PHYSICS OF MANTLE AND CORE MINERALS

Thesis by

Raymond Jeanloz

In Partial Fulfillment of the Requirements

for the Degree of

Doctor of Philosophy

California Institute of Technology

Pasadena, California

1980

(Submitted August 10, 1979)

ACKNOWLEDGMENTS

I am especially grateful to T. J. Ahrens for the generous advice and support that he has given me. I have greatly profitted from the rich intellectual atmosphere provided by the faculty at the Institute, and especially at the Seismological Laboratory; in particular, I have been fortunate to be influenced by and learn a great deal from D. L. Anderson, T. J. Ahrens, I. Jackson and F. M. Richter (the latter two as visitors), and also G. R. Rossman. Most of the work discussed below would not have been possible without the help of the staff at the Laboratory: I thank E. Gelle, R. Smith, J. Long, D. Johnson and H. Richeson, as well as M. McConnell and J. Boike for their considerable efforts. I have also greatly benefitted from collaborations with several individuals from outside the Institute. J. M. Christie, H.-K. Mao, F. M. Richter, G. L. Nord, Jr. and J. S. Lally have generously helped me with this work, and I appreciate the numerous discussions which I have had with D. E. Grady and S. W. Kieffer. These studies have been supported by the National Science Foundation and NASA, for which I am grateful.

ABSTRACT

Shock-wave equation-of-state (Hugoniot) data for initially porous and nonporous samples of iron provide experimental support for theoretically calculated properties of the earth's core, and show that whereas both densities and bulk moduli in the outer core are less than those of Fe under equivalent conditions (by about 10% and 12% respectively) their gradients with pressure are consistent with gross chemical homogeneity through the outer core; simple dynamic models of the core are allowed. New Hugoniot data for wüstite show that oxygen (∿11 wt. %) can be the element which reduces the density of the outer core below that of Fe. The properties of the inner core are consistent with those of iron, suggesting that the inner core-outer core boundary is both a phase and a compositional boundary. The minimum estimated temperature at the top of the outer core is ∿2800K, whereas subsolidus phase equilibria of olivine indicate a temperature near 2000K in the transition zone. Hugoniot data for porous and nonporous MgO and SiO_2 (phases considered representative of the lower mantle) provide an experimentally-constrained (adiabatic) geothermal gradient through the lower mantle which implies the presence of one or (for a more consistent result) more thermal boundary layers in the lower mantle. These suggest that the core is a major heat source for the mantle and that a barrier to convection occurs in (or near the top of) the lower mantle: a chemical discontinuity would be a likely cause. This inference is consistent with new shock-wave data for CaO which show that calcium could be substantially enriched in the lower mantle, as suggested by inhomogeneous accretion theories. A thermal equation of state is determined for anorthite from porous and

nonporous Hugoniot data which, however, show that this refractory mineral can probably not be a major Ca-bearing phase in the lower mantle, except perhaps near the core-mantle boundary. Diamond-cell and Hugoniot data show that CaO undergoes a B1/B2 transition at ∿70 GPa with properties well predicted theoretically. FeO undergoes a similar transition (at ∿70 GPa) and these results suggest that transformation in magnesiowüstite may be important in the lowermost mantle. New Hugoniot data for bronzite are combined with previous shock-wave measurements for olivines and pyroxenes. These data are consistent with static high-pressure results, but suggest the occurrence of post-perovskite phases (density ∿5% greater than perovskite) and they also provide evidence of nonequilibrium effects under shock to pressures above 100 GPa. Spectroscopic and microscopic studies of shock-compressed olivines support this evidence: the structure of olivine achieved under shock is apparently far from equilibrium, as is indicated by phase-transformation theory. Although the bulk properties measured under shock are consistent with the attainment of thermodynamic equilibrium, these properties apparently represent highly transient and nonequilibrium states.

TABLE OF CONTENTS

INTRODUCTION

There is a continuing need to study the physical properties of minerals at high pressures and temperatures in order to better understand the nature of the Earth's deep interior. It is only by combining the measurements of such properties (e.g., density, compressibility, thermal expansion) with direct observations, such as are afforded by seismology, that the composition, thermal state and dynamic processes of the mantle and core can be delineated. The purpose of this thesis is to present new data on the physical properties of several minerals at high pressures, based largely on shock-wave (Hugoniot) experiments, and to apply such data to studies of the lower mantle and core.

The lower mantle comprises the dominant portion of the Earth (62% atomic) and an understanding of its state is of central importance to understanding the nature of the bulk earth. Although the simplest model of the present mantle is based on the assumption of uniform composition, neither this assumption nor its consequences have been fully tested to date. For example, heterogeneous accretion theories for the formation of planets, which predict an enrichment of refractory compounds with depth in the earth, are appealing in light of the current understanding of planetary formation and evolution: without large-scale (whole-mantle) stirring during or after accretion, such enrichment seems inevitable. However, the properties of plausible refractory components at high pressures have virtually not been studied, and hence the possibility of compositional inhomogeneity throughout the mantle has not been critically examined. The Hugoniots of a typical refractory phase (anorthite) and of a refractory oxide component (CaO) are presented

below (Chapters 2, 3, 6 and 7) with this question in mind. Although these data cannot prove that the mantle is inhomogeneous, they do show that an enrichment of refractory components in the lower mantle is completely acceptable on physical grounds.

A related problem concerns the dynamic processes in the mantle and the thermal state which these processes establish. Large scale compositional heterogeneities are very likely to be barriers to through-going convection, therefore favoring the establishment of a relatively complex (small-scale) flow field rather than a single convection cell with depth (considered to be the simplest model of the dynamic state of the mantle). Of course, evidence for a compositional boundary in the present mantle is also evidence against through-going flow. The presence of such a boundary is suggested by the low temperatures implied for the mantle and core without it (Chapter 11).

It is similarly important to determine the nature of the core, although it only corresponds to about 17% (atomic) of the earth. Because the outer core is liquid, the high-pressure liquidus of its constituent (presumably an iron-based alloy) provides an estimate of the lowest possible temperature at the core-mantle boundary. To this end, the density and thermal properties of candidate phases are experimentally constrained at high pressures (Chapters 3 and 5) so that the trade-offs in determining composition and temperature of the core can be more fully evaluated. Surprisingly, a large amount of oxygen (30% atomic) may be present in the core according to these results. This is consistent with recent geochemical arguments for

the presence of oxygen in the core and suggests a relatively high value for the minimum temperature at the core-mantle boundary: above 3000 K.

Taken together, these results show that a chemically inhomogeneous model of the mantle is compatible with the available data and may be preferred with regard to satisfying the current constraints on the thermal state of the earth. Although the degree of inhomogeneity cannot be specified, this conclusion is consistent with heterogeneous accretion theories, but not with whole-mantle convection. The implication is that the tectonic processes which occur near the earth's surface are not directly coupled to the flow field at depth. If this is the case, core formation is unlikely to have occurred at a late stage of the earth's formation since both the physical aggregation of the core material and the potential energy which this releases would be sufficient to homogenize the mantle. These conclusions are based on the assumption that the core is the main heat source driving the tectonic "engine", an inevitable circumstance unless the geotherm through the core is almost exactly isothermal (based on the electrical conductivity of alloys measured at high pressures). However, if the mantle is mainly heated internally (i.e., insignificant thermal flux from the core), this would fortify the conclusion that the mantle consists of more than one chemical and dynamic system (Chapter 11).

Shock-wave techniques are emphasized in the present work because they remain one of the only means of generating the pressures and temperatures of interest ($P \sim 30$ to 350 GPa, or 300 to 3500 kbar; $T \sim$ 1000-5000K). In particular, a large portion of this thesis is concerned with determining thermal as well as compressional properties at high pressures from shock

experiments on minerals (Chapters 5, 6, 7, 11). Among the thermal properties of interest are the coefficient of thermal expansion and the Grüneisen parameter, that is anharmonic properties, to hundreds of GPa and thousands of degrees. By experimentally determining such properties, the measured equations of state of minerals can be corrected to the temperatures existing within the earth, and the tradeoffs between estimated temperature, composition and compressional properties in the mantle and core can be experimentally determined.

Many of the mineral properties considered below have intrinsic interest aside from the direct applications to the earth's interior. For example, arguments are presented to show that although minerals have very high (effective) viscosities under geological conditions, they are extremely inviscid under dynamic (shock-produced) strain rates: viscosity decreases by nearly 1 decade per decade increase in strain rate (Chapter 4). As a consequence, a simplifying assumption (isentropicity) can be used in analyzing the release from shock states, and release data can provide independent constraints on the equation of state. Also, it is because of the low dynamic viscosity that useful thermal data can be extracted from shock experiments on porous samples: the approach to hydrodynamic conditions greatly favors the ability to measure stable averages of properties from highly heterogeneous media (Chapter 7).

Similarly, the observation of glass apparently formed by intense shearing in shocked olivine is interesting in that it is consistent with simple theoretical arguments that the effective core radius (radius of nonelastic interaction) for dislocations is approximately

$4|\underset{\sim}{b}|$ ($\underset{\sim}{b}$: Burgers vector, unit-cell dimension; Chapter 9). That is, when the average dislocation spacing is less than this distance (density exceeding $\sim 10^{17}$ m^{-2} in olivine) the structure becomes randomized, as in a high-angle grain boundary.

Among the most interesting results to emerge from the high-pressure experiments is the generalization that anharmonic properties do not scale directly with volume (Chapters 5, 7). Compressional properties typically vary monotonically with density: for example, bulk modulus increases with increasing density, both under compression and through phase transformations. By contrast, although thermal properties (Grüneisen parameter, thermal expansion) decrease under compression, they increase dramatically with increasing density at major phase transformations. Thus, anharmonic properties appear to be determined by bond length, whereas compressional properties reflect an overall packing efficiency between polyhedral units. Since cation coordination number and bond length increase at major pressure-induced phase transitions, an increased anharmonicity results. An interesting consequence of this is that the local Rayleigh number is likely to increase across a region of phase transformation in the mantle, since an increase in anharmonicity causes an increased thermal expansion and decreased thermal diffusivity (effects which have been experimentally verified). The Rayleigh number describes the driving force for convection against dissipative processes, hence perturbations in the flow field are expected to be localized beneath a transition region.

Despite the advantages of using shock waves to probe the nature of minerals at high pressures and temperatures, considerable difficulties

arise due to the short time scales of the experiments ($\sim 10^{-7}$ s), and the possibility of nonequilibrium effects is always present. Electron microscopy and spectroscopy are used (Chapters 8 - 10) to address this problem by studying in detail the effects of shock on olivine. This is an ideal material for retaining shock-induced microstructures (i.e., resisting thermal annealing), and strong evidence is found for the structural state achieved in olivine under shock being far from equilibrium. This conclusion is expected to hold for most silicates, according to the theory of phase transformations, and it is independently inferred from release-adiabat measurements (Chapters 1 and 6). This implies that the assumption of thermodynamic equilibrium which has been made in reducing Hugoniot data for the complex minerals which appear to transform under shock is fundamentally incorrect. In the simple (e.g., oxide) structures, equilibrium conditions can prevail through phase transformation under shock, as can be verified by independent experiments (e.g., Chapter 2). However, the Hugoniot data for the complex silicates do appear to correspond to equilibrium properties, despite the fact that these data reflect microstructural states which are out of equilibrium. This is an enigmatic result but it does suggest that the geophysical conclusions which have been drawn from the Hugoniot data for silicates are probably (perhaps fortuitously) correct.

The chapters to follow should be considered as independent papers, but they can be grouped under three topics: (1) Hugoniot equations of state of several candidate mantle and core minerals (Chapters 1 to 4); (b) experimentally based thermal equations of state (Chapters 5 to 7); (c) shock-effects in olivine (Chapters 8 to 10). The last chapter (Chapter 11) presents general arguments concerning the thermal, chemical and dynamic state of the lower mantle based largely on the approaches which are developed in the preceding chapters. It also illustrates much of the motivation behind the studies described in the earlier chapters. Experimental techniques are described in detail in Chapters 1, 3 and 6, and data analysis is emphasized in Chapters 3, 5 and 7.

Chapter 1

PYROXENES AND OLIVINES: STRUCTURAL IMPLICATIONS OF SHOCK-WAVE DATA FOR HIGH PRESSURE PHASES

Abstract

A re-examination of Hugoniot equation of state data and three new release adiabat points indicates that results for enstatite-bronzite composition pyroxene are compatible with its transforming to a perovskite phase at high pressure (for En_{90}: $\rho_0 = 4.20$ g/cm^3, $K_0 \sim 2.6 \pm 0.5$ Mbar, $K'_0 \sim 3.5 \pm .65$). The release adiabat data, as well as results from porous samples, imply that the shock-wave data do not define an equilibrium, high-pressure phase Hugoniot below about 1.00 Mbar. These also suggest a further transformation to a phase (or assemblage) with density about 5% (or more) greater than that of orthorhombic perovskite. The data would allow such a transformation to occur at pressures as low as 0.60 Mbar under shock, representing an upper bound for the equilibrium transition pressure.

Hugoniot data on magnesian olivines also appear to represent states of thermodynamic disequilibrium or a mixed-phase region below about 0.80-1.00 Mbar. However, Hugoniot points for Mg-pyroxene and Mg-olivine coincide at pressures above 0.70 Mbar, suggesting that these minerals transform to high-pressure phases (or phase assemblages) of comparable density. Since MgO (presumably as periclase or in a closely related structure) attains relatively low densities at these pressures, the shock-wave data are in strong disagreement with the disproportionation of Mg_2SiO_4 to a $MgSiO_3$ (perovskite) + MgO assemblage above 0.80-1.00 Mbar. Conversely, the shock-wave data do not preclude a transformation

of the type $Mg_2Si_2O_6 \rightarrow Mg_2SiO_4$ ("post-perovskite" phase) + SiO_2 (rutile or fluorite structure). Again, these results would imply polymorphism to very dense "post-perovskite" phases. Based on the arguments made for pyroxene, such a transformation could occur at pressures as low as 0.60 Mbar under equilibrium conditions.

We note that the combined results of high-pressure experiments allow Mg-pyroxene compositions to be as likely candidates for the lower mantle as olivine.

I. INTRODUCTION

Upon recognition that the features associated with plate tectonic processes on the earth (subduction zones, ridges and plumes) may reflect an integral sampling of the mantle convective flow field, and with the perspectives attained from the last decade of terrestrial planetary exploration, experimental high-pressure geophysics has focused increasingly on studying candidate materials of the earth's lower mantle and core.

Current ideas (e.g., Schubert and Anderson, 1974) suggest that active convection in the earth takes place to depths of at least 750 km. However, it is important to discern whether the upper mantle above ∿350 km depth, and possibly the phase transition region extending to depths of at least 670 km, represents a differentiate of the lower mantle and is thus atypical of the silicate zone of the earth as proposed by Anderson et al. (1972) and Anderson (1977). By contrast Ringwood (1975), has emphasized the essential homogeneity of the mantle. Clearcut data specifying the composition of the upper mantle stem largely from inclusions in kimberlites (e.g., Boyd, 1973) and nodules from volcanic rocks of deep-seated origin (e.g., Basu, 1975; MacGregor, 1975) and demonstrate the upper mantle to be largely garnet lherzolite with minor amounts of eclogite. This composition is not unlike the "pyrolite" model originally proposed by Clark and Ringwood (1964) which, by means of variations in temperature, pressure, and degree of partial melting, accounts for the genesis of a large class of effusive and plutonic rocks that penetrate the crust (Green, 1972).

The lower mantle, extending from depths of 670 to 2900 km,

represents 49% of the mass of the earth. Its mineralogy and thermal state can be inferred from comparison of shock-wave and seismological data (Al'tschuler and Sharpidzhanov, 1972a, b; Anderson et al., 1972; Anderson, 1977), and by extrapolation of results based on quench products from static high-pressure, petrological experiments (e.g., Ringwood, 1975; Liu, 1975a, b, 1976; Akimoto et al., 1976) using largely ultrasonic and static-compression equations of state. The composition, structure, and thermal history of the earth must ultimately be related to the composition of the sun, the moon, meteorites and other terrestrial planets, and the processes of planetary accretion (e.g., Hanks and Anderson, 1969; Lewis, 1972; Ringwood, 1975).

In the present study the nature of the shock-induced, high-pressure phases of olivine and pyroxene rocks is examined in the light of data for the densities of a new class of perovskite-related silicate structures synthesized by Liu (1975a, b, 1976) and some new Hugoniot and release adiabat data for bronzite. Previous data for olivine-rich samples in the range Fo_{100} to Fo_{85} and for enstatitic samples of analogous composition are reported by Trunin et al. (1965) and McQueen et al. (1967). Trunin et al. (1965) and recently Simakov and Trunin (1973) have reported single datum points for four different compositions, extending our knowledge of Hugoniot states for ferromagnesian silicates to pressures in excess of 2.40 Mbar.

II. EXPERIMENTAL METHODS

Discs (1 cm in diameter) of Bamle bronzite $(Mg_{.86}, Fe_{.14})SiO_3$ were cored from the same aliquot previously studied to shock

pressures of 0.48 Mbar (Ahrens and Gaffney, 1971) and machined to thickness tolerances of $\sim\pm0.05$ mm. The density of each disc was determined at least twice by weighing in air and in reagent grade toluene using temperature corrections of Berman (1939). The samples were mounted on 0.5 mm thick Cu or Ta driver plates and impacted by flyer-plate bearing projectiles at speeds ranging from 5.4 to 6.1 km/sec with a light-gas apparatus qualitatively similar to that described by Jones et al. (1966). Pure (commercial grade) Cu and Ta flyer plates, 2.5 mm thick, with a minimum diameter of 17 mm (Figure 1) are hot-press welded into lexan projectile blanks using techniques developed by A. Mitchell (private communication). After molding and stress relieving, a polyethylene, gas-sealing rear portion of the projectile was press fitted onto the 6 mm long lexan flyer plate (front) portion of the projectile. The final projectile diameter was machined so as to provide a $\sim$0.03 mm interference fit with the light-gas gun launch tube. The resulting projectiles had masses of 14 and 20 gm for Cu and Ta flyer plates, respectively. The light-gas gun used to accelerate these projectiles employs a 20 m long, 16 cm diameter pump tube in which a $\sim$20 kg high-density polyethylene piston is used to compress the propelling gas, H_2, initially at a pressure of 2 bar. The polyethylene piston achieves speeds of $\sim$0.4 km/sec using approximately 3 kg of double-based propellant. The projectile is launched upon bursting of a diaphram (at a gas pressure of $\sim$0.7 kbar) at the breech of the 25 mm diameter, 7 mm long launch tube. The total flight of the projectile from the muzzle of the launch tube to the target is $\sim$500 mm and occurs in a vacuum of 10 to 30 mtorr. Projectile velocities are measured using

the flash X-ray method of Jones et al. (1966), except that interruption of a continuous X-ray beam (Long and Mitchell, 1972) is used to trigger the first flash X-ray unit (∿15 ns exposure), and the breakage of a 0.05 mm diameter copper wire intercepting the outer edge of the projectile is used to trigger the second flash X-ray unit. The center line of the two flash X-ray units are ∿350 mm apart, and the time interval between X-ray flashes is measured to within an uncertainty of ±0.01 μsec. Since triggering in our initial experiments was not reliable, we have had to rely on the redundancy provided by measuring (1) the electronic delays of both flash X-ray units and (2) the time interval between the second X-ray flash and the closure of the redundant pin switch(es) mounted on the sample assembly (Figure 1) to infer impact velocity. The ∿3° projectile tilt observed in Figure 1, is highly reproducible, and the sample assembly was thus pre-oriented to achieve nearly normal impact.

As in the experiments of Ahrens et al. (1971), an electronically triggered, image-converted streak camera was used to record shock transit-time through the sample. However, in the present experiments, the onset of illumination on shock arrival at the mirrors (presumably arising from the high temperatures behind the shock in the glass) was used to record shock arrivals with the streak camera, and the arrival of the shock at the mirror-free surface was observed to result in the immediate loss of illumination (Figure 2). We infer this effect to be caused by the disintegration of the specular mirror surface, probably upon incongruent vaporization of the glass and the accompanying, sudden adiabatic expansion of the vaporized species. In the present

experiments, the streak camera was writing at a speed of 25 mm/μsec for a duration of ∿2 μsec on 20 X 22.5 cm (4 X 5 inch) Tri-X film. Developing procedures were used to force the film to a sensitivity of ASA 3000. Time calibration was obtained using a Pockel-cell modulated Ar-ion laser beam modulated at 20 Mhz, thus providing time marks at 50 nsec intervals. The writing rate at any point on the streak camera trace was measurable to within ±0.25%, and a practical time resolution of ∿2 nsec was achieved.

Hugoniot states were determined using the impedance match method of Rice et al. (1958), and release adiabat data employ the buffer technique described by Ahrens et al. (1969b). The equations of state for Ta and Cu employed in the impedance match solutions are those given by McQueen et al. (1970).

III. RESULTS FOR GLASS AND BAMBLE BRONZITE

The unexpected self illumination and prompt light decay upon passage of strong shocks through the soda-lime glass mirrors (microscope slide quality, plate glass) provided consistent and, we believe, reliable measurements of shock-wave velocities in this material. The resulting data are given in Table 1 and plotted in Figures 3 and 4. The shock-wave velocity (U_s) - particle velocity (u_p) relation in Figure 3 is concordant with data reported by Dremin and Adadurov (1964) to pressures of 0.41 Mbar for a glass of similar zero-pressure density (2.48 g/cm^3) but of slightly different composition. The linear U_s-u_p relation indicated in Figure 3 fits the present four data points, and Dremin and Adadurov's data points at 0.33 and 0.41 Mbar with a coefficient of correlation

$r^2 = 0.997$. This fit was used to obtain the release adiabat points for the Bamle bronzite (Table 2, Figure 5).

Qualitatively, the behavior of Na-Ca glass is observed to be similar to that first reported by Wackerle (1962) for fused quartz. It appears that above ~0.15 Mbar, the Si^{4+} ion begins to transform from tetrahedral to octahedral coordinations with the O^{2-} ion, as in the case of the quartz to stishovite transition (McQueen et al., 1963). This, and the possible coordination increases of the Na^{+} and Ca^{+} ions account for the incompressible behavior indicated above 0.50 Mbar. The zero-pressure density (ρ_0) shown in Figure 4 is calculated using our microprobe analyses and standard oxide molar volumes assuming a molar volume of 14.014 cm^3 for SiO_2 (stishovite) (Robie and Waldbaum, 1968).

Although the uncertainties in the measurement of projectile and shock velocity can be obtained from the scatter of redundant projectile time-interval measurements and the uncertainties of discerning shock arrival times on the streak records, the estimation of uncertainties in the pressure-density plane (Figures 4 and 5) is less straightforward. The non-orthogonality of the uncertainty brackets shown in both figures for the Hugoniot data arise from the fact that the particle velocity and, hence, pressure and density, are not independently related to uncertainties in projectile and shock velocity via the impedance match solution. The uncertainties arising from both the density and pressure are calculated from the uncertainties in projectile velocity holding the shock velocity fixed (at its average value), and vice versa. The uncertainties in the three release points

take into account only the uncertainties in shock velocity through the buffer (1-mm-thick glass).

IV. DISCUSSION

Shock-wave data for magnesian pyroxenes are summarized in Figure 5, including results for porous (synthetic aggregate) samples, nonporous samples, and our new data on Bamle bronzite (cf. Table 2). At pressures below about 0.70-1.00 Mbar, it is clear that the porous Hugoniot data bear an anomalous relation with respect to the nonporous data since the former should lie on "hot compression" curves, systematically displaced to lower densities (at a given pressure) from the principal Hugoniot presumably defined by nonporous data. The energy associated with irreversible compaction of porosity represents a thermal pressure as a function of initial density, via Grüneisen's γ (V, T), which defines this displacement. For this reason, the porous data have, in general, been very scantily discussed, considered uninterpretable, or outright dismissed as wrong (McQueen et al., 1967; McQueen, 1968; Ahrens et al., 1969a, Davies and Gaffney, 1973; Simakov and Trunin, 1973).

The relatively high density attained by the porous materials on shocking can, nevertheless, be explained as a kinetic effect (cf. McQueen et al., 1967, 1970). Assuming that pyroxene transforms to a dense phase or assemblage above a given pressure, this transformation, even once initiated under shock, may not have time to go to completion without substantial overdriving. Because porous samples become much hotter on shocking, their rate of transformation is expected to be

significantly enhanced, thus yielding a larger proportion of high-pressure phase material for a given pressure compared with nonporous samples. Assuming this model applies, it is easy to explain the distribution of Hugoniot data in the figure.

The pressure-release points shown in Figure 5 provide independent support for such a model. Since the release path is adiabatic (isentropic to within the approximation of reversibility) while entropy increases monotonically up a materials' Hugoniot, the P-V slope of the release path should be no steeper than the Hugoniot slope at a given pressure (e.g., see Duvall and Fowles, 1966). Because the measured release adiabat points lie below the Hugoniot data, it is indicated that a mixed-phase region extends to pressures around 0.70-1.00 Mbar with transformation to a high-density assemblage complete at pressures no lower than these. This high-pressure assemblage must have a metastable Hugoniot with a P-V slope at least as great as the release paths, which supports the hypothesis of an extended mixed-phase (or disequilibrium) region probably associated with the rate of phase transformation under shock.

At pressures above about 1.00 Mbar the nonporous samples achieve densities that are generally (and consistently) higher than the porous points. So, we believe that the shock-wave data begin to define an equilibrium, high-pressure assemblage Hugoniot at these pressures, below which one or more phase transformations result in a wide, mixed-phase region.

Similarly, Hugoniot data for Mg-rich olivines are summarized in Figure 6. These show the same anomalous relations between porous

and nonporous samples, implying transformation to a high-density phase (or assemblage) subject to kinetic effects (though release adiabat data for such compositions are not yet available). This conclusion fits in with the discussion by Ahrens and Petersen (1969).

Aside from these results with porous data and steep, measured release paths (cf. Ahrens et al., 1969b; Grady et al., 1974, 1977), a comparison of shock-recovery and static high-pressure experiments (Ahrens and Graham, 1972; Liu, 1974, 1975c; Schneider and Hornemann, 1976) also indicate that overdriving beyond equilibrium transition pressures is commonly needed in silcates to achieve a given phase transformation under shock, clearly implying control by kinetics of nucleation and growth of high-pressure phases (but note Podurets and Trunin, 1974). Thus, porous samples may well indicate the presence and nature of high-pressure phases (or assemblages) more readily than nonporous samples under shock. Also, high-pressure phase Hugoniots will tend to be significantly steeper (and therefore centered at higher zero-pressure densities) than would be apparent from the distribution of the data.

Zero-pressure densities for high-pressure phases interpreted from pyroxene and olivine shock-wave data by several workers are summarized in Figure 7. The tendency has been to assign higher densities (for a given Mg:Fe ratio) to olivine (A_2BO_4) than to pyroxene (ABO_3) stoichiometries. One problem is apparent near the magnesian end, however, in that interpreted densities seem to actually decrease with increasing Fe content. Barring very complex phase relations, this is highly unlikely due to the enormous difference

in the atomic masses of Fe and Mg. Rather, it appears that the density estimates for the magnesian endmembers have been biased upward relative to the Fe-bearing compositions by the high densities implied by the porous data (which only exist for the endmembers, forsterite and enstatite). Based on the arguments developed above, it is not appropriate to directly compare the porous data with the data for (nonporous) Fe-bearing compositions.

Liu's recent (1975a, 1975b, 1976; Liu and Ringwood, 1975) static high-pressure experiments have confirmed the previously suspected occurrence and significance of perovskite-related structures in silicates (Reid and Ringwood, 1969, 1974, 1975; Shimizu et al., 1970; Ringwood and Major, 1971). Distorted (non-cubic), perovskite-like structures have been quenched from diamond-anvil experiments on both magnesian olivines and pyroxenes. These structures, apparently of the orthorhombic, rare-earth, orthoferrite type (Marezio et al., 1970) will be loosely termed perovskites. Densities versus composition for the perovskite phases and assemblages of pyroxene (ABO_3) and olivine (ABO_3 + AO) derived from Liu's (1975a, 1975b) X-ray parameters are also shown in Figure 7. It is interesting to note that an olivine stoichiometry actually results in a lower density perovskite assemblage than a pyroxene stoichiometry. This is a direct consequence of the low density of (Mg, Fe)O in the ABO_3 + AO assemblage. The densities of such (Mg, Fe)O recovered from high pressure lie directly between the densities of MgO (periclase) and FeO (stoichiometric wüstite), as can be seen in Figure 7. This is compatible with the shock-wave data on MgO, which shows no evidence for phase transformations to pressures

over 1.00 Mbar (McQueen and Marsh cited in Birch, 1966; McQueen, 1968; Carter et al., 1971).

In order to compare the static results with the shock-wave data, theoretical metastable Hugoniots were constructed for perovskite of appropriate composition ($Mg_{0.9}$ $Fe_{0.1}$ SiO_3) based on Birch-Murnaghan principal adiabats. This approach is philosophically and computationally similar to that of Davies and Gaffney (1974). Necessary parameters are shown in Table 3 along with the values used here. Density and the energy of the pyroxene-perovskite transformation (at P = 0) were derived from Liu's work (1975a, 1975b, 1976), via Figure 7 and by using $\Delta E_{tr} \leq (-P\Delta V + T\Delta S)_{tr}$. Since the last term is not known, it is assumed to be negligibly small (i.e., $\frac{dP}{dT} = 0$ for the phase boundary). Because the experimental data bound the equilibrium pressure of transition, and most likely $T\Delta S \leq 0$, the resulting estimate for ΔE_{tr} is probably a strict upper bound (and rather high). Incidentally, though we discuss the direct transformation from pyroxene to perovskite structures under shock, this obviously represents a metastable phase boundary (based on our current knowledge from Liu's work). Intermediate structures may well be involved.

Estimates of the bulk modulus K_0 and $K_0' = (dK/dP)_{P=0}$ were based on their empirical correlation with density, with particular emphasis given to data for perovskite-structured compounds (Beattie and Samara, 1971; Davies, 1976). The wide range in values given easily overlap estimates based on the various K-ρ relations that have been proposed (Anderson, 1967, 1969; Anderson et al., 1968; Anderson and Anderson, 1970; Anderson, 1972). Similarly, Grüneisen's (bulk or thermodynamic)

γ was estimated from typical values for various compounds, with a volume dependence that has been found to be not unreasonable for those cases where it has been studied. Temperature dependence was assumed to have a negligible effect, and, again, rather wide bounds were given for reasonable values. Finally, a family of theoretical perovskite Hugoniots was constructed for the best estimate of values given in Table 3 and by varying each of the parameters within the stated bounds. An envelope containing this family of curves along with the Hugoniot based on the best values are shown in Figure 5.

It is immediately clear that the shock-wave data are compatible with Mg-pyroxene transforming to a perovskite structure at pressures above approximately 0.80 Mbar. This is contrary to the conclusions of Simakov and Trunin (1973). In fact, by considering the most porous data (which achieve high densities at relatively low pressures) and the arguments presented above, it seems that perovskite-like densities can be achieved by about 0.50 Mbar. If anything, the left half of the envelope in Figure 5 agrees with the data as well as the best estimate; this could be consistent with an even lower pressure for transformation to the perovskite structure. This, then, is an upper bound for the pressure of transformation based solely on Hugoniot data yet it still represents a significant overdriving compared to the static experiments (Liu, 1975b, 1976).

Compared with the theoretical Hugoniots, the release paths still appear to have very steep slopes, and the most porous data cross over to yet higher densities. These latter data may be erroneous (Simakov and Trunin, 1973), but assuming that they are not, they suggest, along

with the release adiabats, the possibility of a phase (or assemblage) with a zero-pressure density even higher than perovskite. Transformation to such a "post-perovskite" phase could occur at pressures as low as about 0.60 Mbar, according to the shock data; this would therefore be an upper limit for the equilibrium transition pressure. An initial density of 5% or so greater than for orthohombic perovskite could be consistent with the data.

In similar fashion, a theoretical Hugoniot (Figure 6) was constructed for a perovskite assemblage corresponding to olivine stoichiometry ($MgSiO_3$ [perovskite] + MgO [periclase]) based on the best-estimate Hugoniot in Figure 5 and the rather well-determined Hugoniot of MgO (McQueen and Marsh cited in Birch, 1966; McQueen, 1968; Carter et al., 1971) shown in Figure 8. Because the left half of the envelope in Figure 5 appeared most consistent with the pyroxene points, a corresponding band is shown in Figure 6.

In this case, perovskite-like densities are achieved in the 0.60-0.80 Mbar range. Once more, the shock-wave data are consistent with the static results that demonstrate olivine transforming to perovskite at high pressures (but again at pressures significantly lower than under shock). On the other hand, the olivine points are clearly shifted to higher densities than the perovskite-assemblage Hugoniot at pressures above about 0.70 Mbar. Because the theoretical curve for the perovskite assemblage cannot be shifted without causing a significant deviation from the pyroxene points, the olivine data are in strong disagreement with a perovskite assemblage at high pressure.

If the olivine points did not deviate so systematically from the

theoretical Hugoniot, which is consistent with the pyroxene shock data, this divergence might well be ascribed to be within experimental error. However, the same discrepancy emerges from Figure 8, quite apart from any theoretical curves. The point here is that above about 0.70 Mbar, the olivine and pyroxene data overlap, whereas a perovskite model would predict olivine densities to be lower than pyroxene densities (i.e., shifted toward the MgO Hugoniot) as was mentioned above and can be inferred from Figure 7. Although we have discussed kinetic effects and a mixed-phase region to the 1.00 Mbar range, the overlap continues to much higher pressures. Furthermore, the nature of the perovskite-forming transformations would suggest that pyroxene (which involves no disproportionation) would form perovskite at least as readily as olivine, whereas in the high-pressure data of Figure 8 one must either consider the olivine too dense or the pyroxene not dense enough to agree with a self-consistent perovskite model.

V. CONCLUSIONS

After reviewing experimental techniques, we presented new Hugoniot data for Bamle bronzite including simultaneously measured release paths, based on the mirror-buffer technique. Calculation of Hugoniot states for the mirror glass provides a satisfactory internal check, with the soda-lime glass behaving in a fashion similar to fused quartz under shock.

Re-examining available shock data for magnesian pyroxenes and olivines leads to the conclusion that these data define a mixed-phase (or disequilibrium) region to about the 1.00 Mbar range, related

to the kinetics of phase transformation in these silicates. By recognizing this point, certain discrepancies in previous interpretations of shock data can be explained. A set of theoretical Hugoniots for pyroxene and olivine stoichiometry, perovskite-bearing assemblages was constructed based on the properties deduced from high-pressure work, showing that the shock data is compatible with transformations to perovskites in the 0.45-0.70 Mbar region (decidedly above the equilibrium pressure of transformation).

A perovskite model implies different densities for pyroxene and olivine stoichiometries, however. We note that by considering an extremely simplistic assemblage for the lower mantle, consisting of high-pressure phases of only olivine and pyroxene, varying the proportions of these components results in a significant variation in the overall density of the assemblage. In other words, any compelling evidence for density variations within the lower mantle (based, say, on seismological data) can be readily explained without resorting, for example, to variations in Mg:Fe ratios. This degree of freedom is likely to exist whatever the pertinent, multi-phase assemblage may be for the lower mantle. In fact, we consider our two-phase model simplistic if for no other reason than that we have ignored for lack of data the effects on phase relations of other likely components, such as Al or Ca.

In addition, the high-pressure shock data suggest the presence of a yet higher density phase (or assemblage) than perovskite. In particular, the results on olivine diverge from predicted estimates and from densities consistent with pyroxene Hugoniot points. Taken together,

the data do not preclude transformations involving a "post-perovskite" phase of Mg_2SiO_4 at pressures above 0.80-1.00 Mbar, and including a reaction of the type $Mg_2Si_2O_6 \rightarrow Mg_2SiO_4$ ("post-perovskite" phase) + SiO_2 (rutile, α-PbO_2, or fluorite structure) (cf., German et al., 1974; Jamieson, 1977).

We reiterate that the static high-pressure results (and thus our analysis) involve an orthorhombic (i.e., non-ideal) modification of perovskite. Since this class of structures includes a wide variety of related modifications (succinctly summarized by Salje, 1976), it is quite possible that the higher pressure phase suggested by the shock data is, in fact, a perovskite such as the ideal cubic form. Indeed, it is quite possible that the phase quenched from high pressure is a modification of the actual structure attained under pressure. Bearing in mind the well-known difficulties of recovering these high-pressure polymorphs on quenching (e.g., Liu and Ringwood, 1975) and the important effects of environmental conditions on the perovskite modifications (e.g., see Sis et al., 1973), it is not unlikely that they are involved in higher density assemblages than have yet been described. Recently discussed hexagonal forms may be an example of this (cf., Burbank and Evans, 1948; Kawai et al., 1974). However, there are other structure types that could also be likely, some of which have only begun to be discussed as possible high-pressure polymorphs (e.g., Reid and Ringwood, 1970; Ringwood, 1975; Moore, 1976).

Finally, the shock data indicate very similar properties for olivine and pyroxene at high pressures, making them both equally likely candidates for the lower mantle.

Acknowledgments. This is the first scientific report of results obtained with the light-gas gun apparatus housed in the Helen and Roland W. Lindhurst Laboratory of Experimental Geophysics. The physical facilities of this laboratory owe their existence to the generosity of Mrs. Helen W. Lindhurst. We appreciate the skilled operation and maintenance of our apparatus by H. Richeson, D. Johnson, and V. Nenow. We also thank I. Jackson for helpful comments.

REFERENCES

Ahrens, T. J., Shock-wave equations of state of minerals, in Mantle and Core in Planetary Physics, L. Corso (ed.), Academic Press, New York, 157-187, 1971.

Ahrens, T. J. and E. S. Gaffney, Dynamic compression of enstatite, J. Geophys. Res., 76, 5504-5513, 1971

Ahrens, T. J. and E. K. Graham, Shock-induced phase change in iron-silicate garnet, Earth Planet. Sci. Lett., 14, 87-90, 1972.

Ahrens, T. J. and C. F. Petersen, Shock wave data and the study of the earth, in The Application of Modern Physics to the Earth and Planetary Interiors, S. K. Runcorn (ed.), Wiley-Interscience, New York, 449-461, 1969.

Ahrens, T. J., D. L. Anderson, and A. E. Ringwood, Equations of state and crystal structures of high-pressure phases of shocked silicates and oxides, Rev. Geophys., 7, 667-707, 1969a.

Ahrens, T. J., J. H. Lower and P. L. Lagus, Equation of state of forsterite, J. Geophys. Res., 76, 518-528, 1971.

Ahrens, T. J., C. F. Petersen, and J. T. Rosenberg, Shock compression of feldspars, J. Geophys. Res., 74, 2727-2746, 1969b.

Akimoto, S., M. Akaogi, K. Kawada and O. Nishizawa, Mineralogic distribution of iron in the upper half of the transition zone in the earth's mantle, in The Geophysics of the Pacific Ocean Basin and Its Margin, G. H. Sutton, M. H. Manghnani and R. Moberly (eds.), 399-405, Am. Geophys. Union Monograph 19, 1976.

Al'tschuler, L. and I. Sharpidzhanov, Additive equation of state of silicates at high pressure, Izv. Earth Phys., 3, 11-21, 1971a.

Al'tschuler, L. and I. Sharpidzhanov, Distribution of iron in the earth and its chemical differentiations, Izv. Earth Phys., 4, 3-16, 1971b.

Anderson, D. L., A seismic equation of state, Geophys. J. R. astr. Soc., 13, 9-30, 1967.

Anderson, D. L., Bulk Modulus-density systematics, J. Geophys. Res., 74, 3857-3864, 1969.

Anderson, D. L., Composition of the mantle and core, Ann. Rev. Earth Planet. Sci., 5, 179-202, 1977.

Anderson, D. L. and O. L. Anderson, The bulk modulus-volume relationship for oxides, J. Geophys. Res., 75, 3494-3500, 1970.

Anderson, D. L., C. Sammis, and T. Jordan, Composition of the mantle and core, in The Nature of the Solid Earth, E. C. Robertson (ed.), McGraw-Hill Co., New York, 41-66, 1972.

Anderson, O. L., Patterns in elastic constants of minerals important to geophysics, in The Nature of the Solid Earth, E. C. Robertson, (ed.), McGraw-Hill Co., New York, 557-613, 1972.

Anderson, O. L., E. Schreiber, R. C. Liebermann and N. Soga, Some elastic constant data on minerals relevant to geophysics, Rev. Geophys., 6 491-524, 1968.

Basu, A. R., Hot-spots, mantle plumes and a model for the origin of ultramafic xenoliths in alkali basalts, Earth Planet. Sci. Lett., 28, 261-274, 1975.

Beattie, A. G., and G. A. Samara, Pressure dependence on the elastic constants of $SrTiO_3$, J. Appl. Phys., 42, 2376-2381, 1971.

Bénard, J., Sur les paramètres limites de la phase FeO, Acta Cryst., 7, 214, 1954.

Berman, H., A torsion microbalance for the determination of specific gravities of minerals, Am. Mineralogist, 24, 434-440, 1939.

Birch, F., Compressibility: elastic constants, in Handbook of Physical Constants, S. P. Clark, Jr., (ed.), Geol. Soc. Am. Mem. 97, 97-173, 1966.

Boyd, F. R., A pyroxene geotherm, Geochim. Cosmochim. Acta, 37, 2533-2546, 1973.

Burbank, R. D., and H. T. Evans, Jr., The crystal structure of hexagonal barium titanate, Acta Cryst., 1, 330-336, 1948.

Carter, W. J., S. P. Marsh, J. N. Fritz and R. G. McQueen, The equation of state of selected materials for high-pressure reference in Accurate Characterization of the High-Pressure Environment, E. C. Lloyd (ed.), 147-158, Nat. Bur. Stds. Pub. 326, 1971.

Clark, S. P., Jr. and A. E. Ringwood, Density distribution and constitution of the mantle, Rev. Geophys., 2, 35-88, 1964.

Davies, G. F., The estimation of elastic properties from analogue compounds Geophys. J. R. astr. Soc., 44, 625-647, 1976.

Davies, G. F. and D. L. Anderson, Revised shock-wave equations of state for high-pressure phases of rocks and minerals, J. Geophys. Res., 76, 2617-2627, 1971.

Davies, G. F. and E. S. Gaffney, Identification of high-pressure phases of rocks and minerals from Hugoniot data, Geophys. J. Roy. astr. Soc., 33, 165-183, 1973.

Dremin, A. N. and G. A. Adadurov, The behavior of glass under dynamic loading, Soviet Physics - Solid State, 6, 1379-1384, 1964.

Duvall, G. E. and G. R. Fowles, Shock waves, in High Pressure Physics and Chemistry, 2, R. S. Bradley (ed.) Academic Press, New York, 209-299, 1966.

German, V. N., N. N. Orlova, L. A. Tarasova and R. F. Trunin, Synthesis of the orthorhombic phase of silica in dynamic compression, Izv. Earth Phys., 7, 50-56, 1974.

Grady, D. E., W. J. Murri and G. R. Fowles, Quartz to stishovite: wave propagation in the mixed phase region, J. Geophys. Res., 79, 332-338, 1974.

Grady, D. E., Processes occurring in shock wave compression of rocks and minerals, in High Pressure Research: Applications to Geophysics, M. H. Manghnani and S. Akimoto (eds.), Academic Press, New York, 1977.

Green, D. H., Magmatic activity as the major process in the chemical evolution of the earth's crust and mantle, Tectonophys., 13, 47-71, 1972.

Hanks, T. C. and D. L. Anderson, The early thermal history of the Earth, Phys. Earth Planet. Int., 2, 19-29, 1969.

Jamieson, J. C., Phase transitions in rutile-type structures, in High-Pressure Research: Applications to Geophysics, M. H. Manghnani and S. Akimoto (eds.), Academic Press, New York, 1977.

Jones, A. H., W. M. Isbell and C. J. Maiden, Measurement of the very high pressure properties of materials using a light-gas gun, J. Appl. Phys., 37, 3493-3499, 1966.

Kalinin, V. A. and V. L. Pan'kov, Equations of state of rocks, Izv. Earth Physics, 7, 10-20, 1974.

Katsura, T., B. Iwasaki, S. Kimura and S. Akimoto, High-pressure synthesis of the stoichiometric compound FeO, J. Chem. Phys., 47, 4559-4560, 1967.

Kawai, N., M. Tachimori and E. Ito, A high pressure hexagonal form of $MgSiO_3$, Proc. Japan Academy, 50, 378-380, 1974.

Lewis, J. J., Metal/silicate fractionation in the solar system, Earth Planet. Sci. Lett., 15, 286-290, 1972.

Liu, L., Disproportionation of kyanite to corundum plus stishovite at high pressure and temperature, Earth Planet. Sci. Lett., 24, 224-228, 1974.

Liu, L., Post-oxide phases of forsterite and enstatite, Geophys. Res. Lett., 2, 417-419, 1975a.

Liu, L., Post-oxide phases of olivine and pyroxene and mineralogy of the mantle, Nature, 258, 510-512, 1975b.

Liu, L., High-pressure reconnaissance investigation in the system $Mg_3Al_2Si_3O_{12}$-$Fe_3Al_2Si_3O_{12}$, Earth Planet. Sci. Lett., 26, 425-433, 1975c.

Liu, L., The high pressure phases of $MgSiO_3$, Earth Planet. Sci. Lett., 31, 200-208, 1976.

Liu, L. and A. E. Ringwood, Synthesis of a perovskite-type polymorph of $CaSiO_3$, Earth Planet. Sci. Lett., 28, 209-211, 1975.

Long, J. R. and A. C. Mitchell, A dc X-ray fiducial pulse generator for light-gas gun work, Rev. Scient. Instr., 43, 914-917, 1972.

MacGregor, I. D., Petrologic and geophysical significance of mantle xenoliths in basalts, Rev. Geophys. Space Phys., 13, 90-93, 1975.

Marezio, M., J. P. Remeika and P. D. Dernier, The crystal chemistry of the rare earth orthoferrites, Acta Cryst., B26, 2008-2022, 1970.

McQueen, R. G., Shock-wave data and equations of state, in Seismic Coupling, G. Simmons (ed.), Advanced Research Projects Agency Meeting, National Technical Information Service, Springfield, Virginia, pp. 53-150, 1968.

McQueen, R. G., J. N. Fritz and S. P. Marsh, On the equation of state of stishovite, J. Geophys. Res., 68, 2319-2322, 1963.

McQueen, R. G., S. P. Marsh and J. N. Fritz, Hugoniot equation of state of twelve rocks, J. Geophys. Res., 72, 4999-5036, 1967.

McQueen, R. G., S. P. Marsh, J. W. Taylor, J. N. Fritz, and W. J. Carter, The equation of state of solids from shock wave studies, in High Velocity Impact Phenomena, R. Kinslow (ed.), Academic Press, New York, 294-419, 1970.

Moore, P. B., The glaserite, $K_3Na(SO_4)_2$, structure type as a "super" dense-packed oxide: evidence for icosahedral geometry and cation-anion mixed layer packings, N. Jb. Miner. Abh., 127, 187-196, 1976.

Pan'kov, V. L. and V. A. Kalinin, Thermodynamic characteristics of rocks and minerals under the conditions obtaining in the earth's mantle, Izv. Earth Phys., 3, 3-15, 1975.

Podurets, M. A. and R. F. Trunin, On the microstructure of the dense phase of shock-compressed quartz, Izv. Earth Phys., 7, 21-24, 1974.

Reid, A. F. and A. E. Ringwood, High-pressure scandium oxide and its place in the molar volume relationships of dense structures of M_2X_3 and ABX_3 type, J. Geophys. Res., 74, 3238-3252, 1969.

Reid, A. F. and A. E. Ringwood, The crystal structure of dense M_3O_4 polymorphs: high pressure Ca_2GeO_4 of K_2NiF_4 structure type, J. Solid State Chem., 1, 557-565, 1970.

Reid, A. F. and A. E. Ringwood, New dense phases of geophysical significance, Nature, 252, 681, 1974.

Reid, A. F., and A. E. Ringwood, High-pressure modification of $ScAlO_3$ and some geophysical implications, J. Geophys. Res., 80, 3363-3370, 1975.

Rice, M. H., R. G. McQueen and J. M. Walsh, Compression of solids by strong shock waves, in Solid State Physics, 6, F. Seitz and D. Turnbull (eds.), Academic Press, New York, 1-63, 1958.

Ringwood, A. E., Composition and Petrology of the Earth's Mantle, McGraw-Hill Co., New York, 1975.

Ringwood, A. E. and A. Major, Synthesis of majorite and other high pressure garnets and perovskites, Earth Planet. Sci. Lett., 12, 411-418, 1971.

Robie, R. A. and D. R. Waldbaum, Thermodynamic properties of minerals and related substances at 298.15°K (25.0°C) and one atmosphere (1.013 bars) pressure and at high temperatures, U. S. Geol. Surv. Bull. 1259, 256 pp., 1968.

Robie, R. A., P. M. Bethke, M. S. Toulmin and J. L. Edwards, X-ray crystallographic data, densities and molar volumes of minerals, in Handbook of Physical Constants, S. P. Clark, Jr. (ed.), Geol. Soc. Am. Mem. 97, 27-73, 1966.

Salje, E., Symmetry and lattice dynamics of oxides with perovskite-like structures, Acta Cryst., A32, 233-238, 1976.

Schneider, H. and U. Hornemann, Disproportionation of andalusite (Al_2SiO_5) into Al_2O_3 and SiO_2 at very high dynamic pressures, Am. J. Sci., in press, 1976.

Schubert, G. and O. L. Anderson, The earth's thermal gradient, Physics Today, 27, 28-34, 1974.

Shimizu, Y., Y. Syono and S. Akimoto, High-pressure transformations in $SrGeO_3$, $SrSiO_3$, $BaGeO_3$, and $BaSiO_3$, High Temp.-High Press., 2, 113-120, 1970.

Simakov, G. V. and R. F. Trunin, On the existence of overdense perovskite structures in magnesium silicates under conditions of high pressure, Izv. Earth Phys., 9, 80-81, 1973.

Sis, L. B., G. P. Wirtz and S. C. Sorensen, Structure and properties of reduced $LaCoO_3$, J. Appl. Phys., 44, 5553-5559, 1973.

Trunin, R. F., V. I. Gon'Shakova, G. V. Simakov and N. E. Galdin, A study of rocks under the high pressures and temperatures created by shock compression, Izv. Earth Phys., 9, 1-12, 1965.

Wackerle, J., Shock-wave compression of quartz, J. Appl. Phys., 33, 922-932, 1962.

Table 1

Hugoniot Data, Soda-Lime Glass[a]

Shot No.	Flyer Plate	Projectile Velocity, km/sec	Shock Velocity, km/sec	Pressure, Mbar	Density g/cm^3
LGG9	Cu	5.76 ± 0.18[b]	8.90 ± 0.13	0.919	4.66
LGG11	Cu	5.86 ± 0.02[b]	8.91 ± 0.12	0.934	4.72
LGG14	Ta	5.541± 0.010[c]	9.094± 0.013	0.981	4.756
LGG12	Ta	5.66 ± 0.10	9.11 ± 0.02	1.005	4.85

a. Na_2O, 0.1; MgO, 0.02; SiO_2, 0.75; CaO, 0.13.
Initial Density, 2.49 ± 0.01 g/cm^3

b. 1-mm-thick sample.

c. 2-mm-thick sample.

Table 2

HUGONIOT AND RELEASE ADIABAT DATA, BAMLE BRONZITE

Shot No.	Flyer Plate	Initial Density g/cm^3	Flyer Plate Velocity km/sec	Shock Velocity, km/sec	Pressure, Mbar	Shock Density, g/cm^3	Buffer Shock Velocity, km/sec	Release Pressure Mbar	Release Density g/cm^3
LGG6	Cu	3.2923±0.0003	5.375[a]	10.08±0.13	1.126	4.963	9.14±0.11	0.803	4.950
LGG8	Cu	3.2943±0.0012	6.09±0.13	10.37±0.05	1.324	5.261	9.62±0.16	0.923	5.260
LGG14	Ta	3.3021±0.0007	5.54±0.01	10.07±0.03	1.335	5.491	8.83±0.15	0.730	5.258

a. Projectile velocity inferred from shock velocity through arrival mirrors.

Table 3

PARAMETERS FOR THEORETICAL HUGONIOT OF (Mg, Fe) SiO_3 PEROVSKITE

Composition: $(Mg_{0.9}Fe_{0.1})SiO_3$	Source
$\rho_0 = 4.20$ g/cm^3	(1)
$K_0 = \sim 2.6$ ($\pm$ .35) Mbar	(2)
$K'_0 = \sim 3.5$ ($\pm$ 1.0)	(2)
$\Delta E_{tr} < \sim 166$ KJ/mol	(1)
$\gamma = \gamma_0 (V/V_0)^n$	
$\gamma_0 \cong 1.5$ ($\pm$ 0.5)	
$n \cong 1.0$ ($\pm$ 0.5)	

(1) From data of Liu (1975a, 1975b).

(2) See Davies (1976), for example.

FIGURE CAPTIONS

Figure 1. Flash radiographs of projectile taken at stations 390 mm (upper) and 33 mm (lower) from target. Nominal exposure times are ∿15 sec. Projectile speed is 5.5 km/sec. Shot LGG14.

Figure 2. Static (a) and dynamic (b) streak camera photograph of bronzite Hugoniot and release adiabat experiment. Shot LGG14.

Figure 3. Shock velocity versus particle velocity data for soda-lime glass.

Figure 4. Shock pressure versus density for soda-lime glass.

Figure 5. Compilation of shock data of Mg-rich pyroxenes. Hugoniot points for samples of varying porosities (synthetic, polycrystalline aggregates) and pyroxene-rich (>90%) rocks are included, as are newly determined release paths (arrows). Theoretical Hugoniot (solid curve) and envelope (dashed curve) are discussed in the text and Table 3. McQueen and Marsh (unpublished) are cited in Birch (1966).

Figure 6. Compilation of shock data for Mg-rich olivines, including results on porous samples (synthetic, polycrystalline aggregates) and olivine-rich (>90%) rocks. Theoretical Hugoniot (solid curve) for a Mg-endmember and high-pressure assemblage are discussed in the text. Dashed curve corresponds to the left

FIGURE CAPTIONS - continued

side of the envelope in Figure 5. McQueen and Marsh (unpublished) are cited in Birch (1966).

Figure 7. Summary of zero-pressure densities for high-pressure phases of olivines and pyroxenes as a function of composition based on interpretation of shock-wave data (symbols), and calculated from X-ray parameters for ABO_3 (perovskite) and AO quenched from high-pressure diamond-anvil experiments (lines through points). MgO (periclase) and FeO (stoichiometric wüstite) values are from Bénard (1954), Robie et al. (1966), Katsura et al. (1967), and Robie and Waldbaum (1968) with error bars showing variations in measurement and estimate, while error bars on the remaining points are based on Liu's (1975a, 1975b) estimates of error in the X-ray parameters. The dashed line (ABO_3 + AO) corresponds to the density of a perovskite assemblage with olivine stoichiometry (assuming K_D^{Mg-Fe} ol-perov. = 1). Symbols are keyed as follows:

A Ahrens (1971)
AAR Ahrens, Anderson & Ringwood (1969a)
AG Ahrens and Gaffney (1971)
AS Al'tschuler and Sharpidzhanov (1971a)
DA Davies and Anderson (1971)
DG Davies and Gaffney (1973)
KP Kalinin and Pan'kov (1974)
MMF McQueen, Marsh & Fritz (1967)
PK Pan'kov and Kalinin (1975)

FIGURE CAPTIONS - concluded

Figure 8. Representative Hugoniot data from Figures 5 and 6 compared with the Hugoniot for MgO (McQueen and Marsh, unpublished, as cited in Birch, 1966; McQueen, 1968; Carter *et al.*, 1971).

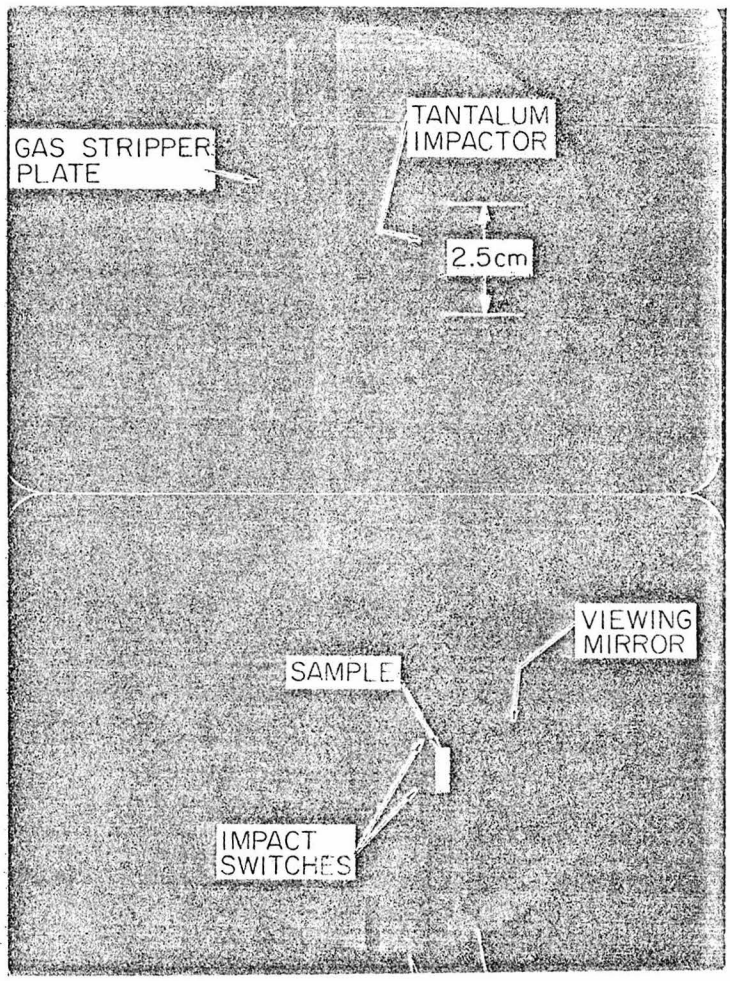
GAS STRIPPER PLATE
TANTALUM IMPACTOR
2.5cm
VIEWING MIRROR
SAMPLE
IMPACT SWITCHES

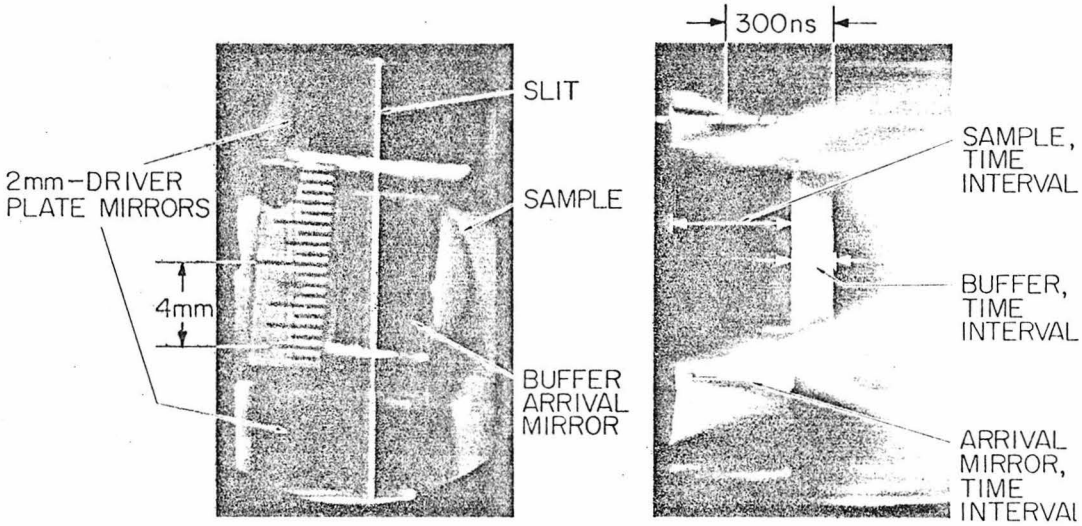
SLIT
2mm-DRIVER PLATE MIRRORS
SAMPLE
4mm
BUFFER ARRIVAL MIRROR
300ns
SAMPLE, TIME INTERVAL
BUFFER, TIME INTERVAL
ARRIVAL MIRROR, TIME INTERVAL
(a)
(b)

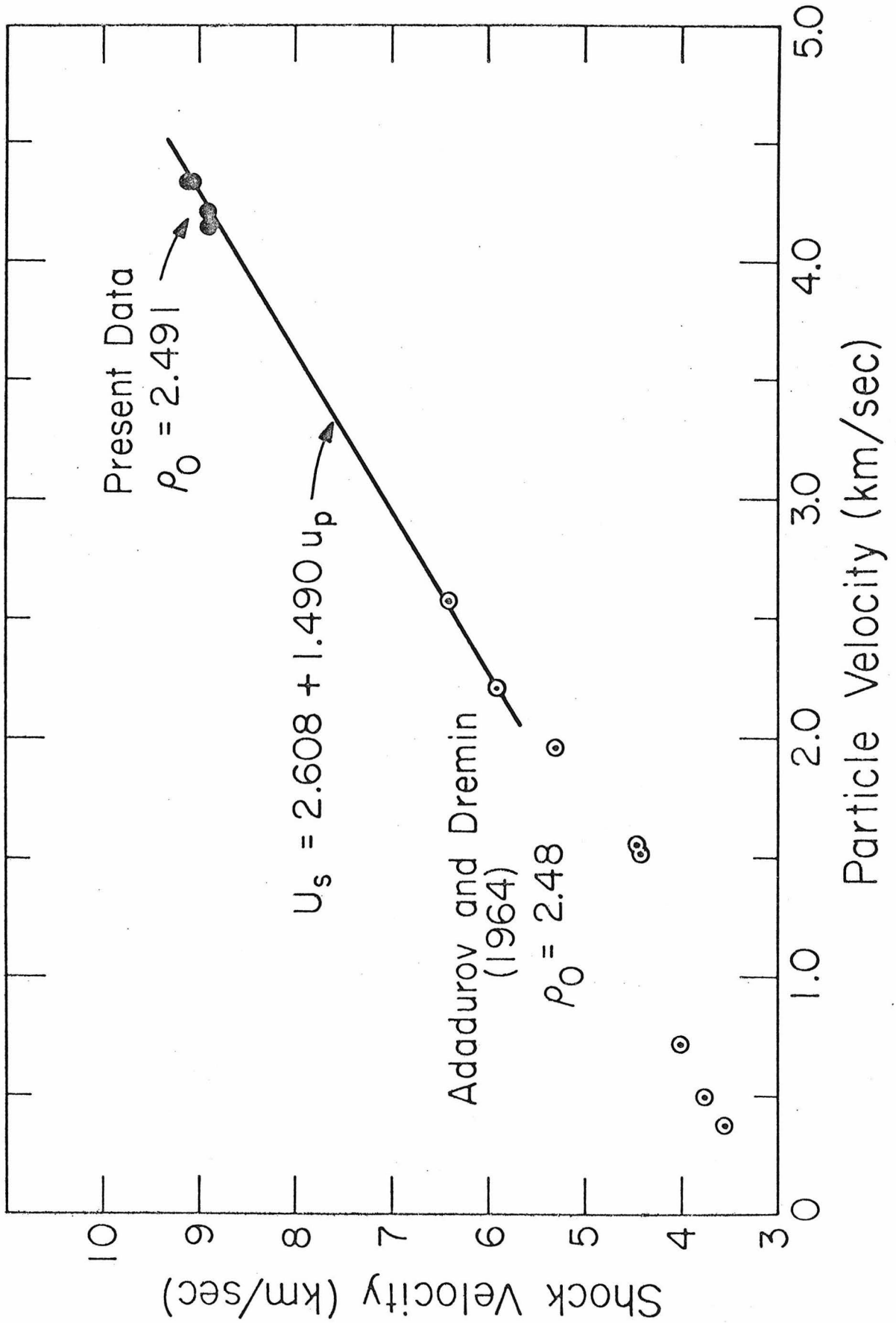
Present Data
$\rho_0 = 2.491$
$U_s = 2.608 + 1.490\, u_p$
Adadurov and Dremin
(1964)
$\rho_0 = 2.48$
Shock Velocity (km/sec)
Particle Velocity (km/sec)
3
4
5
6
7
8
9
10
0
1.0
2.0
3.0
4.0
5.0

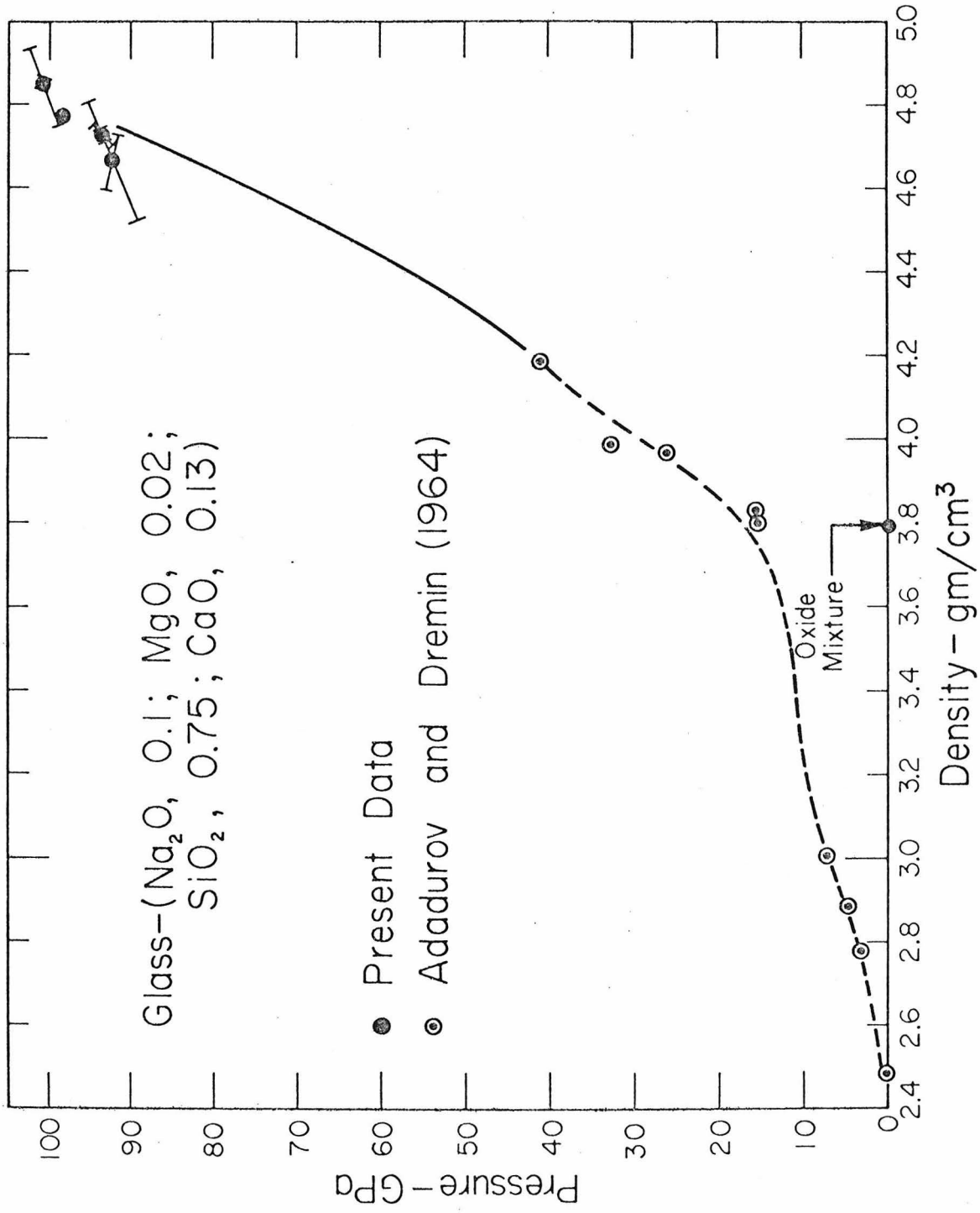
Glass–(Na_2O, 0.1; MgO, 0.02; SiO_2, 0.75; CaO, 0.13)
Present Data
Adadurov and Dremin (1964)
Oxide Mixture
Pressure – GPa
Density – gm/cm³
0
10
20
30
40
50
60
70
80
90
100
2.4
2.6
2.8
3.0
3.2
3.4
3.6
3.8
4.0
4.2
4.4
4.6
4.8
5.0

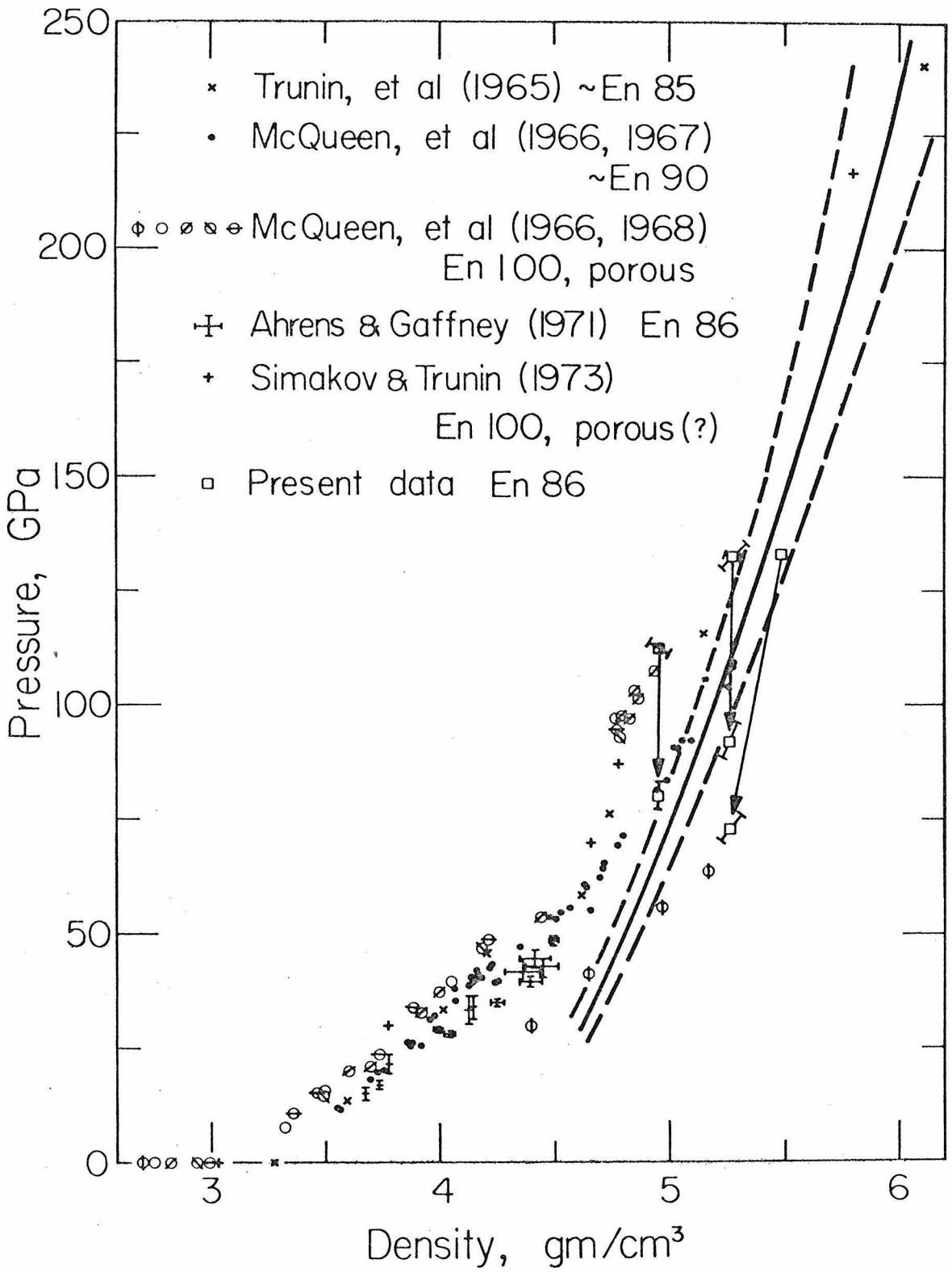
Trunin, et al (1965) ~En 85
McQueen, et al (1966, 1967) ~En 90
McQueen, et al (1966, 1968) En 100, porous
Ahrens & Gaffney (1971) En 86
Simakov & Trunin (1973) En 100, porous (?)
Present data En 86
Pressure, GPa
Density, gm/cm³
0
50
100
150
200
250
3
4
5
6

Fig. 5

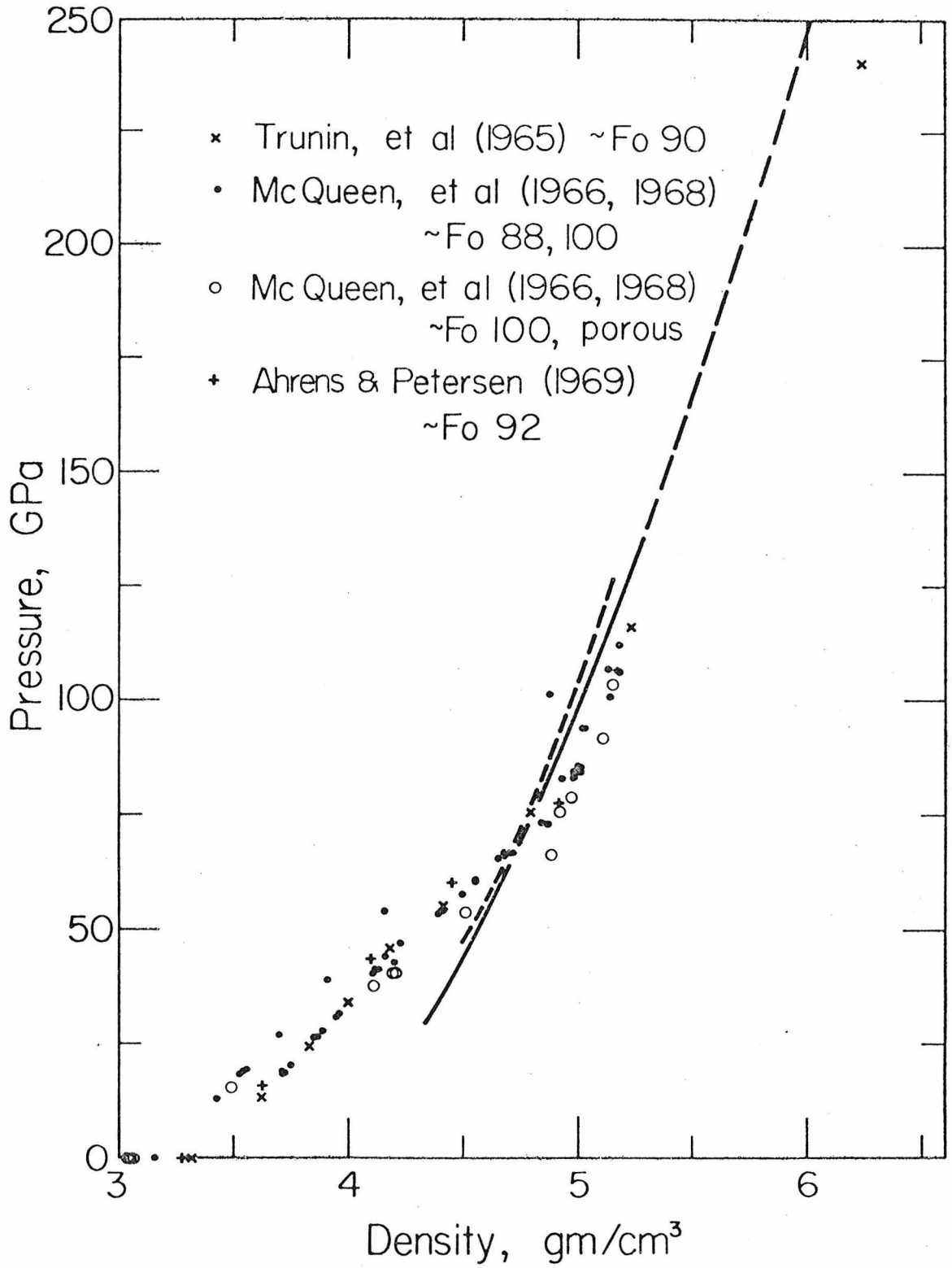
250
200
150
100
50
0
Pressure, GPa
3
4
5
6
Density, gm/cm³
× Trunin, et al (1965) ~Fo 90
• McQueen, et al (1966, 1968) ~Fo 88, 100
○ McQueen, et al (1966, 1968) ~Fo 100, porous
+ Ahrens & Petersen (1969) ~Fo 92

Fig. 6

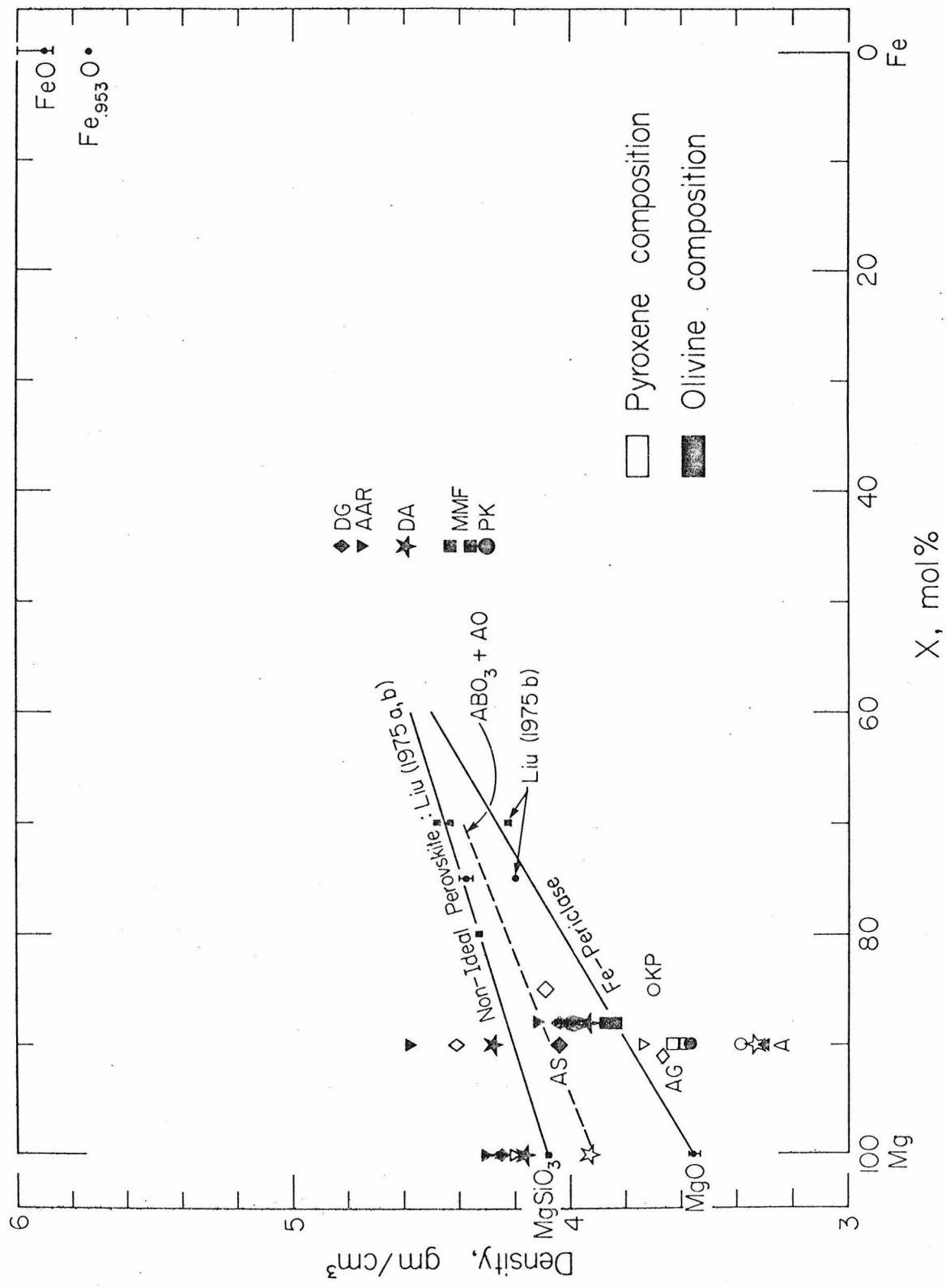
FeO
$Fe_{.953}O$
Pyroxene composition
Olivine composition
DG
AAR
DA
MMF
PK
ABO_3 + AO
Liu (1975 b)
Perovskite; Liu (1975 a,b)
Non-Ideal
Fe-Periclase
AS
AG
KP
A
$MgSiO_3$
MgO
Density, gm/cm³
X, mol%
Fe
Mg
0
20
40
60
80
100
3
4
5
6

Fig. 2

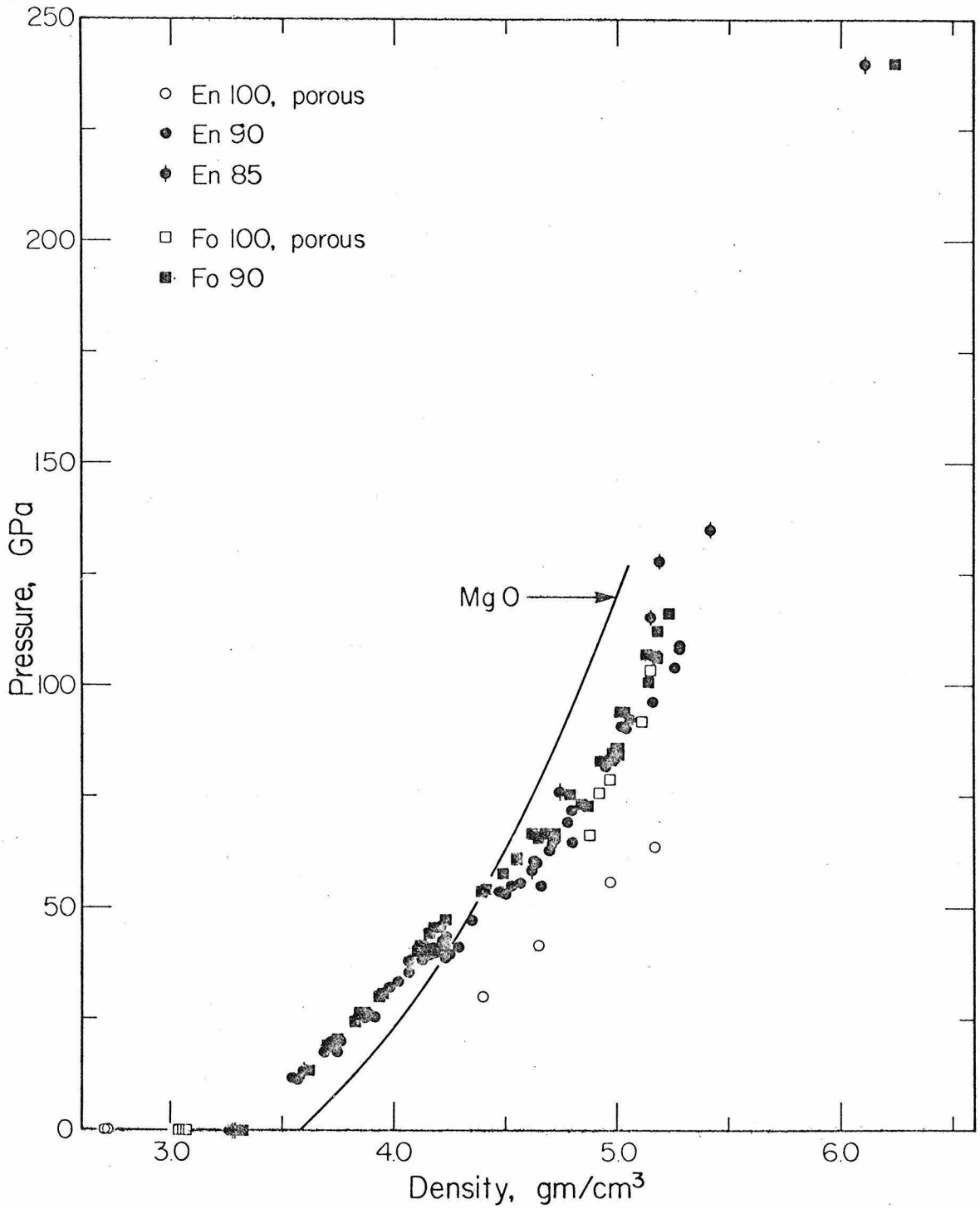
250
200
150
100
50
0
Pressure, GPa
3.0
4.0
5.0
6.0
Density, gm/cm3
En 100, porous
En 90
En 85
Fo 100, porous
Fo 90
Mg O

Fig. 8

Chapter 2

B1/B2 TRANSITION IN CaO FROM SHOCK-WAVE AND DIAMOND-CELL EXPERIMENTS

Abstract

Volume and structural data obtained by shock-wave and diamond-cell techniques demonstrate that CaO transforms from the B1 (NaCl-type) to the B2 (CsCl-type) structure at 60-70 GPa (0.6-0.7 Mbar) with a volume decrease of 11%. The agreement between the shock-wave and diamond-cell results independently confirms the ruby-fluorescence pressure scale to about 65 GPa. The shock-wave data agree closely with equations of state derived from *ab initio* calculations. The discovery of this B1/B2 transition is significant in possibly allowing considerable enrichment of calcium components in the earth's lower mantle, consistent with inhomogeneous accretion theories.

Calcium oxide, initially in the B1 (NaCl-type) structure is expected to transform to the B2 (CsCl-type) structure at high pressure by analogy with the B1/B2 transitions found in alkali halides (Pistorius, 1976; Liu, 1971; Liu and Bassett, 1972). There is considerable interest in such transitions both in theoretical studies of oxide structures (Tosi and Arai, 1966; Cohen and Gordon, 1976; Demarest, et al., 1977) and also due to their possible occurrence in the earth's lower mantle. We have carried out shock-wave, equation-of-state (Hugoniot) experiments[1] as well as X-ray diffraction, under static high pressure, through a diamond cell[2]: Both techniques demonstrate a B1/B2 transition in CaO at 60-70 GPa (0.6-0.7 Mbar). This is the first documentation of the B2 structure in an oxide of direct geophysical interest.

---

[1]Shock experiments were performed on synthetic, single crystals in [100] orientation, prepared under controlled conditions to prevent hydration. Samples were impacted by projectiles launched from either a two-stage light-gas gun or a 40 mm propellant gun. Experimental techniques are described in Jeanloz and Ahrens (1978) and further details are in Jeanloz and Ahrens (in preparation). The datum in parentheses (Figure 1) results from only a partially successful experiment and hence has a considerable uncertainty, estimated at ±1-2% in density and pressure. The open symbol represents an alternative (and less preferred) interpretation of the results of the 70 GPa shock experiment. In the preferred interpretation, a two-wave structure is inferred for the shock front with the first wave (70.2 ± 0.4 GPa) being associated with the phase transition. The alternative interpretation (open symbol) yields a transition pressure of about 63 (±3) GPa.

[2]Powdered CaO from the same sample material as used in the shock experiments was mounted in a gasketed, high-pressure diamond cell in 4:1 methanol:ethanol fluid (see Mao and Bell, 1978; Mao and Bell, 1978b; Piermarini et al., 1973). Lattice parameters and structures were determined by X-ray diffraction ($Ag_{\alpha}K_{\alpha}$ and MoK_{α} radiation) at pressures between 60 and 67 GPa (±2 GPa precision) as determined on the ruby-fluorescence scale (Barnett et al., 1973; Mao et al., 1978). The B2 structure was identified by its 100, 110, 111 and 200 X-ray lines.

Our new data are given in Table 1 and Figure 1 along with previous results for CaO (Perez-Albuerne and Drickamer, 1965; Sato et al., 1973). For comparison, theoretical Hugoniots based on finite strain theory and *ab initio* (Modified Electron Gas, see Cohen and Gordon, 1976) calculations for the B1 and B2 phases are also given[3]. The shock data provide an accurate dynamic compression curve for CaO and the X-ray data from the diamond cell confirm the nature of the structural transition. The diamond-cell experiments indicate the transition beginning at 60 (±2) GPa on the ruby-fluorescence pressure scale (Mao and Bell, 1977; Mao and Bell, 1978; Piermarini et al., 1973; Barnett et al., 1973; Mao et al., 1978) and at room temperature (295K), whereas the shock-wave data indicate a slightly higher transition pressure: about 63 to 70 GPa but at approximately

---

[3]Theoretical Hugoniots based on third order finite strain theory were constructed (e.g., Davies and Gaffney, 1973) from the ultrasonic data of Chang and Graham (1977) for the B1 phase, using the following values: ρ_0 = 3.345 Mg/m^3, K_{0s} = 112.5 GPa, K_0' = 4.79, γ_0 = 1.505 (γ/V = const.). All necessary parameters are experimentally constrained except for the volume dependence of γ, which introduces only a minor uncertainty. These parameters were estimated for the B2 phase, guided by systematics (Davies, 1976; Jamieson, 1977; Demarest et al., 1978) ρ_0 = 3.76 Mg/m^3, K_{0s} = 115 GPa, K_0' = 5, E_{tr} = 80 kJ/mol, γ_0 = 1.51 (γ/V = const.). Theoretical Hugoniots for the B1 and B2 phases based on the Modified Electron Gas theory (Cohen and Gordon, 1976) were constructed using the same thermal properties as above, and correcting the theoretical bulk moduli according to Hite and Kearney (1967), and Bartels and Vetter (1972). Shock temperatures were estimated by determining the thermal offset between adiabat and Hugoniot based on the finite strain calculations and a Debye-Grüneisen model for the specific heat (e.g., Ahrens et al., 1969).

1350K[4]. A volume decrease of 11 ± 1% is found at the transition in both sets of experiments, which is in agreement with simple systematics among the data for B1/B2 transitions among halides (Jamieson, 1977; Demarest et al., 1978) and provides additional support for applying such systematics to oxides. The consistency between the shock-wave and diamond cell results on the transition pressure in CaO provides an approximate but independent confirmation of the ruby-fluorescence scale calibration at about 65 (±5) GPa. Thus the B1/B2 transition in CaO may provide a convenient and readily reversible pressure-calibration point for ultra-high pressure static experiments.

The shock-wave data corresponding to the B1 phase are in excellent agreement (Figure 1) with the theoretical Hugoniot calculated from recent ultrasonic data for CaO (Chang and Graham, 1977) and also compare favorably with the theoretical Hugoniot based on the Modified Electron Gas theory. Hence, the equation of state of CaO in the B1 structure appears to be very well constrained both experimentally and theoretically. Although the *ab initio* results underestimate somewhat the density of the B2 phase, they predict its compressional behavior

---

[4]The apparent difference in transition pressures may be due to either thermal or kinetic effects: for example, a few GPa offset due to kinetics is found for the [100] orientation of NaCl transforming under shock (Fritz et al., 1971). Alternatively, this difference in transition pressures could be due completely to the higher temperatures achieved under shock, implying an entropy decrease on the order of 4 to 13 J/mol K at the transition (see footnote 3).

quite well. Our Hugoniot data are consistent with essentially identical zero-pressure bulk moduli (and pressure derivatives) for the B1 and B2 phases of CaO, as expected from systematics.

Similar B1/B2 transitions are also considered to be plausible in the geophysically important (Mg,Fe)O series. From simple, ionic-radius ratio concepts (Wells, 1975; Shannon and Prewitt, 1969), the B1 monoxides might be expected to transform at successively higher pressures in the following order (cation/anion radius ratios in parentheses): BaO (0.97), SrO (0.83), CaO (0.71), MgO (0.51). Barium oxide is known to transform from a B1 to a B2-related structure at about 14 GPa (Liu, 1971; Liu and Bassett, 1972), and hence SrO is expected to transform at about 45 (±10) GPa and MgO above 100-110 GPa, from the present results on CaO combined with these systematics. No B1/B2 transitions have been found in SrO to 34 GPa and MgO to 95 GPa or higher (Liu and Bassett, 1973; Mao and Bell, in press; Carter et al., 1971), and the only other oxide for which a B1/B2 transition is known is EuO (but after undergoing an electronic transition) (Jayaraman, 1972). Hence, CaO appears to be the only oxide for which an uncomplicated B1/B2 transition has been found to date. Despite the relatively simple nature of B1/B2 transitions, however, their theoretical characterization is still imperfect, particularly for the purposes of predicting their occurrence. This conclusion is illustrated by the data for CaO which disagree with the B1/B2 transition pressures expected from either *ab initio* calculations (Cohen and Gordon, 1976),

120 GPa, or from a semi-empirical, lattice-instability model which predicts a transition pressure between 28 and 40 GPa (Demarest et al., 1977).

A significant consequence of the B1/B2 transition in calcium oxide is that because of the resulting density increase a considerable amount of CaO component is allowed within the earth's lower mantle, at least below about 1550 km depth (corresponding to 65 GPa pressure). As shown in Figure 1, the Hugoniot of the B2 phase of CaO is within 1-2% of the seismologically determined pressure-density relation for the lower mantle (Dziewonski et al., 1975; Anderson and Hart, 1976). The reduction of this Hugoniot to estimated mantle temperatures results in only a small correction which, if anything, improves the comparison[5]. Although calcium might well occur in a complex oxide or silicate mineral, simple oxide-mixing models have proved rather successful in modeling the properties of the mantle and candidate minerals at high pressure (Birch, 1952; McQueen et al., 1967; Al'tshuler and Sharipdzhanov, 1971; Anderson et al., 1971; Liu and Ringwood, 1975). Hence from purely geophysical considerations, a significant enrichment of refractory, calcium-bearing phases is allowed within the earth's deep interior. Such enrichment might, for example, be consistent with inhomogeneous accretion theories of the terrestrial planets and would imply that the mantle is not chemically homogeneous throughout (Turekian and Clark, 1969; Grossman and

---

[5]For example, at 110 GPa the temperature on the Hugoniot, about 2850 K (footnote 3), is identical to estimated mantle temperatures (e.g., Stacey, 1977).

Larimer, 1974; Ringwood, 1975).

Acknowledgement

We are very grateful to Professor R. A. Bartels (Trinity University, San Antonio, Texas), and to Drs. M. M. Abraham and Y. Chen (Oak Ridge National Laboratory) for generously providing sample material. We thank Professors R. G. Gordon and J.C. Jamieson for helpful comments and discussions.

REFERENCES

Ahrens, T. J., C. F. Petersen and J. T.Rosenberg, J. Geophys. Res., 74, 2727, 1969.

Al'tshuler, L. V. and I. I. Sharipdzhanov, Izv. Acad. Sci. USSR Earth Phys., No. 3, 167, 1971.

Anderson, D. L. and R. S. Hart, J. Geophys. Res., 81, 1976.

Anderson, D. L., C. Sammis and T. Jordan, Science, 171, 1103, 1971.

Barnett, J. D., S. Block and G. J. Piermarini, Rev. Sci. Instr., 44, 1, 1973.

Bartels, R. A. and V. H. Vetter, J. Phys. Chem. Solids, 33, 1991, 1972.

Birch, F., J. Geophys. Res., 57, 227, 1952.

Carter, W. J., S. P. Marsh, J. N. Fritz and R. G. McQueen, in Accurate Characterization of the High-Pressure Environment, E. C. Loyd (ed.) Nat. Bur. Stand. (U.S.) Spec. Publ. 326, 146, 1971.

Chang, Z. P. and E. K. Graham, J. Phys. Chem. Solids, 38, 1355, 1977.

Cohen, A. J. and R. G. Gordon, Phys. Rev., B14, 4593, 1976.

Davies, G. F., Geophys. J. R. astr. Soc., 44, 625, 1976.

Davies, G. F. and E. S. Gaffney, Geophys. J. R. astr. Soc., 33, 165, 1973.

Demarest, H. H., Jr., C. R. Cassell and J. C. Jamieson, J. Phys. Chem. Solids, 39, 1211, 1978.

Demarest, H., R. Ota and O. L. Anderson, in High Pressure Research, M. Manghnani and S. Akimoto (eds.), Academic Press, New York, 281, 1977.

Dziewonski, A. M., A. L. Hales and E. R. Lapwood, Phys. Earth Planet. Int., 10, 12, 1975.

Fritz, J. N., S. P. Marsh, W. J. Carter and R. G. McQueen, in Accurate Characterization of the High Pressure Environment, E. C. Lloyd, (ed.), Nat. Bur. Stand. (U.S.) Spec. Pub. 326, 201, 1971.

Grossman, L. and J. W. Larimer, Rev. Geophys. Space Phys., 12, 71, 1974.

Hite, H. E. and R. J. Kearney, J. App. Phys., 38, 5424, 1967.

Jamieson, J. C., in High Pressure Research, M. Manghnani and S. Akimoto, (eds.), Academic Press, New York, 209, 1977.

Jayaraman, A., Phys. Rev. Lett., 29, 1674, 1972.

Jeanloz, R. and T. J. Ahrens, Proc. Lunar Planet. Sci. Conf., 9th, 2789, 1978.

Liu, L., J. Appl. Phys., 42, 3702, 1971.

Liu, L. and W. A. Bassett, J. Geophys. Res., 77, 4934, 1972.

Liu, L. and W. A. Bassett, J. Geophys. Res., 78, 8470, 1973.

Liu, L. and A. E. Ringwood, Earth Planet. Sci. Lett., 28, 209, 1975.

Mao, H. K. and P. M. Bell, Carnegie Inst. Washington Ybook., 76, 644, 1977.

Mao, H. K. and P. M. Bell, Carnegie Inst. Washington Ybook., 77, 904, 1978.

Mao, H. K. and P. M. Bell, J. Geophys. Res., in press.

Mao, H. K., P. M. Bell, J. W. Shaner and D. J. Steinberg, J. Appl. Phys., 49, 3276, 1978.

McQueen, R. G., S. P. Marsh and J. N. Fritz, J. Geophys. Res., 72, 4999, 1967.

Perez-Albuerne, E. A. and H. G. Drickamer, J. Chem. Phys., 43, 1381, 1965.

Piermarini, G. J., S. Block and J. D. Barnett, J. Appl. Phys., 44, 5377, 1973.

Pistorious, C. W. F. T., Progr. Solid State Chem., 11, 1, 1976.

Ringwood, A. E., Composition and Petrology of the Earth's Mantle, McGraw-Hill Book Co., New York, 618 pp., 1975.

Sato, Y., Y. Ida and S. Akimoto, High Temp.-High Press., 5, 679, 1973.

Shannon, R. D. and C. T. Prewitt, Acta Cryst., B25, 925, 1969.

Stacey, F. D., Phys. Earth Planet. Int., 15, 341, 1977.

Tosi, M. and T. Arai, Adv. High Pressure Research, 1, 265, 1966.

Turekian, K. K., and S. P. Clark, Jr., Earth Planet. Sci. Lett., 6, 346, 1969.

Wells, A. F., Structural Inorganic Chemistry, Fourth Ed., Oxford Univ. Press, Oxford, 1095 pp., 1975.

TABLE 1

CaO: Diamond Cell Results

Run No.	Pressure[1] (GPa)	Molar Volume (cm^3)[2] B1 Phase	B2 Phase	Relative Intensity[2] I(B1)/I(B2)
14Y1	60.6	12.44	11.10	1.7
14Y2	61.2	12.36	11.06	0.7
14Y3	63.4	12.26	10.90	0.5
14Y4	63.7	12.28	10.87	0.5
14Y5	66.8	12.18	10.91	0.2

Notes:

(1) Precision of ±2 GPa; absolute accuracy of calibration is within 6% (footnote 2).

(2) Based on 200 and 110 X-ray lines for B1 and B2 patterns, respectively; estimated precision of molar volume is about ±0.7%. Relative intensities of X-ray lines based on visual estimates.

FIGURE CAPTION

Figure 1. New shock-wave data for CaO compared with previous, static compression data and theoretical Hugoniots based on finite-strain (P_{3H}) and *ab initio* (MEG) calculations (see text). Also shown are two seismological models for the lower mantle (Dziewonski et al., 1975; Anderson and Hart, 1976). Error bars for the shock-wave data are approximately of the size of the symbols (or smaller), except for the datum in parentheses which is considerably less certain. The open symbol represents an alternative interpretation of the 70 GPa result.

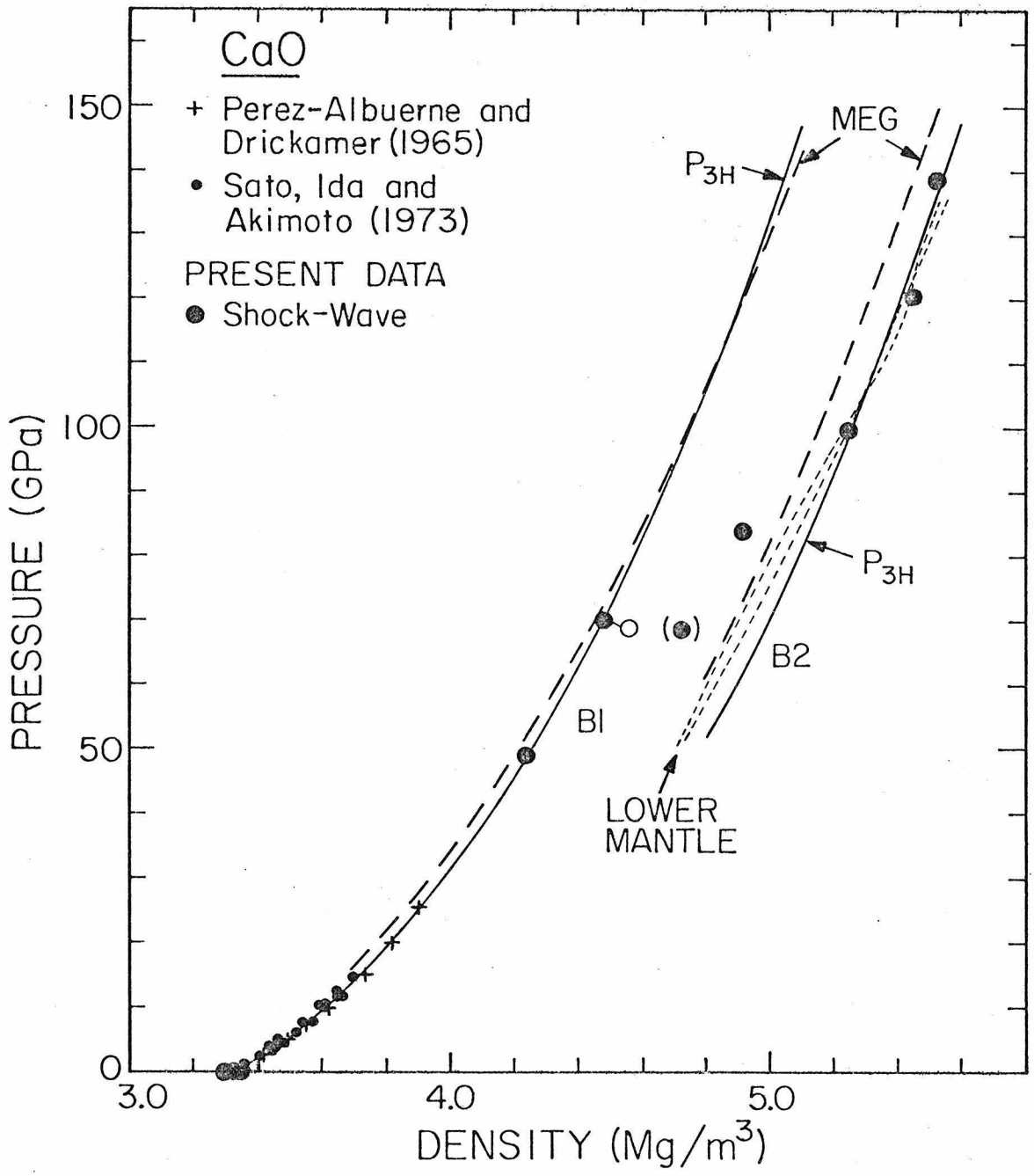
CaO
+ Perez-Albuerne and Drickamer (1965)
• Sato, Ida and Akimoto (1973)
PRESENT DATA
● Shock-Wave
MEG
P3H
P3H
(●)
B2
B1
LOWER MANTLE
PRESSURE (GPa)
DENSITY (Mg/m3)
150
100
50
0
3.0
4.0
5.0

Chapter 3

FeO and CaO: HUGONIOT EQUATIONS OF STATE OF TWO OXIDES

Abstract

New shock-wave (Hugoniot) and release-adiabat data for $Fe_{0.94}O$ and CaO, to 230 and 175 GPa (2.3 and 1.75 Mbar) respectively, show that both oxides transform from their initial B1 (NaCl-type) structures at about 70 (±10) GPa. CaO transforms to the B2 (CsCl-type) structure and FeO is inferred to do the same. Alternatively, FeO may undergo an electronic transition, but it does not disproportionate under shock to Fe and Fe_2O_3 or Fe_3O_4. The Hugoniot data for the B1 phases of FeO and CaO agree with the ultrasonically-determined bulk moduli (K_0 = 185, 112GPa, respectively), and the pressure derivative for CaO (K_0' = 4.8); $K_0' \sim 3.2$ for FeO is determined from the present data. The Hugoniot data are consistent with low- and high-pressure phases of FeO and CaO having nearly identical K_0 and K_0'. Volume changes for B1/B2 transitions in oxides agree with theoretical expectations and with trends among the halides: $-\frac{\Delta V}{V_1} \sim 4\%$ and 11% for FeO and CaO respectively. Also, the transition pressures increase with decreasing cation/anion radius ratio for the oxides. The Hugoniot data show that the density of the outer core is equal to that of a 50-50 mix (by weight) of Fe and FeO (∿11 wt. % oxygen), consistent with geochemical arguments for the presence of oxygen in the core. In terms of a mixture of simple oxides, the density of the lower mantle is satisfied by $\frac{Fe}{Mg+Fe} \sim 0.12$, however arbitrarily large amounts of CaO can be present; an enrichment of refractory components in the lower mantle is allowed by the shock-wave data. Because of the relatively low transition pressure in FeO, a B1/B2 transition in (Mg, Fe)O is likely to

occur in the lower mantle even if MgO transforms at 150-170 GPa. Such a transition may contribute to the scattering of seismic waves and change in velocity gradient found near the base of the mantle.

INTRODUCTION

FeO and CaO are the only major-element oxides which have not previously been studied at the high pressures existing in the earth's mantle and core. We report the first Hugoniot (shock-wave), equation-of-state measurements for these oxides to pressure of 150 GPa (1.5 Mbar) and above. We believe that our results have special application to interpreting the state of the lower mantle and, in the case of FeO, that of the core.

The most important result of this work is the discovery of phase transitions in both oxides at about 70 GPa, which allow for the presence of considerably more CaO and FeO in the lower mantle and core, respectively, than has previously been thought. Similar transitions may occur in (Mg,Fe)O, which is thought to be prevalent throughout the lower mantle.

Although the phase assemblages which occur in the earth's deep interior are unknown, it has long been recognized that the close-packed oxides have properties similar to those of the mantle [Birch, 1952; Al'tshuler and Sharipdzhanov, 1971]. Hence, the simple oxides provide a model, high-pressure assemblage which is a convenient standard against which to reference other candidate phase assemblages. The present shock-wave data show that a wide range of oxide compositions can satisfy the properties of the lower mantle consistent, for example, with inhomogeneous accretion theories [Turekian and Clark, 1969; Clark, et al., 1972]. Some of the data for CaO which are presented below have been discussed by Jeanloz, et al., [1979] who compare these with independent measurements made with the diamond-cell. They also compare the new data with the results of quantum mechanical calculations

[Cohen and Gordon, 1976], and find remarkable agreement between many of the predicted and observed properties of CaO at high pressures. In the following sections a description of the samples, an analysis of the shock-wave data, and their application to the mantle and core are discussed.

SAMPLES AND PREPARATION

The iron oxide samples studied here are hot-pressed polycrystals from the same batch as studied by Graham and Bonczar [1978]. Petrographic, and microprobe analyses reveal the presence of 2.0% (vol.) Fe, whereas a lattice parameter of 430.8 (±0.4)pm was determined by X-ray diffraction. This indicates a stoichiometric coefficient $x = 0.94$ (in Fe_xO) according to Hentschel [1970], and hence a crystal density of 5.731 (±0.004) Mg/m^3. A recent EXAFS study [Chen, et al., 1978] demonstrates that no interstitial defects occur for $x \gtrsim 0.90$, indicating that the present samples correspond structurally to stoichiometric wüstite [cf. Roth, 1960; Kofstad, 1972].

Archimedean densities were measured using reagent-grade Toluene and the correction factors of Berman [1939], but bulk densities were determined by directly measuring the volume of each sample (cf. Table 1). The porosity of the samples, derived from the bulk and crystal densities, is about 4% and the near equivalence of bulk and Archimedean densities indicates that most of this porosity is not interconnected.

The CaO samples used in this study were all cut in {100} orientation (shock-wave propagation direction) from synthetic single crystals. These were grown by arc-fusion techniques and were acquired from two sources: (1) Oak Ridge National Laboratory (ORNL), samples grown and described

by Abraham, et al. [1971]; (2) CaO from the same batch (MRC) as used in the study of Son and Bartels [1972]. X-ray diffraction and electron microprobe analyses produced no evidence of impurities. Because CaO is hygroscopic it was immersed in mineral oil for storage and cutting. Final sample preparation was carried out in a glove box under a controlled atmosphere and no evidence was found for even partial or surficial hydration of the samples used in this study.

The MRC samples are of variable color ranging from clear to light brown (darker portions of the crystals were avoided), whereas the ORNL samples are uniformly clear; presumably the color is due to carbon impurities [Freund, et al., 1977, 1978]. Archimedean densities of virtually all of the CaO samples were found to be slightly less than the X-ray value ρ_o = 3.345 Mg/m^3 (Table 2). Infrared absorption spectra revealed a strong OH peak at 3645 cm^{-1} in several 1 to 2 mm thick chips from the ORNL crystals, indicating the presence of $Ca(OH)_2$ (portlandite) within these samples [eg, Nakamoto, 1970]. Care was taken to prevent surface contamination or hydration, and the low values of density can be accounted for by the presence of up to 2.9 wt% portlandite within the CaO crystals. Briggs [1977] has similarly documented evidence for a brucite ($Mg(OH)_2$) precipitate within MgO grown by identical techniques as used for the CaO crystals.

SHOCK EXPERIMENTS AND DATA ANALYSIS

Driver plates made of 2024 aluminum alloy, tantalum or tungsten were used, with fused quartz or Lexan arrival mirrors mounted on the back and on each side of the sample [eg, Ahrens et al., 1977]. The

driver plates are impacted by projectiles which are accelerated either by a two-stage light-gas gun or by a 40 mm propellant gun. The primary measurements consist of timing the projectile velocity and measuring the shock-wave travel time through the sample and mirrors (of known thickness) by way of a streak image such as is shown in Figure 1, and schematically in Figure 2. Timing calibration marks are included directly on the streak image. Further experimental details are given in Jeanloz and Ahrens [1977, 1978], Ahrens, et al. [1977], and Jackson and Ahrens [1979].

Impact velocities are measured with typical accuracies of about 0.1%. The largest uncertainties in these experiments arise from reading the streak records which are interpreted from both a direct visual reading and also by means microdensitometer scans [Jeanloz and Ahrens, 1978; Jackson and Ahrens, 1979]. Between 25 and 50 scans are made across each streak record in a direction parallel to the time axis, and each of the boundaries corresponding to the shock wave entering or exiting the sample or mirrors is picked at the midpoint of the maximum gradient in light intensity (Figure 1). Time resolution is strictly limited by the graininess of the film at about 0.5-1.0 ns, however the actual boundary locations are only determined to about 1.5 ns, or more, due to the fuzziness of the boundaries. This reflects, in part, the finite rise-time of the shock front.

A common difficulty arises from non-normal impacts as illustrated in Figures 1 and 2. The tilt of the projectile can reach up to 3-5° at impact, however the particle velocity vector is still oriented normal to the driver plate and the boundaries on the streak record need only be fit by parallel lines which are not normal to the time axis. Ignoring

for the moment projectile bowing (discussed below), the best fit to the boundaries corresponding to the shock entering the arrival mirrors (simultaneously, entering the samples), the buffer mirror (exiting the sample) and the buffer arrival mirror (exiting the buffer mirror) is given by the least-squares solution to a set of straight, parallel lines [eg, Draper and Smith, 1966]. A weighting matrix can be determined by the sharpness of each boundary crossing, however this is usually unnecessary. For convenience, the time axis is centered at the midpoint of the slit image. The least-squares analysis gives a direct estimate of the standard error of the intercept for each boundary, which is then used to evaluate the error in the determination of the shock-wave velocity.

A more difficult problem arises from bowing of the projectile, as schematically shown in Figure 2. This commonly occurs at velocities above about 5.7 km/s (for Ta flyer plates) and produces a curved boundary on the streak record where the shock enters the sample. Corrections due to projectile bowing are large, up to about 15 ns (3-5% of the travel time), although they only correspond to a 50-100 μm maximum flexure of the flyer plate. In reducing the data, a quadratic least-squares fit to the first boundary is found by an iterative scheme such that the slope at the centroid (intercept with the time axis) is parallel to the simultaneous least-squares fit to the remaining boundaries, which are taken to be parallel and straight. As is illustrated in Figure 2, the straight line approximation is not good for the first boundary when the projectile is bowed, although it is a good approximation for the remaining boundaries (only one is shown) because these are relatively short and involve little

extrapolation. The shortest travel time through the sample, which determines the shock-wave velocity, is given by the time interval measured along the centered time axis. Independent experiments in which the bowing is directly observed suggest that a quadratic fit and extrapolation of the first boundary, as used here, is adequate.

An important source of error results from nonuniform writing rate of the image-converter streak camera used for experiments with the light-gas gun (Figure 1). Although timing calibrations are performed for each experiment, the nonuniformity in writing rate can at times be determined only to 10 or 20%. In reducing the data, a time-dependent writing rate is used which corresponds to the portion of the record being read.

Combining the errors just enumerated, the shock-wave velocity is usually determined to about 1% (cf. Tables 1 and 2). A standard error analysis is used [e.g., Mood et al., 1974, p. 181], with most of the terms in the matrix of partial derivatives employed for the error propagation being given in Jackson and Ahrens [1979]; additional terms have been included for uncertainties in initial density. The remaining data reduction employs the usual impedance matching conditions to determine Hugoniot states [e.g., Walsh and Christian, 1955]; the Riemann-integral equation is applied for release-path determinations [see Rice, et al., 1958; Lyzenga and Ahrens, 1977; Jeanloz and Ahrens, 1977, 1978]. The standard equations of state of McQueen et al. [1970] for 2024 aluminum alloy, tantalum and tungsten, from Wackerle [1962] and Jackson and Ahrens [1979] for fused quartz, and from Carter and Marsh [1979] for Lexan were used in this study.

Results

The new shock-wave data for $Fe_{0.94}O$ and CaO are shown in Figures 3 and 4, and listed in Tables 1 and 2; both Hugoniot states and release adiabats are presented. For both compounds, there is clear evidence for a shock-induced phase transformation at approximately 70 GPa from the initial, B1 (NaCl-type) structure.

The properties of the B1 phases of both FeO and CaO have been studied extensively, in part because of the geophysical interest in these compounds [e.g., Mao et al., 1969; Akimoto, 1972; Jackson, et al., 1978; Graham and Bonczar, 1978; Son and Bartels, 1972; Sato, et al., 1973; Chang and Graham, 1977]. The present data are in good agreement with the results of most of these studies. For example, a least-squares fit (third order, Eulerian finite strain: see Jeanloz and Ahrens [1979a] for details) to the CaO Hugoniot data determine the zero-pressure bulk modulus and its pressure derivative, K_{0S} = 111 ± 3 GPa and K'_{0S} = 4.7 ± 0.2, in excellent agreement with the ultrasonically determined values of Chang and Graham [1977]: 112.5 GPa and 4.8, respectively [cf. Jeanloz, et al., 1979]. These values are compatible with the results of previous static-compression [Perez-Albuerne and Drickamer, 1965; Sato, et al., 1973] and ultrasonic [Son and Bartels, 1972] studies, however the more recent work of Dragoo and Spain [1977] yields values that are significantly different. The best estimates of the properties of the B1 phases of FeO and CaO are listed in Table 3, which also provides the values of the Grüneisen parameters used in the present analysis.

In the case of Fe_xO, the present data are in excellent agreement with the value K_{0S} = 185 ± 5GPa measured ultrasonically by Jackson et al., [1978] and Graham and Bonczar [1978]. This is illustrated in Figure 5, in which the Hugoniot shown is based on the ultrasonic value of the bulk modulus, but with K_0' unconstrained. With the K_{0S} thus constrained, the data require K_0' = 3.2 ± 0.3, whereas an unconstrained fit to the three shock-wave data results in K_{0S} = 190 ± 5 (GPa), K_0' = 3.0 ± 0.3 (Table 3). The isotherm corresponding to the Hugoniot is also shown in Figure 5, and it is evident that the earlier static-compression data [Clendenen and Drickamer, 1966; Mao, et al., 1969] are not in agreement with the ultrasonic and Hugoniot measurements. The initial density (ρ_0) of FeO is not well determined (Table 3) because of the effect of nonstoichiometry on the lattice parameter of wüstite [e.g., Bénard, 1954; Katsura, et al., 1967; Hentschel, 1970; Hayakawa, et al., 1972].

Because many compounds with a B1 structure transform to the B2 (CsCl-type) structure at high pressures [e.g., Pistorius, 1976], the transitions exhibited by FeO and CaO (Figures 3 and 4) might be expected to be of this type. Sluggish kinetics are not likely to seriously affect the shock data for a displacive transition, such as a B1/B2 type [Johnson and Mitchell, 1972]. Although {100}-oriented crystals, such as used here for CaO, may transform at slightly higher pressure than {111} crystals due to kinetics, this is likely to be a relatively small effect [see Fritz, et al., 1974; Duvall and Graham, 1977]. From in-situ X-ray diffraction at high pressures, the transition in CaO is known to be of B1/B2 type and it begins under shock within 10 GPa of the static transition pressure [Jeanloz, et al., 1979]. The present data can not

conclusively determine the nature of the FeO transition, however for both CaO and FeO the transition begins between about 70 and 80 GPa under shock. Although the record for experiment LGG 060 on CaO can not be unambiguously interpreted, the preferred interpretation is that it documents a two-wave structure with the first (70 GPa) wave being associated with the B1/B2 transition. The alternative interpretation of that record is also given in Figure 3 and Table 2, and would imply a transition pressure between 60 and 70 GPa for CaO. Similarly, experiment LGG 034 (datum in parentheses, Figure 4) was only partially successful and its interpretation is uncertain.

Systematic relations suggest that B1 and B2 phases should have similar values of K_{0S} and K_0' [e.g., Davies, 1976], and this is consistent with the present data for CaO and FeO. The properties of the high-pressure phases of these oxides can be derived from the Hugoniot data of Figures 3 and 4, the results being listed in Table 3. The same approach has been used as discussed above: a third order finite-strain equation of state is found by a least-squares fit [Jeanloz and Ahrens, 1979a]. High values of γ_0 have been assumed for the high-pressure phases based on the work of Ramakrishnan, et al. [1979; see also Jeanloz, 1979; Jeanloz and Ahrens, 1979a] who show that γ increases significantly on transforming from B1 to B2 phases. The transformation energies ($E_{tr} \sim P_{tr} \Delta V_{tr}$) have been determined by extrapolation of the high-pressure phase Hugoniots to the approximate transition pressures, using the least squares-fit shock velocity (U_S) vs. particle velocity (u_p) relations given in Table 3. The CaO data from shots LGG 024 and 033 are considered separately, below.

Because the B2 structure is a likely candidate for the high-pressure phase of FeO, theoretical Hugoniots were constructed based on the predicted properties of this structure [e.g., Jeanloz and Ahrens 1977; Jeanloz, et al., 1979]. The envelope of the family of Hugoniots thus calculated from third order finite-strain theory and for a plausible range of parameters is shown in Figure 3. The high-pressure data fall within this envelope, consistent with the predicted occurrence of the B2 phase, however they exhibit a curvature which is not seen in the calculated Hugoniots. Since the four highest pressure Hugoniot points define a straight U_S-u_P trend, it is not likely that a further transition occurs in the 100 to 230 GPa pressure range. This suggests that a higher than third-order finite strain expansion is required, and the solid curve shows one possible fourth-order solution (ρ_o = 6.2 Mg/m^3, K_{0S} = 192 GPa, K_0' = 3.55, ξ_2 = 1.5, γ_o = 2, n = 1, E_{tr} = 31 kJ/mol), which corresponds to a (constrained) least-squares fit to the data. The datum at 152 GPa is not discrepant because it derives from a sample with a slightly lower initial porosity than the other samples: correcting for this effect shifts the point to the solid curve. This solution is consistent with the parameters listed in Table 3 and is used for the subsequent analysis of the high-pressure data of FeO. Whether these data correspond to the B2 structure or not does not strongly affect this analysis.

Once the properties of the high-pressure phases have been determined by a fit to the Hugoniot data, temperatures along the Hugoniot can be directly calculated [cf. Jeanloz and Ahrens, 1979a, and references therein].

The results for CaO and FeO are given in Figure 6, along with recent estimates of the geotherm in the lower mantle and core, for comparison. A Debye-Grüneisen model is used for calculating the specific heat, and anharmonic contributions of higher order are neglected. CaO is in the high-temperature regime above about 80 GPa and 1000 K on the Hugoniot, whereas FeO enters the high-temperature range at 300-400 K and low pressure. The main reason for the steeper rise in temperature along the Hugoniot of CaO as compared with that of FeO is due to the significantly higher density of the latter. Nevertheless, for both compounds a direct comparison of the Hugoniot with the measured properties of the earth can be made approximately within the pressure range of 100 to 140 GPa.

For CaO and FeO, the agreement between the expected properties of the B2 phase and the observed properties of the shock-produced, high-pressure phase is rather good. Both from considerations of a simple ionic model for B1/B2 transitions [e.g., Pauling, 1960; Wells, 1975] and from experimental data [e.g., Demarest, et al., 1978], the volume change at the transition is expected to be determined by the ratio of ionic radii of the compound in question. As is illustrated in Figure 7, such systematics are remarkably good for both halides and oxides (BaO involves complications due to the occurrence of distorted structures: Liu [1971]; Liu and Bassett [1972]). Similarly, the transition pressure from B1 to B2 structures is expected to increase with decreasing cation/anion radii, at least qualitatively. Figure 8 shows this to be the case for the data currently available for oxides. Both SrO and MgO are known not to transform to the B2 phase to pressures of 34 and 95 (to 120) GPa,

respectively [Liu and Bassett, 1973; Mao and Bell, 1979; Carter, et al., 1971], hence only lower bounds can be given for the transition pressures of these compounds. The only other oxide for which a B1/B2 transition is known, EuO at 40 GPa, can not be directly compared in this respect since it is known to undergo a valence transition at about 30 GPa [Jayaraman, 1972; Jayaraman, et al., 1974]. It is interesting to note that EuO does fit on the trend of Figure 8 if the ionic radii for valence 2 are nevertheless used.

The high-pressure data for FeO can not be discussed further without considering what phase they may reflect. Several alternatives are listed in Table 4, and these can be distinguished as either structural or electronic transitions; a combination may also obtain. The occurrence of a distorted structure or of an unknown structure-type can not be ruled out, but these would likely have densities similar to or less than that of the B2 phase (as in BaO); FeO would be expected to further transform to a B2 structure. Disproportionation reactions of the type discussed by Mao [1974] and Mao and Bell [1977] do not satisfy the present data, however. As is shown in Figure 9, combinations of Fe_2O_3 or Fe_3O_4 and Fe result in densities significantly less than those of FeO at high pressures, based on the shock-wave data of McQueen and Marsh [quoted in Birch, 1966] and McQueen et al., [1970]. Such assemblages would result in densities virtually identical to those of the B1 (low pressure) phase of FeO.

Pressure-induced electronic transitions must be considered more speculative candidates for explaining the phase transformation in FeO

since few such transitions are known among oxides. Also, there are difficulties in understanding the electronic structure of FeO [e.g., Adler, 1968, 1975; Falicov and Koiller, 1975], and only crude predictions can be made, as is illustrated by the example of a spin-pairing transition. According to most estimates [Fyfe, 1960; Burns, 1970; Gaffney and Anderson, 1973; Strens, 1976; Ohnishi, 1978] such a transition would involve a large volume change (about 20%) occurring between 25 and 55 GPa, and involving a significant increase in bulk modulus [Ohnishi and Mizutani, 1978]. This is inconsistent with the present data, and a spin transition could be ruled out except that Tossell [1976] has argued that it might involve only a 5% volume decrease in FeO based on the work of Clack and Smith [1974] on fluorine analogs. This, along with Tossell's predicted transition pressure of 60-70 GPa, is consistent with the present data.

The possibility of a valence transition in FeO can similarly not be ruled out, although it would require the gap between 3d and 4s bands to decrease by about 2.4 eV (or more) as a compression $\frac{V}{V_0} \sim 0.77$ is achieved [cf. Bowen, et al., 1975]. This would require a significantly ($\sim$50%) larger decrease in the band-gap upon compression than is found in EuO [Jayaraman, et al., 1974], which only has a 1.1 eV gap at zero pressure. The density change at such a transition could be large but need not be, as is the case for EuO [$\sim$4%: Jayaraman, 1977]. However, the zero-pressure density of metallic FeO of 7.34 Mg/m^3 as calculated by Ringwood [1978] would, if correct, completely rule out metallization as the cause of the FeO transition observed in this study. Ross [1972]

has argued for the validity of the Herzfeld theory of metallization which would predict an electronic collapse in FeO only at a density greater than 10.1 Mg/m^3, corresponding to a pressure well above 200-250 GPa. This also suggests that the present transition in FeO is not due to metallization, although it is worth noting that the density required for the electronic collapse in EuO is itself overestimated by the Herzfeld theory. Therefore, the possibility of either a spin-pairing transition or a valence transition in FeO can not be critically tested.

On the other hand, there is close agreement between the observed transition in FeO and the behavior predicted for a B1/B2 transition, as shown by Figures 3, 7 and 8. Hence, the preferred interpretation is that FeO, like CaO, undergoes a B1/B2 transition, although the possibility of an electronic transition cannot be ruled out. The correlation in Figure 8 is unexpectedly good, particularly since the relatively low ratio of shear to bulk moduli in FeO suggest that the B1 structure is somewhat less stable in this than in the other oxides [Jackson, et al., 1978]; the slight deviation of FeO from the trend is therefore not surprising. Although crystal-field stabilization has been invoked to explain the high-pressure phase equilibria among iron-bearing minerals [e.g., Syono et al., 1971; Burns, 1976; Yagi, et al., 1978], such an effect would tend to increase the relative stability of FeO in the B1 structure, contrary to what is shown in Figure 8.

The release adiabats determined for FeO and CaO in both their low and high-pressure phases (Figures 3 and 4) are of interest in that they are generally internally consistent, with slopes less than the

slope of the Hugoniot. This is not the case for many silicates which typically exhibit anomalous (steep) release paths from their Hugoniot states, suggesting the presence of a mixed-phase region or of non-equilibrium effects [Ahrens, et al., 1969b; Grady, et al., 1974, 1975; Jeanloz and Ahrens, 1977, 1978]. Entropy production due to viscous dissipation can not account for such anomalous release adiabats [Jeanloz and Ahrens, 1979b]. The present results for simple oxides lend further confidence to the previous measurements of release adiabats, despite their often anomalous nature [see also Grady, 1977]. Other than the release from 161 GPa (LGG 043), which may be anomalous, the release adiabats from the Hugoniot states of CaO are shallower than would be expected for the isentropes of a solid. Although vaporization upon decompression could explain this observation, the calculated Hugoniot temperatures are lower than the melting temperature, and other effects may be involved [Lyzenga and Ahrens, 1977]. By contrast, the FeO release adiabats are quite similar to isentropes expected for solids. Also, the release paths in the mixed-phase region (eg, 84 GPA for CaO) are as expected for a momentarily "frozen-in" transition [Ahrens, et al., 1969b; Grady, et al., 1974, 1975].

The Hugoniot data for CaO at 134 and 149 GPa (LGG 024 and 033 in Table 2, not shown in Figure 4) have not been considered in the foregoing discussion. These data are anomalous (Figure 4), both in their extremely high densities and in their steep release adiabats. A misreading of the raw data would tend to result in anomalously shallow release paths for an erroneously high Hugoniot density, contrary to

observation, and the errors associated with these data appear to be too small to account for the discrepancy. In fact, all of the data at high pressures in Figure 4 appear to contain more scatter than is usual [e.g., Jeanloz and Ahrens, 1978], and it is possible that these anomalies reflect an incipient instability in CaO. As with FeO, an electronic collapse is expected in CaO at pressures (or densities) above those achieved in this study, however the relatively high Hugoniot temperatures which are reached above 120 GPa might help to promote such a transition (or other instability). Speculation aside, the two high density data are considered to be anomalous, and are not further discussed.

DISCUSSION

Recently, the idea has been revived that oxygen may be an important constituent of the earth's core [Ringwood, 1978; cf, Jacobs, 1975]. Thus, one of the reasons for interest in the properties of FeO at high pressures has been in order to test its viability as a component in the core. The comparison between iron, FeO and the outer core is presented in Figure 9, in which the shock-wave data have been reduced to core temperatures according to the analysis given above and that in Jeanloz [1979]. Stacey's [1977] geotherm for the core has been used, however, the results do not depend critically on the assumed temperatures: 1500K affects the densities by about 1%, the estimated accuracy of the reduced Hugoniot data.

With the discovery of the new high-pressure phase of FeO, somewhat more oxygen can be allowed in the core, from the seismological bounds, than has previously been thought. As is evident from Figure 9, both the

density and the compressibility (not well constrained) of an Fe-FeO mixture can reproduce the properties of the core: about 50 wt.% FeO (11 wt.% O) is required in combination with iron. This corresponds to approximately 30 atomic % O, or nearly a composition of Fe_2O, comprising the liquid outer core, and hence supports Ringwood's [1978] hypothesis. Although Dubrovskiy and Pan'kov [1972] had also proposed that iron oxide is present in the core, the new shock-wave data preclude their inferred composition of 100% FeO. The results of this study can not be used to critically evaluate the Fe_2O hypothesis of Bullen [1973; Strens, 1976], since this is predicated on an assumed electronic transition in iron oxide, but the present data are not exactly consistent with Fe_2O comprising the outer core (by about 2% in density).

In order to evaluate these latter hypotheses, it is crucial to resolve whether the 70 GPa transition in FeO involves an electronic transition or not. The shock-wave data allow considerable amounts of oxygen in the core on physical grounds (density, bulk modulus), however the geochemical considerations (nature of bonding, whole-earth composition) can not be addressed. If oxygen occurs in the core, immiscible liquids may tend to form, as happens at zero pressure, unless FeO becomes semimetallic [Ringwood, 1978]. A two-phase melt would, in this case, be highly unstable due to the large density differences between the two liquids (Figure 9). Hence adequately vigorous stirring in the core would be required in order to prevent unmixing, unless the endmember components become more compatible at high pressures than they

are at zero pressure. Although a hypothesized electronic transition in FeO is compatible with the present data, none is required and a structural transition is quite adequate for explaining the shock-wave measurements.

An important consequence of allowing oxygen in the core is that this increases the estimated minimum temperature of the outer core, probably to about 3500K, based on the high-pressure experiments of Usselman [1975a,b; see Jeanloz and Richter, 1979; Ringwood, 1978]. The upper bound for temperature is still determined by the melting point of iron, which presumably can not be exceeded at the inner core/ outer core boundary.

The new data for CaO and FeO can also be applied to models of the earth's lower mantle. For example, one of the main results discussed by Jeanloz, et al., [1979] is that CaO, as a consequence of its phase transition, has essentially the same density as the mantle at pressures above 60-70 GPa (Figure 4). Therefore, CaO is an "invisible" component of the lower mantle in that virtually any amount can be accommodated in accordance with seismological observations. An enrichment of CaO within the lower mantle would be compatible with an enrichment in refractory components, as suggested by inhomogenous accretion theories.

Similarly, SiO_2 is essentially an invisible component of the lower mantle according to the available shock-wave data [e.g., Davies, 1972]. Although SiO_2 may have a density slightly lower than that of the mantle at high pressures (and mantle temperatures), there is significant uncertainty in the reduction of the Hugoniot data [e.g., McQueen, et al., 1963, 1964; Ahrens, et al., 1969a; Davies, 1974]; the difference in

densities is within about 1% and hence probably not resolvable. Consequently, in terms of the major element oxides, only the relative proportions of MgO, Al_2O_3 and FeO in the lower portions of the mantle can be constrained with any assurance. At pressures less than 60-70 GPa (depths less than about 1550 km), CaO would also be considerably less dense than the mantle, unless its B2 structure is stabilized by solid solution or unless it can enter another high density phase [e.g., Liu and Ringwood, 1975].

The new data for FeO do not significantly alter previous conclusions about the relative proportions of Fe in the mantle [Ringwood, 1975]. A value of $\frac{Mg}{Mg+Fe} \sim 0.88$ (± 0.02) satisfies mantle properties for essentially any combination of MgO, FeO and SiO_2, whereas slightly lower values are required for more than about 3-4 mol% Al_2O_3. On the other hand, it is possible that phases with densities slightly higher than the component oxides occur within the lower mantle, thus tending to increase this Mg-value for the total assemblage.

Of greater interest, however, is considering FeO as a candidate phase (rather than component oxide) of the lower mantle. Upper mantle olivine transforms to a perovskite + magnesiowüstite assemblage at high pressures, with iron being enriched in the oxide; these are considered likely to be the most important phases of the lower mantle [Liu, 1976, 1977, 1978; Yagi, et al., 1978; Mao, et al., 1979]. Therefore, it is of interest to extrapolate the present results across the MgO-FeO solid solution series, to plausible mantle compositions.

MgO might be expected to transform at high pressure to the B2 phase, with about a 2% density increase (Figure 7). However, shock-wave data [Carter, et al., 1971] indicate no evidence of a transition in MgO to about 120 GPa, and this has been confirmed to 95 GPa in diamond-cell experiments [Mao and Bell, 1979]. But even if MgO transforms at a pressure in excess of 150 GPa, its B2 structure could still be of significance for the mantle. Interpreting the high-pressure phase of FeO as a B2 structure, a phase diagram can be constructed for (Mg,Fe)O based on the new Hugoniot data, the systematics of Figure 7, and an assumed transition pressure for MgO. The result is Figure 10, in which MgO is shown transforming at 150 or 170 GPa, as two examples. The plausible range of composition for (Mg,Fe)O in the mantle is indicated, as is the appropriate composition of magnesiowüstite in equilibrium with perovskite in a pyrolite-like mantle [Yagi, et al., 1978]. Thus, because of the relatively low transition pressure which has been found for FeO, a B1/B2 transition in magnesiowüstite may be of significance in the lower mantle, particularly in the D" layer at its base.

Jeanloz and Richter [1979] recently discussed several possible explanations for the nature of the D" region which is characterized by anomalous gradients in seismic velocities, scattering of seismic waves and possible heterogeneities [see Cleary's, 1974, review and references therein; also Julian and Sengupta, 1973; Sacks and Beach, 1974; Haddon and Cleary, 1974; Kanasewitch and Gutowski, 1975; Wright and Lyons, 1975; Dornboos, 1976; Chang and Cleary, 1978]. Although both compositional and thermal heterogeneities have been invoked to explain the properties of the D" layer, the present data suggest that a third alternative, phase

transition could strongly accentuate slight variations in the temperature field near the base of the mantle, assuming a non-zero Clapeyron slope; the transition shown in Figure 10 involves a density increase $\delta\rho \sim 5$ to 8% in (Mg,Fe)O. A comparable density contrast requires temperature variations of 5000 to 10000K, which are highly unlikely, or compositional variations corresponding to about 10 mol percent MgO (ideal mixing assumed throughout).

The phase assemblage near the base of the mantle is unknown, but for an olivine-rich composition perovskite might be expected as the dominant phase with up to 30 vol. % magnesiowüstite [$\sim$ 15 vol. % for a perovskite-bearing pyrolite assemblage; see Ringwood, 1975; Mao, et al., 1979]. From velocity-density systematics [e.g., Birch, 1961], this immediately suggests local velocity variations of 2 - 4% in the D" region which could readily cause scattering. Alternatively, noting that neither bulk nor shear moduli change very much upon transforming from B1 to B2 structures [Table 3; Davies, 1976; Jeanloz, et al., 1979; Cohen and Gordon, 1975], the velocity is expected to decrease by about 1% (for pyrolite composition) due to transformation in (Mg,Fe)O near the base of the mantle. This could contribute to the anomalous change in velocity gradient which is observed, and the need for compositional heterogeneity in the D" region may be precluded.

CONCLUSIONS

New shock-wave data have been presented for CaO and FeO to about 175 and 230 GPa, respectively. In both cases, a phase transformation is found at approximately 70 (±10) GPa; it is known to be of B1/B2 type in CaO. Alternative explanations (eg, electronic transitions) can not be precluded in the case of FeO, but the preferred interpretation is that this oxide also undergoes a B1/B2 transition.

The shock-wave data for the B1 phases of FeO and CaO are in excellent agreement with several ultrasonic and static-compression measurements on these compounds, as well as with Modified Electron Gas calculations for CaO [Cohen and Gordon, 1976]. Combining the available data allows a value $K_0' \sim 3.2$ to be determined for FeO. Similarly, the properties of the high-pressure phases of CaO and FeO have been determined from a reduction of the shock-wave data (Table 3). In both cases, these properties are consistent with expectations for B2 structures based on systematics.

The main application of the FeO data is towards evaluating the possible oxygen content of the core. The new data allow a considerable amount of oxygen to be present in the core, as has recently been suggested from geochemical considerations [Ringwood, 1978]. However, only the physical constraints on this hypothesis can be considered here, and establishing the nature of the transition in FeO may provide important geochemical constraints. About 30 atomic percent substitution of oxygen in the core (the remainder being Fe) is consistent with the shock-wave data.

CaO is found to have densities essentially equivalent to those of the mantle at pressures in excess of 70 GPa. Hence it, along with SiO_2, is an invisible oxide component of the lower mantle in that there are no constraints on the amounts of these oxides which may be present. In terms of a model, mixed-oxide assemblage for the lower mantle only the relative proportions of MgO and Al_2O_3 versus FeO can be determined from density and bulk modulus data. More realistic, candidate phase assemblages (eg, perovskite-bearing) have similar properties, but probably require slightly less iron-enrichment to achieve mantle densities than the simple oxides. Nevertheless, the data for oxides allow a considerably different composition in the lower mantle than in the upper mantle. For example, an enrichment of refractory components in the lower mantle, as is suggested by inhomogeneous accretion theories [Turekian and Clark, 1969], is consistent with its measured properties.

On the other hand, an application of the present data to the perovskite and oxide assemblage which is presumed to be abundant in the lower mantle, suggests that a phase transition in magnesiowüstite may be of significance within the mantle. In particular, such a transition may occur within the D" region, suggesting the presence of only a simple thermal boundary layer at the base of the mantle and hence the possibility of another boundary layer elsewhere within the lower mantle. The most plausible cause of such a boundary layer within the mantle, and its requisite barrier to convection, is a major chemical discontinuity. The results of this study are compatible with, and perhaps suggestive of, the earth's mantle consisting of more than one chemical and dynamic system.

ACKNOWLEDGEMENTS

We thank E. K. Graham (Pennsylvania State University), M. M. Abraham and Y. Chen (Oak Ridge National Laboratory), and R. A. Bartels (Trinity University) for providing the samples used in this study. We have benefitted from discussions with I. Jackson, M.S.T. Bukowinski, E. K. Graham, J. A. Tossell, A. E. Ringwood and L. M. Falicov. We thank R. Smith, E. Gelle, J. Long and H. Richeson for their assistance with the experiments. Work supported by NSF grants EAR 75-15006A01 and EAR 77-23156. Contribution number 3302, Division of Geological and Planetary Sciences, California Institute of Technology, Pasadena, CA 91125.

REFERENCES

Abraham, M., Butler, C. T. and Chen, Y., 1971. Growth of high-purity and doped alkaline earth oxides: I. MgO and CaO. J. Chem. Phys., 55, 3752-3756.

Adler, D., 1968. Mechanisms for metal-nonmetal transitions in transition-metal oxides and sulfides. Rev. Mod. Phys., 40, 714-736.

Adler, D., 1975. Fundamental problems in the electronic structure of transition - metal oxides. J. Solid State Chem., 12, 332-340.

Ahrens, T. J., Anderson, D. L. and Ringwood, A. E., 1969a. Equations of state and crystal structures of high-pressure phases of shocked silicates and oxides. Rev. Geophys., 7, 667-707.

Ahrens, T. J., Petersen, C. F. and Rosenberg, J. T., 1969b. Shock compression of feldspars. J. Geophys. Res., 74, 2727-2746.

Ahrens, T. J., Jackson, I. and Jeanloz, R., 1977. Shock compression and adiabatic release of a titaniferous mare basalt. Proc. Lunar Sci. Conf. 8th, 3437-3455.

Akimoto, S., 1972. The system MgO-FeO-SiO_2 at high pressures and temperatures - phase equilibria and elastic properties. Tectonophysics, 13, 161-187.

Al'tshuler, L. V. and Sharipdzhanov, I. I., 1971. Additive equations of state of silicates at high pressures. Izv. Acad. Sci. USSR, Earth Phys., no. 3, 167-177.

Anderson, D. L. and Hart, R. S., 1976. An earth model based on free oscillations and body waves. J. Geophys. Res., 81, 1461-1475.

Benard, J., 1954. Sur les parametres limites de la phase FeO. Acta Cryst., 7, 214.

Berman, H., 1939. A torsion microbalance for the determination of specific gravities of minerals. Am. Min., 24, 434-440.

Birch, F., 1952. Elasticity and constitution of the earth's interior. J. Geophys. Res., 57, 227-286.

Birch, F. 1961. The velocity of compressional waves in rocks to 10 kilobars, part 2. J. Geophys. Res., 66, 2199-2224.

Birch, F., 1966. Compressibility; elastic constants, in: Handbook of Physical Constants (S. P. Clark, Jr., editor) Geol. Soc. Am. Mem. 97, 97-123.

Bowen, H. K., Adler, D. and Anker, B. H., 1975. Electrical and optical properties of FeO. J. Solid State Chem., 12, 355-359.

Briggs, A., 1977. Direct evidence for a brucite precipitate in a melt-grown MgO crystal. J. Mat. Sci., 12, 637-640.

Bullen, K. E., 1973. Cores of the terrestrial planets. Nature, 243, 68-70.

Burns, R. G., 1970. Mineralogical Applications of Crystal Field Theory, Cambridge University Press, Cambridge, 244.

Burns, R. G., 1976. Partitioning of transition metals in mineral structures of the mantle, in: The Physics and Chemistry of Minerals and Rocks, J. Wiley & Sons, New York, pp. 555-572.

Carter, W. J. and Marsh, S. P., 1979. Hugoniot equations of state of polymers. J. Chem. Phys. (in press).

Carter, W. J., Marsh, S. P., Fritz, J. N. and McQueen, R. G., 1971. The equation of state of selected materials for high-pressure reference, in: Accurate Characterization of the High-Pressure Environment (E.C. Lloyd editor), Nat. Bur. Stds. (U.S.) Pub. 326, pp. 147-158.

Chang, A. C. and Cleary, J. R. 1978. Precursors to PKKP. Bull. Seism. Soc. Am., 68, 1059-1079.

Chang, Z. P. and Graham, E. K., 1977. Elastic properties of oxides in the NaCl-structure. J. Phys. Chem. Solids, 38, 1355-1362.

Chen, H., Knapp, G. S. and Chen, W. K., 1978. Extended X-ray absorption fine-structure (EXAFS) study of point defects in iron-oxides. Ceram. Bull, 57, 314.

Clack, D. W. and Smith, W., 1974. Molecular orbital calculations on transition metal complexes. Part VIII. J. Chem. Soc., Dalton, 2015-2020.

Clark, S. P., Turekian, K. K. and Grossman, L., 1972. Chemical models of the Earth, in: The Nature of The Solid Earth (E. C. Robertson, ed.), McGraw-Hill, New York, pp. 3-18.

Clendenen, R. L. and Drickamer, H. G., 1966. Lattice parameters of nine oxides and sulfides as a function of pressure. J. Chem. Phys., 44, 4223-4228.

Cohen, A. J. and Gordon, R. G., 1975. Theory of the lattice energy, equilibrium structure, elastic constants and pressure-induced phase transitions in alkali-halide crystals. Phys. Rev.,B 12, 3228-3241.

Cohen, A. J. and Gordon, R. G., 1976. Modified electron-gas study of the stability, elastic properties, and high-pressure behavior of MgO and CaO crystals. Phys. Rev., B14, 4593-4605.

Davies, G. F., 1972. Equations of state and phase equilibria of stishovite and a coesitelike phase from shock-wave and other data. J. Geophys. Res., 4920-4933.

Davies, G. F., 1974. Limits on the constitution of the lower mantle. Geophys. J. R. astr. Soc., 38, 479-503.

Davies, G. F., 1976. The estimation of elastic properties from analogue compounds. Geophys. J. R. astr. Soc., 44, 625-647.

Demarest, H. H., Cassell, C. R., and Jamieson, J. C., 1978. The high pressure transitions in KF and RbF. J. Phys. Chem. Solids, 39, 1211-1215.

Doornbos, D. J., 1976. Characteristics of lower mantle inhomogeneities from scattered waves. Geophys. J. R. astr. Soc., 44, 447-470.

Dragoo, A. L. and Spain, I. L., 1977. The elastic moduli and their pressure and temperature derivatives for calcium oxide. J. Phys. Chem. Solids, 38, 705-710.

Draper, N. and Smith, H., 1966. Applied Regression Analysis, J. Wiley & Sons, New York, 407 pp.

Dubrovskiy, V. A. and Pan'kov, V. L., 1972. On the composition of the earth's core. Izv. Acad. Sci. USSR Earth Phys., no. 7, 452-455.

Duvall, G. E. and Graham, R. A., 1977. Phase transitions under shock-wave loading. Rev. Mod. Phys., 49, 523-579.

Dziewonski, A. M., Hales, A. L. and Lapwood, E. R., 1975. Parametrically simple earth models consistent with geophysical data. Phys. Earth Planet. Int., 10, 12-48.

Falicov, L. M. and Koiller, B., 1975. Low temperature conductivity of transition-metal oxides. J. Solid State Chem., 12, 349-354.

Freund, F.,and Demortier, G., 1978. Carbon content of high-purity alkaline earth oxide single crystals grown by arc fusion. J. Am. Ceram. Soc., 61, 429-439.

Freund, F., Debras, G. and Demortier, G., 1977. Carbon content of magnesium oxide single crystals grown by the arc fusion method. J. Cryst. Growth, 38, 277-280.

Fritz, J. N., Marsh, S. P., Carter, W. J. and McQueen, R. G., 1971. The Hugoniot equation of state of sodium chloride in the sodium chloride structure, in: Accurate Characterization of the High-Pressure Environment (E. C. Lloyd, editor), Nat. Bur. Stand. (U.S.) Spec. Pub. 326, pp. 201-208.

Fyfe, W. S., 1960. The possibility of d-electron coupling in olivine at high pressures. Geochim. Cosmochim. Acta, 19, 141-143.

Gaffney, E. S. and Anderson, D. L., 1973. Effect of low-spin Fe^{2+} on the composition of the lower mantle. J. Geophys. Res., 78, 7005-7014.

Grady, D. E., 1977. Processes occurring in shock wave compression of rocks and minerals, in: High-Pressure Research (M. H. Manghnani and S. Akimoto, eds.) Academic Press, New York, pp. 389-438.

Grady, D. E., Murri, W. J. and DeCarli, P. S., 1975. Hugoniot sound velocities and phase transformations in two silicates. J. Geophys. Res., 80, 4857-4861.

Grady, D. E., Murri, W. J. and Fowles, G. R., 1974. Quartz to stishovite: wave propagation in the mixed phase region. J. Geophys. Res., 79, 332-338.

Graham, E. R. and Bonczar, L. J., 1978. Elasticity of the magnesiowüstite solid solution. EOS, 59, 373.

Haddon, R. A. W. and Cleary, J. R. 1974. Evidence for scattering of seismic PKP waves near the mantle-core boundary. Phys. Earth Planet. Int., 8, 211-234.

Hayakawa, M., Cohen, J. B. and Reed, R. B., 1972. Measurement of the lattice parameter of wüstite of high temperatures. J. Am. Ceram. Soc., 55, 160-164.

Hentschel, B., 1970. Stoichiometric FeO as a metastable intermediate of the decomposition of wüstite at 255°C. Z. Naturforsch., 25a, 1996-1997.

Jackson, I. and Ahrens, T. J., 1979. Shock-wave compression of single-crystal forsterite. J. Geophys. Res., 84, 3039-3048.

Jackson, I., Liebermann, R. C. and Ringwood, A. E., 1978. The elastic properties of $(Mg_xFe_{1-x})O$ solid solutions. Phys. Chem. Min., 3, 11-31.

Jacobs, J. A., 1975. The Earth's Core, Academic Press, New York, pp. 253.

Jayaraman, A., 1972. Pressure - induced electronic collapse and semi-conductor-to-metal transition in EuO. Phys. Rev. Lett., 29, 1674-1676.

Jayaraman, A., Singh, A. K., Chatterjee, A. and Devi, S. U., 1974. Pressure-volume relationship and pressure-induced electronic and structural transformations in Eu and Yb monochalcogenides. Phys. Rev., B9, 2513-2520.

Jeanloz, R., 1979. Properties of iron at high pressures and the state of the core. J. Geophys. Res., 84.

Jeanloz, R. and Ahrens, T. J., 1977. Pyroxenes and olivines: structural implications of shock-wave data for high pressure phases, in: High-Pressure Research (M. H. Manghnani and S. Akimoto, eds.) Academic Press, New York, pp. 439-461.

Jeanloz, R. and Ahrens, T. J., 1978. The equation of state of a lunar anorthosite: 60025. Proc. Lunar Planet. Sci. Conf. 9th, 2789-2803.

Jeanloz, R. and Ahrens, T. J., 1979a. Anorthite: Thermal equation of state to high pressures. Submitted for publication.

Jeanloz, R. and Ahrens, T. J., 1979b. Release adiabat measurements on minerals: the effect of viscosity. J. Geophys. Res. (submitted).

Jeanloz, R., Ahrens, T. J., Mao, H. K. and Bell, P. M., 1979. B1/B2 transition in CaO from shock-wave and diamond cell experiments. Science. (in press)

Jeanloz, R. and Richter, F. M., 1979. Convection, composition and the thermal state of the lower mantle. J. Geophys. Res., in press.

Johnson, Q. and Mitchell, A. C., 1972. First x-ray diffraction evidence for a phase transition during shock-wave compression. Phys. Rev. Lett., 29, 1369-1371.

Julian, B. R. and Sengupta, M. K., 1973. Seismic travel time evidence for lateral inhomogeneity in the deep mantle. Nature, 242, 443-447.

Kanasewitch, E. R. and Gutowski, P. R., 1975. Detailed seismic analysis of a lateral mantle inhomogeneity. Earth Planet. Sci. Lett., 25, 379-384.

Katsura, T., Iwasaki, B., Kimura, S. and Akimoto, S., 1967. High-pressure synthesis of the stoichiometric compound FeO. J. Chem. Phys., 47, 4559-4560.

Kofstad, P., 1972. Nonstoichiometry, Diffusion and Electrical Conductivity in Binary Metal Oxides, J. Wiley & Sons, New York, 382 pp.

Liu, L.-G., 1971. A dense modification of BaO and its crystal structure. J. App. Phys., 42, 3702-3704.

Liu, L.-G., 1976. Orthorhombic perovskite phases observed in olivine, pyroxene and garnet at high pressures and temperatures. Phys. Earth Planet. Int., 11, 289-298.

Liu, L.-G., 1977. Mineralogy and Chemistry of the earth's mantle above 1000 km. Geophys. J. R. astr. Soc., 48, 53-62.

Liu, L.-G., 1978. High pressure Ca_2SiO_4, the silicate K_2NiF_4-isotype with crystalchemical and geophysical implications. Phys. Chem. Minerals, 3.

Liu, L.-G. and Bassett, W. A., 1972. Effect of pressure on the crystal structure and the lattice parameters of BaO. J. Geophys. Res., 77, 4934-4937.

Liu, L.-G. and Bassett, W. A., 1973. Changes of the crystal structure and the lattice parameter of SrO at high pressure. J. Geophys. Res., 78, 8470-8473.

Liu, L.-G. and Ringwood, A. E., 1975. Synthesis of a perovskite-type polymorph of $CaSiO_3$. Earth Planet. Sci. Lett., 28, 209-211.

Lyzenga, G. and Ahrens, T. J., 1978. The relations between the shock-induced free-surface velocity and post-shock density of solids. J. App. Phys., 49, 201-204.

Mao, H.-K., 1974. A discussion of the iron oxides at high pressures with implications for the chemical and thermal evolution of the earth. Carnegie Inst. Wash. Yearbook, 73, 510-518.

Mao, H.-K. and Bell, P. M., 1977. Disproportionation equilibrium in iron-bearing systems at pressures above 100 kbar with applications to chemistry of the earth's mantle, in: Energetics of Geological Processes (S. K. Saxena and S. Bhattacharji editors), Springer-Verlag, New York, pp. 236-249.

Mao, H.-K, Yagi, T. and Bell, P. M., 1979. Experimental study of the relations between $(Mg,Fe)SiO_3$ perovskite and coexisting phases in the system MgO-FeO-SiO_2 under conditions equivalent to those in the deep mantle (150-500 kbars, 1000-1500°C). EOS, 60, 388 (abstract).

Mao, H.-K. and Bell, P. M., 1979. J. Geophys. Res. (in press)

Mao, H.-K., Takahashi, T., Bassett, W. A., Weaver, J. S. and Akimoto, S., 1969. Effect of pressure and temperature on the molar volumes of wüstite and of three $(Fe,Mg)_2SiO_4$ spinel solid solutions. J. Geophys. Res., 74, 1061-1069.

McQueen, R. G., Fritz, J. N. and Marsh, S. P., 1963. On the equation of state of stishovite. J. Geophys. Res., 68, 2319-2322.

McQueen, R. G., Fritz, J. N. and Marsh, S. P., 1964. On the composition of the earth's interior. J. Geophys. Res., 69, 2947-2965.

McQueen, R. G., Marsh, S. P., Taylor, J. W., Fritz, J. N. and Carter, W. J., 1970. The equation of state of solids from shock wave studies, in: High Velocity Impact Phenomena (R. Kinslow, ed) Academic Press, New York, pp. 294-419 and Appendices.

Mood, A. M., Graybill, F. A. and Boes, D. C., 1974. Introduction to the Theory of Statistics, McGraw-Hill, New York, 564 pp.

Ohnishi, S., 1978. A theory of the pressure-induced high-spin - low-spin transition of transition-metal oxides. Phys. Earth Planet. Int., 17, 130-139.

Ohnishi, S. and Mizutani, H., 1978. Crystal-field effect on the bulk moduli of transition - metal oxides. J. Geophys. Res., 83, 1852-1856.

Nakamoto, K., 1970. Infrared Spectra of Inorganic and Coordination Compounds, second edition, J. Wiley & Sons, New York, 338 pp.

Pauling, L., 1960. The Nature of the Chemical Bond, third edition, Cornell University Press, Ithaca, New York, 644 pp.

Perez-Albuerne, E. A. and Drickamer, H. G., 1965. Effect of high pressures on the compressibilities of seven crystals having the NaCl or CsCl structure. J. Chem. Phys., 43, 1381-1387.

Pistorius, C. W. F. T., 1976. Phase relations and structures of solids at high pressures. Progr. Solid State Chem., 11, 1-151.

Ramakrishnan, J., Hardy, R. J. and Kennedy, G. C., 1979. The Grüneisen parameter γ of KBr, RbCl, and Bi through high pressure phase transitions. J. Phys. Chem. Solids, 40, 297-303.

Rice, M. H ., McQueen, R. G. and Walsh, J. M., 1958. Compressibility of solids by strong shock waves, Solid State Physics, 6, 1-63.

Ringwood, A. E., 1975. Composition and Petrology of the Earth's Mantle, McGraw-Hill, New York, 618 pp.

Ringwood, A. E., 1978. Composition of the core and implications for origin of the earth. Geochem. J., 11, 111-136.

Robie, R. A., Hemingway, B. S. and Fisher, J. R., 1978. Thermodynamic Properties of Minerals and Related Substances, U.S. Geol. Survey. Bull. 1452, Washington, D.C., pp. 456.

Ross, M., 1972. On the Herzfeld theory of metallization. Application to rare gases, alkali halides, and diatomic molecules. J. Chem. Phys., 56, 4651-4653.

Roth, W. L., 1960. Defects in the crystal and magnetic structures of ferrous oxide. Acta Cryst., 13, 140-149.

Sacks, I. S. and Beach, L., 1974. Lateral heterogeneity at the base of the mantle - an indication of whole mantle convection. Carnegie Inst. Wash. Yearbook, 73, 1020-1032.

Sato, Y., Ida, Y. and Akimoto, S., 1973. Equation of state determined with the Bridgman-anvil high-pressure apparatus. High Temp.-High Press., 5, 679-688.

Shannon, R. D. and Prewitt, C. T., 1969. Effective ionic radii in oxides and flourides. Acta Cryst., B25, 925-946.

Son, P. R. and Bartels, R. A., 1972. CaO and SrO single crystal elastic constants and their pressure derivatives. J. Phys. Chem. Solids, 33, 819-828.

Stacey, F. D., 1977. A thermal model of the earth. Phys. Earth Planet. Int., 15, 341-348.

Strens, R. G. J., 1976. Behavior of iron compounds at high pressure, and the stability of Fe_2O in planetary mantles, in: The Physics and Chemistry of Minerals and Rocks (R.G.J. Strens, editor), J. Wiley & Sons, New York, pp. 545-554.

Syono, Y., Tokonami, M. and Matsui, Y., 1971. Crystal field effect on the olivine - spinel transformation. Phys. Earth Planet. Int., 4, 347-352.

Tossell, J. A., 1976. Electronic structures of iron-bearing oxidic minerals at high pressure. Am. Min., 61, 130-144.

Touloukian, Y. S., Kirby, R. K., Taylor, R. E. and Lee, T. Y. R., 1977. Thermal Expansion, Nonmetallic Solids, IFI/Plenum, New York, pp. 1658.

Turekian, K. K. and Clark, S. P., Jr., 1969. Inhomogeneous accretion model of the earth from the primitive solar nebula. Earth Planet. Sci. Lett., 6, 346-348.

Usselman, T. M., 1975a. Experimental approach to the state of the core: Part I. Am. J. Sci., 275, 278-290.

Usselman, T. M., 1975b. Experimental approach to the state of the core: Part II. Am. J. Sci., 275, 291-303.

Wackerle, J., 1962. Shock-wave compression of quartz. J. App. Phys., 33, 922-937.

Walsh, J. M. and Christian, R. H., 1955. Equation of state of metals from shock wave measurements. Phys. Rev., 97, 1544-1556.

Wells, A. F., 1975. Structural Inorganic Chemistry, Fourth edition, Oxford University Press, New York, 1095 pp.

Wright, C. and Lyons, J. A., 1975. Seismology, $dT/d\Delta$ and deep mantle convection. Geophys. J. R. astr. Soc., 40, 115-138.

Yagi, T., Mao, H. K., and Bell, P. M., 1978. Effect of iron on the stability and unit-cell parameters of ferromagnesian silicate perovskite. Carnegie Inst. Washington Yearbook, 77, 837-841.

Table 1

FeO Shock-Wave Data

	EXPERIMENT			SAMPLE		HUGONIOT STATE				RELEASE STATE				
	Shot No.	Flyer/ Driver	Impact Velocity (km/s)	Bulk Density (Mg/m^3)	Archimedean Density (Mg/m^3)	Shock-wave Velocity (km/s)	Particle Velocity (km/s)	Pressure (GPa)	Density (Mg/m^3)	Buffer Material	Shock-wave Velocity (km/s)	Particle Velocity (km/s) (1)	Pressure (GPa)	Density (Mg/m^3)
	457	W	1.705 ±0.001	5.499 ±0.004	5.525 ±0.008	6.435 ±0.050	1.220 ±0.003	43.2 ±0.2	6.785 ±0.016	Lexan	5.379 ±0.079	1.942 ±0.050	12.5 ±0.5	6.084 ±0.099
	438	W	2.296 ±0.002	5.494 ±0.004	5.557 ±0.014	6.954 ±0.078	1.629 ±0.005	62.2 ±0.5	7.175 ±0.031	Lexan	6.117 ±0.115	2.412 ±0.073	17,7 ±0.9	6.530 ±0.124
	471	W	2.500 ±0.003	5.504 ±0.007	5.522 ±0.010	7.173 ±0.045	1.766 ±0.004	69.7 ±0.3	7.301 ±0.020	Lexan	6.738 ±0.115	2.808 ±0.073	22.6 ±1.0	6.248 ±0.146
										Free surface velocity:		3.165 ±0.329	0	6.058 ±0.485
LGG	062	Al	5.101 ±0.004	5.484 ±0.005	5.563 ±0.014	7.221 ±0.042	2.034 ±0.007	80.6 ±0.2	7.635 ±0.027	fused quartz	5.922 ±0.111	3.034 ±0.070	39.6 ±1.7	6.435 ±0.184
LGG	046	Al	5.999 ±0.006	5.514 ±0.014	5.555 ±0.014	7.592 ±0.066	2.414 ±0.012	101.1 ±0.5	8.085 ±0.051	fused quartz	6.338 ±0.124	3.297 ±0.110	46.0 ±2.8	7.256 ±0.229
LGG	064	Cu	5.456 ±0.006	5.555 ±0.012	5.576 ±0.008	8.701 ±0.106	3.147 ±0.014	152.1 ±1.3	8.703 ±0.081	fused quartz	8.298 ±0.058	4.532 ±0.037	82.9 ±1.2	7.012 ±0.111
LGG	044	Ta	5.776 ±0.003	5.494 ±0.012	5.562 ±0.012	9.640 ±0.165	3.743 ±0.018	198.2 ±2.5	8.981 ±0.125	fused quartz	9.316 ±0.328	5.174 ±0.207	106.2 ±8.0	7.485 ±0.476
LGG	065	Ta	6.300 ±0.006	5.505 ±0.005	5.526 ±0.008	10.230 ±0.053	4.055 ±0.007	228.4 ±0.9	9.120 ±0.040	fused quartz	10.030 ±0.072	5.624 ±0.045	124.3 ±1.9	7.502 ±0.106

Note:

(1) Calculated from the shock-wave velocity measured throught the buffer-mirror using:

$\rho_0 = 2.204\ Mg/m^3$, $U_S = 1.11 + 1.59\ u_p$ (km/s) [fused quartz]

$\rho_0 = 1.196\ Mg/m^3$, $U_S = 2.33 + 1.57\ u_p$ (km/s) [Lexan]

Table 2

CaO SHOCK-WAVE DATA

Single Crystals, <100> Orientation

EXPERIMENT				SAMPLE		HUGONIOT STATE				RELEASE STATE				
	Shot No.	Flyer/ Driver	Impact Velocity (km/s)	Source[1]	Archimedean Density (Mg/m^3)	Shock-wave Velocity (km/s)	Particle Velocity (km/s)	Pressure (GPa)	Density (Mg/m^3)		Shock-wave Velocity (km/s)	Particle[2] Velocity (km/s)	Pressure (GPa)	Density (Mg/m^3)	
	428	W	2.342 ±0.060	B	3.306 ±0.001	8.204 ±0.101	1.801 ±0.048	48.9 ±1.4	4.236 ±0.036		5.202 ±0.210	2.581 ±0.132	29.6 ±2.7	3.737 ±0.237	
										Free surface velocity:		4.316 ±0.084	0	2.735 ±0.081	
LGG	060	Al	5.099 ±0.014	B	3.339 ±0.002	9.086 ±0.074	2.314 ±0.012	70.2 ±0.4	4.480 ±0.019						(3)
						8.789 ± 0.070	2.350 ± 0.012	69.0 ±0.4	4.558 ±0.020		5.813 ± 0.062	2.966 ± 0.039	38.0 ± 0.9	4.317 ± 0.043	(4)
LGG	034	Al	5.226 ±0.020	B	3.305 ±0.003	8.312 ±0.166	2.491 ±0.020	68.4 ±0.7	4.719 ±0.050		No	Data			(5)
LGG	057	Al	5.992 ±0.004	0	3.325 ±0.002	8.831 ±0.063	2.846 ±0.009	83.6 ±0.6	4.906 ±0.024		6.516 ±0.122	3.409 ±0.077	49.0 ±2.0	4.695 ±0.072	
LGG	027	Ta	4.510 ±0.020	0	3.345 ±0.004	9.068 ±0.100	3.285 ±0.011	99.6 ±0.9	5.245 ±0.041		7.334 ±0.150	3.924 ±0.095	63.4 ±2.8	4.952 ±0.111	
LGG	040	Ta	5.197 ±0.004	B	3.307 ±0.006	9.630 ±0.048	3.782 ±0.005	120.5 ±0.5	5.446 ±0.022		8.723 ±0.034	4.800 ±0.21	92.3 ±0.8	4.537 ±0.054	
LGG	024 (6)	Ta	5.680 ±0.110	0	3.319 ±0.002	9.706 ±0.097	4.151 ±0.087	133.7 ±3.0	5.798 ±0.104		7.422 ±0.148	4.295 ±0.010	75.0 ±3.2	5.786 ±0.119	

Table 2 (continued)

CaO SHOCK-WAVE DATA

Single Crystals, <100> Orientation

EXPERIMENT				SAMPLE		HUGONIOT STATE				RELEASE STATE			
	Shot No.	Flyer/ Driver	Impact Velocity (km/s)	Source[1]	Archimedean Density (Mg/m^3)	Shock-wave Velocity (km/s)	Particle Velocity (km/s)	Pressure (GPa)	Density (Mg/m^3)	Shock-wave Velocity (km/s)	Particle[2] Velocity (km/s)	Pressure (GPa)	Density (Mg/m^3)
LGG	055	Ta (thin)	5.608 ±0.005	0	3.347 ±0.002	10.253 ±0.082	4.038 ±0.008	138.6 ±0.9	5.521 ±0.035	9.270 ±0.110	5.145 ±0.069	105.1 ±2.7	4.593 ±0.159
LGG	052	Ta (thin)	5.817 ±0.006	0	3.338 ±0.002	10.579 ±0.087	4.174 ±0.009	147.4 ±1.0	5.513 ±0.036	9.467 ±0.098	5.269 ±0.062	109.9 ±2.4	4.686 ±0.127
LGG	033 (6)	Ta	6.075 ±0.006	0	3.312 ±0.005	10.159 ±0.102	4.421 ±0.010	148.7 ±1.2	5.864 ±0.054	7.960 ±0.160	4.319 ±0.101	75.8 ±3.3	5.859 ±0.054
LGG	049	Ta (thin)	6.101 0.006	B	3.315 ±0.002	10.577 ±0.110	4.402 ±0.011	154.3 ±1.3	5.678 ±0.052	9.869 ±0.150	5.523 ±0.095	120.1 ±3.9	4.697 ±0.230
LGG	043	Ta (thin)	6.219 ±0.004	B	3.320 ±0.002	10.877 ±0.188	4.465 ±0.018	161.3 ±2.2	5.630 ±0.084	9.200 ±0.321	5.101 ±0.202	103.4 ±7.7	5.417 ±0.177
LGG	047	Ta (thin)	6.473 ±0.004	B	3.328 ±0.002	11.233 ±0.170	4.628 ±0.016	173.0 ±2.0	5.659 ±0.215	10.149 ±0.073	5.699 ±0.139	127.5 ±5.9	4.951 ±0.245

Notes:

(1) B: MRC samples
O: ORNL samples

(2) Calculated from the measured shock-wave velocity through the fused quartz buffer-mirror using: $\rho_0 = 2.204\ Mg/m^3$, $U_S = 1.11 + 1.59\ u_p$ (km/s)

(3) Based on first wave arrival: preferred interpretation

(4) Based on second wave arrival

(5) Poor record, results depend on interpretation

(6) Not shown in Figure 4

Table 3

Properties of FeO and CaO

B1 Phase	FeO	CaO
ρ_0 (Mg/m^3)	5.864 ±0.045 (1)	3.345 ±0.003 (2)
K_{0s} (GPa):	185 ±5 (3)	112 ±1 (4)
$\frac{dK_0}{dP}$	3.2 ±0.3 (5)	4.8 ±0.1 (4)
γ_0:	1.63 ±0.25 (2,6)	1.51 ±0.11 (2,6)
	γ/V = constant (7)	
B2 Phase		
ρ_0 (Mg/m^3)	6.05 ±0.15 (8)	3.76 ±0.05 (8,9)
K_{0s} (GPa):	195 ±10 (8)	115 ±8 (8)
$\frac{dK_0}{dP}$:	3.4 ±0.5 (8)	4.9 ±0.8 (8)
E_{tr} (kJ/mol):	29 ±3 (8)	90 ±5 (8,9)
γ_0:	1.8 ±0.2 (7,10)	1.8 ±0.2 (7,10)
$n = \frac{d\ln\gamma}{d\ln V}$	1 to 1.5 (7)	1 to 1.5 (8)
	$U_S = 3.72 + 1.59\ u_p$ (km/s) (8)	$U_S = 3.80 + 1.59$ (km/s) (8,11

Table 3 (continued)

Notes and References

Zero subscript indicates evaluated at zero pressure. Values for FeO are corrected for nonstoichiometry where necessary.

(1) Hentschel [1970]

(2) Robie, et al [1978]

(3) Jackson, et al [1978]; Graham and Bonczar [1978]; this study

(4) Chang and Graham [1977]; this study

(5) From shock-wave data, with K_{0s} constrained within stated range

(6) Touloukian, et al [1977]; data in table

(7) assumed

(8) This study, from fits to Hugoniot data. The high-pressure phase of FeO may not be of B2 type: see text.

(9) Jeanloz, et al [1979]

(10) See Ramakrishnan, et al [1979]

(11) Data from experiments LGG 024 and 033 excluded

Table 4

FeO Phase Transition

STRUCTURAL	PREDICTED BEHAVIOR
a) B1(NaCl) → B2(CsCl)	$\frac{-\Delta V}{V} \sim 4\%$, $P_{tr} \sim 90$ GPa
b) Distorted Structures	? $\frac{-\Delta V}{V} \lesssim 4\%$
c) Disproportionation	$\frac{-\Delta V}{V} \sim 0\%$
ELECTRONIC	
a) High spin → Low spin	$\frac{-\Delta V}{V} \sim 20\%$, $K_0 \sim 250$ GPa, $P_{tr} \sim 25$–40 GPa
	$\frac{-\Delta V}{V} \sim 5\%$, $P_{tr} \sim 60$–70 GPa
b) Valence Transition	? $P_{tr} > 200$ GPa, $\rho_0 \sim 7.34$ Mg/m^3
OBSERVED BEHAVIOR:	$\frac{-\Delta V}{V} \sim 4\%$, $P_{tr} \sim 70$–80 GPa, $K_0 \sim 200$ GPa

Figure Captions

Figure 1. Experimental record for shot LGG 057 on CaO. (a) Still photograph of back side of target showing side arrival mirrors (A and E) and sample on driver plate. Buffer mirror and scale are placed on back of sample, and buffer arrival mirror is placed on back of buffer mirror. Position of slit is also indicated.

(b) Streak photograph produced by sweeping the image, as viewed through the slit, of the back side of the target to the right. The successive destruction of shock-arrival, buffer and buffer-arrival mirrors by the shock wave is recorded by the disappearance of the light reflected from these mirrors. Time calibration shown at top. Note the tilt due to non-normal impact.

(c) Microdensitometer records corresponding to the three traces shown on the streak record (not corrected for tilt). Shock arrival times are indicated.

(d) Calibration of image-converter streak camera: writing rate is determined from microdensitometer scan of time calibration on streak record (stack of ten records shown).

Figure 2. Schematic illustration (highly exaggerated) of projectile tilt and bowing, and their effect on the streak record. Particle-velocity vector (u_p) is normal to target (seen edge-on) despite tilt. The arrival on the streak record corresponding to the shock-wave entering the sample is significantly curved due to the bowing of the projectile.

Figure 3. Hugoniot (solid points) and release-adiabat (error bars, no points) data for $Fe_{0.94}O$ (Table 1). The initial densities of the present samples, wüstite of the same stoichiometry and the nonporous equivalent (wüstite + iron) are shown. Dashed curves indicate envelope of theoretical Hugoniots calculated for the B2 phase (see Table 3). Free-surface result (shot 471) excluded for clarity.

Figure 4. Hugoniot and release-adiabat data for CaO in B1 and B2 structures (Table 2); symbols are as in Figure 3. Seismologically determined compression curves for the lower mantle are given as short-dashed lines. Open Hugoniot point shows the alternative interpretation of experiment LGG 060, and the datum in parentheses (LGG 034) is highly uncertain. Data from shots LGG 024 and 033 are not included (see text).

Figure 5. Compression data for wüstite in the B1 structure. The theoretical Hugoniot calculated from ultrasonic data (see text, K_0' unconstrained) is shown, along with the corresponding isotherm. Isothermal static-compression and shock-wave data are given as open and closed symbols, respectively.

Figure 6. Calculated temperatures along the Hugoniots of CaO and $Fe_{0.94}O$; dashed portions indicate regions of phase transformation. Recently estimated geotherms for the lower mantle and outer core are also shown.

Figure 7. Correlation of relative volume decrease at the B1/B2 transition with ratio of cation/anion radii, from data and an ionic bonding model (solid lines; after Demarest, et al., 1978). Two cases for repulsive potentials with r^{-9} and r^{-12} dependencies are given, and the ionic radii of Shannon and Prewitt [1969] were used. The nature of the FeO transition is uncertain and the case of BaO is complex (open symbols: see text). The radius ratio for MgO is also indicated.

Figure 8. Correlation of transition pressures in B1 monoxides with radius ratio (see Figure 7).

Figure 9. Shock-wave data for FeO (present results), Fe (McQueen et al., 1970), Fe_2O_3 and Fe_3O_4 (McQueen and Marsh, in: Birch, 1966) (Heavy curves) compared with the seismologically determined compression curve of the core [Dziewonski, et al., 1975; Anderson and Hart, 1976]. The Fe and FeO data, corrected to core temperatures, are shown as thin dashed curves. Mixtures of oxides and Fe corresponding to FeO are given as thin solid curves: 1/3 (Fe + Fe_2O_3) 1/4 (Fe + Fe_3O_4) and (Fe_3O_4 - Fe_2O_3), with increasing density; open squares are from Al'tshuler and Sharipdzhanov [1971]. Hugoniots for only the high-pressure phases are shown, and the wüstite data are corrected to the stoichiometric endmember.

Figure 10. Calculated phase diagram for magnesiowüstite based on the present data for FeO. The pressure at the core-mantle boundary (CMB) is indicated as is the range of plausible compositions of (Mg, Fe)O in the mantle: arrow is derived from Yagi, et al., [1978]. Ideal mixing and a zero Clapeyron slope are assumed. Two possible transition pressures for MgO are used as examples, and a temperature of 3000K is assumed in the calculation.

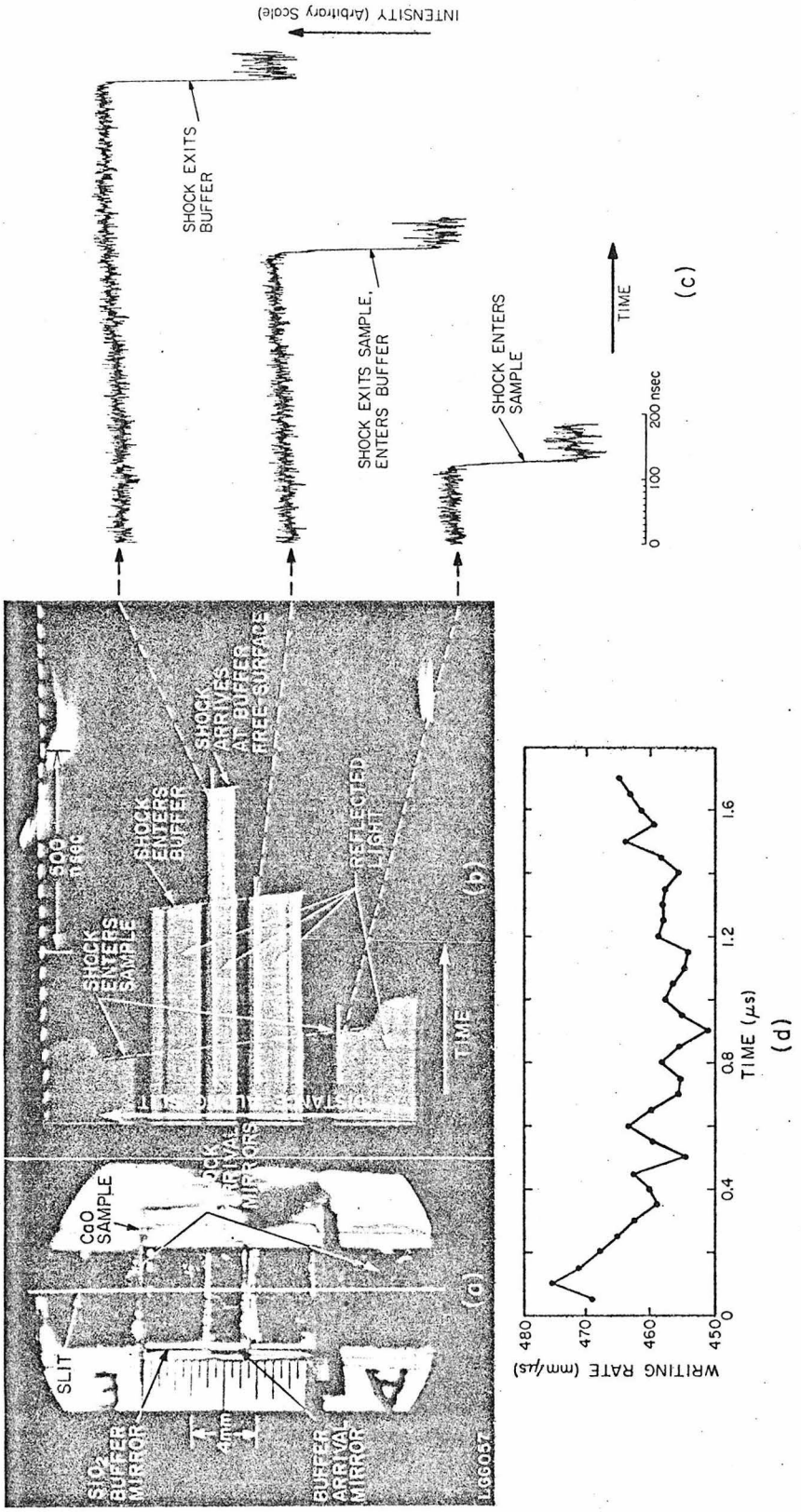
INTENSITY (Arbitrary Scale)
SHOCK EXITS BUFFER
SHOCK EXITS SAMPLE, ENTERS BUFFER
SHOCK ENTERS SAMPLE
0
100
200 nsec
TIME
(c)
SiO2 BUFFER MIRROR
4mm
SLIT
CaO SAMPLE
BUFFER ARRIVAL MIRROR
LGC057
(a)
500 nsec
SHOCK ENTERS SAMPLE
SHOCK ENTERS BUFFER
SHOCK ARRIVES AT BUFFER FREE SURFACE
REFLECTED LIGHT
TIME
(b)
WRITING RATE (mm/μs)
480
470
460
450
0
0.4
0.8
1.2
1.6
TIME (μs)
(d)

Fig. 1

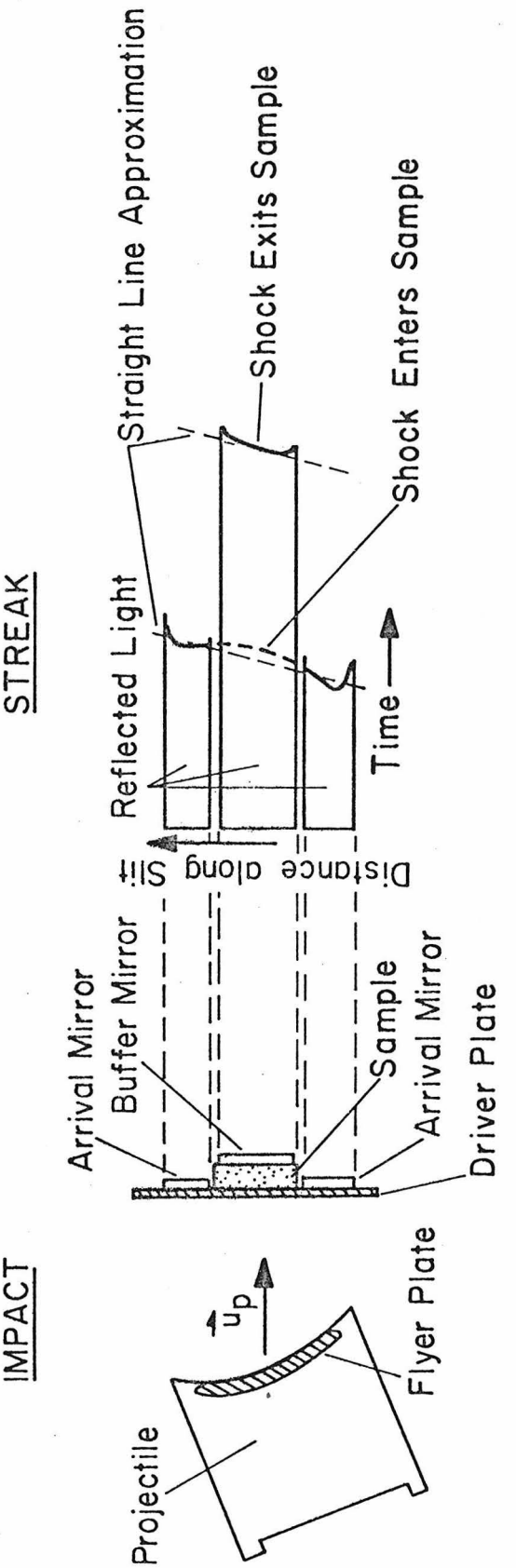
STREAK
Straight Line Approximation
Shock Exits Sample
Shock Enters Sample
Reflected Light
Time
Distance along Slit
Arrival Mirror
Buffer Mirror
Sample
Arrival Mirror
Driver Plate
IMPACT
u_p
Projectile
Flyer Plate

Fig. 3

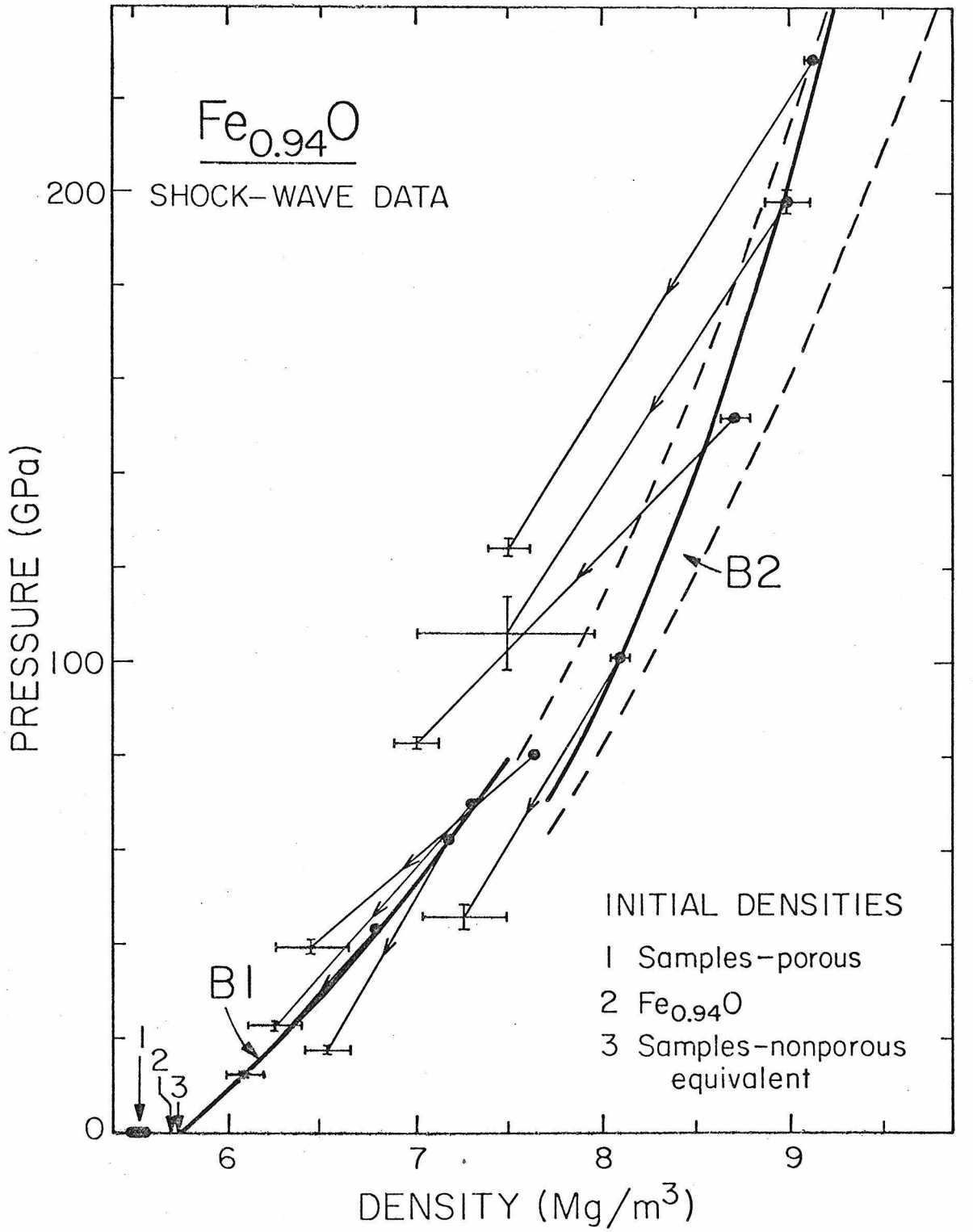
$Fe_{0.94}O$
SHOCK-WAVE DATA
PRESSURE (GPa)
200
100
0
6
7
8
9
DENSITY (Mg/m^3)
B1
B2
1
2
3
INITIAL DENSITIES
1 Samples-porous
2 $Fe_{0.94}O$
3 Samples-nonporous equivalent

Fig. 3

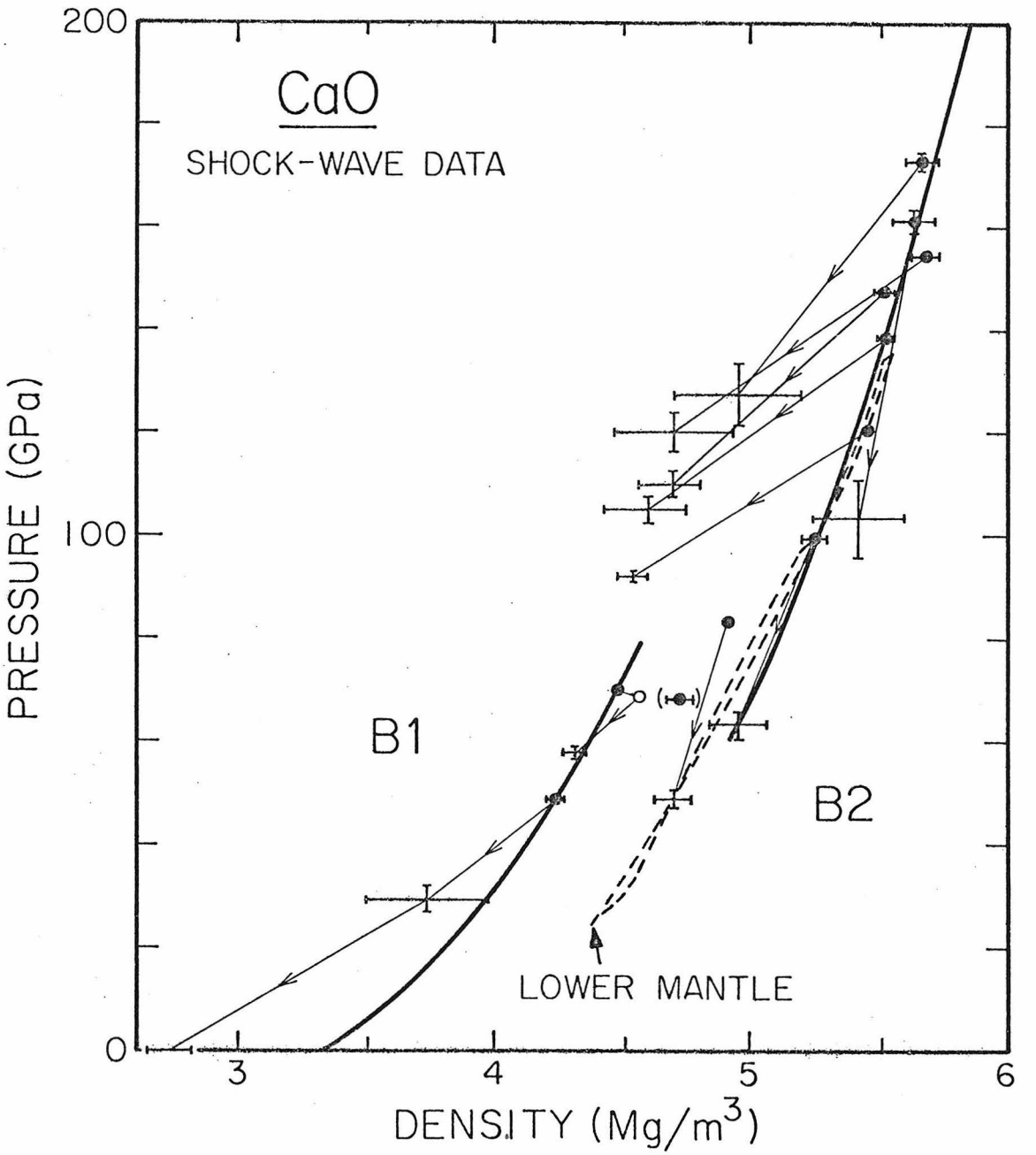
CaO
SHOCK-WAVE DATA
PRESSURE (GPa)
200
100
0
B1
B2
LOWER MANTLE
3
4
5
6
DENSITY (Mg/m3)

Fig. 4

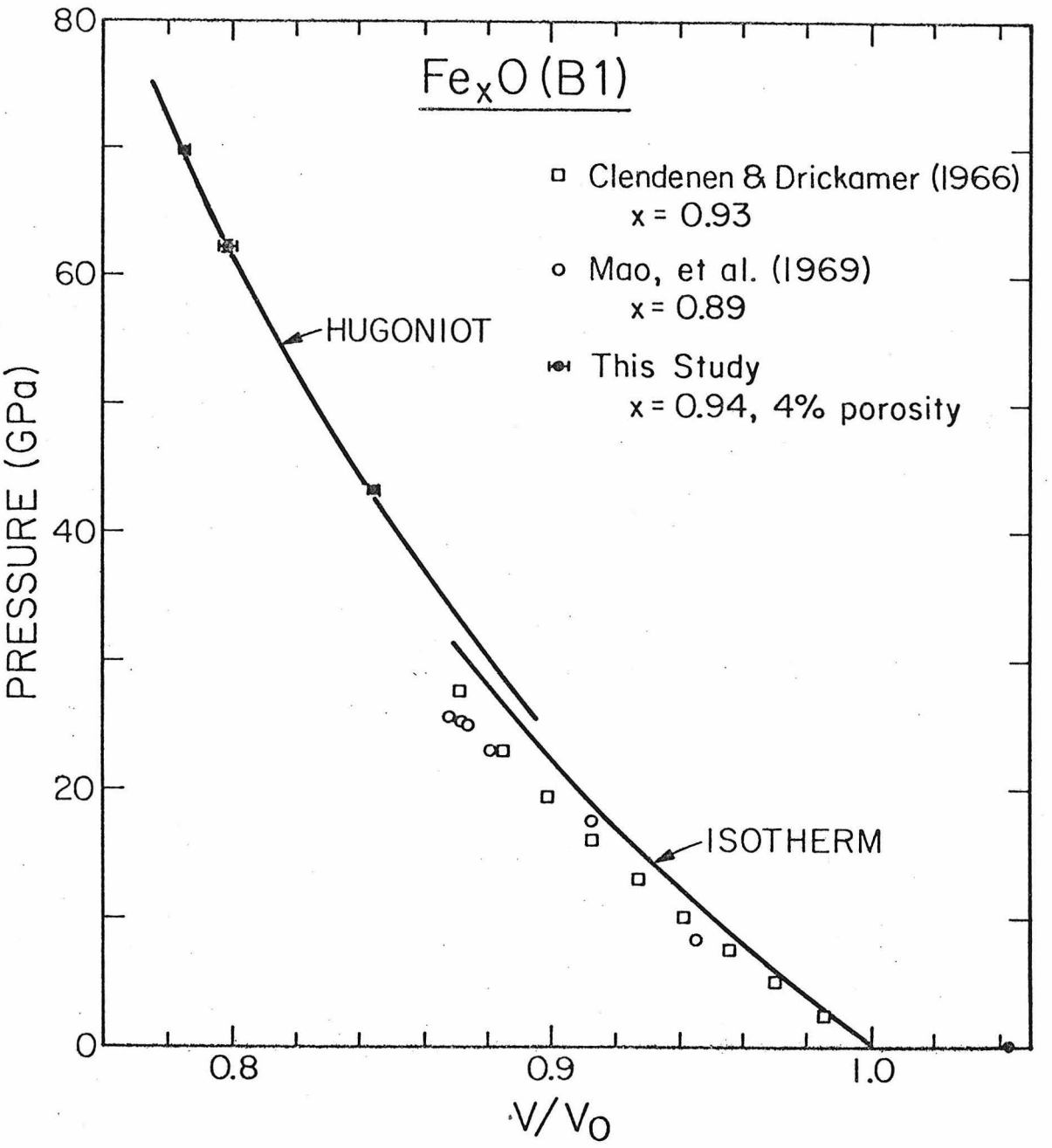
Fe_xO (B1)
Clendenen & Drickamer (1966)
x = 0.93
Mao, et al. (1969)
x = 0.89
This Study
x = 0.94, 4% porosity
HUGONIOT
ISOTHERM
PRESSURE (GPa)
V/V0
0
20
40
60
80
0.8
0.9
1.0

Fig. 5

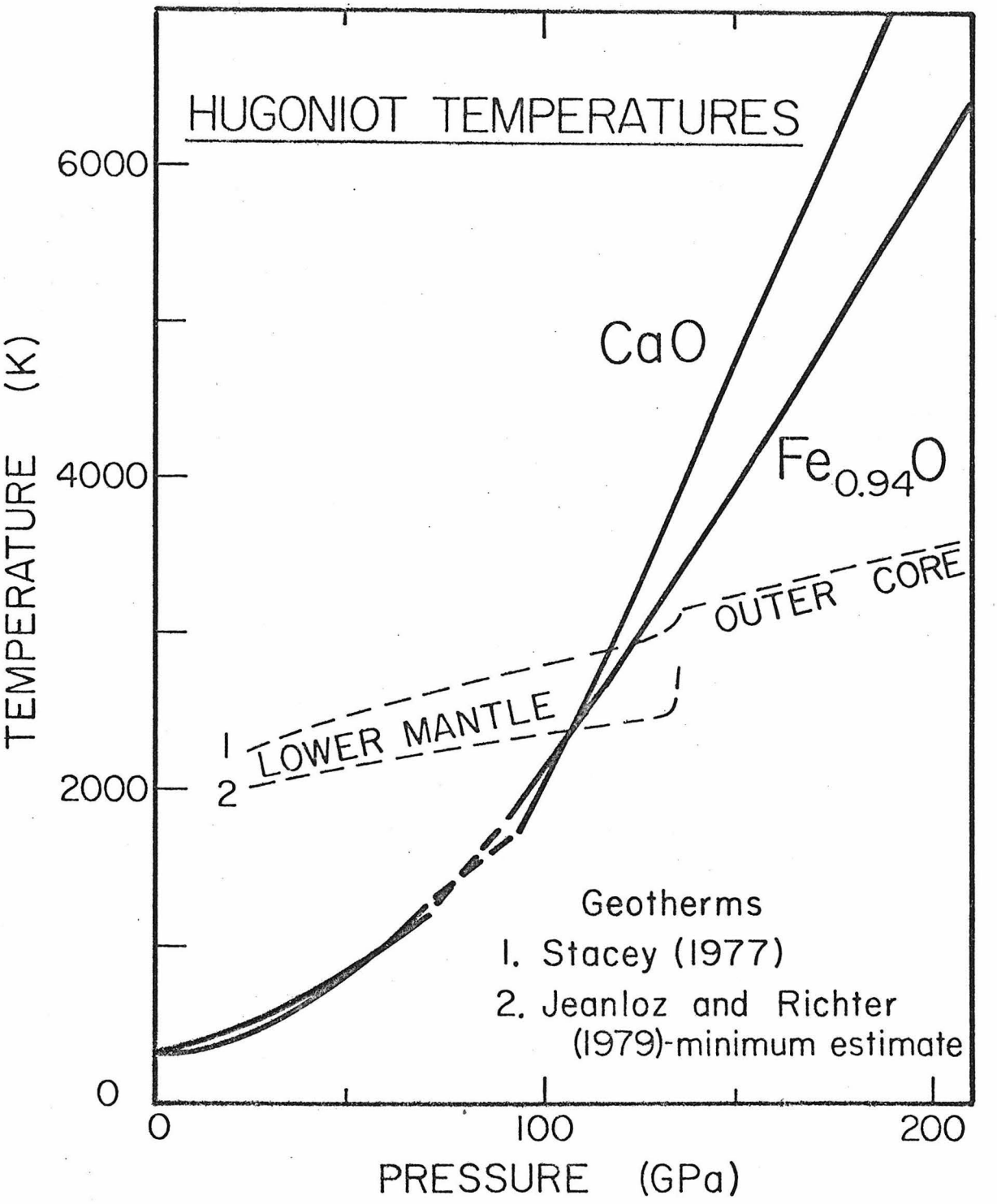
HUGONIOT TEMPERATURES
6000
4000
2000
0
TEMPERATURE (K)
CaO
$Fe_{0.94}O$
OUTER CORE
LOWER MANTLE
1
2
Geotherms
1. Stacey (1977)
2. Jeanloz and Richter (1979)-minimum estimate
0
100
200
PRESSURE (GPa)

Fig. 6

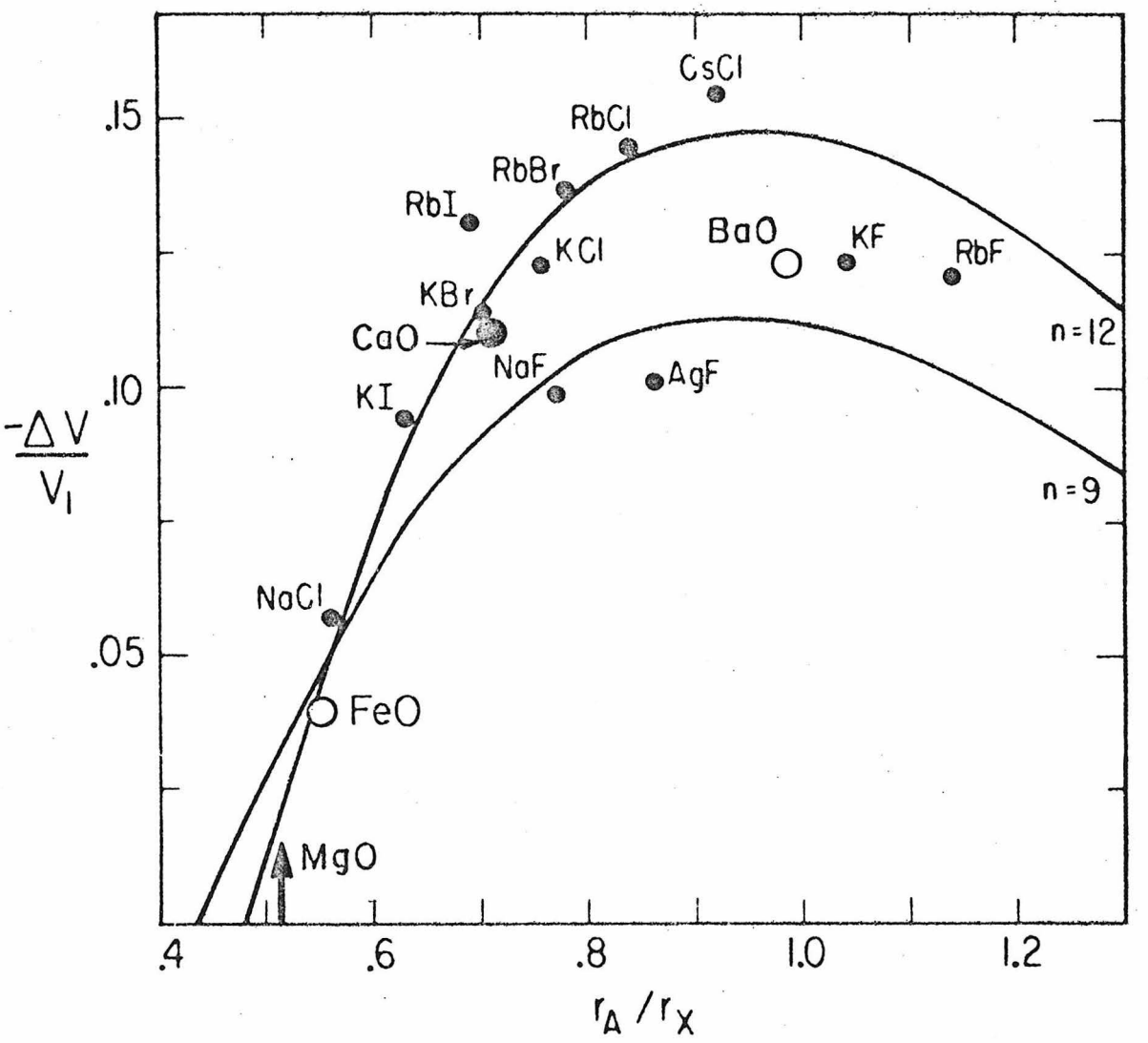
CsCl
RbCl
RbBr
RbI
KCl
BaO
KF
RbF
KBr
CaO
NaF
AgF
KI
NaCl
FeO
MgO
n=12
n=9
.15
.10
.05
-ΔV/V_I
.4
.6
.8
1.0
1.2
r_A / r_X

Fig. 7

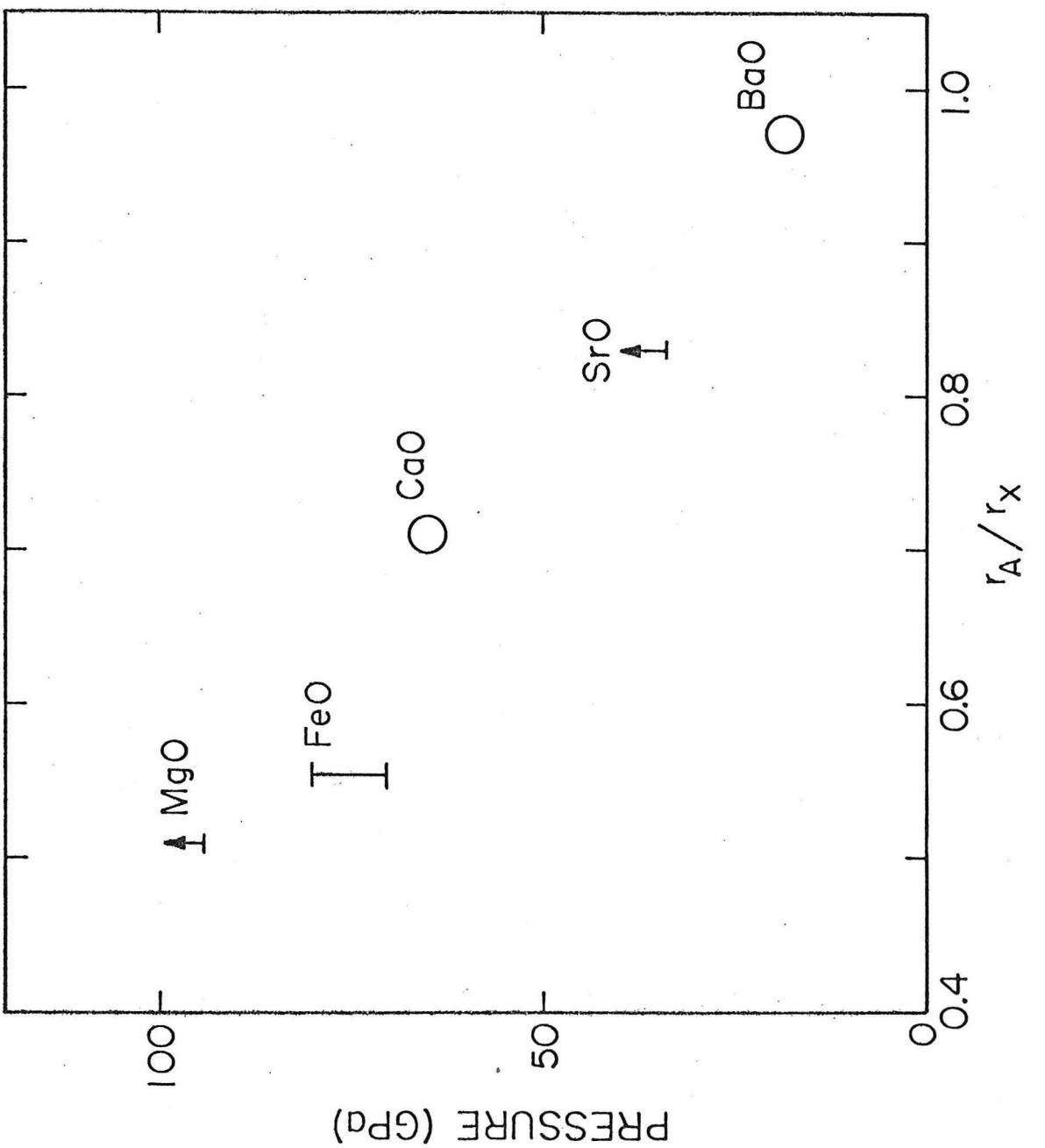

Fig 2

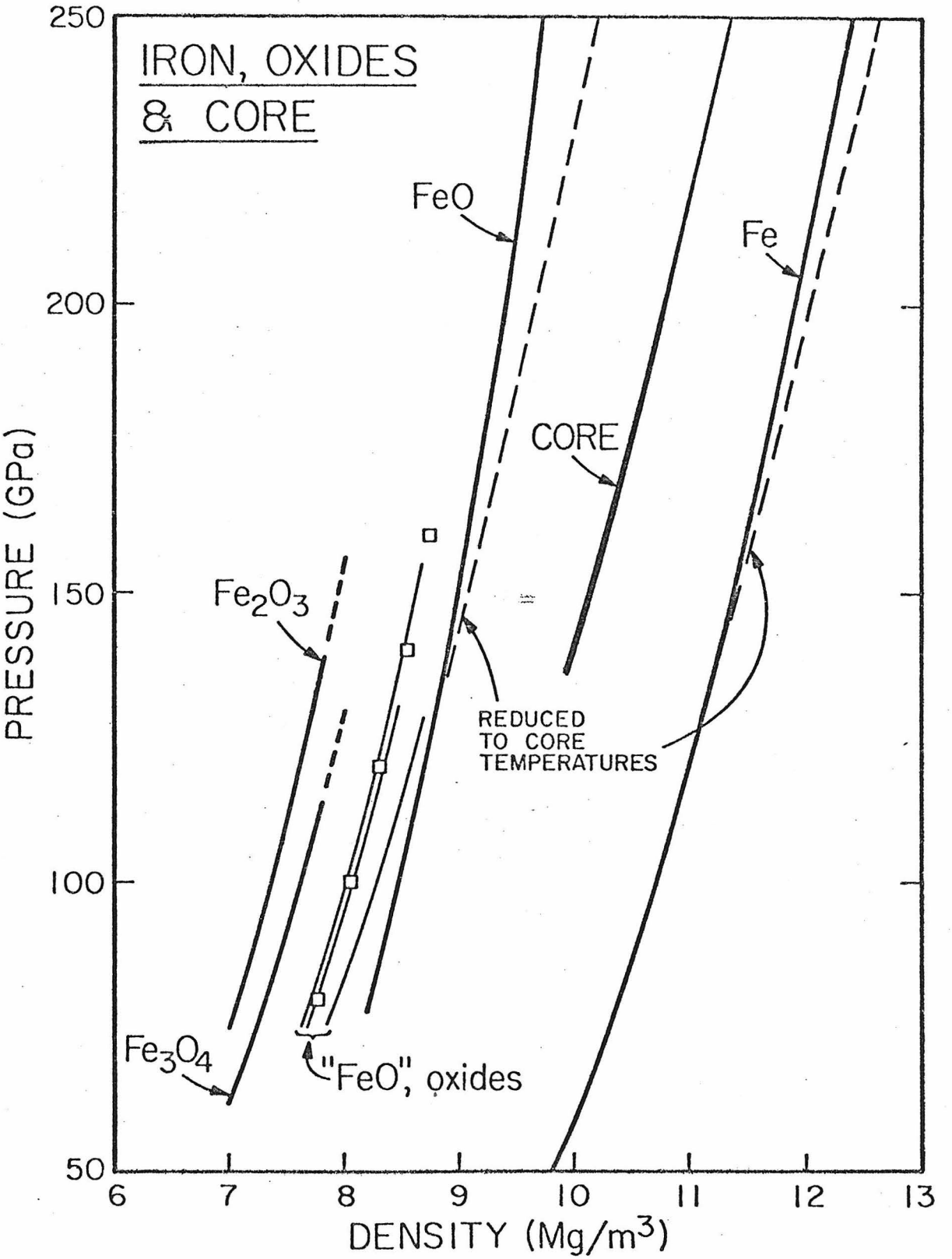
IRON, OXIDES
& CORE
FeO
Fe
CORE
Fe_2O_3
REDUCED
TO CORE
TEMPERATURES
Fe_3O_4
"FeO", oxides
PRESSURE (GPa)
DENSITY (Mg/m^3)
250
200
150
100
50
6
7
8
9
10
11
12
13

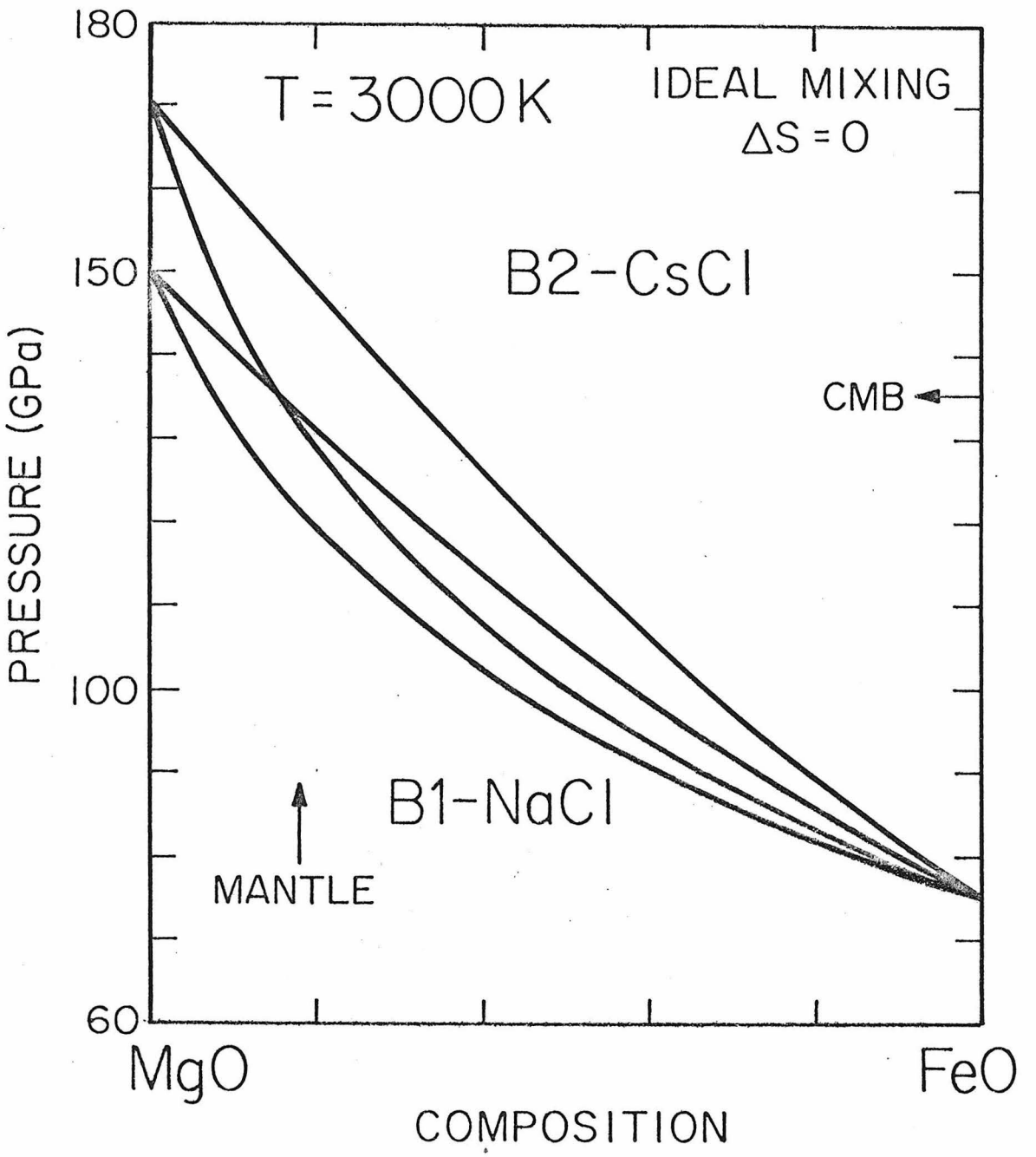
180
150
100
60
T = 3000 K
IDEAL MIXING
ΔS = 0
B2-CsCl
CMB
B1-NaCl
MANTLE
PRESSURE (GPa)
MgO
FeO
COMPOSITION

Chapter 4

RELEASE ADIABAT MEASUREMENTS ON MINERALS: THE EFFECT OF VISCOSITY

Abstract

The current inversion of pressure-particle velocity data for release from a high-pressure shock state to a pressure-density path usually depends critically upon the assumption that the release process is isentropic. It has been shown by Kieffer and Delaney that for geological materials below stresses of $\sim$150 GPa, the effective viscosity must be $\lesssim 10^3$ kg m^{-1} s^{-1} (10^4 poise) in order that the viscous (irreversible) work carried out on the material in the shock state remains small compared to the mechanical work recovered upon adiabatic rarefaction. The available data pertaining to the offset of the Rayleigh line from the Hugoniot for minerals, the magnitude of the shear stress in the high-pressure shock state for minerals and the direct measurements of the viscosities of several engineering materials shocked to pressures below 150 GPa yield effective viscosities of $\sim 10^3$ kg m^{-1} s^{-1} or less. We infer that this indicates that the conditions for isentropic release of minerals from shock states are achieved, at least approximately, and we conclude that the application of the Riemann integral to obtain pressure-density states along the release adiabats of minerals in shock experiments is valid.

Over the last decade an increasing number of measurements of dynmaic unloading from high pressure shock (Hugoniot) states have been reported for rocks and minerals, including porous samples and soils (Ahrens et al., 1969; Petersen et al., 1970; Lysen, 1970; Grady et al. 1974, 1976; Ahrens, 1975; Grady and Murri, 1976; Jeanloz and Ahrens, 1977, 1978; Jackson and Ahrens, 1979). The release-path measurements have been motivated by the information provided which is complementary to that given by Hugoniot data in constraining the high-pressure equation of state as well as the nature of yielding and apparent phase transformations under shock conditions. Upon unloading, variables such as particle velocity or pressure in the sample are measured, either discretely or continuously in time (Ahrens et al., 1969; Cowperthwaite and Williams, 1971; Grady, 1973; Seaman, 1974). These are usually converted to release paths in the pressure-density plane by way of the Riemann integral formulation which, however, is strictly valid only for isentropic (or isothermal) flows (e.g., Rice et al., 1958; Fowles and Williams, 1970; Lyzenga and Ahrens, 1978).

Recently Kieffer and Delaney (1979) have demonstrated how the non-dimensionalized expressions of Thompson (1972) for the conservation equations of a compressible, viscous fluid may be utilized to obtain criteria to determine whether the release processes from high pressure shock states in materials of geophysical interest are indeed isentropic. The object of the present note is both to clarify the derivation of these isentropic flow criteria and to point out how existing data, quite surprisingly, demonstrate that the effective viscosity of solids shocked to high pressures is sufficiently low that dynamic unloading

appears to be isentropic.

Isentropic flow is assumed in the Riemann integral formulation because the change in pressure (P) with density (ρ) is assumed to be given by the square of the isentropic bulk sound speed, $c^2 \equiv (\partial P/\partial \rho)_s$. Hence the appropriate criterion for isentropic flow upon decompression is that the change in pressure associated with a change in entropy is negligibly small in comparison with the isentropic change in pressure. Since the change in pressure in a volume element within the flow is given by

$$\frac{DP}{Dt} = c^2 \frac{D\rho}{Dt} + \left(\frac{\partial P}{\partial s}\right)_\rho \frac{Ds}{Dt} \quad , \tag{1}$$

with t being time, s being specific entropy and D denoting Lagrangian differentiation, the criterion for isentropic flow is:

$$\left| c^2 \frac{D\rho}{Dt} \right| >> \left|\left(\frac{\partial P}{\partial s}\right)_\rho \frac{Ds}{Dt}\right| \quad . \tag{2}$$

However, $\frac{D\rho}{Dt} = -\rho \underline{\nabla} \cdot \underline{u}$ from conservation of mass while the right hand side of (2) can be expanded by way of the following thermodynamic identity:

$$\left(\frac{\partial P}{\partial s}\right)_\rho = -\left(\frac{\partial \rho}{\partial T}\right)_P \left(\frac{\partial T}{\partial s}\right)_P c^2 \tag{3}$$

Hence (2) becomes

$$|\underline{\nabla}\cdot\underline{u}| >> \left|\frac{1}{\rho}\left(\frac{\partial \rho}{\partial T}\right)_P \left(\frac{\partial T}{\partial s}\right)_P \frac{Ds}{Dt}\right| \tag{2a}$$

where c^2 has been cancelled from both sides, $\underline{u}$ is the particle velocity vector field and T is temperature. We consider two sources of entropy production, namely those associated with mechanical dissipation and thermal dissipation (cf. Thompson, 1972, Eq. 2.1b):

$$\rho \frac{Ds}{Dt} = \frac{\Gamma}{T} - \frac{\nabla \cdot q}{T} \tag{4}$$

Here, Γ is the viscous dissipation function (units of energy/time) and $\underline{q}$ is the heat-flux vector. In principle, both bulk and shear viscosities enter into Γ, however, we will not differentiate between these but rather use an effective viscosity, η. We note that Eq. (4) does not account for any reactions (including phase transformations) which might occur in the flow, such processes requiring an extra set of terms involving the affinities of the components (eg., DeGroot and Mazur, 1969). Also, this equation does not apply to a discontinuous production of entropy, such as occurs across the shock front. Substituting (4) into (2a) and using the heat conduction equation (κ is the thermal diffusivity, which is assumed constant) yields

$$|\nabla \cdot \underline{u}| \gg \left| \frac{1}{\rho^2} \left(\frac{\partial \rho}{\partial T}\right)_P \left(\frac{\partial T}{\partial s}\right)_P \left[\frac{\Gamma}{T} + \rho C_p \frac{\kappa}{T} \nabla^2 T\right] \right| \tag{5}$$

For one-dimensional flow and non-negligible compression this reduces to

$$|\nabla \cdot \underline{u}| \sim |u_{,x}| \gg \left| \left(\frac{\partial V}{\partial T}\right)_P \frac{T}{C_P} \left[\frac{\Gamma}{T} + \rho C_p \frac{\kappa}{T} T_{,x,x}\right] \right| \tag{5a}$$

where subscript ,x indicates differentiation in the x direction, while V and C_P are the specific volume and specific heat at constant pressure,

respectively.

Following Thompson (1972, p. 140), Eq. 5a can be normalized in terms of a characteristic length (ℓ), particle velocity (u_o), volume (V_o), and temperature (T_o). With $X = x/\ell_o$ and $\Gamma_o = \eta u_o^2/\ell_o^2$ this becomes

$$\left|\frac{u_o}{\ell_o}\left(\frac{u}{u_o}\right)_{,X}\right| >> \left|\left(\frac{\partial V}{\partial T}\right)_P \frac{T}{C_P}\left\{\frac{\eta u_o^2}{\ell_o^2 T}\left(\frac{\Gamma}{\Gamma_o}\right)+\frac{\kappa}{T}\rho C_p \frac{T_o}{\ell_o^2}\left(\frac{T}{T_o}\right)_{,x,x}\right\}\right| \quad (6)$$

and rearranging terms yields

$$\left|\left(\frac{u}{u_o}\right)_{,X}\right| >> \left|\left(\frac{\eta V_o}{u_o \ell_o}\right)\frac{T_o}{V_o}\left(\frac{\partial V}{\partial T}\right)_p\left\{\frac{u_o^2}{C_P T_o}\left(\frac{\Gamma}{\Gamma_o}\right)+\frac{\kappa\rho}{\eta}\left(\frac{T}{T_o}\right)_{,X,X}\right\}\right| \quad (7)$$

Because the normalized variables $(u/u_o)_{,X}$ (Γ/Γ_o), and $(T/T_o)_{,X,X}$ have values near unity (see Thompson, 1972; Kieffer and Delaney, 1979) Eq. 7 may be rewritten as

$$1 >> \left|\frac{1}{Re_o} T_o \alpha \left\{\frac{u_o^2}{C_P T_o}+\frac{1}{Pr}\right\}\right|$$

where $(u_o \ell_o / V_o \eta)$ is the Reynolds number Re_o, α is the coefficient of thermal expansion and $Pr = \dfrac{\eta}{\kappa\rho}$ is the Prandtl number. As Kieffer and Delaney (1979) pointed out, at temperatures of geophysical interest $\alpha T_o \simeq 0.1$ for shocked minerals and liquids and the inequality of (8) reduces to the two inequalities

$$\left|\frac{\kappa}{u_o \ell_o}\right| << 10 \quad (9a)$$

$$\left|\frac{\eta}{\rho_o u_o \ell_o}\frac{u_o^2}{C_P T_o}\right| << 10 \quad (9b)$$

which are identical to their Eq. 17a and 17b. For shock waves in

rocks and minerals the density is on the order of 5 Mg/m^{-3}, characteristic particle velocities are on the order of 10^3 m s^{-1}, while C_p and κ are very nearly 10^3 J kg^{-1} K^{-1} and 10^{-6} m^2 s^{-1} respectively. The rise time of shock fronts provide a lower bound for ℓ_o, and hence conservative bounds for the inequalities, of about 10^{-5} m (Grady, 1977). The thermal inequality given by equation 9(a) is easily satisfied since the left hand side is of magnitude $\sim 10^{-4}$. Hence heat flow contributes negligibly to entropy production and release from the Hugoniot state is clearly adiabatic, as is commonly assumed.

On the other hand, the left hand side of equation 9(b) requires an effective viscosity $\eta \lesssim 10^3$ kg m^{-1} s^{-1} (10^4 poise) for flow behind a shock wave to be isentropic (Kieffer and Delaney, 1979; T_o is of order 10^3 K). What then is the viscosity in the material behind a shock front in a solid? Duvall (1962) suggested, in a rather simple argument, that the thickness of a stable transition zone from the unshocked to the shocked state (ΔX) is related to the difference at constant volume between the Rayleigh line and a static (equilibrium) curve lying near the Hugoniot, ΔP_V (see Figures 1 and 2). Thus ΔX is determined by the effective viscosity η times the ratio of the pressure jump, P, to the maximum pressure gradient along the front (given by the maximum value of $\rho_o U_S \Delta P_V$, where U_S is the shock wave velocity):

$$\Delta X = \frac{\eta P}{\rho_o U_S \Delta P_V)_{max}} = \eta \frac{u_o}{\Delta P_V)_{max}} \qquad (12)$$

This means that as the viscosity increases the rise time of the shock increases, as is expected. For shock fronts in silicates $\Delta X \simeq 10^{-4}$ m while $\Delta P_V/P$ is of order 10^{-1} (or less) in the 10 to 100 GPa range.

Appropriate values of $\rho_o U_S \sim 10^7$ kg m^{-2} s^{-1} and therefore $\eta \simeq 10^3$ kg m^{-1} s^{-1} is a conservative estimate from Eq. 12.

We note that this approach is analogous to the simple dimensional argument that the effective viscosity is given by the ratio of the deviatoric stress (σ) to the strain rate ($\dot{\varepsilon}$). Approximating the strain by

$$\dot{\varepsilon} \sim \frac{1}{\tau} \frac{\Delta V}{V} = \frac{U_S}{\Delta X} \frac{\Delta V}{V} \qquad (13)$$

where τ is the rise time of the shock and $\frac{\Delta V}{V}$ is the compression, we arrive at a value of $\dot{\varepsilon} \sim 10^8$ s^{-1}. In virtually all silicates and in many oxides the stress difference between the Hugoniot and the hydrostatic compression curve appears to be quite small at pressures in the 10-100 GPa range. For example in the case of quartz, this difference amounts to no more than 100 MPa at 10GPa (Ahrens and Linde, 1968), while Ahrens et al. (1968) found a stress difference as large as about 3 GPa in polycrystalline corundum. Identifying these stress differences with σ, we arrive at effective viscosities $\eta \sim \sigma \dot{\varepsilon} < 10^2$ kg m^{-1} s^{-1}. This conclusion is corroborated by recent rise-time measurements in metals using velocity-interferometer techniques (Chhabildas and Asay, 1979). We therefore conclude, on the basis of arguments such as those presented by Duvall (1962), that the effective viscosities of silicates and oxides appear to be low enough under shock conditions to satisfy the criteria for isentropic flow during release. It is also worth noting that the nature of the shock front is likely to reflect the properties of the material at high pressure behind the front. For a steady shock, any perturbation behind the front is communicated forward toward the shock front, and overtakes the shock front, in the laboratory

reference frame, at a speed u+c where c is the local sound speed. Since u+c > U_S, the shock and particle velocity reflect the properties of the material encompassed by the shock (Duvall, 1978) and estimates of the viscosity from the rise time of the front should approximately correspond to the effective viscosity in the shocked state (cf. Chhabildas and Asay, 1979).

Probably the most conclusive evidence that the effective viscosity behind shock fronts in such solids as Al, Pb, Fe and NaCl is low, in the range 10^3 to 10^4 kg m^{-1} s^{-1}, are the experiments of Sakharov et al. (1965) and more recently Mineev and Savinov (1967) at shock pressures ranging from ∿12 to 250 GPa. In these experiments the decay of perturbations to the shock front induced by impact of an explosively driven, sinusoidally corrugated piston into the sample material have demonstrated that virtually all of these materials have similar effective viscosities. Moreover, experiments carried out by independent techniques on mercury and water (Mineev and Zaidel, 1968; Al'tshuler et al., 1977) demonstrate that the substances have comparable viscosities, ∿10^3 kg m^{-1} s^{-1}, in the 4 to 44 GPa range. Also studies of jet formation during oblique impact of several metals by Godunov and colleagues (1971, 1974, 1975) imply similarly low viscosities for several metals at strain rates achieved upon shock-loading. These results independently suggest that silicates may likewise have low, fluid-like viscosities under shock.

Finally, we note that the sound speed measurements of Grady et al. (1975) indicate velocities in quartz shocked to 22 to 35 GPa which are well below the longitudinal velocity but consistent with velocities

expected for a fluidlike mixture of quartz and stishovite. Similar results were obtained for feldspar shocked to pressures of 46 GPa, and Grady et al. (1975) infer from these anomalously low sound speeds that these minerals contain very hot and probably liquid zones (see also Grady, 1977). This again suggests that the effective viscosity of silicates under shock conditions may be quite low. We note, however, that alternative interpretations can be found to explain the reduced sound speeds. For example, these may be ascribed to a modulus defect associated with dispersion and due to an unknown absorption mechanism (eg. Nowick and Berry, 1972; Thompson, 1972); this would actually imply increased viscosities. Phase transformations are not involved in reducing the sound speeds, however, since both corundum and periclase exhibit such reduced velocities under shock while undergoing no phase changes (Bless and Ahrens, 1976; Grady, 1977).

We conclude, on the basis of several lines of evidence, that the effective viscosity in shocked oxides and silicates is probably very low compard to unshocked materials, perhaps as low as 10^3 kg m^{-1} s^{-1} or less. Such low values may represent a purely transient effect or may be the result of massive dynamic yielding, among other processes. Godunov et al. (1974) present a simple, phenomenological model which yields the observed low viscosities at the high strain rates achieved in shock. Although direct measurements of the viscosity of silicates and oxides in the shocked state have yet to be carried out we conclude that the viscous inequality Eq. 9(a) is satisfied and that the rarefaction process described by release adiabats from the shock state is nearly isentropic (see also Chhabildas and Asay, 1979). The major assumptions

in our analysis arise from our neglecting the effects of dissipation due to reactions and our not distinguishing between bulk and shear viscous dissipation, however our result justifies the use of the Riemann integral formulation which converts pressure-particle velocity states to pressure-density states along the release adiabat (Rice et al., 1958; Ahrens et al., 1969; Grady, 1977; Lyzenga and Ahrens, 1978). Thus the additional data inferred from such release adiabat measurements provide valid, and in most cases, useful constraints on the equations of state of minerals.

ACKNOWLEDGEMENTS

We appreciate having received a preprint of the Kieffer and Delaney paper, and are particularly indebted to D. E. Grady as well as D. L. Anderson and S. W. Kieffer for their helpful comments.

REFERENCES

Ahrens, T.J., Compaction by impact of unconsolidated lunar fines, The Moon, 14, 291-299, 1975.

Ahrens, T. J., W. H. Gust and E. B. Royce, Material strength effect on the shock compression of alumina, J. Appl. Phys., 39, 4610-4616, 1968.

Ahrens, T.J. and R. K. Linde, Response of brittle solids to shock compression, in Behavior of Dense Media Under High Dynamic Pressures, J. Berger (ed.) Gordon and Breach, New York, 325-336, 1968.

Ahrens, T. J., C. F. Peterson, and J. T. Rosenberg, Shock compression of feldspars, J. Geophys. Res., 74, 2727-2746, 1969.

Al'tshuler, L. V., G. I. Kanel' and B. S. Chekin, New measurements of the viscosity of water behind a shock wave front, Soviet Phys. JETP, 45, 348-350, 1977.

Bless, S. J. and T. J. Ahrens, Measurement of release wave speed in shock-compressed polycrystalline alumina and aluminum, J. Geophys. Res., 81, 1935-1942, 1976.

Chhabildas, L. C. and J. R. Asay, Rise-time measurements of shock transitions in aluminum, copper and steel, J. Appl. Phys., 50, 2749-2756.

Cowperthwaite, M. and R. F. Williams, Determination of constitutive relationships with multiple gauges in nondivergent waves, J. Appl. Phys., 42, 456-462, 1971.

DeGroot, S. R. and P. Mazur, Non-Equilibrium Thermodynamics, North-Holland Publ. Co., Amsterdam, 510 pp., 1969.

Duvall, G. E., Concepts of shock wave propagation, Bull. Seism. Soc. Am., 52, 869-893, 1962.

Duvall, G. E., Maxwell-like relations in condensed materials. Decay of shock waves, Iranian J. Sci. and Tech., 7, 57-69, 1978.

Fowles, R. and R. F. Williams, Plane stress wave propagation in solids J. Appl. Phys., 41, 360-363, 1970.

Godunov, S. K., A. A. Deribas, I. D. Zakharenko and V. I. Mali, Investigation of the viscosity of metals in high-velocity collisions, Combusion, Explosion and Shock Waves, 7, 114-118, 1971.

Godunov, S. K., A. F. Demchuk, N. S. Kozin and V. I. Mali, Interpolation formulas for Maxwell viscosity of certain metals as a function of shear-strain intensity and temperature, J. Appl. Mech. Tech. Phys., 15, 526-529, 1974.

Godunov, S. K., A. A. Deribas and V. I. Mali, Influence of material viscosity on the jet formation process during collisions of metal plates, Combustion, Explosion and Shock Waves, 11, 1-13, 1975.

Grady, D. E., Experimental analysis of alternating wave propagation, J. Geophys. Res., 78, 1299-1308, 1973.

Grady, D. E., W. J. Murri and G. R. Fowles, Quartz to stishovite: Wave propagation in the mixed phase region, J. Geophys. Res., 79, 332-338, 1974.

Grady, D. E., W. J. Murri and P. S. DeCarli, Hugoniot sound velocities and phase transformation in two silicates, J. Geophys. Res., 80, 4857-4861, 1975.

Grady, D. E. and W. J. Murri, Dynamic unloading in shock compressed feldspar, Geophys. Res. Lett., 3, 472-474, 1976.

Grady, D. E., Processes occurring in shock-wave compression of rocks and minerals, in High-Pressure Research: Applications to Geophysics, M.H. Manghnani and S. Akimoto (eds.) Academic Press, N.Y., 389-438, 1977.

Jackson, I. and T. J. Ahrens, Shock wave compressions of single crystal forsterite, J. Geophys. Res., 84, 3039-3048, 1979.

Jeanloz, R. and T. J. Ahrens, Pyroxenes and olivines: Structural implications of shock-wave data for high pressure phases, in High-Pressure Research: Applications to Geophysics, M. Manghnani and S. Akimoto (eds.) Academic Press, New York, 439-462, 1977.

Jeanloz, R. and T. J. Ahrens, The equation of state of a lunar anorthosite: 60025, Proc. Lunar Planet. Sci. Conf. 9th, 2789-4803, 1978.

Kieffer, S. W. and J. M. Delany, Isentropic decompression of fluids from crustal and mantle pressures, J. Geophys. Res., 84, 1611-1620, 1979.

Lysne, P. C., A comparison of calculated and measured low-stress Hugoniots and release adiabats of dry and water-saturated tuff, J. Geophys. Res., 75, 4375-4386, 1970.

Lyzenga, G. and T. J.Ahrens, The relations between the shock-induced free-surface velocity and post-shock density of solids, J. Appl. Phys., 49, 201-204, 1977.

McQueen, R. G., S. P. Marsh and J. N. Fritz, Hugoniot equation of state of twelve rocks, J. Geophys. Res., 72, 4999-5036, 1967.

Mineev, V. N., and E. V. Savinov, Viscosity and melting point of aluminum, lead and sodium chloride subjected to shock compression, Sov. Phys. JETP, 25, 411-415, 1967.

Nowick, A. S. and B. S. Berry, Anelastic Relaxation in Crystalline Solids, Academic Press, New York, 677 pp., 1972.

Petersen, C. F., W. T. Murri and M. Cowperthwaite, Hugoniot and release adiabat measurements for selected geological materials, J. Geophys. Res., 75, 2063-2072, 1970.

Rice, M. H., R. G. McQueen and J. M. Walsh, Compression of solids by strong shock waves, Solid State Phys., 6, 1-63, 1958.

Sakharov, A. D., R. M. Zaidel', V. N. Mineev and A. G. Oleinik, Experimental investigations of the stability of shock waves and the mechanical properties of substances at high pressures and temperatures, Soviet Physics-Doklady, 91, 1091-1094, 1965.

Seaman, L., Langrangian analysis for multiple stress or velocity gages, in attenuating waves, J. Appl. Phys., 45, 4303-4314, 1974.

Thompson, P. A., Compressible Fluid Dynamics, McGraw-Hill Book Co., New York, 665 pp., 1972.

Figure Captions:

Figure 1: Relation of Hugoniot state (P, V) and thermodynamic path (Rayleigh line) to Rankine-Hugoniot curve. The pressure difference $(\Delta P_V)_{max}$ is considered a measure of the effective viscosity at the shock front.

Figure 2: Shock wave profile with finite-width, ΔX, resulting from intrinsic material viscosity, η, at the shock front.

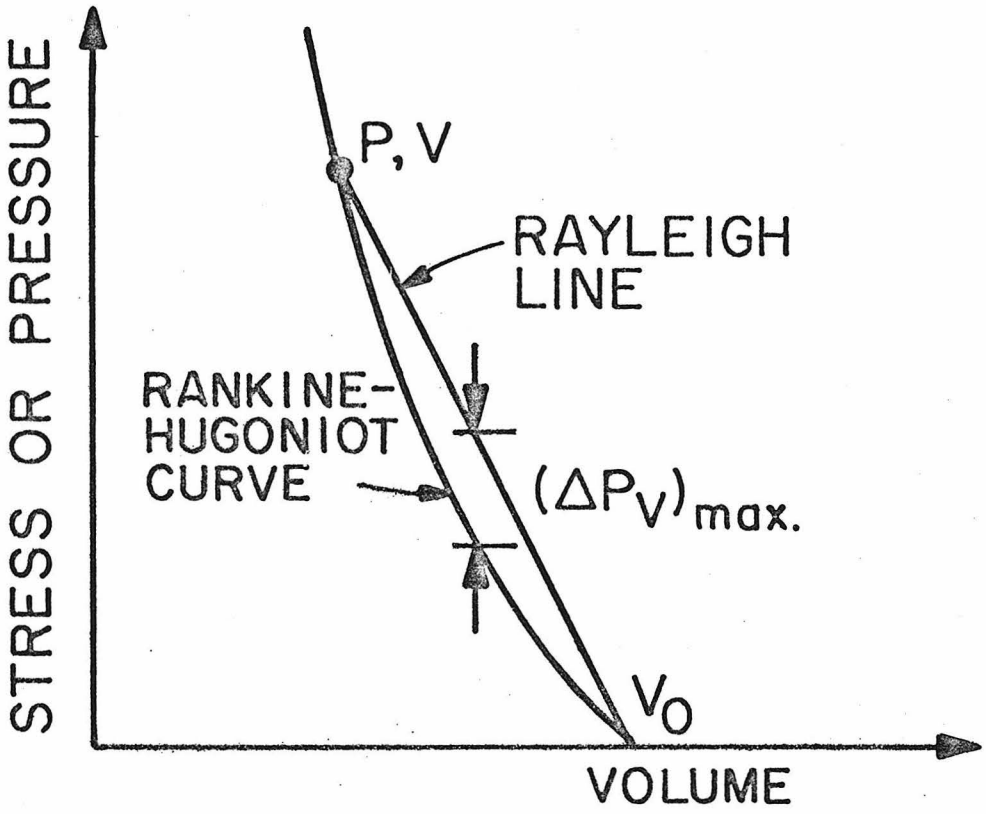
STRESS OR PRESSURE
P, V
RAYLEIGH LINE
RANKINE-HUGONIOT CURVE
$(\Delta P_V)_{max.}$
V_0
VOLUME

Figure 1

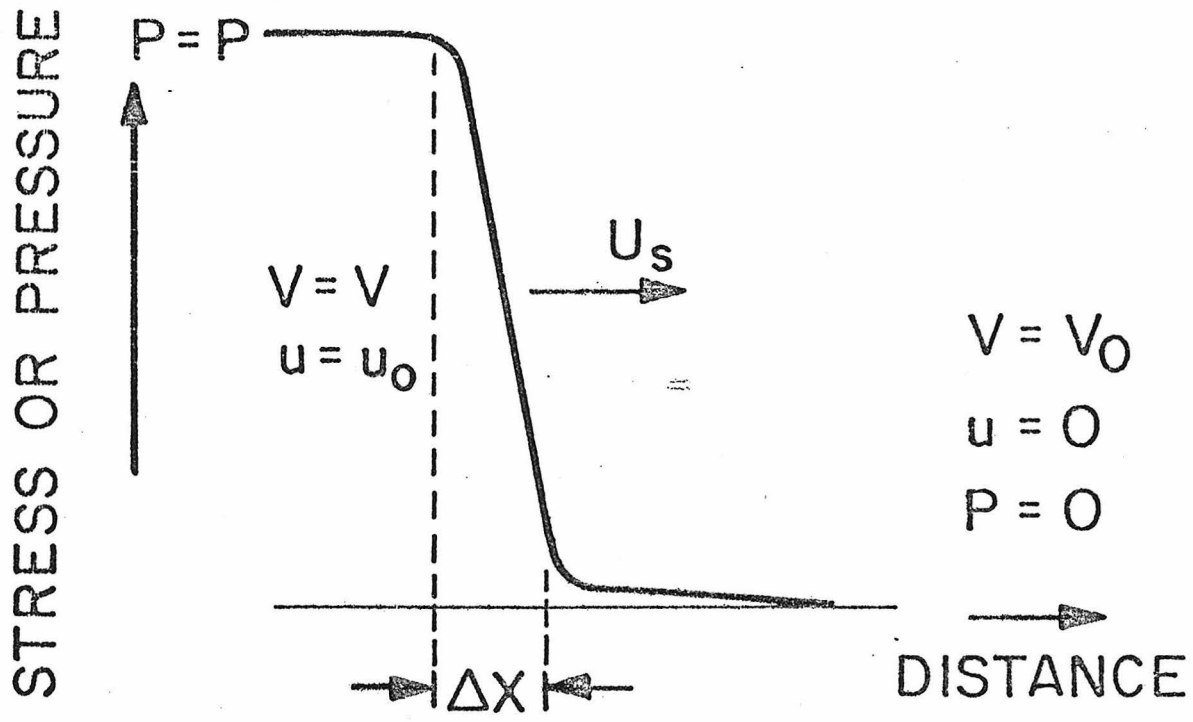

Figure 2

Chapter 5

PROPERTIES OF IRON AT HIGH PRESSURES AND THE STATE OF THE CORE

Abstract

Shock-wave (Hugoniot) data for initially porous and nonporous samples of iron are inverted to yield values of the Grüneisen parameter (γ), adiabatic bulk modulus (K_s) and coefficient of thermal expansion (α) along the Hugoniot to pressure of about 150 GPa (1.5 Mbar). This represents the first reliable estimate of thermal properties (e.g., α) to such high pressures based directly on experimental data. The values of γ fit the conventional function $\gamma = \gamma_0(V/V_0)^n$ but with n significantly larger than 1, while extrapolation formulas suggested to date for α appear not to provide the best fit to the data. The present analysis yields values of γ between about 1.4 and 1.0 (essentially temperature independent) and α between about 1.0 and 0.4 x 10^{-5} K^{-1} throughout the earth's core, therefore implying that simple dynamical models of the core are quite viable. These results provide experimental confirmation of the Vaschenko-Zubarev/Irvine-Stacey (or "free-volume") formulation for γ of iron at high pressures, as well as support for Stacey's recent model of the thermal state of the core. The data on density, sound speed and bulk modulus of iron are extrapolated and corrected to pressures and temperatures existing throughout the earth's core, and compared with current seismological information. This leads

to the following conclusions: (i) both densities and bulk moduli in the outer core are less than those of Fe under equivalent conditions (by about 10% and 12%, respectively); but (ii) their gradients through the outer core are consistent with gross chemical homogeneity (i.e., uniform intermixing of Fe and a lighter, more compressible element or compound); (iii) both densities and bulk moduli for the inner core are compatible with those of iron, suggesting that (iv) the inner core-outer core boundary is likely to be a compositional as well as a phase boundary. Assuming that the outer core consists of Fe and a lighter element or compound, X, the constraints on density, bulk modulus and mass fraction of X which must be simultaneously satisfied are given.

INTRODUCTION

It has long been recognized from seismological evidence that the bulk of the earth's core has a density slightly less than that of iron under equivalent conditions [Birch, 1952, 1964]. This has been interpreted as indicating that the core most likely consists mainly of iron, intermixed with a lighter element. Further information about the nature of the core is less well constrained, however, and although its static (e.g., compressional) properties are reasonably well understood (mainly from shock-wave data on iron and closely related compounds), its thermal and dynamic properties have been particularly difficult to establish. Rather complete thermodynamic models do exist for the core [e.g., Stacey, 1977a] but these have not, as yet, been tested against any experimental data at the appropriate conditions.

The purpose of this paper is to show that such data are available in the form of shock-wave (Hugoniot) measurements on initially porous samples. Although such data have been presented and analysed to a certain degree [for example, Al'tshuler et al., 1958; McQueen et al., 1970; also Birch, 1972; Jamieson et al., 1979], I believe that they have not been fully appreciated for the geophysical information which they provide. Whereas shock-wave measurements have mainly been used to constrain static properties, the present analysis is intended to demonstrate that such measurements can also provide important information on the thermal properties of materials at extremely high pressures and temperatures.

The present analysis of Hugoniot data on initally porous samples extends that of McQueen et al., [1970], yielding measurements of the high-temperature, high-pressure Grüneisen parameter (γ), adiabatic bulk modulus (K_S), and coefficient of thermal expansion (α) along the Hugoniot of iron. These can then be compared with:

(i) the seismological properties observed for the core [e.g., Dziewonski et al., 1975; Anderson and Hart, 1976];

(ii) the thermal state inferred for the core [e.g., Stacey, 1977a]; and

(iii) current high-pressure equation-of-state models for iron [e.g., Al'tshuler et al., 1960; McQueen et al., 1970].

The properties of the core are quite similar to those inferred from the data on iron in the present study, consistent with the widely held hypothesis that iron is the dominant component of the core.

However, significant differences are evident between the measured properties of iron and those of the core and it is these differences which can help to constrain the nature of the lighter "alloying" element in the core.

ANALYSIS OF POROUS HUGONIOT DATA

Shock-wave data yield measurements of thermal properties at high pressures and temperatures by way of the Grüneisen parameter

$$\gamma = V \left(\frac{\partial P}{\partial E}\right)_V \qquad (1)$$

which can be calculated from a comparison of the measured pressure (P)-volume (V)-internal energy (E) Hugoniot states of a porous material and its nonporous equivalent at constant volume [e.g., Al'tshuler et al., 1958; Kormer et al., 1962; McQueen et al., 1970; Carter et al., 1971]. The γ obtained in this manner from the data of McQueen et al. [1970] on iron are shown as a function of density in Figure 1a.

For this analysis, the nonporous shock-wave data were fit by an empirical relation (quadratic shock-velocity, U_S, vs. particle-velocity, u_P, dependency) defining a reference Hugoniot. Each Hugoniot state for an intially porous sample was then compared for its offset (thermal pressure) at that volume with this reference equation-of-state. The appropriate equations are

$$\gamma(V) = V \frac{2(P_1 - P_0)}{P_1(V_{01} - V) - P_0(V_{00} - V)} \tag{2a}$$

$$P_0(V) = (2s_0'^2 \eta_0^3 V_{00})^{-1}$$

$$\times \{(1-\eta_0 s_0)^2 - 2s_0' c_0^0 \eta_0^2 - (1-\eta_0 s_0)\left[(1-\eta_0 s_0)^2 - 4s_0' c_0^0 \eta_0^2\right]^{1/2}\} \tag{2b}$$

$$\eta = \frac{V_0 - V}{V_0} \neq 0 \tag{2c}$$

where $U_S^0 = c_0^0 + s_0 u_P^0 + s_0' (u_P^0)^2$ $(s_0' \neq 0)$, $V_0 = 1/\rho_0$ is the initial volume, and the 0 and 1 indices are for nonporous (reference) and porous (offset) Hugoniots, respectively. The resultant γ's do not depend on the nature of the fit to the nonporous Hugoniot data and they are in complete agreement with the γ's calculated by McQueen et al. [1970].

The scatter in the values of γ shown in Figure 1a is largely due to the lower experimental precision of the Hugoniot data for the porous samples, and this scatter could, in principle, be avoided by using empirical fits to the porous data as well. This procedure results in smooth $\gamma(V)$ curves which, however, are strongly dependent on the form of the equation used to fit the porous data, thus yielding a spurious precision. Therefore, the present analysis is based on the raw data as shown in Figure 1a.

Two effects require particular attention in order to avoid complications: those of incomplete compaction and of phase transformation. The low density (or low pressure) values of γ are subject to a large and systematic error due to the fact that incomplete compaction of the porous samples at low shock stresses results in an offset of the Hugoniots which is not due to thermal pressure [Lysne and Halpin, 1968; Neal, 1976]. Therefore, the lowest pressure Hugoniot data for porous samples are not included in this study and the following (somewhat arbitrary) lower limits were used for Hugoniot densities and porous samples: 9.50 Mg/m^3 (ρ_0 = 6.97 Mg/m^3), 8.75 Mg/m^3 (ρ_0 = 6.00 Mg/m^3), 8.50 Mg/m^3 (ρ_0 = 4.77 Mg/m^3). These limits could be increased for a more conservative analysis. The highest porosity data (ρ_0 = 3.38 Mg/m^3) were treated separately, as discussed below.

It is worth noting that the results for γ at highest pressures are intrinsically of higher precision than those at lower pressures, not only because the effects of incomplete compaction are then negligible, but also because the ratio $\Delta P/\Delta E$ is much more tightly constrained by the Hugoniot data [see also Neal, 1976].

Furthermore, the data at densities lower than 9.50 Mg/m^3 are based on an extrapolation of the reference Hugoniot downward from 40 GPa. Below about 9.00 Mg/m^3, the measured Hugoniot of iron represents states partially transformed between the α and ε phases [Andrews, 1973; Barker and Hollenbach, 1974]. Thus between 8.6 Mg/m^3 and 9.2 Mg/m^3, the γ's shown in Figure 1a depend on the Hugoniot data and extrapolation which are used to constrain the reference Hugoniot, making these values

of the Grüneisen parameter somewhat less reliable than those at higher densities. The Hugoniot parameters (c_0, s, s') of McQueen et al. [1970] were used (rather than the least squares fit: c_0 = 3.718 (±0.081), s = 1.781 (±0.077), s' = 0.040 (±0.017)) because they represent a reasonable compromise at densities below 9.2 Mg/m^3 while giving a good fit at higher densities.

Iron is known to undergo only one solid-solid phase transformation under shock loading to several hundred GPa: α (bcc) → ε (hcp) at about 13 GPa [Bancroft et al., 1956, McQueen et al., 1970; Barker and Hollenbach, 1974]. All of the data used here are from pressures above 13 GPa and at densities greater than the ρ_0 = 8.31 (±0.07) Mg/m^3 for ε-Fe [Mao et al., 1967]. Therefore, this analysis (excluding the ρ_0 = 3.38 Mg/m^3 data) essentially reflects the properties of ε-Fe at high pressures and temperatures. It is also worth mentioning that the α→ε transformation is considered to be a ferromagnetic → paramagnetic transition under shock [cf., Keeler and Royce, 1971; Andrews, 1973; Wasilewski, 1976] and therefore magnetic contributions to the properties of iron at high pressures need not be separately considered.

It is likely that melting occurs in the samples shock-loaded to high stresses (particularly the porous samples), however the effects of melting are completely negligible for this study. At the high-pressures considered here solid and melt have very similar densities and internal energies at a given pressure. This conclusion is based both on experimental and theoretical grounds; melting is essentially unobservable within the few percent accuracy of P-V Hugoniot data

[Kormer et al., 1965; Urlin, 1966; McQueen et al., 1971]. Also, there is abundant evidence that the volume change on melting decreases to a small (but finite) value at high pressures [Bridgman, 1931; Ross and Alder, 1966; Stishov, 1969]. In any case, the change in volume on melting is known to be only about 3% at low pressures [δ-Fe to liquid: Strong, 1959; Sterrett et al., 1965], while Liu [1975] calculated an upper limit of about 5% at 94 GPa (ε-Fe to liquid) based on his high pressure data. Stacey [1977b] has also concluded that the effects of melting can be ignored at pressures relevant to the core, as have Birch [1972] and Irvine and Stacey [1975].

The possible role of the γ (fcc) phase of iron [cf., Birch, 1972] is more problematical in this analysis. There is certainly no evidence for a transition to γ-Fe in the Hugoniot data (nonporous samples) to 150 GPa and probably higher. Thus, either the γ and ε phases are indistinguishable from shock experiments or the Hugoniot states never intersect the stability field of γ-Fe [there is good reason to doubt that any kinetic phenomena are at work in such a transition: Johnson and Mitchell, 1972]. In the former case, the γ structure can be safely ignored for this study.

It seems more likely, however, that γ-Fe is in fact not formed along the reference Hugoniot and is therefore of no relevance to the core: the core, being at temperatures less than or equal to those along the Hugoniot (see below) would be even more completely within the stability field of the ε phase. Birch [1972] and Liu [1975]

reached the same conclusion, while Stacey and Irvine apparently disagree [Stacey, 1977b].

The state of the porous samples under shock is poorly known, however. These samples may reflect properties much more analogous to those of γ-Fe, at low pressures in particular. In this case, the derived Grüneisen parameters would tend to be higher for the more porous (i.e., hotter) samples. If anything the data reflect the opposite trend at low pressures (Figure 1a) implying that the γ-phase can be ignored in this study. However, these difficulties again emphasize that the present analysis tends to be less reliable at lower compressions.

Because equation (1) is solved as a ratio of finite differences, the γ's calculated from porous Hugoniot data represent averages over rather large temperature intervals. Were γ to be strongly dependent on temperature, data for different porosities would be systematically offset from each other at any given volume. Such systematic behavior is not obvious within the available Fe data (Figure 1a), indicating that γ is effectively independent of temperature [see also McQueen et al., 1970]. This is often assumed to be the case [e.g., Wallace, 1972; Stacey, 1977b] but is contrary to the recent conclusions of Mulargia's [1977] theoretical analysis.

The data preclude a dependency of γ on temperature any larger than of the order of 5-10% per 1000 K (this is the limit of resolution imposed by the data). Temperature effects on γ must be within the scatter of the data: $\Delta\gamma < 30\%$, approximately. At 100 GPa, for example,

the $\rho_0 = 6.00$ Mg/m^3 data are offset from the reference Hugoniot by $\Delta\rho \geq 0.75$ Mg/m^3 which, based on the data for the coefficient of thermal expansion α given below, represents a temperature difference $\Delta T \geq 6 \times 10^3$ K and thus a temperature effect on γ within the stated limit.

The value of γ for Fe at high pressures and temperatures shown in Figure 1a can be fit with an empirical relation of the form

$$\gamma = \gamma_0 \left(\frac{V}{V_0}\right)^n \quad . \tag{3}$$

Using the initial density of ε-Fe as a centering volume, the best values for γ_0 and n are 2.2 and 1.62 (±0.37 estimated standard error), respectively (cf., Table 1).

The value of γ_0 is not very well constrained by the data because of the greater uncertainties at low densities discussed above. However, the value of n is well determined and it appears to be significantly different from 1. Although this conclusion may vary depending on the nature of the fit and the data used, Ramakrishnan et al. [1978] obtained similar results from measurements of γ at lower pressures. This would imply that the assumption often used of $\rho\gamma$ = constant [e.g., McQueen et al., 1970] is not correct for Fe at high pressures and that this assumption results in a smaller dependence of γ on volume than is indicated by the data. Thus, the values of γ assumed by McQueen et al. [1970] are somewhat lower than those given by the data from this study at densities below 10.5 Mg/m^3 (Figure 3).

If the Grüneisen parameter is known along the Hugoniot, the bulk sound speed (c) or adiabatic bulk modulus (K_s) can be calculated in the manner discussed by McQueen and coworkers [1967, 1970]. Assuming a Mie-Grüneisen form of the equation-of-state, they derive an expression for the sound speed which yields the following formula for the bulk modulus along the reference Hugoniot (subscript H indicates evaluated on the Hugoniot):

$$K_s)_H = \left(\frac{dP}{dV}\right)_H \left[(V_{00} - V)\,\frac{\gamma}{2V} - 1\right] V + \frac{P_o\gamma}{2} = \rho\, c_H^2 \qquad (4)$$

Here, P_0 is given by Equation (2b) and

$$\left(\frac{dP}{dV}\right)_H = \frac{3\,P_0}{V_{00}\eta_0} + (2V_{00}^2 s_0'^2 \eta_0^3)^{-1} \left\{ 2s_0(1-\eta_0 s_0) + 4s_0' c_0^0 \eta_0 - s_0\left[(1-\eta_0 s_0)^2 - 4s_0' c_0^0 \eta_0^2\right]^{\frac{1}{2}} - (1-\eta_0 s_0)\,\frac{\left[s_0(1-s_0\eta_0) + 4s_0' c_0^0 \eta_0\right]}{\left[(1-\eta_0 s_0)^2 - 4s_0' c_0^0 \eta_0^2\right]^{\frac{1}{2}}} \right\} . \qquad (5)$$

The resulting values of $K_s)_H$ are shown in Figure 1b as a function of density.

For comparison, the bulk modulus given by the equation-of-state model for Fe of McQueen et al. [1970] is also shown in Figure 1b. Athough they arrived at a $\gamma(V)$ dependence from separate considerations, the agreement is good. This is not surprising, though, since the same data base is being used here and Equation (4) gives the bulk modulus as equal to the slope of the Hugoniot, except for a small thermal correction.

The comparison of Al'tshuler et al.'s [1960] sound speed measurements is much more gratifying. Al'tshuler and coworkers' data is completely independent of the present analysis and the agreement evident in Figure 1b is significant.

Melting at high pressure could affect the bulk modulus of Fe, presumably lowering it. However, there is both experimental and theoretical evidence which indicates that the change in modulus on melting is small if the volume change is small [e.g., Tallon et al., 1977]. Bridgman [1931], for example, emphasized the rapid convergence of solid and melt compressibilities at high pressures as being an important experimental observation with regards to the physics of melting. The concept that the volume change on melting remains finite, although small, up to the highest pressures [this is justified both theoretically and experimentally: see Ross and Alder, 1966 and Stishov, 1969] also forces the bulk moduli of solid and liquid to converge under compression at least as rapidly as the volume change of melting. Thus given that the volume change on melting is negligible at high pressures (within the resolution of the present data set), the change in modulus due to melting is also expected to be negligible in both the analysis of the Hugoniot data and their application to the earth's core. This is an agreement with the work of Irvine and Stacy [1975] but not with that of Anderson [1977].

In theory, it is possible to derive data for $K_S)_H$ (or c_H) along the Hugoniots of the porous samples in an analysis completely analogous to that used for the reference Hugoniot. Such data would constrain the

temperature dependence of $K_S)_H$ at extremely high temperatures and pressures. The porous data unfortunately do not constrain the slope of their Hugoniots well enough for such an analysis to be very useful.

By using the thermodynamic identity

$$\gamma = \frac{\alpha K_S V}{C_P} \tag{6}$$

the value of the coefficient of thermal expansion α_H along the Hugoniot can be directly obtained from the shock data on porous iron. These data are shown in Figure 1c.

Here, the specific heat C_P was set to 3R (the Dulong-Petit value of C_V) which is probably a good approximation given that the temperatures involved are well above the Debye temperature of iron [Gschneider, 1964; Andrews, 1973; Stacey, 1977a; Bukowinski, 1977]. Although C_P is always larger than C_V, the latter tends to decrease below its high temperature value (3R) under compression. Specifically, the $\alpha(V)$ dependency can be used to reduce all of the porous data to a given (thermal) standard state (e.g., the reference Hugoniot, or a theoretical isentrope or isotherm) and, in turn, the correction factor $\alpha\gamma T$ between C_V and C_P can be evaluated. This correction is well within the scatter of the data, being, for example, about 3% between 100-150 GPa (using the Hugoniot temperatures shown below). The correction of C_V due to compression is of the opposite sign but is probably quite small: less than 0.5% at 150 GPa, as estimated with a simple Grüneisen-Debye model [e.g., McQueen et al., 1970].

Clearly the values of α deduced from this analysis represent high-temperature ("saturated") values, which are nearly independent of temperature. This is consistent with the assumptions made for the specific heat: α independent of temperature is essentially equivalent to C_v independent of pressure at high pressures and temperatures [cf., Stacey, 1977b; although his equation (20) is slightly incorrect this conclusion stands because of the small values of α and its pressure derivative at these conditions]. Of course, these high temperature values of α are the ones of greatest geophysical interest.

Further corrections to C_v and C_P may be necessary, however. Schottky anomaly and particularly electronic contributions may be important in increasing the value of C_v above 3R [Shimizu and Terao, 1967; Jamieson et al., 1979], while corrections for melting and extremely high temperatures may significantly decrease the specific heat below its lattice vibrational value [Kormer et al., 1962; Keller and Wallace, 1962; Grover, 1971; Wallace, 1972]. At present it is impossible to quantify these latter effects sufficiently to evaluate them properly and the thermal and electronic contributions are assumed to be unimportant for the purposes of this analysis.

Neglecting these corrections may lead to systematic errors in the calculated values of α_H. However, because they tend to cancel each other the overall effect of the corrections in the subsequent discussion of the core is surely quite small compared to the scatter exhibited by the data. In any case, data for the coefficient of thermal expansion at pressures of tens to hundreds of GPa, even if accurate

only to about ten or twenty percent (Figure 1c), still represent a significant result in that no other experimental technique can at present achieve this combination of accuracy and high pressures. For comparison, the recent work of Yagi [1978] represents virtually the only direct measurements of coefficients of thermal expansion of solids at high temperatures and pressures, extending only to 8 GPa, however.

The samples of largest initial porosity were treated separately since they do no reach Hugoniot densities much higher than the initial density of α-Fe. It is not clear from the Hugoniot data whether or not these samples achieve fully compacted states; however, if they do the resulting thermal properties are expected to represent those of α-Fe (or its molten equivalent) at extremely high temperatures. For the present purposes, the γ and α phases of Fe can be considered indistinguishable.

Because of their scatter, the data above 15.0 GPa were fit with a quadratic U_s-u_p relation and the resulting values of γ, $K_s)_H$ and α_H are shown as dashed curves in Figure 1. It is remarkable, given the uncertainties involved, that these data for samples of highest porosity are significantly displaced from the higher density data pertaining to ε-Fe and that they are quite consistent with the high temperature values of γ, K_s and α for α-Fe at zero pressure [shown in brackets at ρ_0 = 7.85 Mg/m^3 in Figure 1; see also Ramakrishnan et al., 1978]. The discrepancies apparent in Figure 1 can easily be ascribed to the scatter in the original Hugoniot data, whereas the effect of incomplete compaction would be to yield anomalously high values of γ and α.

Finally, it is interesting to notice that $\gamma = 1.5$ in the density range 7.6 to 8.0 Mg/m^3 implies an asymptotic Hugoniot density within this range for the samples with $\rho_0 \sim 3.38$ Mg/m^3 [see Al'tshuler et al., 1958; McQueen et al., 1970]. This result is quite consistent with the original Hugoniot data as well as with the known γ of α-Fe (see Figure 1a). Therefore it seems evident from this analysis that these most porous samples are, in fact, fully compacted (above 15.0 GPa) and that they are truly reflecting thermal properties.

GEOPHYSICAL APPLICATIONS -- STATE OF THE CORE

To the extent that the thermal properties of the core can be approximated by those of Fe, the thermal properties derived from shock data on porous samples and discussed in the previous section can be directly applied. Therefore, the data of Figure 1 have been replotted as a function of pressure in Figure 2 in order to compare them with inferred or observed values of γ, K_s and α in the outer core. As is apparent, the shock-wave data on Fe are broadly consistent with current models for the core [Tolland, 1974; Dziewonski et al., 1975; Stacey, 1977a; Anderson and Hart, 1976; Hart et al., 1977; Jamieson et al., 1979], although systematic differences are present as well. These differences are interpreted as being due to the fact that the core consists not only of Fe but also of an intermixed, lower density component [Birch, 1952, 1964].

Stacey [1977a, b, c] has shown that a Lindemann-type criterion is probably appropriate for the melting gradient in the core and therefore that this gradient will be steeper than the adiabat as long as $\gamma > 2/3$.

The shock data on Fe indicate a $\gamma \sim 1.3$ for the upper portion of the outer core which is consistent (see Figure 2a) both with Stacey's estimate and with that of Jamieson and coworkers. The new data are therefore fully consistent with simple dynamic models of the core.

Stacey's [1977a] values of γ for the core are shown in Figure 3, along with the commonly assumed functional $\gamma\rho$ = constant and with the fit to the results from this study extrapolated through the core.

An important conclusion of this analysis is that the data on Fe are in excellent agreement with the theoretical values of γ_{VZ} (or "free-volume" γ) derived from the Vaschenko-Zubarez/Irvine-Stacey formalism. Stacey's correction for electronic contributions yields values of γ which are not inconsistent with the data, given the scatter in Figure 1a, but which do seem to be systematically high. His value of the electronic Grüneisen parameter (γ_e = 2.2-2.3 in the core) is probably much too high; I agree with Jamieson et al. [1979] in setting $\gamma_e \sim 1.5$ (± 0.3, perhaps) based on the work of Al'tshuler et al. [1962] and of Bukowinski [1977]. Hence, there are effectively no contributions to the Grüneisen parameter of iron which would change it significantly from its lattice vibrational value [Jamieson et al., 1979] and Stacey's estimates of γ in the core should probably be slightly lowered. In any case, the data for γ from Hugoniot measurements on porous Fe

provide an important experimental verification of the formulation given by Vaschenko and Zubarev [1963] and Irvine and Stacey [1975].

The pressure dependence of γ assumed by Stacey [1977a] appears to be smaller than is warranted by the data and is closer to that given by $\rho\gamma$ = constant. As is clear from Figure 3, however, this makes virtually no difference at core pressures. Above 100 to 120 GPa, the present set of data are essentially in agreement with the values of γ assumed by McQueen et al. [1970] as well as those calculated by Stacey, and there is not at present any evidence that the γ of Fe is different from that of the core. On the other hand, Bukowinski's recent [1977] theoretical analysis pertaining to the inner core yields a γ ($\sim$1.8) which is somewhat inconsistent with the data presented here. It is encouraging to note, however, that the completely independent evaluations of γ provided by Stacey, Bukowinski, Jamieson et al. and the present analysis are all compatible with values between about 1.0 and 1.5 for iron under core conditions, re-emphasizing the likelihood of a convecting and adiabatic core.

The values of K_s for Fe along the Hugoniot shown in Figure 2b are clearly larger than the values of K_s observed for the top of the outer core. Since the temperatures at about 150 GPa for the core and the Hugoniot of iron are thought to be close [McQueen et al., 1970; Tolland, 1974; Usselman, 1975; Stacey, 1977a] this difference must reflect the deviation of the core from a pure iron composition.

The data for $K_s)_H$ of iron can be fit by the empirical relations $K_s)_H$ in (GPa) = $113.1 + 5.45P - 0.0058P^2$. Combining the fit for γ

(Equation 3) with Equation (6) then gives the following formula for the coefficient of thermal expansion of Fe along the Hugoniot: $\alpha_H = 0.0293\ V^{0.62}\ K_s)_H^{-1}$, with α in K^{-1} and V in m^3Mg^{-1}.

This dependency of α is shown in Figures 2c and 4 where it is compared with Stacey's [1977a] values for the core. The data agree very well with Stacey's results, the apparent differences being due largely to the high values of γ used by Stacey and to the fact that the core has a bulk modulus lower than that of Fe at equivalent pressures. Therefore, to the extent that Stacey has correctly evaluated C_P in his analysis the agreement with his model indicates that the approximation used here for C_P ($\sim$3R) is quite justified. Again, the shock-wave data on porous Fe lend strong experimental support to the thermal model of the core proposed by Stacey [1977a].

The present data for α up to pressures of 150 GPa cannot be satisfactorily fit with equations of the form given by Birch [1952, 1968]. The new data are best fit by αK_s proportional to $V^{2/3}$ (approximately) rather than this product being a constant. A power law for α analogous to equation (3), as proposed by Anderson [1967], does fit the data although with an exponent somewhat different than would be expected from Anderson's equations [cf., Clark, 1969, as well]. These conclusions are similar to Yagi's [1978] observations at lower pressures. At higher pressures, such as those in the core, the difference between any of these functional dependencies for α is rather small, however. Also, the empirical relation of McLachlan and Foster

[1977] seems not to hold at high pressures. Although they demonstrate that α/C_p ($\equiv\gamma/K_s V$) is approximately independent of temperature at zero pressure, this factor decreases by nearly 50% with a 9% volume decrease (50-100 GPa along the Hugoniot).

Because the temperatures achieved on the Hugoniot of Fe are much higher than those existing in the lower parts of the core, thermal corrections must be made to the shock data in order to pursue any further comparisons with seismological observations. For this purpose, the core temperatures of Stacey [1977a] are used along with the Hugoniot temperatures given by the equation of state model of McQueen et al. [1970] for Fe. The temperature distributions in question are shown in Figure 5. As has been shown above, the present data for γ, K_s and α derived from measurements on porous samples are fully consistent with the analyses of Stacey and McQueen et al. under conditions existing in the core. The Hugoniot temperatures calculated by Al'tshuler et al. [1962] are similar to but consistently lower than those shown at pressures above about 120 GPa. Even if the absolute values of temperature are subject to reinterpretation, the gradients are generally agreed upon [see Stacey, 1972; Verhoogen, 1973; Usselman, 1975; Jacobs, 1975]. It is clear, then, that thermal corrections to the data become increasingly important for comparisons corresponding to greater depths in the core.

Figure 6 presents density data for Fe and for the core. The Hugoniot data, corrected to core temperatures using the thermal expansions and temperatures which are indicated in Figures 4 and 5, clearly

show the well known discrepancy in densities for iron and the outer core. This difference amounts to about 10% throughout the core, with an estimated error of approximately ±2%. The gradients for the core and for Fe are essentially parallel, indicating that a single, lighter component, uniformly distributed throughout the core could account for the observed densities. This disagrees with Usselman's [1975] result, however he did not perform the appropriate temperature reductions [see also Ahrens, 1979].

The situation for the inner core is much less clear in that the density is virtually unconstrained in whole-earth seismological models. Although the wave velocity is well known through the inner core, there is a complete trade-off with bulk modulus as discussed below. The models shown are not compatible with an iron composition, however other models have shown densities well into the range of Fe [e.g., UTD 124 of Dziewonski and Gilbert, 1972]. Furthermore, a recent analysis of PKP phases [Cormier and Richards, 1977] does indicate a large change in properties at the inner core-outer core boundary which is incompatible, for example, with the C2 model. Densities in the inner core as large as those required by the iron are therefore quite plausible, as was concluded by Birch [1964, 1972].

It is worth noting that the densities of iron under core conditions evaluated in this study are by and large very compatible with the isotherm independently calculated by McQueen et al. [1970] and shown in Figure 6.

The bulk sound speeds along the Hugoniot of Fe and in the core are compared in Figure 7. These sound speeds are quite similar, however without the temperature correction they appear to cross. The Hugoniot sound speeds must be corrected by a factor of

$$\frac{\delta c}{c} \sim \frac{1}{2} \left(\alpha + K\left(\frac{\partial \alpha}{\partial P}\right)_H\right) \delta T$$

where δT is the temperature difference between core and Hugoniot, and the present data for $\alpha(P)$ and K_s were used. I should note that these sound speeds are not very compatible with those calculated by McQueen et al. [1970] along the 300 K isotherm of iron. This is one of the only inconsistencies to appear between their calculations and the results given here, and it undoubtedly reflects differences in initial assumptions which ultimately lead to slightly different extrapolations.

The sound speeds for Fe corrected in this manner are much more compatible with the data for the core than has previously been thought, and they no longer imply a crossing over (Figure 7). Using the present estimate for the sound speed along the Hugoniot, the bulk velocity of iron is systematically higher (by 1-2%) than that of the outer core under equivalent conditions. Al'tshuler et al.'s [1960] data would imply much closer agreement, however this difference is probably within the experimental error, as is shown by a more recent measurement at 185 GPa which agrees with the sound speeds calculated here [Figure 7: Al'tshuler et al., 1971]. The fact that the sound speed of iron

converges with the measured sound speed in the inner core lends support to the suggestion that the inner core consists of pure iron.

Alder and Trigueros [1977] also derived sound speeds for iron under core conditions based on the Hugoniot of nonporous Fe. Using different assumptions and an independent approach, their results are virtually coincident with the data given here. However, it is worth noting that dispersion has been ignored in the present study (as well as in previous work), although it could have a significant effect on the comparison with seismic wave velocities [e.g., if the core is at or below its liquidus: Vaišnys, 1968, for example].

The important conclusions are that, along with the densities, the velocity gradient in the outer core is grossly consistent with a homogeneous composition, while the actual values of velocity are close to but probably less than those of Fe under equivalent conditions. These results contradict the conclusions of previous analyses [e.g., Al'tshuler and Kormer, 1961; Anderson et al., 1971; Davies and Dziewonski, 1975; Anderson, 1977] which have not taken thermal effects properly into account. Recent analyses indicate that seismological data are consistent with chemical homogeneity and an adiabatic gradient on a gross scale for the bulk of the outer core [Dziewonski et al., 1975; Butler and Anderson, 1978]. However, more detailed observations based on modeling SKS and SKKS phases do suggest inhomogeneity on a finer scale than has been resolved in whole-earth models [Kind and Müller, 1977].

A similar comparison of bulk moduli is shown in Figure 8. Even with no thermal correction, the bulk modulus along the iron Hugoniot tends to be higher than that in the core. This is to be expected since the sound speeds are similar whereas the density of the outer core is known to be less than that of Fe.

The thermal correction to the bulk modulus along the Hugoniot is substantial. The correction used may be somewhat too small, however, because of the uncertain nature of the extrapolation of α. The thermal correction does increase the bulk sound speed as was just discussed because the correction for the bulk modulus (approximately 10%) is much larger than that for the density (1-2%). As before this correction yields a gradient, in this case for the bulk modulus, which is very consistent with the observed gradients in the core.

Under equivalent conditions, iron has a bulk modulus about 10-15% larger than that of the outer core. This estimate of bulk modulus is perhaps accurate only to about ±3-5%, particularly due to the fact that the effects of melting (which have been ignored) may decrease the bulk modulus by a few percent even under conditions existing in the core. On the other hand, since the thermal correction used for the bulk modulus (or sound speed) is possibly too small, the overall effect on the values shown in Figure 8 is not likely to change them by a large amount. However, the general gradients of K_s shown in Figure 8 may be more accurate than the absolute values.

Davies and Dziewonski [1975] concluded that the bulk modulus of the core is higher than that of iron, based on a theoretical extrapolation to zero pressure and 300 K. Such large extrapolations to room conditions,

however, seem to be less well constrained than the present analysis. Somerville [1979] has used a similar approach to that of Davies and Dziewonski and found that his extrapolation yields a lower bulk modulus for the core than for Fe, consistent with the conclusions reached here [compare Verhoogen, 1973, as well].

The inner core, again, does not allow a unique interpretation. The inner core is quite compatible with the extrapolated bulk modulus of iron as shown in Figure 8. The highest curve is for the bulk modulus which satisfies both the density of iron at core temperatures (Figure 6) and the seismically determined sound speed (Figure 7) in the inner core. This curve lies at slightly higher values than those estimated for Fe but is by no means inconsistent since the present extrapolation may be an underestimate by the requisite 3-5%. It is also interesting that the Poisson ratio inferred for the inner core from seismology (about 0.44) is virtually the same as that measured for Fe at pressures of 100-200 GPa under shock [Al'tshuler et al., 1971]. This implies that not only the bulk modulus but also the shear modulus of the inner core is consistent with that of iron [see also, Al'tshuler and Sharipdzhanov, 1971; Anderson, 1977]. Since the density, bulk modulus and shear modulus of the inner core are fully compatible with values estimated for iron under the same conditions, it is quite plausible that the inner core does in fact consist of solid iron and that the inner core-outer core boundary represents not only a phase boundary but also a compositional boundary.

Alternatively, the inner core may be interpreted as being the solid equivalent of the outer core and its boundary as being a phase change (i.e., melting) only. This is fully consistent with whole-earth seismological models, such as C2 [Anderson and Hart, 1976; Hart et al., 1977], which include a jump of only a few percent in density and bulk modulus at the boundary as might be expected for a melting transition. However, the more detailed analysis of Cormier and Richards [1977] alluded to above appears to preclude such a small change in acoustic impedance at the inner core-outer core boundary. It seems highly unlikely that melting without an accompanying compositional change could account for the changes in density and velocity demanded by their results [c.f., Verhoogen, 1973; Usselman, 1975 as well]. Furthermore, the base of the outer core is known to be incompatible with homogeneity on a large scale (and possibly on a smaller scale, within the outer core) as shown most recently by Butler and Anderson [1978].

Therefore, the available data strongly suggest that the inner core boundary represents more than a simple melting transition and therefore that it is also a compositional boundary. In light of these conclusions, the simplest model for the inner core may well be that it consists of pure iron as indicated above and as suggested by others [e.g., Birch, 1972; Bukowinski, 1977; Ahrens, 1979]. Otherwise yet another compound, different from that in the outer core or from iron, must be considered for the inner core although iron is fully consistent with all of the data presently at hand.

The necessity for nickel in the core is unclear, however since the effect of incorporating Ni is apparently to increase the density without markedly affecting the bulk modulus of iron [McQueen and Marsh, 1966] it is clear that the inner core could only contain a rather small proportion of nickel. On physical grounds none is needed.

The consequences of these alternatives may be important in considering the thermal state of the core. If the inner core represents merely the solidified outer core, then the inner core boundary represents a fixed point on the melting curve of the appropriate (and as yet unknown) iron compound (i.e., a one-component system is assumed). Stacey's [1977a] thermal model of the core, for example, is based in part on such an assumption. However, from the discussion just given, such an assumption does not seem warranted. Rather, the inner core boundary is interpreted here to lie at a temperature above that required for freezing the outer core but below the melting point of pure iron. This conclusion does not necessarily have a strong effect on Stacey's model, and it lends further support to the relatively low temperatures for the core which have been proposed in the last few years [e.g., Tolland, 1974; Stacey, 1977a]. However, this conclusion does suggest that the reason for the outer core being molten is simply that it is contaminated or alloyed such that not only its density but also its melting point is lowered below that of pure Fe [c.f., Birch, 1972 as well].

A change in composition is, of course, expected for melting of a multi-component system (in general), and the arguments given here are

fully consistent with discussions of the core as a eutectic system [e.g., Usselman, 1975]. Nevertheless, the possibility remains that the inner core-outer core boundary is, like the core-mantle boundary, a major chemical discontinuity rather than an equilibrium phase boundary. In any case, if the inner and outer core are taken to be chemically distinct, then their boundary may only serve as a crude bracket on the geotherm.

The combination of bulk modulus and density should provide a powerful discriminant for candidate compositions of the outer core. Assuming the outer core to consist mainly of iron, along with an alloying element or impurity, data on the densities and bulk moduli of various compounds (appropriately corrected for temperature) can be combined with the information given in Figure 9 in order to (i) test whether the properties of this compound are compatible with those of the outer core, and (ii) determine how much of this compound must be in the core. This Core Diagram gives the unique combination of density and bulk modulus as a function of mass fraction of the core which the intermixed compound (X) must possess in order to satisfy the seismological data for the outer core as well as the data on pure iron presented here.

The density of X as a function of mass fraction contained in the core (m_x) along with Fe is given by

$$\rho_x = \frac{m_x}{\rho_{core}^{-1} + \rho_{Fe}^{-1} (m_x - 1)} , \qquad (7a)$$

which implies a volume fraction of X of

$$\nu_x = \frac{\rho_{core} - \rho_{Fe}}{\rho_x - \rho_{Fe}} \quad , \tag{7b}$$

assuming ideal mixing. The bulk modulus of the outer core must then satisfy the Reuss bound (equivalent to the Hashin-Shtrikman value) for the mixture of Fe and X so that

$$K_s = \frac{\nu_x K_{Fe} K_{core}}{K_{Fe} + K_{core} (\nu_x - 1)} \tag{8}$$

[for further details, see Jackson et al., 1978; also Watt et al., 1976].

Figure 9 shows the solutions of Equations (7) and (8) for a depth in the outer core corresponding to 200 GPa (approximately 2860 km radius), based on the densities and bulk moduli of iron and the core which are indicated. Similar diagrams are readily constructed for all depths within the core. Obviously, if X has the same density and bulk modulus as the outer core, it can make up 100% of the mass fraction, and even materials with vanishingly small densities can be present in the outer core. However, using the density as a constraint on the amount of X present (as is commonly done), Figure 9 gives the bulk modulus required by the data. No material with a bulk modulus less than about 45% that of the core can be accommodated in any amount.

Although many candidates have been proposed for the alloy X in the core [Fe-S, Fe-C, Fe-Si, and Fe-O compounds, for example, Jacobs, 1975], the information available for these compositions is as yet too

sparse to make a critical evaluation using Figure 9. The recent calculations of Alder and Trigueros [1977] for a number of compounds do not yield any values of density and bulk modulus which are very compatible with Figure 9. This discrepancy may be due in part to combined errors in the extrapolations which they used and the extrapolations used here. Ahrens' [1979] recent estimate of about 10% S (by weight) being needed to satisfy outer core densities would imply (with $m_x \sim 0.27$) a bulk modulus close to 700 GPa at a pressure of 200 GPa in the core. This in fact is consistent with the values given by Alder and Trigueros' model for the sound speed of FeS. As is well known, mantle compositions (basically, in the system Mg-Si-O) cannot satisfy the constraints of Figure 9 because their relatively low densities and high incompressibilities are mutually exclusive in this context. Iron oxide, however, may fit in very well [c.f., Ringwood, 1978]. Hopefully, additional data at high pressures will allow more complete evaluations of the thermal equation-of-state properties of such compounds, so that they can be more critically considered as candidates for the outer core.

CONCLUSIONS

A new analysis has been presented which yields estimates of the thermal properties of materials at high pressures and temperatures based on shock-wave measurements. This extends previous interpretations of Hugoniot data on initially porous samples and allows a more complete evaluation both of theoretical equations of state and of geophysical

models of the earth's interior. It is hoped that this study will stimulate further measurements of the thermal properties of materials at high pressure using either dynamic or static techniques, and thus provide further physical constraints on the chemical nature of the earth's core.

From the present study, the Hugoniot data on porous iron provide a strong experimental confirmation of Stacey's [1977a] thermal model of the core by verifying his theoretical estimates of thermal properties at high pressures. The Vaschenko-Zubarev/Irvine-Stacey (or "free-volume") formulation for the Grüneisen parameter appears to be very successful for iron at high pressures, while previous (approximate) formulas for the behavior of the coefficient of thermal expansion under compression appear to be less reliable.

This analysis provides new estimates for the bulk modulus and sound speed of iron under core conditions which are in disagreement with the results of previous studies. These earlier studies have not properly accounted for the large differences in temperature between states on the Hugoniot and those within the core. The data presented here demonstrate that the gradients of density, sound speed and bulk modulus within the core are the same as those expected for iron, or a closely related compound, under self-compression. On a gross scale, then, the bulk of the outer core appears to be chemically homogeneous, although more detailed seismic analysis may prove this not to be the case on a smaller scale.

Whereas the bulk velocity in the outer core is close to, but probably somewhat less than that of iron, the bulk modulus in the outer core is clearly some 10-15% less than that of pure Fe under equivalent conditions. Hence the light, "alloying" element present in the outer core decreases both the density and bulk modulus below that of iron by about the same proportions.

The present analysis of the data for pure Fe constrains the density and bulk modulus which the lighter compound in the outer core must have. The Core Diagram shown in Figure 9 should be quite useful in determining what compounds may be present in the outer core (along with iron) and in what proportions, but only when more data are available on the densities and bulk moduli at (or corrected to) the pressures and temperatures appropriate for the core.

From a combination of seismological observations and the results of this study, the properties of the inner core are found to be completely consistent with its being pure iron. Although it may have a composition other than Fe, the inner core is very likely not to be the solidified equivalent of the outer core. Therefore, the simplest hypothesis at present seems to be that the inner core is in fact pure Fe.

This strongly suggests that the inner core-outer core boundary is both a compositional and a phase boundary as might be expected for a multi-component system, for example. This boundary can therefore not be readily used as a fixed temperature point on the melting curve of iron (or a related compound).

Presumably the contaminant which has lowered the density and bulk modulus of the outer core has also lowered its melting point below that of the inner core. This chemical difference would then be the factor allowing melting in the outer core and, ultimately, the operation of the geomagnetic dynamo.

ACKNOWLEDGEMENTS

I thank D. L. Anderson and T. J. Ahrens for very helpful advice and discussions. I appreciate their critical comments on this manuscript, as well as discussions with M. Somerville, I am particularly indebted to J. A. Jacobs for his careful review of the original manuscript, and also thank M.S.T. Bukowinski, F. D. Stacey and J. M. Brown for helpful discussions and comments.

REFERENCES

Ahrens, T. J., Equations of state of iron sulfide and constraints on the sulfur content of the earth, *J. Geophys. Res.*, in press, 1979.

Alder, B. J. and M. Trigueros, Suggestion of a eutectic region between the liquid and solid core of the earth, *J. Geophys. Res.*, *82*, 2535-2539, 1977.

Al'tshuler, L. V., K. K. Krupnikov, B. N. Ledenev, V. I. Zuchikhin and M. I. Brazhnik, Dynamic compressibility and equation of state of iron under high pressure, *Sov. Phys. JETP*, *34*, 606-614, 1958.

Al'tshuler, L. V., S. B. Kormer, M. I. Brazhnik, L. A. Vladimirov, M. P. Speranskaya and A. I. Fynitkov, The isentropic compressibility of aluminium, copper, lead and iron at high pressures, *Sov. Phys. JETP*, *11*, 766-775, 1960.

Al'tshuler, L. V. and S. B. Kormer, On the internal structure of the earth, *Izv. Acad. Sci. USSR Geophys. Ser.*, *1*, 18-21, 1961.

Al'tshuler, L. V., A. A. Bakanova and R. F. Trunin, Shock adiabats and zero isotherms of seven metals at high pressures, *Sov. Phys. JETP*, *15*, 65-74, 1962.

Al'tshuler, L. V., M. I. Brazhnik and G. S. Telegin, Strength and elasticity of iron and copper at high shock-wave compression pressures, *J. Appl. Mec. Tech. Phys.*, *12*, 921-926, 1971.

Al'tshuler, L. V. and L. D. Sharipdzhanov, Distribution of iron in the earth and its chemical differentiations, *Izv. Acad. Sci. USSR Earth Phys.*, *7*, 231-239, 1971.

Anderson, D. L., C. Sammis and T. Jordan, Composition and evolution of the mantle and core, *Science*, *171*, 1103-1112, 1971.

Anderson, D. L. and R. S. Hart, An earth model based on free oscillations and body waves, *J. Geophys. Res.*, *81*, 1461-1475, 1976.

Anderson, D. L., Composition of the mantle and core, *Ann. Rev. Earth Planet. Sci.*, *5*, 179-202, 1977.

Anderson, O. L., Equation for thermal expansivity in planetary interiors, *J. Geophys. Res.*, *72*, 3661-3668, 1967.

Andrews, D. J., Equation of state of the alpha and epsilon phases of iron, *J. Phys. Chem. Solids*, *34*, 825-840, 1973.

Bancroft, D., E. L. Peterson and S. Minshall, Polymorphism of iron at high pressures, *J. Appl. Phys.*, *27*, 291-298, 1956.

Barker, L. M. and R. E. Hollenbach, Shock wave study of the $\alpha \rightleftarrows \varepsilon$ phase transition in iron, *J. Appl. Phys.*, *45*, 4872-4887, 1974.

Birch, F., Elasticity and constitution of the earth's interior, *J. Geophys. Res.*, *57*, 227-286, 1952.

Birch, F., Density and composition of mantle and core, *J. Geophys. Res.*, *69*, 4377-4388, 1964.

Birch, F., Thermal expansion at high pressures, *J. Geophys. Res.*, *73*, 817-819, 1968.

Birch, F., The melting relations of iron and temperatures in the earth's core, *Geophys. J. R. Astr. Soc.*, *29*, 373-387, 1972.

Bridgman, P. W., *The Physics of High Pressure*, Dover Publications, New York, 398 pp., 1931.

Bukowinski, M. S. T., A theoretical equation of state for the inner core, *Phys. Earth Planet. Int.*, *14*, 333-344, 1977.

Butler, R. and D. L. Anderson, Equation of state fits to the lower mantle and outer core, *Phys. Earth Planet. Sci.*, *17*, 147-162, 1978.

Carter, W. J., S. P. Marsh, J. N. Fritz and R. G. McQueen, The equation of state of selected materials for high-pressure references, in: *Accurate Characterization of the High-Pressure Environment*, (E. C. Lloyd, ed.) Nat. Bur. Stand. (U.S.) Spec. Pub. 326, pp. 146-158, 1971.

Clark, S. P., Jr., Remarks on thermal expansion, *J. Geophys. Res.*, *74*, 731-732, 1969.

Cormier, V. F. and P. G. Richards, Full wave theory applied to a discontinuous velocity increase: the inner core boundary, *J. Geophys.*, *43*, 3-31, 1977.

Davies, G. F. and A. M. Dziewonski, Homogeneity and constitution of the earth's lower mantle and outer core, *Phys. Earth Planet. Int.*, *10*, 336-343, 1975.

Dziewonski, A. M. and F. Gilbert, Observations of normal modes from 84 recordings of the Alaskan earthquake of 1964, March 28, *Geophys. J. R. Astr. Soc.*, *27*, 393-446, 1972.

Dziewonski, A. M. and A. L. Hales and E. R. Lapwood, Parametrically simple earth models consistent with geophysical data, *Phys. Earth Planet. Int.*, *10*, 12- 48, 1975.

Grover, R., Liquid metal equation of state based on scaling, *J. Chem. Phys.*, *55*, 3435-3441, 1971.

Gshneider, K. A., Jr. (1964), Physical properties and interrelationships of metallic and semimetallic elements, *Solid State Phys.*, *16*, 275-426, 1964.

Hart, R. S., D. L. Anderson and H. Kanamori, The effect of attenuation on gross earth models, *J. Geophys. Res.*, *82*, 1647-1654, 1977.

Irvine, R. D. and F. D. Stacey, Pressure dependence of the thermal Grüneisen parameter, with application to the earth's lower mantle and outer core, *Phys. Earth Planet. Int.*, *11*, 157-165, 1975.

Jackson, I., R. C. Liebermann and A. E. Ringwood, The elastic properties of $(Mg_x\ Fe_{1-x})O$ solid solutions, *Phys. Chem. Min.*, *3*, 11-31, 1978.

Jacobs, J. A., *The Earth's Core*, Academic Press, New York, 253 pp., 1975.

Jamieson, J. C., H. H. Demarest, Jr., and D. Schiferl, A re-evaluation of the Grüneisen parameter for the earth's core, *J. Geophys. Res.*, in press, 1979.

Johnson, Q. and A. C. Mitchell, First X-ray diffraction evidence for a phase transition during shock-wave compression, *Phys. Rev. Lett.*, *29*, 1369-1371, 1972.

Keeler, R. N. and E. B. Royce, Shock waves in condensed media, in: *Physics of High Energy Density* (P. Caldirola and H. Knoepfel, eds.) Academic Press, New York, pp. 51-150, 1971.

Keller, J. M. and D. C. Wallace, Anharmonic contributions to specific heat, *Phys. Rev.*, *126*, 1275-1282, 1962.

Kind, R. and G. Müller, The structure of the outer core from SKS amplitudes and travel times, *Bull. Seism. Soc. Am.*, *67*, 1541-1554, 1977.

Kormer, S. B., A. I. Funtikov, V. D. Urlin and A. N. Kolesnikova, Dynamic compression of porous metals and the equation of state with variable specific heat at high temperatures, *Sov. Phys. JETP*, *15*, 477-488, 1962.

Kormer, S. B., M. V. Sinitsyn, G. A. Kirillov and V. D. Urlin, Experimental determination of temperature in shock-compressed NaCl and KCl and of their melting curves at pressures up to 700 Kbar, *Sov. Phys. JETP*, *21*, 689-700, 1965.

Liu, L., On the (γ,ε,ℓ) triple point of iron and the earth's core, *Geophys. J. R. Astr. Soc.*, *43*, 697-705, 1975.

Lysne, P. C. and W. J. Halpin, Shock compression of porous iron in the region of incomplete compaction, *J. Appl. Phys.*, *39*, 5488-5495, 1968.

Mao, H.-K., W. A. Bassett and T. Takahashi, Effect of pressure on crystal structure and lattice parameters of iron up to 300 kbar, *J. Appl. Phys.*, *38*, 272-276, 1967.

McLachlan, D. and W. R. Foster, The relationship between coefficients of expansion and heat capacities of simple metals, *J. Solid State Chem.*, *20*, 257-259, 1977.

McQueen, R. G. and S. P. Marsh, Shock-wave compression of iron-nickel alloys and the earth's core, *J. Geophys. Res.*, *71*, 1751-1756, 1966.

McQueen, R. G., S. P. Marsh and J. N. Fritz, Hugoniot equation of state of twelve rocks, *J. Geophys. Res.*, *72*, 4999-5036, 1967.

McQueen, R. G., S. P. Marsh, J. W. Taylor, J. N. Fritz and W. J. Carter, The equation of state of solids from shock wave studies, in: *High-Velocity Impact Phenomena* (R. Kinslow, ed.) Academic Press, New York, pp. 293-417 and appendices, 1970.

McQueen, R. G., W. J. Carter, J. H . Fritz and S. P. Marsh, The solid-liquid phase line in Cu, in: *Accurate Characterization of the High-Pressure Environment* (E. C. Lloyd, ed.) Nat. Bur. Stand. (U.S.) Spec. Publ. 326, pp. 219-227, 1971.

Mulargia, F., Is the common definition of the Mie-Grüneisen equation of state inconsistent?, *Geophys. Res. Lett.*, *4*, 590-592, 1977.

Neal, T., Dynamic determinations of the Grüneisen coefficient in aluminum and aluminum alloys for densities up to 6 Mg/m^3, *Phys. Rev., B14,* 5172-5181, 1976.

Ramakrishnan, J., R. Boehler, G. H. Higgins and G. C. Kennedy, Behavior of Grüneisen's parameter of some metals at high pressures, *J. Geophys. Res., 83,* 3535-3538, 1978.

Ringwood, A. E., Composition of the core and implications for origin of the earth, *Geochem. J., 11,* 111-136, 1978.

Ross, M. and B. J. Alder, Melting curve at high pressure, *Phys. Rev. Lett., 16,* 1077-1079, 1966.

Shimizu, M. and K. Terao, Calculation of electronic specific heat for iron and nickel metals by the band model, *J. Phys. Soc. Japan, 23,* 771-776, 1967.

Somerville, M., An equation of state of solids at high temperature, *J. Geophys. Res.,* in press, 1979.

Stacey, F. D., Physical properties of the earth's core, *Geophys. Surveys, 1,* 99-119, 1972.

Stacey, F. D., A thermal model of the earth, *Phys. Earth Planet. Int., 15,* 341-348, 1977a.

Stacey, F. D., Applications of thermodynamics to fundamental earth physics, *Geophys. Surveys, 3,* 175-204, 1977b.

Stacey, F. D., *Physics of the Earth,* 2nd Ed., J. Wiley & Sons, New York, 414 pp., 1977c.

Stishov, S. M., Melting at high pressures, *Sov. Phys. Uspekki, 11,* 816-830, 1969.

Sterrett, K. F., W. Klement, Jr. and G. C. Kennedy, Effect of pressure on the melting of iron, *J. Geophys. Res., 70,* 1979-1984, 1965.

Strong, H. M., The experimental fusion curve of iron to 96,000 atmospheres, *J. Geophys. Res.*, *64*, 653-659, 1959.

Tallon, J. T., W. H. Robinson and S. I. Smedley, A mechanical instability hypothesis for melting in the alkali halides, *Phil. Mag.*, *36*, 741-751, 1977.

Tolland, H. G., Thermal regime in the earth's core and lower mantle, *Phys. Earth Planet. Int.*, *8*, 282-286, 1974.

Urlin, V. D., Melting at ultra high pressures in a shock wave, *Sov. Phys. JETP*, *22*, 341-346, 1966.

Usselman, T. M., Experimental approach to the state of the core: Part II. Composition and thermal regime, *Am. J. Sci.*, *275*, 291-303, 1975.

Vaišnys, J. R., Propagation of acoustic waves through a system undergoing phase transformations, *J. Geophys. Res.*, *73*, 7675-7683, 1968.

Vaschenko, V. Y. and V. N. Zubarev, Concerning the Grüneisen constant, *Sov. Phys. Solid State*, *5*, 653-655, 1963.

Verhoogen, J., Thermal regime of the earth's core, *Phys. Earth Planet. Int.*, *7*, 47-58, 1973.

Wallace, D. C., *Thermodynamics of Crystals*, J. Wiley & Sons, New York, 484 pp., 1972.

Wasilewski, P., Shock-loading meteoritic b.c.c. metal above the pressure transition: remnant-magnetization stability and microstructure, *Phys. Earth Planet. Int.*, *11*, p5-p11, 1976.

Watt, J. P., G. F. Davies, and R. J. O'Connell, The elastic properties of composite materials, *Rev. Geophys. Space Phys.*, *14*, 541-563, 1976.

Yagi, T., Experimental determination of thermal expansivity of several alkali halides at high pressures, *J. Phys. Chem. Solids*, *39*, 563-571, 1978.

TABLE 1

Grüneisen Parameter of Fe

$\gamma_0 = 2.2 \pm 0.5$*

$n = 1.62 \pm 0.37$

$\gamma = \gamma_0 (V/V_0)^n$ assumed

$\rho_0 = 8.31$ Mg/m^3 assumed

Reference Hugoniot: $U_s = c_0 + su_p + s'u_p^2$

$\rho_0 = 7.850$

$c_0 = 3.574$

$s = 1.920$

$s' = -0.068$

McQueen *et al.* [1970]*

*See discussion in text

FIGURE CAPTIONS

Figure 1: Thermal properties of Fe derived from shock-wave data on porous samples [McQueen et al., 1970]: (a) Grüneisen parameter, γ, (b) adiabatic bulk modulus, K_s, along the reference (solid) Hugoniot, and (c) the coefficient of thermal expansion, α, all shown as a function of density. The values of K_s measured for Fe under shock by Al'tshuler et al. [1960] are also shown. In each case, values for the high-temperature properties of α-Fe are shown as brackets at $\rho = 7.85$ Mg/m^3. Dashed curves at low densities represent the fits to the data of highest initial porosity ($\rho_0 = 3.38$ Mg/m^3). The solid line in (a) is a fit of Equation (3) to the data while that in (b) represents the bulk modulus along the Hugoniot as given by the equation of state model of McQueen et al. [1970].

Figure 2: High pressure, high temperature thermodynamic properties of Fe taken from Figure 1 (same symbols), are plotted as a function of pressure and compared with the equivalent properties inferred for the core [Stacey, 1977a; Dziewonski et al., 1975; Anderson and Hart, 1977; Hart et al., 1977; Jamieson et al., 1979]. The curve for the Grüneisen parameter of Fe is from the fit shown in Figure 1a. Stacey's best estimates for the Grüneisen parameter in the outer core are labeled γ and γ_{VZ}. Also shown are the fits to the data for $\left(K_s\right)_H$ and α_H discussed in the text.

Figure 3: The Grüneisen parameter for pressures extending through the core as estimated by Stacey and as extrapolated from the present data on iron (Figure 1a). The function $\gamma\rho$ = constant assumed by McQueen et al. [1970] is also shown.

Figure 4: The values of α extrapolated from the present results on Fe (Figure 2c) are compared with the estimate of Stacey for the core.

Figure 5: The Hugoniot temperatures of iron as given by McQueen et al. [1970] are contrasted with Stacey's [1977a] estimates of temperatures in the core.

Figure 6: Densities through the core from whole-earth seismological models [PEM: Dziewonski et al., 1975; C2: Anderson and Hart, 1977; Hart et al., 1977] are compared with those of pure iron at high pressures. The measured Hugoniot and calculated 300K isotherm of Fe given by McQueen et al. [1970] are compared with the present estimates of density under conditions appropriate to the core.

Figure 7: Bulk sound speeds of iron along the Hugoniot according to this study and the work of McQueen et al. [1970] (essentially identical), and the measurements of Al'tshuler et al. [1960, 1971] are shown along with the values corrected to core temperatures from the present analysis. For comparison, seismologically measured bulk sound speeds in the core are also shown.

Figure 8: The bulk modulus of iron along the Hugoniot and at core temperatures is compared with that observed in the core from seismology. The sources of data are the same as in Figures 6 and 7. The curve labeled "ρ_{Fe}-inner core" gives that bulk modulus which satisfies both the density data for iron and the measured sound speeds in the inner core.

Figure 9: Core Diagram showing the values of density and bulk modulus which must be simultaneously satisfied by a candidate compound (X) which is coexisting in a given mass fraction with Fe in the outer core, at a pressure of 200 GPa (radius $\sim$ 2860 km). Errors in density may be as much as $\pm$3-5% while those in bulk modulus may be up to $\pm$5-10%. The densities and bulk moduli of the core and of iron (under the same conditions) used to construct this figure are also shown. Ideal mixing is assumed.

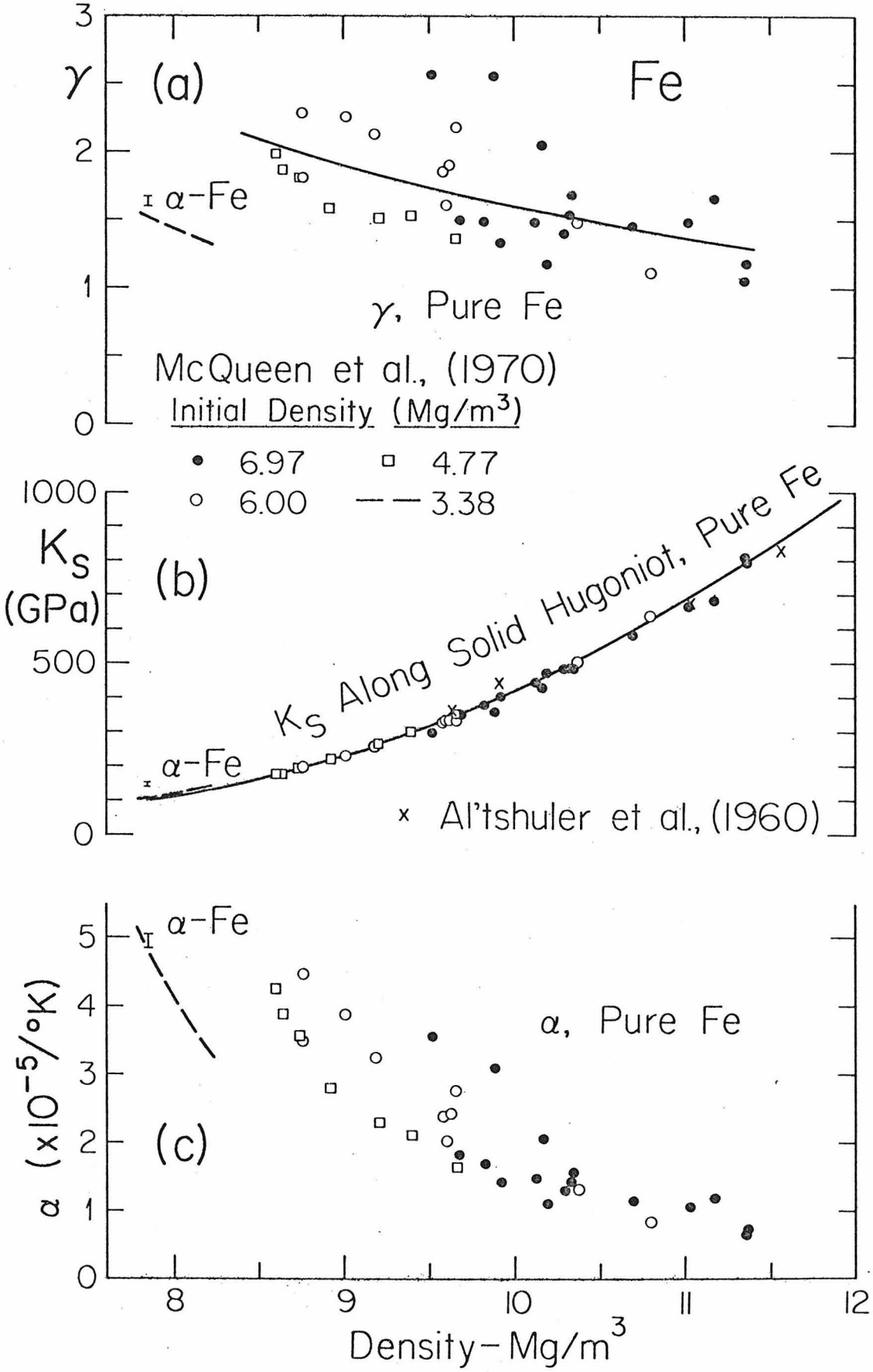
(a)
Fe
γ
α-Fe
γ, Pure Fe
McQueen et al., (1970)
Initial Density (Mg/m³)
6.97
6.00
4.77
3.38
(b)
Ks (GPa)
Ks Along Solid Hugoniot, Pure Fe
α-Fe
Al'tshuler et al., (1960)
(c)
α (x10⁻⁵/°K)
α-Fe
α, Pure Fe
Density - Mg/m³

Fig. 1

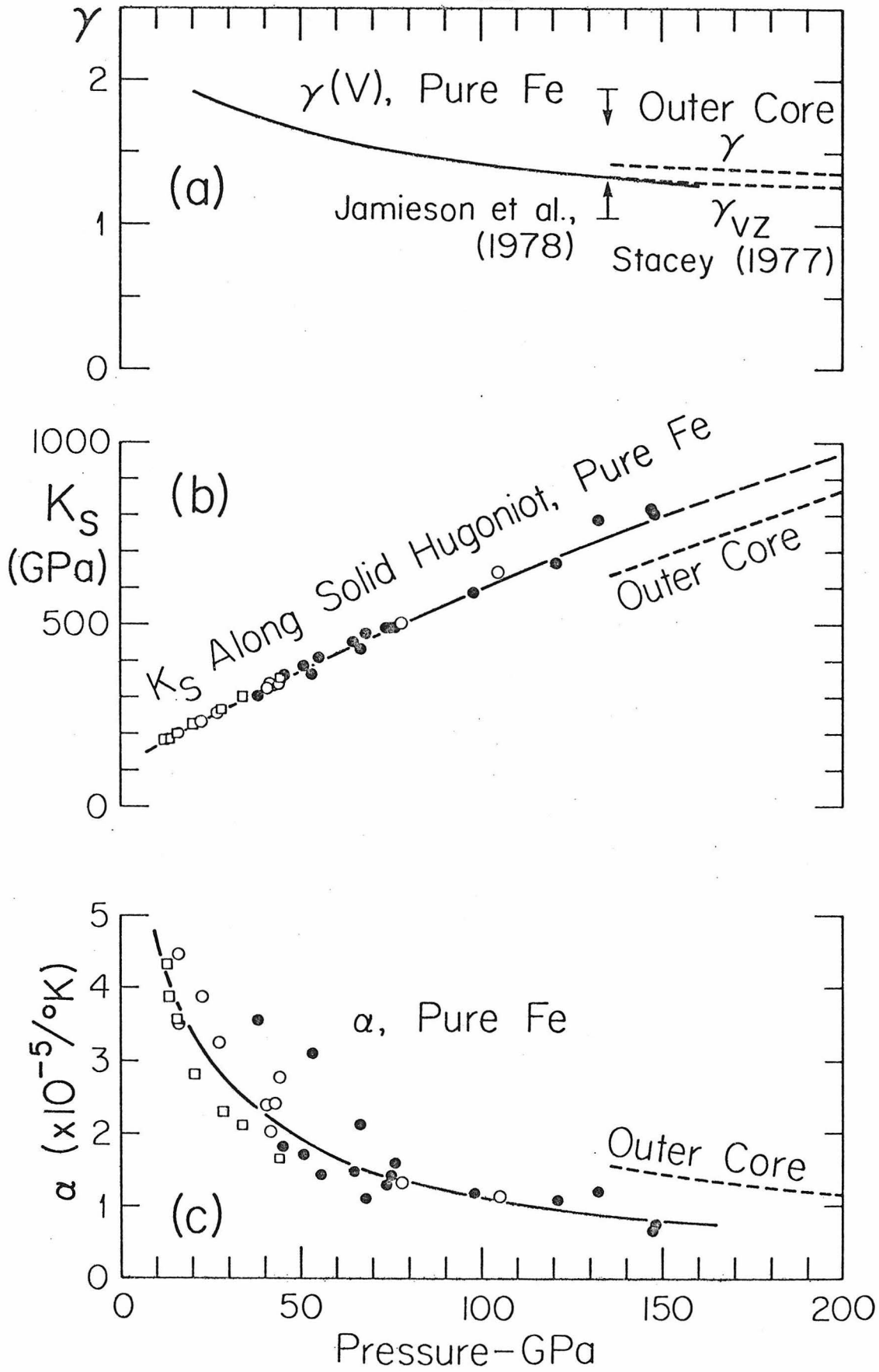
γ
2
1
0
γ(V), Pure Fe
Outer Core
γ
(a)
Jamieson et al., (1978)
γVZ
Stacey (1977)
1000
Ks (GPa)
500
0
(b)
Ks Along Solid Hugoniot, Pure Fe
Outer Core
α (x10⁻⁵/°K)
5
4
3
2
1
0
α, Pure Fe
Outer Core
(c)
0
50
100
150
200
Pressure–GPa

Fig. 2

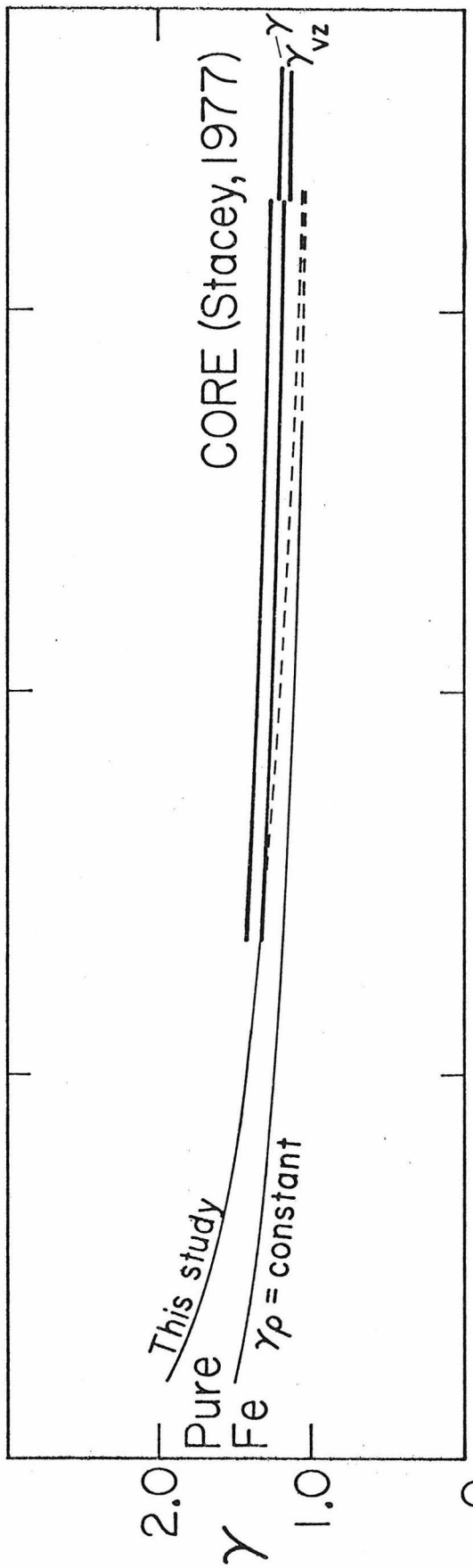
CORE (Stacey, 1977)
γ_{vz}
This study
Pure Fe
$\gamma\rho$ = constant
γ
2.0
1.0
0
100
200
300
Pressure (GPa)

Fig. 3

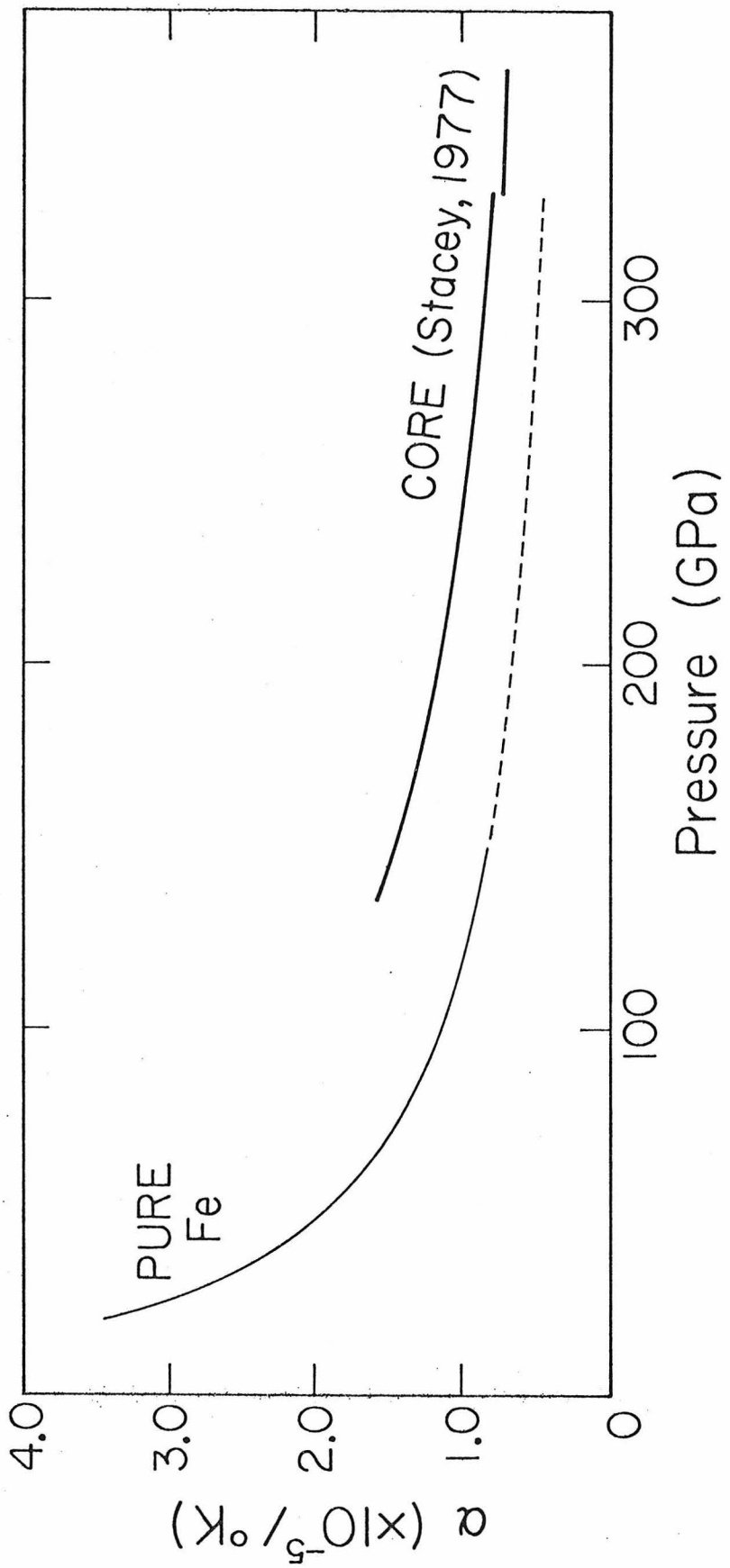
CORE (Stacey, 1977)
PURE Fe
Pressure (GPa)
0
100
200
300
1.0
2.0
3.0
4.0
α (x10⁻⁵/°K)

Fig. 4

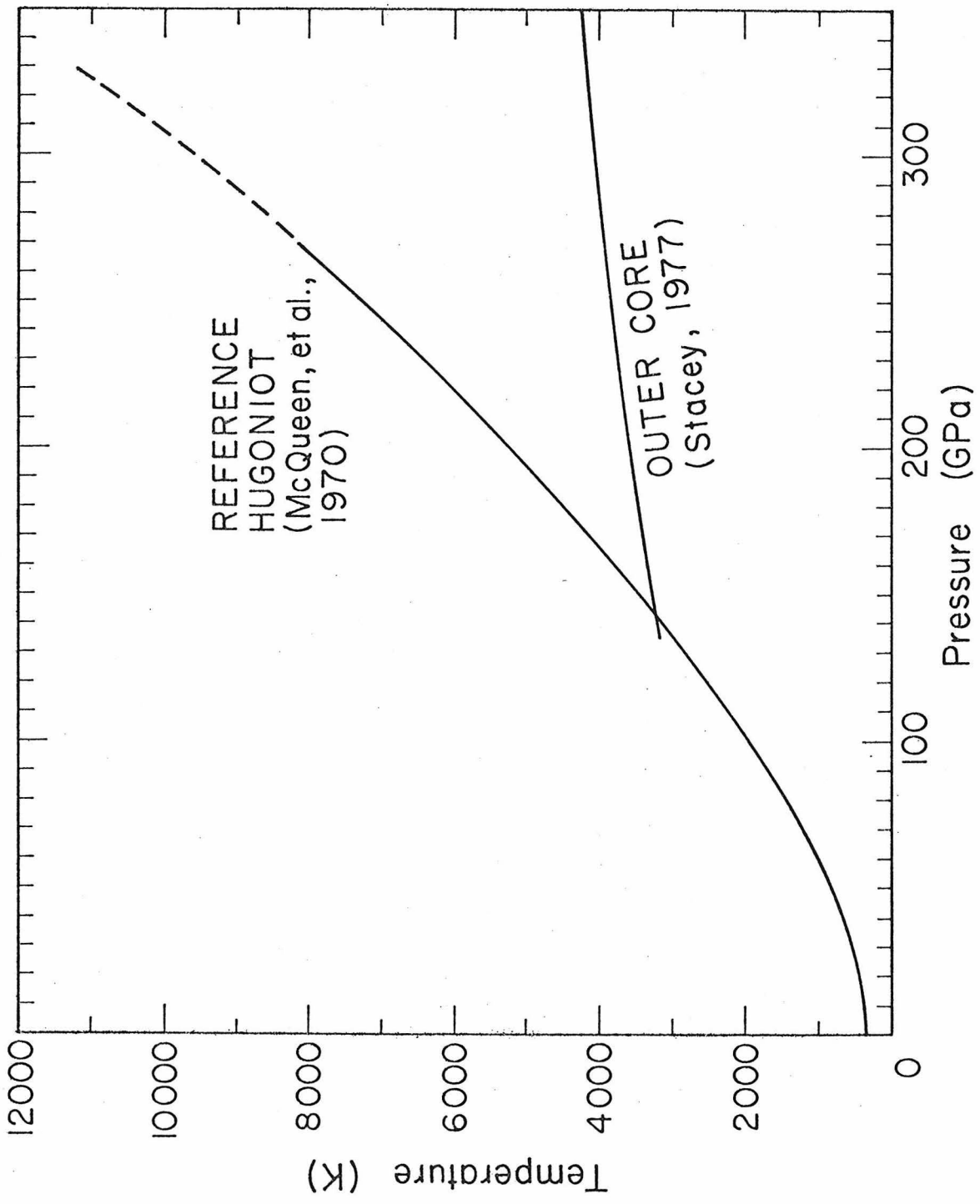
REFERENCE
HUGONIOT
(McQueen, et al.,
1970)
OUTER CORE
(Stacey, 1977)
Temperature (K)
12000
10000
8000
6000
4000
2000
0
100
200
300
Pressure (GPa)

Fig 5

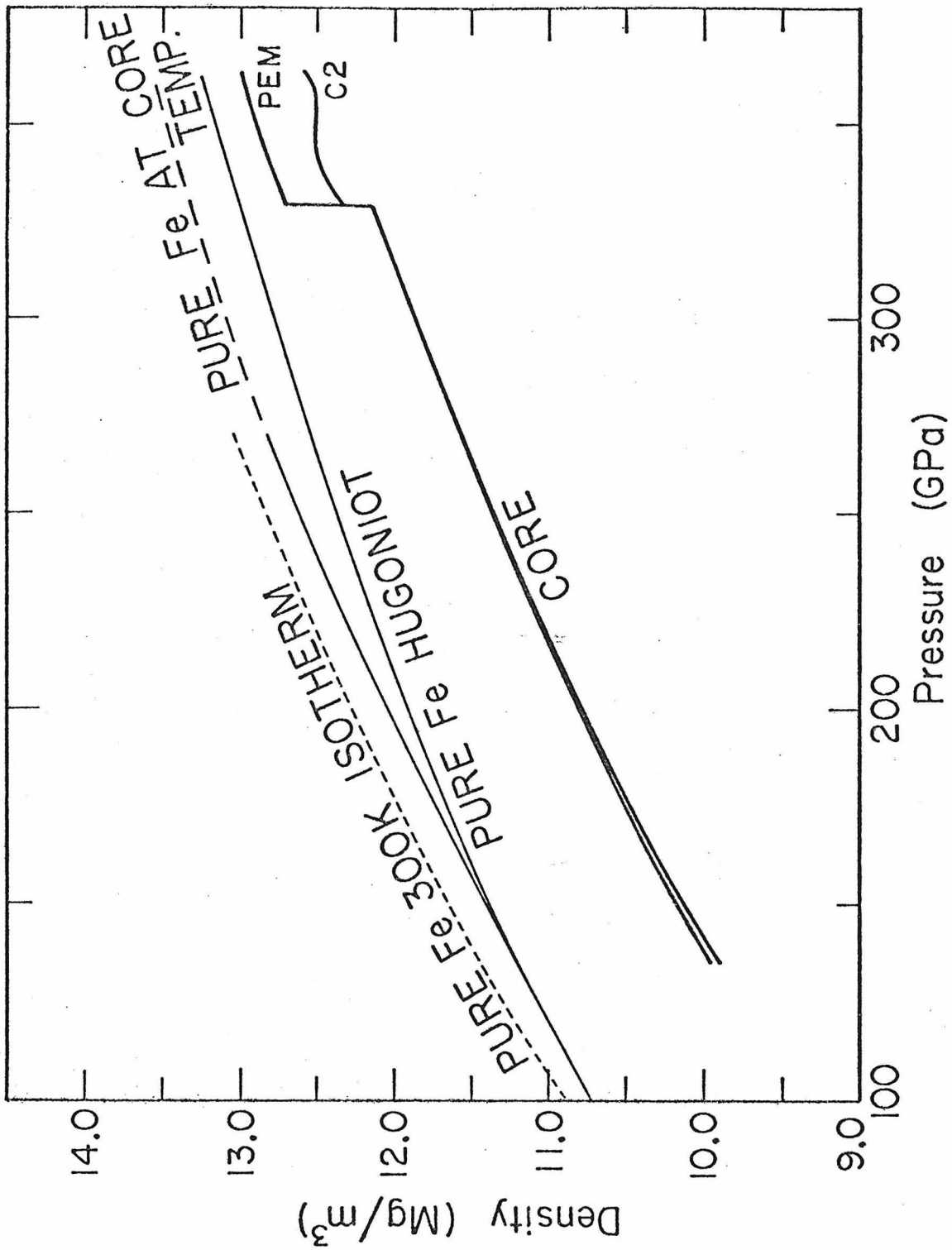
PURE Fe AT CORE TEMP.
PEM
C2
PURE Fe 300K ISOTHERM
PURE Fe HUGONIOT
CORE
Density (Mg/m³)
Pressure (GPa)
14.0
13.0
12.0
11.0
10.0
9.0
100
200
300

Fig. 1

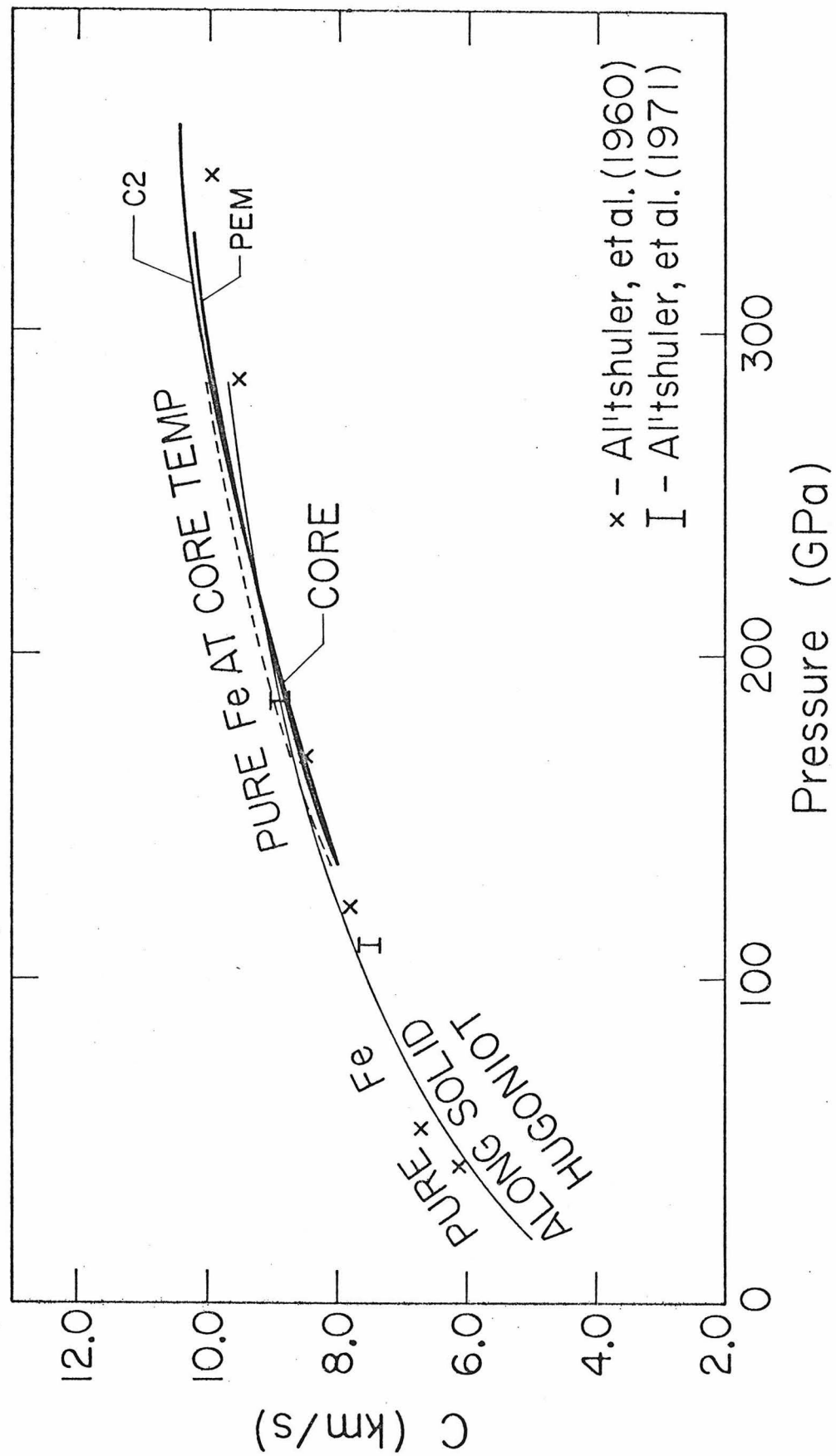
C2
PEM
PURE Fe AT CORE TEMP
CORE
PURE Fe
ALONG SOLID HUGONIOT
x - Al'tshuler, et al. (1960)
I - Al'tshuler, et al. (1971)
C (km/s)
Pressure (GPa)
12.0
10.0
8.0
6.0
4.0
2.0
0
100
200
300

Fig. 7

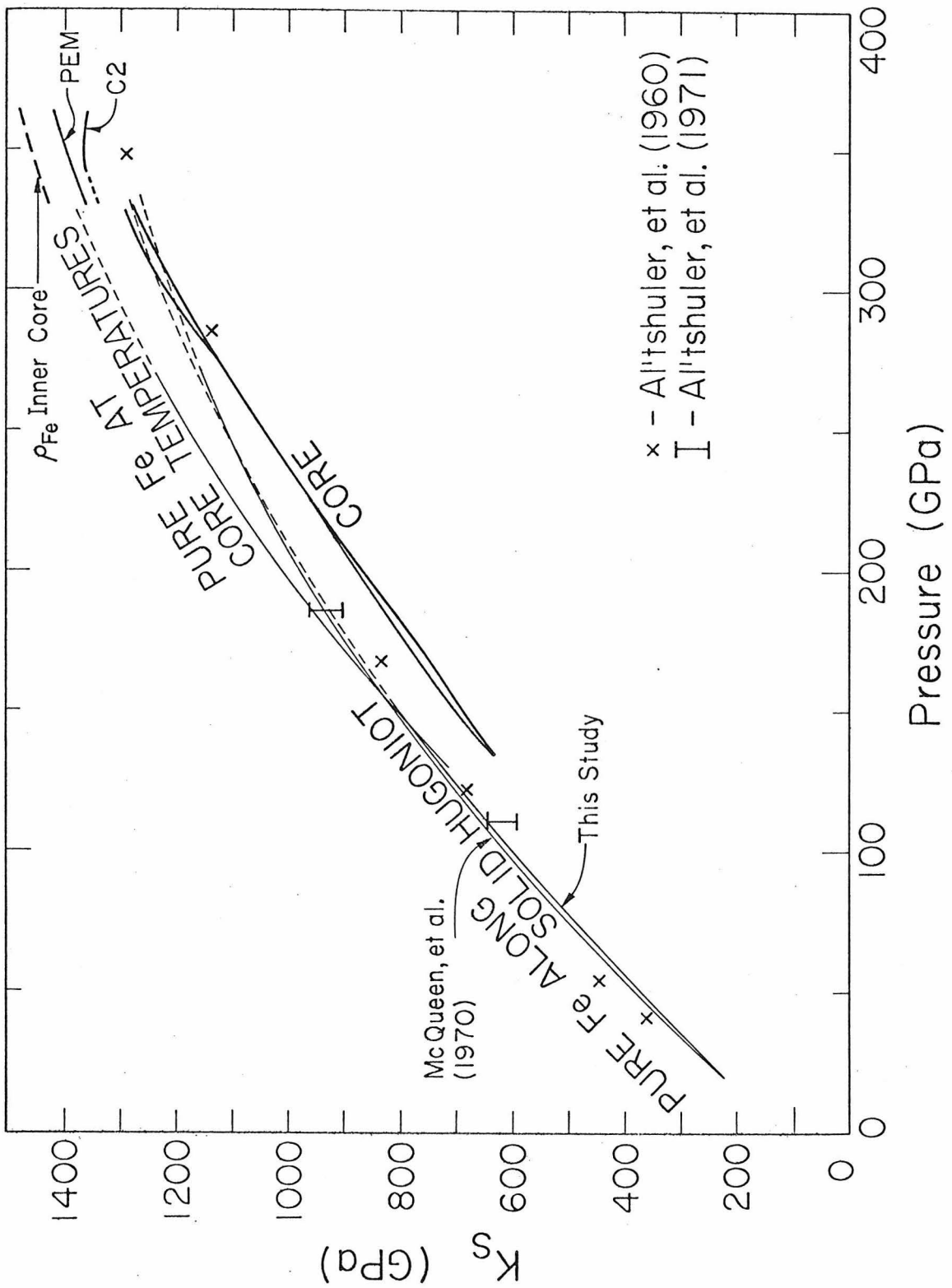
K_S (GPa)
Pressure (GPa)
ρ_{Fe} Inner Core
PEM
C2
PURE Fe AT CORE TEMPERATURES
CORE
PURE Fe ALONG SOLID HUGONIOT
McQueen, et al. (1970)
This Study
× - Al'tshuler, et al. (1960)
I - Al'tshuler, et al. (1971)
0
200
400
600
800
1000
1200
1400
100
300

Fig. 8

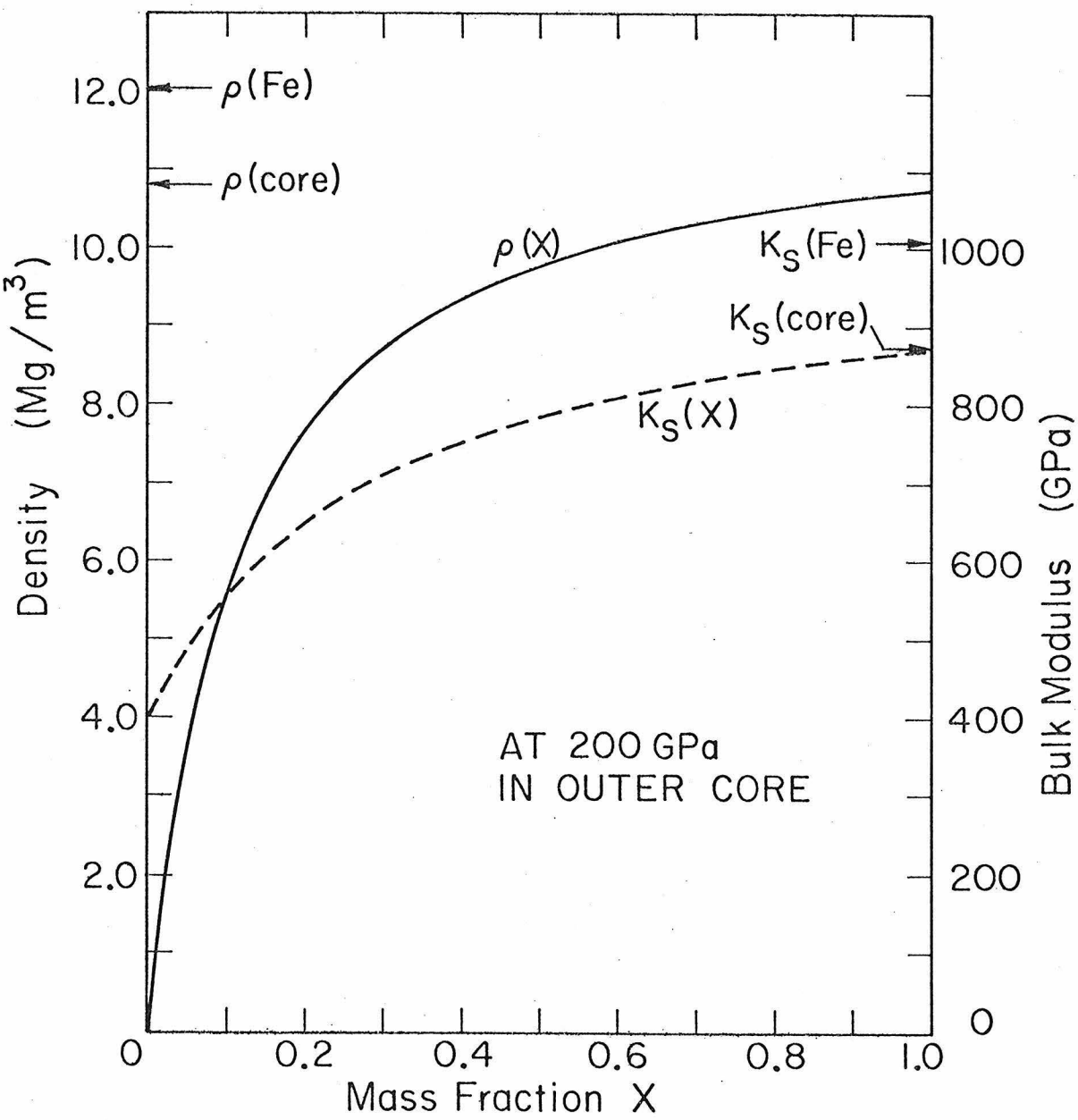
12.0
10.0
8.0
6.0
4.0
2.0
0
Density (Mg/m³)
ρ(Fe)
ρ(core)
ρ(X)
K_S(Fe)
K_S(core)
K_S(X)
1000
800
600
400
200
0
Bulk Modulus (GPa)
AT 200 GPa
IN OUTER CORE
0
0.2
0.4
0.6
0.8
1.0
Mass Fraction X

Fig. 9

Chapter 6

THE EQUATION OF STATE OF A LUNAR ANORTHOSITE: 60025

Abstract

New, shock-wave equation-of-state measurements of lunar anorthosite 60025 (18% initial porosity) and single crystal anorthite in the 40 to 120 GPa (0.4-1.2 Mbar) pressure range are presented and compared, along with previous results on nonporous anorthosite and lunar samples. The porous lunar anorthosite exhibits a lower shock impedance than nonporous anorthosite which, in turn, has a lower impedance than either nonporous gabbroic anorthosite (15418) or high-titanium, mare basalt (70215). This suggests that crater statistics (and, hence, apparent cratering ages) for different lunar terranes are biased by the properties of the different target rocks: for a given set of impacts, systematically smaller craters will tend to be formed in (nonporous) high-Ti mare basalt, gabbroic anorthosite and anorthosite, respectively. The effect of initial porosity in anorthosite 60025 is significant: for a given impact, peak stresses are distinctly lower in the porous anorthosite (typically by about 20% in the 40-100 GPa range) than in the nonporous equivalent, whereas both shock and post-shock temperatures are considerably higher. For example, shock temperatures (at a given pressure) differ by about 10^3 to 5×10^3 K over the range 40-100 GPa. Thus, maturing of a planetary surface by repeated impact (resulting in even mild brecciation and, hence, porosity) strongly enhances the thermal energy partitioning into the planet during meteoritic bombardment. The coupling of kinetic energy on impact is,

however, decreased leading to a decrease in cratering efficiency due to increased porosity. These results imply that, as a result of successive impact events, the dynamic properties of a given rock unit as well as the entire planetary surface will evolve such that the efficiency in the trapping of thermal energy associated with impact will tend to increase with time.

INTRODUCTION

We present the first high-pressure equation-of-state data for calcic anorthosite, an important lunar rock-type. Our new data help to illustrate the range of dynamic (shock-wave) properties among the major lithologies found on the moon and, in particular, the profound effects of mechanical properties (e.g., porosity) on the response of target rocks to impact.

An anorthositic component is thought to make up some two-thirds of the lunar highland crust, as the result of early lunar differentiation (e.g., Adler et al., 1973; Walker et al., 1973a; Taylor and Jakes, 1974, 1977; Taylor and Bence, 1975, 1978; Bielefeld et al., 1977; Schonfeld, 1977). Indeed, anorthosite 60025, the subject of the present study, is a likely representative of the primitive lunar crust (as suggested, for example, by its low $^{87}Sr/^{86}Sr$ values: Papanastassiou and Wasserburg, 1972; see also Taylor and Bence, 1975). It is therefore, a particularly interesting rock to subject to shock-wave studies, in view of the current interest in modeling (and understanding) the early evolution of the moon and the response of its surface to meteoritic bombardment associated with the late stages of accretion. In fact, sample 60025 itself has apparently been affected by a rather ancient (basin-forming?) impact (about 4.2 AE ago, according to $^{40}Ar/^{39}Ar$ data: Schaefer and Husain, 1974), which has left a textural imprint of fracturing and mild brecciation.

Finally, we are interested in acquiring Hugoniot (shock-wave) equation-of-state data on Ca- and Al-bearing oxides and silicates (in the present case, anorthite): i.e., phases of early, high-temperature

condensates from the primitive solar nebula (Grossman, 1972). Such data in conjunction with component mixing models (e.g., Birch, 1952; McQueen, 1968; McQueen et al., 1970; Al'tshuler and Sharipdzhanov, 1971), help to constrain physical models of the growth and evolution of planetary bodies, and may be of direct interest in the study of the deep interiors of terrestrial planets (e.g., Anderson, 1972, 1973; Taylor and Bence, 1975; Ruff and Anderson, 1977).

EXPERIMENTAL

Although most of the experimental procedures used in this study have been previously described (Jeanloz and Ahrens, 1977; Ahrens et al., 1977; Jackson and Ahrens, 1979), details specific to this study, as well as changes and improvements in techniques, are discussed in this section.

Samples approximately 15 mm x 10 mm x 5 mm (0.9-1.2 gm) were cut from a block of specimen 60025.36, and ground and lapped into the shape of a rectangular solid to within dimensional tolerances of 0.1-0.3% (thickness was controlled to 0.04-0.17%, i.e., ±1-6μm). After thorough cleaning and washing in acetone, each sample was heated to 105°C in a partial vacuum ($<10^{-1}$ torr) for 12 hours or more, and then weighed. Values of the bulk density were calculated from the sample dimensions and mass (see Table 1); these are accurate to better than 0.5% (based on repeated measurements).

Archimedean ("intrinsic" or crystal) density was measured using toluene (cf., Ahrens et al., 1977). Rather than placing the sample in a toluene bath as we have previously done, the sample was evacuated (to $<10^{-1}$ torr, at 20°C) inside a flask and then the toluene let in.

In this way, vaporized toluene soaks into the sample very effectively, yielding highly reproducible density determinations. We tried to exclude pyroxene aggregates from our samples; however, despite these precautions, our values of crystal density may be low by as much as 1-2% (indicating less than complete saturation by the toluene) for a pyroxene content of up to 2-3% in our sample (cf., Dixon and Papike, 1975). For the samples listed in Table 1, crystal densities range between 2.709 and 2.751 (±0.003) Mg/m^3, using the correction factors of Berman (1939). These values are very consistent with the composition of 60025 (>98% plagioclase of composition An_{96} and density 2.75 Mg/m^3; Walker et al., 1973b; Dixon and Papike, 1975; Hodges and Kushiro, 1973). Finally, the crystal and bulk densities of each sample were used to calculate the porosities given in Table 1 (listed to the nearest 1/2%, their probable accuracy).

The samples were mounted along with fused quartz arrival and buffer mirrors on pure tantalum or 2024 aluminum driver plates, and impacted by projectiles launched from a two-stage light-gas gun at velocities ranging between 4.5 and 5.8 km/s (see Jeanloz and Ahrens, 1977, and Ahrens et al., 1977). The impacts were produced in a chamber evacuated to about 2×10^{-2} torr. Data, in the form of a streak record from an image-converter streak camera (Figure 1), were read both visually and with a scanning microdensitometer (see Figure 2). Boundaries were picked at 1/2 amplitude of the maximum gradient in light intensity, and the sharpness of the boundary was taken from the slope of the gradient in light intensity. The boundaries were fit by straight lines (all forced to be parallel for a given record) using a least-squares

criterion weighted by the sharpness of each boundary crossing. These fits were then used in a statistical reduction of the shock and partial release data similar to that discussed by Jackson and Ahrens (1979), using the Hugoniot equations of state of McQueen et al. (1970) for Ta and 2024 Al, and of Wackerle (1962) for fused SiO_2.

We have confirmed the reliability of using shock-induced self-illumination to measure shock-wave travel times through the mirrors on the target (cf., Jeanloz and Ahrens, 1977) by mounting small, supplementary arrival mirrors on the main mirrors (as described above) in several experiments (six to date) and comparing the extinction of applied illumination to the onset in self-illumination.

RESULTS

The Hugoniot and release data for anorthosite 60025 are shown in three alternative representations in Figures 3, 4 and 5 and are listed in Table 1. For comparison, data on nonporous plagioclase is also shown in these figures. These latter data represent a baseline against which the effects of porosity on the high-pressure equation-of-state of anorthite are dramatically evident.

Two datum points, the early results of a separate study which is underway on nonporous anorthite (composition of An_{95}; results to be reported elsewhere), are shown in these figures. These data are consistent with previous results for Tahawus Anorthosite (McQueen et al., 1967). Although the Tahawus Anorthosite consists mainly of intermediate plagioclase (An_{49}), it also contains about 10% augite (density $\sim$3.4 Mg/m^3) such that its initial density and, hence, its impedance are

fortuitously very close to that of single-crystal anorthite (see Figure 3; McQueen et al., 1967).

The Tahawus Anorthosite data above 30 GPa have been interpreted by McQueen et al. (1967) as representing a high-density polymorph (or assemblage) formed at high pressure; this is suggested by the anomalous compressibility below 30 GPa (Figure 3) and the linear trend of the shock-wave velocity (U_s) versus particle velocity (u_p) data with an intercept below the bulk sound speed of anorthite (Figure 4, McQueen et al., 1967; Liebermann and Ringwood, 1976; cf. also Ahrens et al., 1969a and b). McQueen et al. (1967) inferred a zero-pressure density of about 3.5 Mg/m^3 corresponding to these high-pressure data; this is also consistent with one release adiabat measurement of Ahrens and Rosenberg (1968) but see Ahrens et al. (1969a and b) as well.

Also shown in Figures 3 and 4 is a pre-experimental estimate of the Hugoniot state of anorthite (An_{96}) at 120 GPa (1.2 Mbar) based on the inversion of Hugoniot data for various rocks, using an additive (noninteracting continua) mixture theory (Ahrens et al., 1977). This theoretical estimate is consistent with the Hugoniot data shown in these figures, thus lending further conficence to the validity and usefulness of the mixture model in extracting the properties of components or in predicting the behavior of aggregates which have not been (and perhaps cannot be) studied at high pressures.

The equation-of-state of nonporous anorthite, then, is well described by (i) the new single-crystal data, (ii) existing data on anorthosite (fortuitously), and (iii) a theoretical estimate.

It is clear from the figures, however, that the data for porous

anorthite (anorthosite 60025) are dramatically offset from the nonporous Hugoniot. Presumably, this is due to the large amount of thermal energy imparted to the porous samples in the form of irreversible work done in compacting void space (see e.g., Ze'ldovich and Raizer, 1967; McQueen et al., 1970). It is worth noting that sample #036 (91 GPa shock state) with an initial porosity which was approximately 2% higher than that of the other samples (about 18 ± 1/2%; Table 1), has a slightly larger offset from the nonporous Hugoniot than do the other porous samples, thus supporting the present interpretation. Correcting for the extra 2% in initial porosity (based on the effect of 18% porosity on the other three samples, when compared with the nonporous data) brings the Hugoniot state of sample #036 down in pressure (to about 83 GPa; See Figure 3) and well in line with the three other Hugoniot points for 60025.

The streak record shown in Figure 1b demonstrates an unusual feature. There is a bright flash of light at the back surface of the sample as the shock-wave emerges. We have seen this feature in all four experiments on 60025 (Figure 2), but it has not been seen in experiments either on single-crystal anorthite or other nonporous samples (despite the high pressures to which these have been shocked). This seems to indicate that a considerable quantity of thermal energy resides in the porous samples (compared to the nonporous samples) at high pressures. We do not believe that this flash is associated with a second wave because its width does not correlate with shock pressure (see Figure 2), and because preliminary results of an experiment at about 25 GPa with an inclined mirror assembly (cf., Ahrens et al., 1969b) do not show a multiple wave

structure.

In the shock-wave velocity versus particle velocity plane (Figure 4) the lunar anorthosite data lie on a straight line which is remarkably parallel to the line defined by the high-pressure Hugoniot points for nonporous anorthite, but offset towards lower U_s. Using the conventional, hydrodynamic interpretation of the linear U_s-u_p equation-of-state (e.g., Ruoff, 1967; McQueen et al., 1967), this observation would imply a slightly lower initial bulk sound speed (but similar pressure derivative of the bulk modulus) for the porous anorthite when compared to the nonporous anorthite. Assuming no further complications due to phase transformations (e.g., kinetic effects: Jeanloz and Ahrens, 1977; see also Davies, 1972; and McQueen et al., 1967), this is exactly what might be expected as a thermal effect: a lower "effective" initial bulk modulus for the porous (much hotter) anorthite. The lower initial density tends to counteract the thermal effect, raising the initial sound speed somewhat.

Release adiabat data are also shown in Figure 3, but their interpretation is problematical. The data are reduced from buffer-mirror, travel times (see Jeanloz and Ahrens, 1977 and Ahrens et al., 1977), and exhibit the steep initial release slopes that have been documented for several silicates and rocks (Ahrens and Rosenberg, 1968; Ahrens et al., 1969b; Grady et al., 1974; Grady and Murri, 1976; Grady, 1977; Jeanloz and Ahrens, 1977; Ahrens et al., 1977). Unfortunately, there are several possible explanations for such steep slopes.

In the simplest (nontransforming, hydrodynamic) case, the release path is expected to be isentropic (Courant and Friedericks, 1948;

Ze'ldovich and Raizer, 1967). This "normal" release path, then, is nearly parallel to but somewhat less steep than the Hugoniot. However, deviations from these conditions can lead to steeper release adiabats. Grady (1977), for example, believes that material strength (nonhydrodynamic behavior) can be regained by a sample while it is at peak pressure, based on a specific model in which yielding and transformation under shock are associated with hot shear zones. Material strength will, in general, result in a steep, initial release path (corresponding to elastic unloading: e.g., Courant and Friedericks, 1948; Fowles, 1961; Al'tshuler, 1965; Murri et al., 1974). On the other hand, one could argue that a material which has lost virtually all of its strength during shock compression due to its dynamic strength being significantly surpassed (see Rice et al., 1958; Ahrens and Duvall, 1966; van Thiel and Kusubov, 1968; Fowles and Williams, 1970; however, cf., also Ahrens et al., 1968, and Gust and Royce, 1971), could retain enough strength to affect the release slope (Ahrens and Rosenberg, 1968; and Ahrens et al., 1969b, document a Hugoniot elastic limit of about 5 GPa for plagioclase). Although such an interpretation seems consistent with the fact that the highest pressure experiment on 60025 (#026: 94 GPa shock state) resulted in an apparently "normal" release path, the observed, steep release adiabats for the other experiments carried out on porous anorthite (for which the shock temperatures were presumably very high) make it appear quite unlikely that the steep release paths are due to strength effects. In particular, the steep slope for #036 (91 GPa shock pressure) compared with that for the single-crystal anorthite (at slightly lower pressure and a temperature which is less

by about 4×10^3 K, according to preliminary analyses), make it virtually inconceivable that material strength is significantly affecting the release paths.

A more likely class of effects are those involving transformations (reactions, phase transformations, changes in material properties) or, in general, entropy production during release. A simple case is that in which partial phase transformation has occurred on shock-loading so that the release path is a better representation of a true compression curve than the Hugoniot itself (Ahrens and Rosenberg, 1968; Grady et al., 1974; Grady and Murri, 1976; Jeanloz and Ahrens, 1977). Since the present data do not fall in what would normally be called a "mixed phase region" (McQueen et al., 1967; Ahrens et al., 1969a), such phase transformation effects may not seem likely. However, it is possible that: (i) phase transformation is still not complete in states beyond the "mixed-phase region" (Jeanloz and Ahrens, 1977; Jeanloz, 1977; Jackson and Ahrens, 1979), or (ii) other kinetic effects are involved. For example, further phase transformation may still be under way even as the sample is beginning to unload, so that density could even increase (momentarily) as unloading begins. (Given the large amount of "overdriving" that typically occurs under shock conditions, such continued transformation is quite conceivable, e.g., McQueen et al., 1967.)

Also, we note that an additional factor affecting the slope of the release adiabats is the use of a finite difference in evaluating the Riemann integral (by necessity, since only one release state is measured in each experiment). As shown by Lyzenga and Ahrens (1978), this yields an upper bound to the actual density on release. Thus, a

number of factors may be invoked to explain the steep release adiabats for 60025. Unfortunately, it is not clear what role each of these factors plays (quantitatively) in the apparent behavior observed on release.

DISCUSSION

The present results, when combined with previous data on the shock properties of lunar rocks, provide several interesting implications for the dynamics of impact phenomena on the lunar surface.

Our work to date suggests that essentially all of the major lunar rock types will have Hugoniots (see Figure 5) bracketed by the Hugoniots of 70215 (a high-titanium, mare basalt; Ahrens et al., 1977) and of non-porous anorthite (labeled An_{95}) for solid (nonporous) target materials. For example, a point for gabbroic anorthosite (15418), calculated via the additive mixing model (see ablve) and shown in Figure 5, has an impedance ($\rho_0 U_s$) = slope in this Figure), intermediate between that of the basalt and anorthite. Highland rocks appear, then, to have somewhat lower impedances than mare rocks implying the generation of higher pressures in the latter for a given impact velocity. As an example, a curve indicating the peak pressure generated by an iron projectile impacting at 6.0 km/s is shown in Figure 5, showing that a given phase (a plagioclase, for example) might experience peak stresses different by about 20% for the same impact velocity, depending on whether it was located in a mare or in a highland terrane. These differences will increase with increasing pressure (or impact velocity). However, most solid lunar rock types will probably fall in between the bounds set by

the anorthite and the mare basalt in Figure 5.

More dramatic, though, is the substantially lower impedance exhibited by 60025, compared to the solid rocks (Figure 5). For a given impact event, this porous rock clearly attains much lower pressures than the solid rocks, but much higher shock and post-shock temperatures than the nonporous samples. For the 6.0 km/s iron impact, although peak pressures in the porous anorthosite are about 20% lower than for the nonporous equivalent, a preliminary analysis indicates peak temperatures on the order of 4,000 K higher than in the single-crystal anorthite. This same analysis yields a difference of about 1-4 x 10^3 K in shock temperature (at a given pressure) between 60025 and nonporous anorthite over the pressure range 40-100 GPa. Thus, porosity can have a very substantial effect on the thermal energy partitioning and the shock pressures reached in an impact process, ultimately affecting the nature and degree of shock-metamorphism as well as the residual ("post-shock") heating.

The porosity in 60025 is due to mild brecciation and fracturing (Walker et al., 1973; Hodges and Kushiro, 1978; Dixon and Papike, 1975) resulting from light shocking after crystallization. In general, a planetary surface is expected to "mature" with time in that continued bombardment tends to fracture and brecciate the surface, forming a regolith-like layer. Safronov (1972, 1978) and Kaula (1978) have discussed the importance of such a regolith in the thermal evolution of young planetary bodies in that it acts both as an insulating layer which traps impact-produced thermal energy, and also controls the loss of this energy by stirring due to subsequent overturn. Our data emphasize

a separate (perhaps equally important) effect of such a layer indicating that, with its higher initial porosity (lower impedance), it could allow substantially increased partitioning of thermal energy into a planet during accretion or bombardment of its surface.

Therefore, with time, the dynamic properties of the pristine planetary surface will tend to mature (with the appropriate Hugoniots sweeping downward, to the right in Figure 5), resulting in a more substantial shock-heating associated with any given impact. The porosity needed for such dramatic changes can result from very mild shocking (as in the case of 60025). Of course, this effect can be counterbalanced by several processes: for example, the eruption of fresh volcanic flows onto a planetary surface.

CONCLUSION

We have presented the first high-pressure, equation-of-state data for a calcic, aluminous silicate: anorthite. Our shock-wave results on lunar anorthosite 60025, which has an average initial porosity of about 18%, contrast sharply with the equation-of-state of nonporous anorthite due to the large amount of thermal energy associated with pore closure under shock-loading. This thermal energy results in a substantial offset (e.g., as a significant thermal pressure) of the high-pressure states achieved by the porous anorthosite (compared to the nonporous anorthite), illustrating the important role of porosity in determining the response of a target material. For a given impact, although peak pressures are less in a porous than a nonporous target, both shock and post-shock temperatures can be considerably larger, as

in the case of 60025. Cratering efficiency (per mass of target) is therefore significantly reduced for the porous case as a given projectile will impart a higher proportion of its kinetic energy to a smaller mass of target.

The present data provide a shock-wave equation-of-state for an important lunar rock-type and a prime candidate for material representative of the primordial lunar crust. These data can be used to describe the dynamic response of much of the lunar surface to meteoritic impact (e.g., during the late stages of accretion). The combined results on lunar samples to date indicate significant variations in the dynamic properties among the major lunar lithologies. These imply that for a given distribution of high impedance meteorites, the resulting crater sizes will tend to be systematically larger for lunar anorthosite, gabbroic anorthosite, and high-Ti mare basalt respectively. Hence, such lateral variations in crater-forming processes will be reflected as a systematic bias in apparent cratering ages (e.g., in mare vs. terrae). More significantly, however, the present study of a porous highland rock illustrates quite clearly the time-dependence of the dynamic properties of a petrologically well-defined rock unit or planetary surface due to its continual "maturing" under meteoritic bombardment. This results in a general (and potentially very substantial) enhancement, with time, in the production of thermal energy due to the impact of this planetary surface.

ACKNOWLEDGEMENTS

We thank E. Gelle and R. Smith for their dedicated assistance with

the experiments and Dr. Y. Syono for providing samples of anorthite. We also appreciate the helpful comments of Malcolm Somerville and James Long. The critical reviews of Rex V. Gibbons and Jon F. Bauer also improved the paper.

Adler I., Trombka J. I., Schmadeback R., Lowman P., Blodget H., Yin L., Eller E., Podwysocki M., Weidner J. R., Bickel A. L., Lum R. K. L., Gerard J., Gorenstein P., Rjorkholm P., and Harris B. (1973) Results of the Apollo 15 and 16 X-ray experiment. Proc. Lunar Sci. Conf. 4th, p. 2783-2791.

Ahrens T. J., Anderson D. L., and Ringwood A. E. (1969a) The equation of state and crystal structures of high-pressure phases of silicates and oxides. Rev. Geophys. Space Phys. 7, 667-707.

Ahrens T. J. and Duvall G. E. (1966) Stress relaxation behind elastic shock waves in rock. J. Geophys. Res. 71, 4349-4360.

Ahrens T. J., Gust W. H., and Royce E. B. (1968) Material strength effect in the shock compression of alumina. J. Appl. Phys. 39, 4610-4616.

Ahrens T. J., Jackson I., and Jeanloz R. (1977) Shock compression and adiabatic release of a titaniferous mare basalt. Proc. Lunar Sci. Conf. 8th, p. 3437-3455.

Ahrens T. J., O'Keefe J. D., and Gibbons R. V. (1973) Shock compression of a recrystallized anorthositic rock from Apollo 15. Proc. Lunar Sci. Conf. 4th, p. 2575-2590.

Ahrens T. J., Petersen C. F., and Rosenberg J. T. (1969b) Shock compression of feldspars. J. Geophys. Res. 74, 2727-2746.

Ahrens T. J. and Rosenberg J. T. (1968) Shock metamorphism: Experiments on quartz and plagioclase. In Shock Metamorphism of Natural Materials (B. M. French and N. M. Short, eds.), p. 59-81. Mono Book, Baltimore.

Al'tshuler L. V. (1965) Use of shock waves in high-pressure physics. Sov. Phys. Uspekhi 8, 52-91.

Al'tshuler L. V. and Sharipdzhanov I. I. (1971) Additive equations of state of silicates at high pressures. Izv. Earth Phys. 3, 11-28.

Anderson D. L. (1972) Implications of the inhomogeneous planetary accretion hypothesis, Comments on Earth sciences. Geophysics 2, 93-98.

Anderson D. L. (1973) The formation of the moon (abstract). In Lunar Science IV, p. 40-42. The Lunar Science Institute, Houston.

Berman H. (1939) A torsional microbalance for the determination of specific gravities of minerals. Amer. Mineral. 24, 434-440.

Bielefeld M. J., Andre C. G., Eliason E. M., Clark P. E., Adler I., and Trombka J. I. (1977) Imaging of lunar surface chemistry from orbital X-ray data. Proc. Lunar Sci. Conf. 8th, p. 901-908.

Birch F. (1952) Elasticity and constitution of the Earth's interior. J. Geophys. Res. 57, 227-286.

Courant R. and Friedrichs K. (1948) Supersonic Flow and Shock Waves. Interscience, New York. 464 pp.

Davies G. F. (1972) Equations of state and phase equilibria of stishovite and a coesitelike phase from shock-wave and other data. J. Geophys. Res. 77, 4920-4933.

Dixon J. R. and Papike J. J. (1975) Petrology of anorthosites from the Descartes region of the moon: Apollo 16. Proc. Lunar Sci. Conf. 6th, p. 263-291.

Fowles G. R. (1961) Shock wave compression of hardened and annealed 2024 aluminum. J. Appl. Phys. 32, 1475-1487.

Fowles G. R. and Williams R. F. (1970) Plane stress wave propagation in solids. J. Appl. Phys. 41, 360-363.

Grady D. E. (1977) Processes occurring in shock wave compression of rocks and minerals. In High-Pressure Research: Applications to Geophysics (M. H. Manghnani and S. Akimoto, eds.), p. 389-438. Academic Press, New York.

Grady D. E. and Murri W. J. (1976) Dynamic unloading in shock compressed feldspar. Geophys. Res. Lett. 3, 472-474.

Grady D. E., Murri W. J., and Fowles G. R. (1974) Quartz to stishovite: Wave propagation in the mixed phase region. J. Geophys. Res. 79, 332-338.

Grossman L. (1972) Condensation in the primitive solar nebula. Geochim. Cosmochim. Acta 36, 597-619.

Gust W. H. and Royce E. B. (1971) Dynamic yield strengths of B_4C, BeO, and Al_2O_3 ceramics. J. Appl. Phys. 42, 276-295.

Hodges F. N. and Kushiro I. (1973) Petrology of Apollo 16 lunar highland rocks. Proc. Lunar Sci. Conf. 4th, p. 1033-1048.

Jackson I. and Ahrens T. J. (1978) The equation of state of forsterite. Submitted to J. Geophys. Res.

Jeanloz R. (1977) Shocked olivines and the spinel phase: IR spectra, observations and implications (abstract). Geol. Soc. Am. Abstracts with Programs 9, 1036.

Jeanloz R. and Ahrens T. J. (1977) Pyroxenes and olivines: Structural implications of shock-wave data for high-pressure phases. In High-Pressure Research: Applications to Geophysics (M. H. Manghnani and S. Akimoto, eds.), p. 439-461. Academic Press, New York.

Kaula W. M. (1978) Planetary thermal evolution during accretion (abstract). In Lunar and Planetary Science IX, p. 615-717. The Lunar Science Institute, Houston.

Liebermann R. C. and Ringwood A. E. (1976) Elastic properties of anorthite and the nature of the lunar crust. Earth Planet. Sci. Lett. 31, 69-74.

Lyzenga G. A. and Ahrens T. J. (1978) The relation between the shock-induced free-surface velocity and the post-shock specific volume of solids. J. Appl. Phys. 49, 201-204.

McQueen R. G. (1968) Shock-wave data and equations of state. In Seismic Coupling, p. 53-106. Proceedings of a meeting sponsored by Advanced Research Projects Agency, Stanford Research Institute, Jan. 15-16, 1968.

McQueen R. G., Marsh S. P., and Fritz J. N. (1967) Hugoniot equation of state of twelve rocks. J. Geophys. Res. 72, 4999-5036.

McQueen R. G., Marsh S. P., Taylor J. W., Fritz J. N., and Carter W. J. (1970) The equation of state of solids from shock wave studies. In High Velocity Impact Phenomena (R. Kinslow, ed.), p. 294-419. Academic Press, New York.

Murri W. J., Curran D. R., Petersen C. F., and Crewdson R. C. (1974) Response of solids to shock waves. In Advances in High-Pressure Research (R. H. Wentorf, Jr., ed.), V. 4, p. 1-163. Academic Press, New York.

Papanastassiou D. A. and Wasserburg G. J. (1972) Rb-Sr systematics of Luna 20 and Apollo 16 samples. Earth Planet. Sci. Lett. 17, 52-63.

Rice M. H., McQueen R. G., and Walsh J. M. (1958) Compression of solids by strong shock waves. Solid State Phys. 6, 1-63.

Ruoff A. L. (1967) Linear shock-velocity--particle-velocity relationship. J. Appl. Phys. 38, 4976-4980.

Ruff L. and Anderson D. L. (1977) A geophysical model for core convection due to lateral heat sources (abstract). E⊕S 58, 1129.

Safronov V. S. (1972) Evolution of the Protoplanetary Cloud and Formation of the Earth and the Planets. NASA TT F-677 (trans. from Nauka, Moscow, 1969).

Safronov V. S. (1978) The heating of the Earth during its formation. Icarus 33, 3-12.

Schaeffer O. A. and Husain L. (1974) Chronology of lunar basin formation. Proc. Lunar Sci. Conf. 5th, p. 1541-1555.

Schonfeld E. (1977) Comparison of orbital chemistry with crustal thickness and lunar sample chemistry. Proc. Lunar Sci. Conf. 8th, p. 1149-1162.

Taylor S. R. and Bence A. E. (1975) Evolution of the lunar highland crust. Proc. Lunar Sci. Conf. 6th, p. 1121-1141.

Taylor S. R. and Bence A. E. (1978) Chemical constraints on lunar highland petrogenesis (abstract). In Lunar and Planetary Science IX, p. 1155-1157. The Lunar Science Institute, Houston.

Taylor S. R. and Jakeš P. (1974) The geochemical evolution of the moon. Proc. Lunar Sci. Conf. 5th, p. 1287-1305.

Taylor S. R. and Jakeš P. (1977) Geochemical evolution of the moon revisited. Proc. Lunar Sci. Conf. 8th, p. 433-446.

Van Thiel M. and Kusubov A. (1968) Effect of 2024 aluminum alloy strength on high-pressure shock measurements. In Accurate Characterization of the High-Pressure Environment (E. C. Lloyd, ed.), p. 125-130. National Bureau of Standards Special Publication 326.

Wackerle J. (1962) Shock-wave compression of quartz. J. Appl. Phys. 33, 922-930.

Walker D., Grove T. L., Longhi J., Stolper E. M., and Hays J. F. (1973) Origin of lunar felspathic rocks. Earth Planet. Sci. Lett. 20, 325-336.

Walker D., Longhi J., Grove T. L., Stolper E., and Hays J. F. (1973) Experimental petrology and origin of rocks from the Descartes Highlands. Proc. Lunar Sci. Conf. 4th, p. 1013-1032.

Ze'ldovich Y. B. and Raizer Y. P. (1966) Physics of Shock Waves and High-Temperature Hydrodynamic Phenomena. Academic Press, New York. 916 pp. (2 vols.).

TABLE 1

SHOCK-WAVE, EQUATION-OF-STATE DATA FOR LUNAR ANORTHOSITE, 60025

SHOT NUMBER	026	029	036	042
Initial Density-Bulk (Mg/m^3)	2.234(±0.001)	2.244(±0.002)	2.199(±0.001)	2.239(±0.009)
Initial Porosity	18%	18%	20%	18½%
Impact Velocity (km/s)	5.762(±0.012)	4.467(±0.003)	5.668(±0.003)	4.971(±0.002)
Flyer/Driver Material	Ta	Ta	Ta	Al-2024
HUGONIOT STATE				
Shock Wave Velocity (km/s)	9.17(±0.13)	7.73(±0.05)	9.15(±0.07)	6.75(±0.04)
Particle Velocity (km/s)	4.591(±0.015)	3.617(±0.004)	4.525(±0.006)	2.964(±0.009)
Pressure (GPa)	94.0(±1.1)	62.7(±0.3)	91.1(±0.6)	44.8(±0.2)
Density (Mg/m^3)	4.473(±0.075)	4.216(±0.027)	4.351(±0.039)	3.990(±0.025)
RELEASE STATE				
Particle Velocity (km/s)	3.682(±0.164)	3.355(±0.069)	4.417(±0.054)	2.783(±0.023)
Pressure (GPa)	56.4(±4.6)	47.5(±1.8)	79.0(±1.8)	33.9(±0.5)
Density (Mg/m^3)	4.074(±0.096)	4.137(±0.039)	4.333(±0.039)	3.943(±0.025)

Figure 1. (a) Still photograph taken through image converter camera, viewing the back-side of the target (#029): the sample and mirrors can be seen, as well as the location of the slit.

(b) Streak photograph for shot #029 taken by sweeping the image of the slit towards the right (at nearly constant velocity) as the projectile impacted the target. Note the intense flash of light as the shock-wave crosses the sample/buffer mirror interface.

Figure 2. Microdensitometer scans taken from the streak records of experiments on 60025, showing the region of the flash (sample/buffer mirror interface) only. Intensity of light is shown as a function of time (10 μm spatial resolution on the film), at constant position along the slit (approximately at the center of the sample). Note the nearly constant flash duration. Arrival of the shock-wave into the buffer mirror and (in two cases) exit of the shock-wave from the back surface of the buffer mirror is also indicated. The noise in these traces is due wholly to the grain of the film.

Figure Captions (Cont'd)

Figure 3. Hugoniot (shock-wave) equation-of-state data for sample 60025 (including the datum from shot #036 at 91 GPa, corrected for extra porosity: see text) compared with single crystal anorthite (labelled An_{95}; source: Miyake-zima, Izu Islands, JAPAN), a terrestrial (intermediate plagioclase) anorthosite (from Tahawus, NY: McQueen et al., 1967), and a theoretical estimate at 120 GPa (cf., Ahrens et al., 1977), in the pressure-density plane. Note the steep release adiabat slopes for the three, low-pressure experiments on 60025.

Figure 4. Shock-wave velocity (U_s) versus particle velocity (u_p) data pertaining to calcic plagioclase (symbols are defined in Fig. 3). Only data above 30 GPa are shown. The bulk sound speed (c_o) from Liebermann and Ringwood (1976) is indicated for comparison. The porous (60025) and non-porous data define two, linear and essentially parallel trends, and the consistency of the combined results on non-porous samples is evident (despite significant variations in chemical composition: see text).

Figure 5. Shock pressure versus particle velocity data for anorthosite 60025, single-crystal anorthite, terrestrial anorthosite (Tahawus, NY) and mare basalt 70215, and a theoretical estimate for gabbroic anorthosite 15418 (Ahrens et al., 1977). Only data above 30 GPa are shown. The Hugoniot of iron is shown to illustrate the impedance-matching conditions for the 6.0 km/s impact of an iron projectile onto a lunar target.

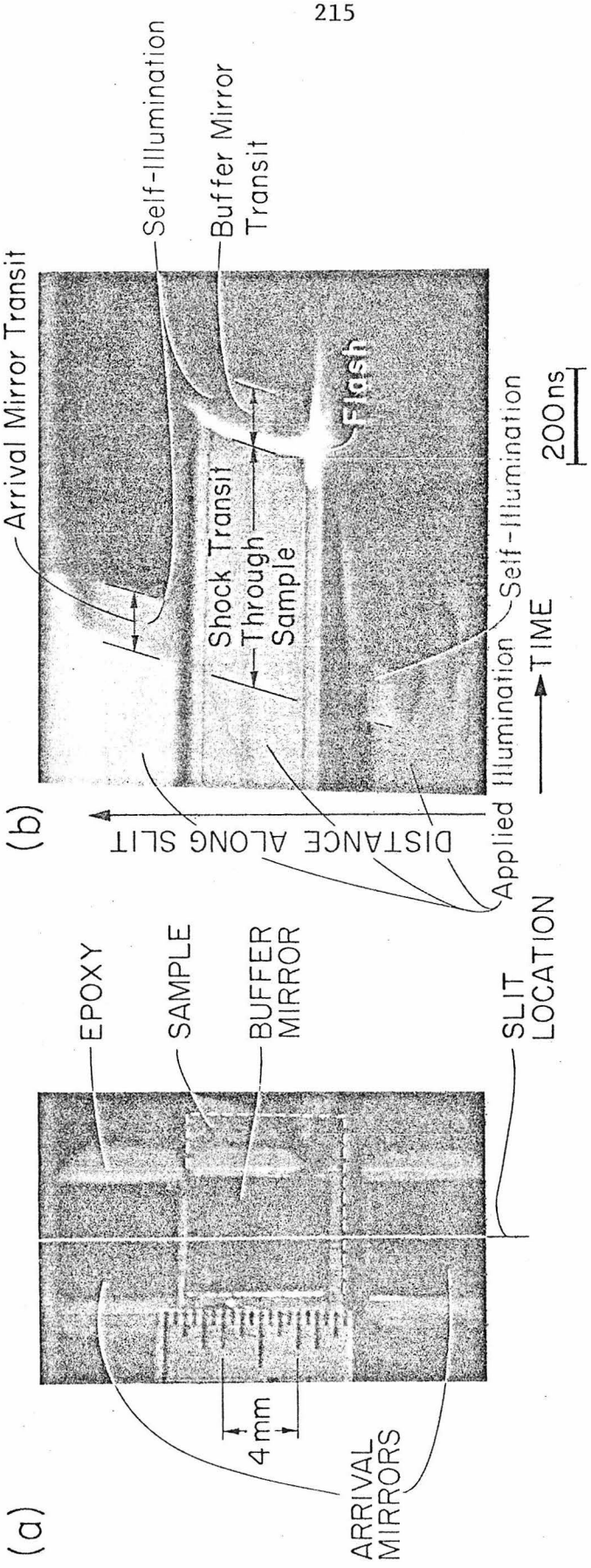
(a)
EPOXY
SAMPLE
BUFFER MIRROR
SLIT LOCATION
4 mm
ARRIVAL MIRRORS
(b)
Arrival Mirror Transit
Self-Illumination
Buffer Mirror Transit
Shock Transit Through Sample
Flash
Self-Illumination
200ns
DISTANCE ALONG SLIT
Applied Illumination
TIME

Fig. 1

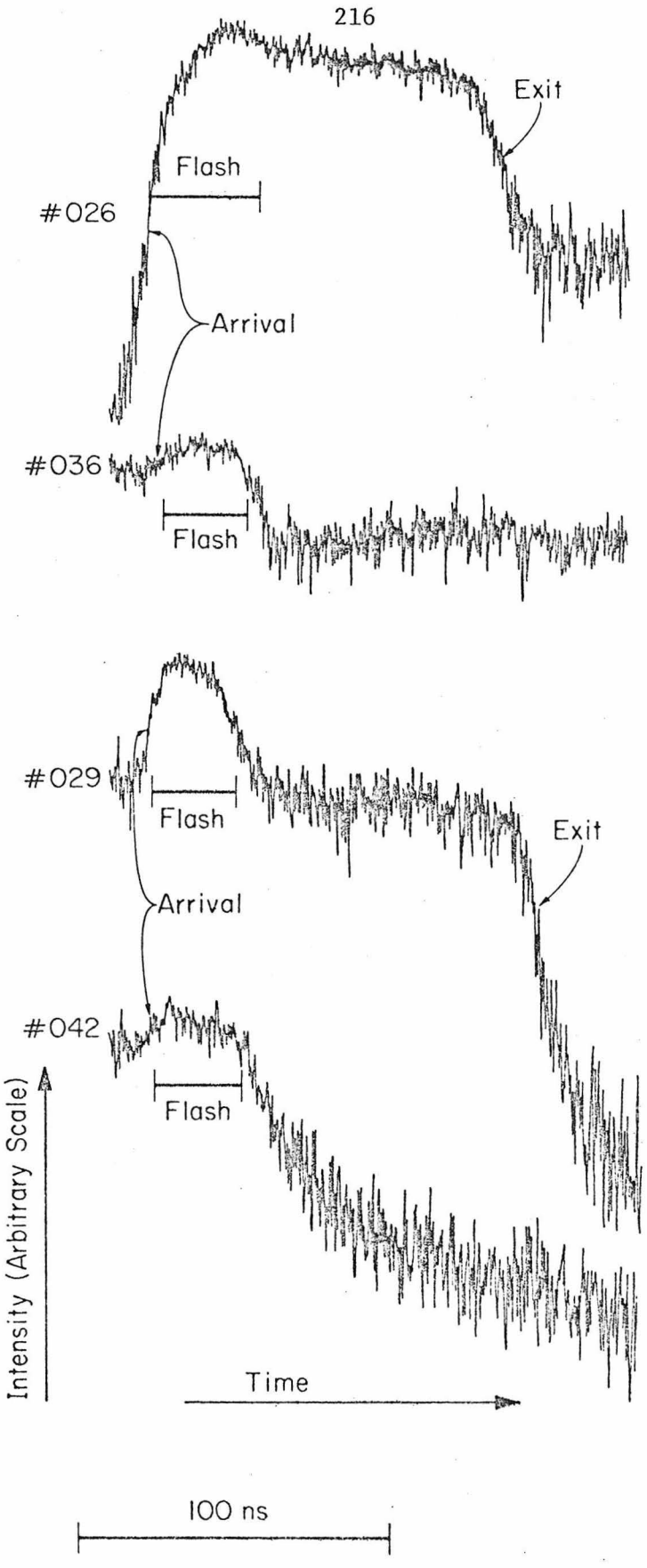
216
Exit
Flash
#026
Arrival
#036
Flash
#029
Flash
Exit
Arrival
#042
Flash
Intensity (Arbitrary Scale)
Time
100 ns

Fig. 2

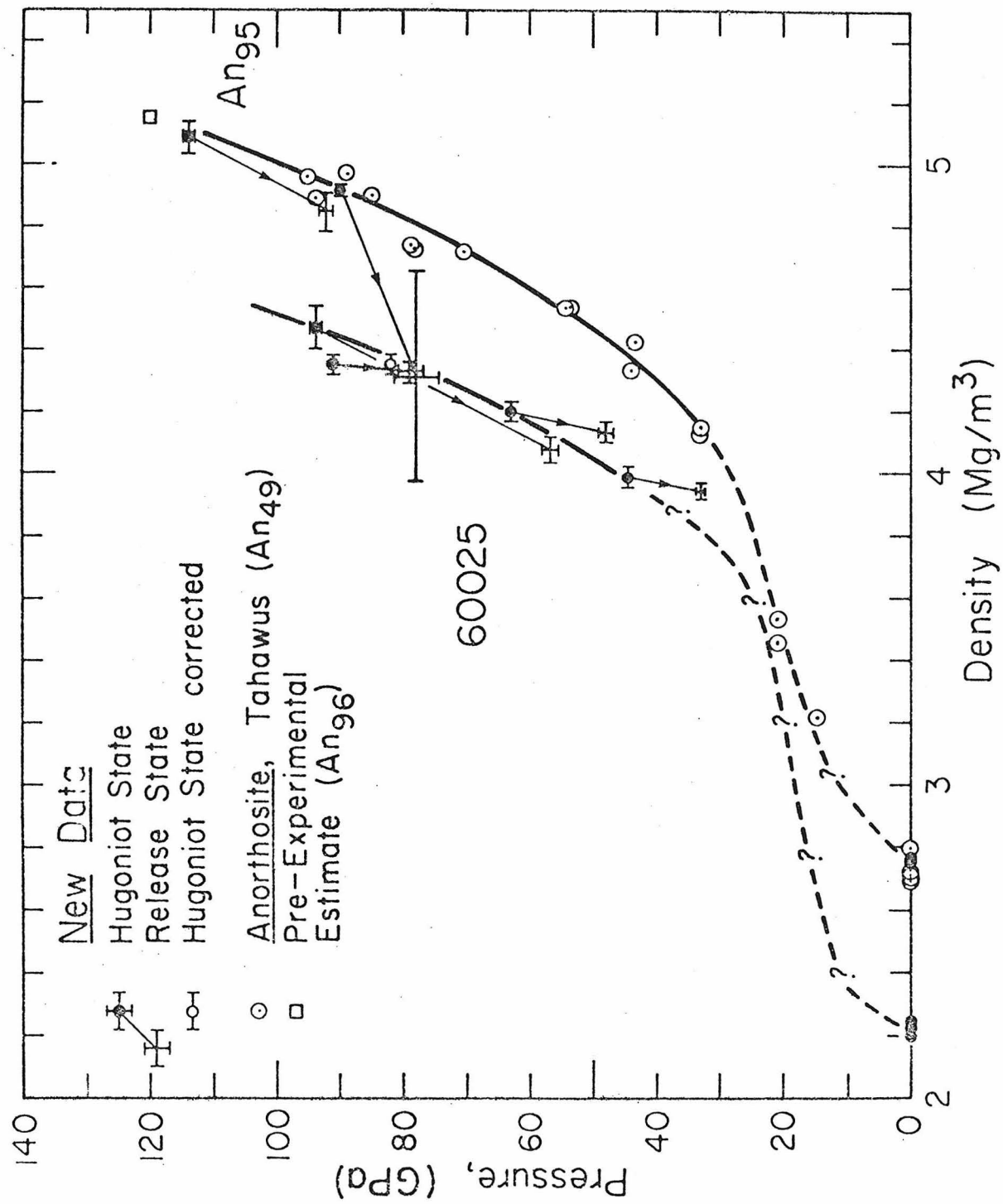
New Data
Hugoniot State
Release State
Hugoniot State corrected
Anorthosite, Tahawus (An49)
Pre-Experimental
Estimate (An96)
An95
60025
Pressure, (GPa)
Density (Mg/m3)
0
20
40
60
80
100
120
140
2
3
4
5

Fig. 3

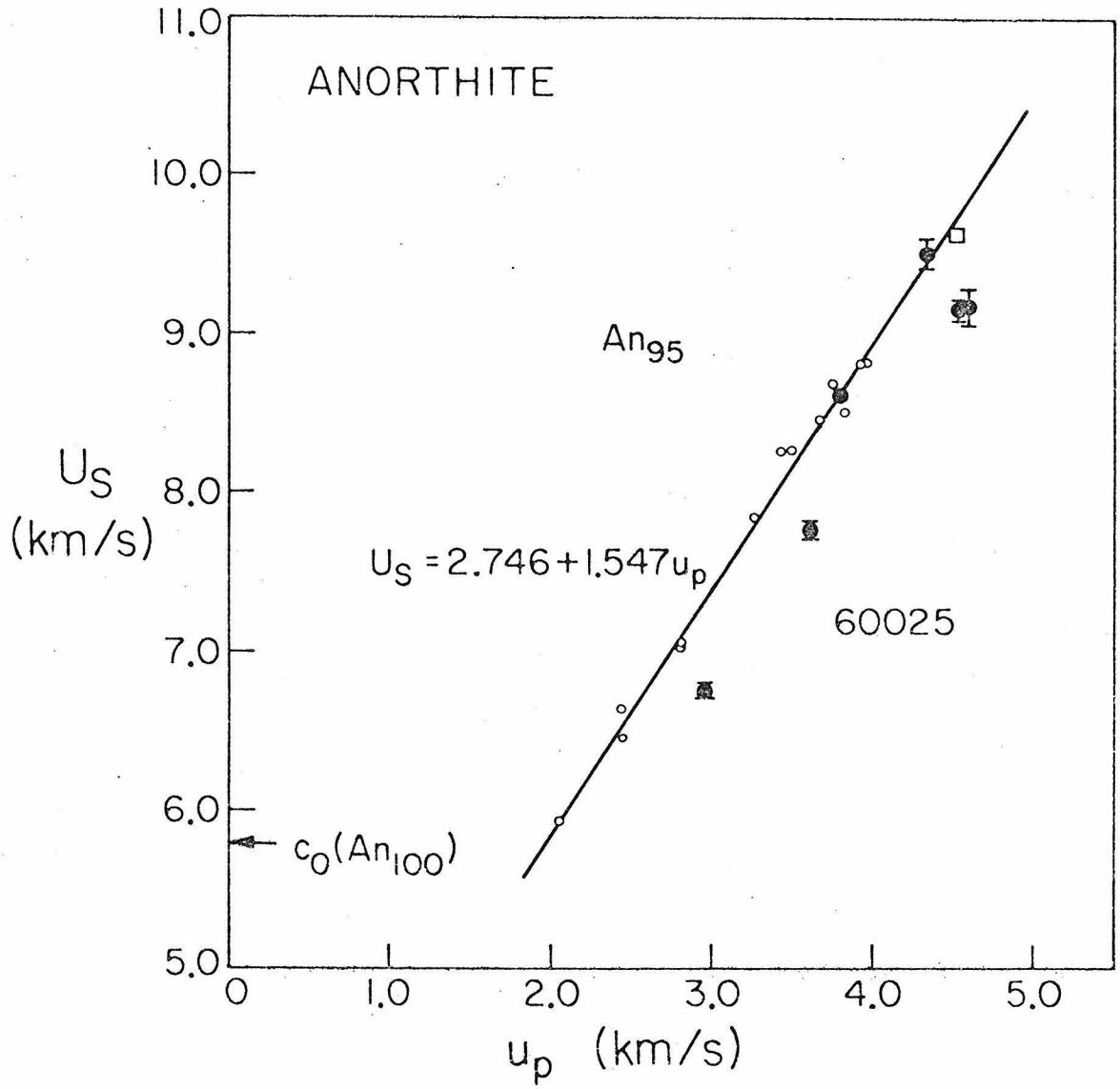
ANORTHITE
An95
Us = 2.746 + 1.547up
60025
c0(An100)
Us (km/s)
up (km/s)
11.0
10.0
9.0
8.0
7.0
6.0
5.0
0
1.0
2.0
3.0
4.0
5.0

Fig. 4

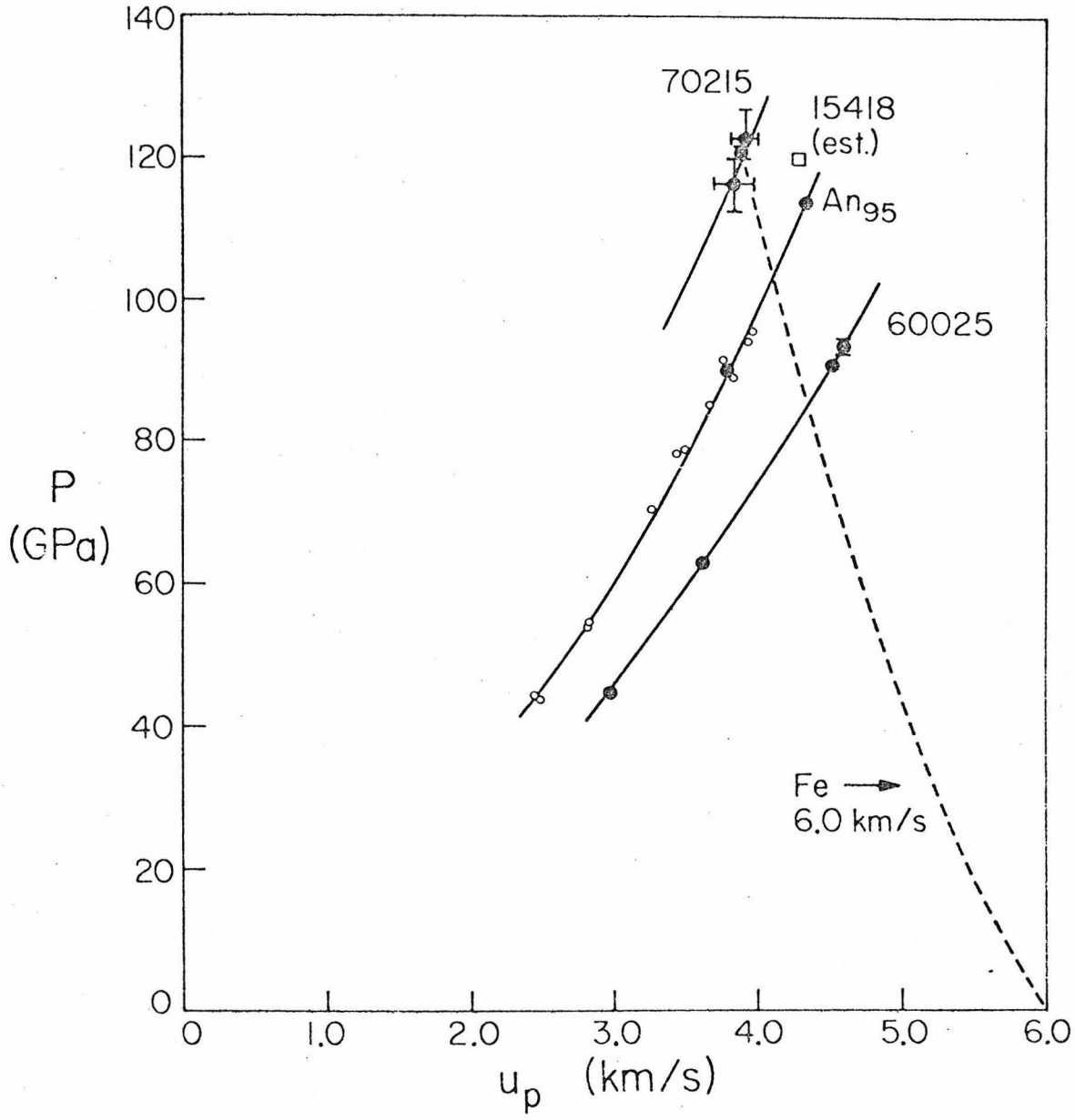
140
120
100
80
60
40
20
0
P
(GPa)
0
1.0
2.0
3.0
4.0
5.0
6.0
u_p (km/s)
70215
15418
(est.)
An_{95}
60025
Fe
6.0 km/s

Fig. 5

Chapter 7

ANORTHITE: THERMAL EQUATION OF STATE TO HIGH PRESSURES

Abstract

We present shock-wave (Hugoniot) data on single-crystal and porous anorthite ($CaAl_2Si_2O_8$) to pressures of 120 GPa. These data can be inverted to yield high pressure values of the Grüneisen parameter (γ) adiabatic bulk modulus (K_s) and coefficient of thermal expansion (α) over a broad range of pressures and temperatures which in turn are used to reduce the raw Hugoniot data and construct an experimentally-based high-pressure thermal equation of state for anorthite. We find surprisingly high values of γ which decrease from about 2.2 to 1.2 over the density range 3.4 to 5.0 Mg/m^3. Our data clearly indicate that whereas the zeroth order anharmonic (quasi-harmonic) properties such as γ and α decrease upon compression for a single phase, these properties apparently increase dramatically (200% or more) in going from a low to a high pressure phase. The results for anorthite also support the hypothesis that higher-order anharmonic contributions to the thermal properties decrease more rapidly upon compression than the lowest order anharmonicities. We find an initial density $\rho_0 \sim 3.4$ Mg/m^3 for the "high-pressure phase" portion of the Hugoniot, with an initial value of K_s essentially identical to that of anorthite at zero pressure (90 GPa). This is surprising in light of recently documented candidate high-pressure assemblages for anorthite with significantly higher densities, and it raises the question of the nonequilibrium nature of Hugoniot data. By

correcting the properties of anorthite to lower mantle conditions we find that although the density of anorthite is comparable to that of the lowermost mantle, its bulk modulus is considerably less, hence making enrichment in the mantle implausible except perhaps near its base.

INTRODUCTION

Anorthite is a mineral of particular geochemical interest because of its refractory nature. Both theoretical and observational evidence suggest that it is among the first high temperature condensates that form from the solar nebula and as such may be an important phase in the earliest accretional history of the planets (e.g., Marvin et al., 1970; Grossman and Larimer, 1974). Indeed, according to inhomogeneous accretional models the present internal zonation of the planets is thought to reflect, at least in a broad sense, the accumulation of first the more refractory condensates followed by successively more volatile-rich material (e.g., Turekian and Clark 1969; Clark et al., 1972). Hence anorthite and other calcium-aluminum minerals may well be enriched deep within the earth and, if stable against buoyancy forces, may remain there from the earliest times of the earth's formation. Recent evidence has, in fact, suggested that a significant portion of the earth's mantle could be quite enriched in a calcium component: the mineral CaO at high pressures has properties which are virtually indistinguishable from those of much of the lower mantle (Jeanloz, et al., 1979). Except for the few hundred kilometers near its base, however, the lower mantle appears to be relatively homogeneous according to seismological observations, and the most plausible location of a chemically distinct zone might be near the bottom of the mantle (Anderson, 1975; Jeanloz and Richter, 1979).

The purpose of this paper is to present new high pressure data on anorthite which provide among the most complete high-pressure, high-temperature characterizations of any silicates to date. We have carried

out shock-wave experiments both on single-crystal anorthite and on anorthite containing a substantial initial porosity. Because the states achieved in the latter are much hotter than those produced in the nonporous (single-crystal) samples under shock the temperature-dependence of the high-pressure equation of state can be directly evaluated. Thus, we derive a thermal equation of state for anorthite to pressures in excess of 120 GPa based on our data and with virtually no theoretical constraints on the form of such an equation of state. As a result, we have measurements over a wide range of pressures and temperatures of such thermal properties as the Grüneisen parameter and coefficient of thermal expansion, as well as the pressure- and temperature-dependent bulk modulus. This in turn allows us to make a direct comparison between anorthite at high pressures and the earth's interior and leads us to the conclusion that although the density of anorthite is consistent with that of the lower mantle the bulk modulus probably precludes significant amounts of anorthite being present except, possibly, in the lowermost portion of the mantle (D" region). A modest enrichment of anorthite is allowed by our data which would be stable at the base of the mantle, however none is required.

The porous anorthite used in our experiments is a lunar highlands rock (sample 60025). Its response to dynamic compression is of intrinsic interest for better understanding the cratering properties of the lunar surface. Because of its extremely primitive character, the properties of 60025 are of particular interest for modeling the late-stage accretion and early evolution of the moon. These considerations have been discussed more fully by Jeanloz and Ahrens (1978), in which some of the data which

are described below were first presented.

EXPERIMENTAL

Euhedral, single-crystals of a "transitional" anorthite from Miyake-zima, Izu Islands, Japan (cf. Gay, 1954; Müller, et al., 1972; McLaren, 1973) were used as nonporous samples; their composition corresponds to $An_{95.4}$ $Ab_{4.5}$ $Or_{0.1}$ (representative analysis in Table 1). Samples were oriented morphologically for shock-wave propagation along the [010] direction and were prepared so as to avoid the small amounts of olivine ($Fo_{83}Fa_{17}$) inclusions present in the anorthite crystals. The porous anorthite samples were cut from lunar anorthosite 60025.36, .174 as previously described (Jeanloz and Ahrens, 1978).

The experimental techniques used in this study have been presented elsewhere and are only briefly discussed here (see Ahrens et al., 1977; Jeanloz and Ahrens, 1977, 1978, 1979a). The initial densities of samples are determined by an Archimedean and a bulk technique for nonporous and porous samples respectively. Properly characterizing the initial densities of the porous samples is particularly important for obtaining data of high quality (Jeanloz and Ahrens, 1978). Shock experiments were carried out using a two-stage light-gas gun or a 40 mm-bore propellant gun to accelerate projectiles to velocities between 2.3 and 6.6 km/s. In each experiment, the impact velocity of the projectile is measured, as is the velocity of the shock wave which is generated in the sample upon impact by the projectile. The shock-wave velocity is determined by measuring the travel time of the shock-wave through the sample (of known thickness) by way of a rotating-mirror or

an image-converter streak camera; details of the data reduction procedure are given in Jeanloz and Ahrens (1979a). The Hugoniot state is then determined by applying impedance-matching conditions (Hugoniot equations) to the measured initial density, impact velocity and shock-wave velocity. A partially- or fully-released state is also determined by a free-surface or buffer impedance mismatch measurement, reduced by way of the Riemann-integral formalism (e.g., Rice et al., 1958; Lyzenga and Ahrens, 1978). The standard equations of state of McQueen et al. (1970) for W, Ta and 2024Al alloy, and of Wackerle (1962) and Jackson and Ahrens (1979) for fused quartz were used in reducing these data.

RESULTS

The results of the present experiments on single-crystal and porous anorthite are given in Tables 2 and 3, respectively, and are shown in Figures 1 and 2; for convenience, the data from Jeanloz and Ahrens (1978) for anorthosite 60025 are included, with slight corrections. Despite variations in composition and porosity, the present data can essentially be considered representative of endmember anorthite ($CaAl_2Si_2O_8$) with 0% and 19% initial porosity. Although the data of McQueen et al. (1967) for Tahawus anorthosite correspond to a more sodic plagioclase (An_{49}), these are indistinguishable from the present (nonporous) data because the Tahawus anorthosite contains enough pyroxene to increase its initial density to that of anorthite (Figures 1 and 2). Hence the single-crystal anorthite and Tahawus anorthosite data are reduced together for determining the properties of anorthite at high pressures (see Jeanloz and Ahrens, 1978).

All of the present data are in the "high-pressure phase" regime (e.g., McQueen et al., 1967) and for comparison a theoretical Hugoniot is shown in Figures 1 and 2 for the zero-pressure structure of anorthite. This is constructed (McQueen et al., 1963; Davies and Gaffney, 1973) from a third-order Eulerian finite-strain adiabat, constrained by recent ultrasonic data for anorthite (Liebermann and Ringwood, 1976). The Tahawus anorthosite data extrapolate to this theoretical Hugoniot at about 10.3 (±0.5) GPa pressure, indicating that the "mixed-phase" region extends from approximately 10.3 to 33.0 GPa for the non-porous samples. The porous and nonporous data in the "high-pressure phase" regime can be characterized by the least squares-fit, quadratic shock-wave velocity (U_s) versus particle velocity (u_p) relations given in Table 4 along with the average initial densities (ρ_0). Although the porous data require a quadratic U_s-u_p relation, this is not the case (statistically) for the nonporous data. It is interesting to note, however, that the porous and nonporous data define essentially parallel trends in Figure 2.

The release paths shown in Figure 1 are schematic in that they are constrained by only a single measurement in each case, as shown. In using the Riemann integral to derive these data, the release process is assumed to be isentropic, and hence the release paths are expected to have similar (but slightly smaller) slopes in the pressure-density plane as the Hugoniot. Although strictly isentropic release might seem implausible, Jeanloz and Ahrens (1979b) have recently shown that the effects of entropy production (excluding reactions or phase transformations) are not likely to be large enough to influence the release paths. The

results for single-crystal anorthite and, at the higher pressures, porous anorthite are consistent with isentropic unloading. These release paths are significantly different from those documented in the "mixed phase" region of feldspars in previous studies (Ahrens et al., 1969b: Grady and Murri, 1976)., consistent with the present data being in the "high-pressure phase" regime of the Hugoniot. It is difficult to understand, however, why several of the release paths for porous anorthite are steeper than the Hugoniot. Finite-strength effects appear not to be responsible and, although several possible explanations can be advanced, these results are enigmatic (cf. Jeanloz and Ahrens, 1978).

THERMAL PROPERTIES

By combining shock-wave data from samples of different initial densities, thermal properties at high pressures can be derived with virtually no theoretical constraints involved (e.g., Kormer et al., 1962; McQueen et al., 1970; Jeanloz, 1979a). In the following, thermal properties will be derived based on successively more extensive assumptions or approximations, however none of the results are strongly dependent on an assumed form of the high-temperature, high-pressure equation of state because each Hugoniot point represents a direct measurement of a pressure (P - volume (V) - internal energy (E) state. The most important assumption is that the porous and nonporous data represent identical (or at least very similar) thermodynamic states, except for the temperatures involved; because of the large energies involved, this appers to be a good approximation (see Jeanloz, 1979a). For example, despite the fact that the porous Hugoniot probably represents molten

anorthite to a large extent, the effect of melting on density at a given (high) pressure is small: at zero pressure, a volume change on melting of only 4% is found (Skinner, 1966), and at high pressures this undoubtedly decreases to within the few percent accuracy of the Hugoniot data. Hence the effect of melting on the energies or compressibilities involved are not likely to be resolvable, and no anomalies which could be ascribed to melting are seen among the data considered here. Each datum probably represents an average over a heterogeneous thermal state achieved on the Hugoniot, particularly for the porous anorthite in which extremely high temperatures can be achieved along grain boundaries (e.g., Belyakov et al., 1974, 1977; also Grady, 1977). However, for the hydrostatic condition which is (at least approximately) achieved along the Hugoniot, temperature perturbations result in density (rather than pressure) variations. Thus, temperature variations between 10^4 and 10^5 K, and concentrated within about 10% of the sample, could readily be concealed within the 1-2% accuracy to which Hugoniot densities were determined in this study. At these high temperatures other processes, such as radiative thermal conductivity are likely to become important enough to preclude more extreme temperature variations. The reproducibility of the present data also suggest that an adequate thermal average has been measured.

The porous and nonporous data are directly inverted to yield values of the Grüneisen parameter ($\gamma \equiv V \left(\frac{\partial P}{\partial E}\right)_V$) based on the Hugoniots given in Table 4. At a given volume (V_H) the Grüneisen parameter is given by

$$\gamma(V_H) = V_H \frac{2(P_H^P - P_H^N)}{P_H^P (V_O^N - V_H) - P_H^N (V_O^P - V_H)} \qquad (1)$$

where O and H subscripts represent zero-pressure and Hugoniot states, while P and N indices refer to porous and nonporous samples respectively (further details are given in Jeanloz, 1979a). Equation 1 yields values of γ which are averaged over large temperature intervals and it is assumed here, as is commonly done (e.g., McQueen et al., 1970; Wallace, 1972), that γ is essentially independent of temperature. Independent analyses show this to commonly be the case (e.g., Anderson et al., 1968; Jeanloz, 1979a), and the porous data for anorthite, although available within only a small variation of initial porosities, are also consitent with a temperature-independent Grüneisen parameter.

The resulting values of γ are shown in Figure 3 in which each datum point represents the offset of a porous Hugoniot point from the nonporous Hugoniot. The error bars largely reflect uncertainties in the nonporous Hugoniot which must be extrapolated downward considerably in pressure (or density) for this analysis. Because the porous Hugoniot is quite well constrained by our data, a smooth (γ) curve can be derived from the parameters listed in Table 4 (Figure 3) which compares favorably with a power-law fit to the data

$$\gamma = 2.20\ (3.40V)^{1.66(\pm 0.42)} \qquad (2)$$

with V in m^3/Mg (based on ρ_o = 3.40 Mg/m^3: see below). It is interesting to note that the exponent in Equation 2 is larger than 1, as in the case of iron (Jeanloz, 1979a), although a value of unity is often assumed for the volume dependence of the Grüneisen parameter (e.g., McQueen et al., 1967, 1970; Brennan and Stacey, 1979).

The most striking feature in Figure 3 is the dramatic increase in

γ from its zero-pressure value, for the high density states achieved along the anorthite Hugoniot. The Grüneisen parameter is expected to decrease upon compression (as shown by the present data), hence the increase shown in Figure 3 at $\rho < 3.7$ Mg/m^3 directly reflects the large increase in zeroth-order anharmonic (quasi-harmonic) contributions to the thermal properties of anorthite as it is compressed through the "mixed-phase" region. It may seem surprising that anharmonic properties increase across such a density jump, however this effect is seen in other cases, such as the phase transitions in Fe, Bi and halides (Jeanloz, 1979a; Ramakrishnan et al., 1979). This is consistent with the standard interpretation of the "mixed-phase" region of the Hugoniot (e.g., McQueen et al., 1967) as representing a polymorphic transformation to a high-density, high-pressure phase, perhaps with increased cation-coordination number. In general, an increase in coordination number is accompanied by an increase in average bond length and hence an increase in anharmonicity might be expected. However, other effects are also available to explain the observed increase in γ with density, such as slight changes in the nature of the interatomic bonding (e.g., Megaw, 1938). In any case, an increase in anharmonic contributions to the thermodynamic properties of anorthite when shock-compressed into its high-density state is clearly indicated by the present data.

Given a knowledge of the Grüneisen parameter, an isentropic bulk modulus (K_S) or bulk sound speed (c) can be determined from the slope of the Hugoniot at any given density (or pressure) by means of the following equation (e.g., Al'tshuler et al., 1960; McQueen et al., 1967, 1970)

$$\rho_H c_H^2 = K_S)_H = \left(\frac{dP_H}{dV_H}\right)\left[\left(V_0{}^P - V_H\right)\frac{\gamma}{2V_H} - 1\right] V_H + \frac{1}{2} P_H{}^N \gamma \qquad (3)$$

This equation is derived by assuming a Mie-Grüneisen form for the equation of state, however the thermal correction to the Hugoniot slope is small and is experimentally constrained (through γ), therefore minimizing the effect of this assumption. The resulting values of K_S along the Hugoniot of anorthite are shown in Figure 4. Again, the individual points are determined by the offset of the porous anorthite data while the curves for K_S along the porous and nonporous Hugoniots are determined from the parameters given in Table 4 (cf. Jeanloz, 1979a). The error bars on the data mainly reflect uncertainties in the fit to the nonporous Hugoniot, particularly of its slope. Significantly, both the porous and nonporous Hugoniots are well enough constrained to directly yield independent measurements of the bulk modulus of anorthite at high pressures and at widely varying temperatures (corresponding to different initial porosity). However, in order to quantitatively separate the thermal and compressional effects on the bulk modulus, a more complete model must be derived for anorthite under shock conditions, as is done below. Such a model yields estimates of the temperatures along the porous and nonporous Hugoniots, thus allowing the isotherms shown in Figure 4 to be determined.

Sound velocities have been independently measured in (alkali) feldspars under shock by means of unloading waves (Grady et al., 1975). These velocities were considered to be anomalously low, and hence were interpreted as being bulk (rather than longitudinal) velocities, suggesting the possibility of partial melting during shock loading. The present results, however, yield lower bulk sound speeds along the Hugoniot than

were expected by Grady and coworkers, thus precluding the need to invoke their "shear-band" melting. In fact, a direct comparison of their velocities with the present data allows the shear modulus along the Hugoniot of feldspar to be calculated. This yields $\mu \sim 117.3$ and 118.3 GPa (Poisson's ratio of 0.21-0.26) at pressures of 34.5 and 46.0 GPa respectively, assuming that Grady et al. measured longitudinal velocities. These values for the shear modulus are not unreasonable, but they are only approximate since there are significant uncertainties in the data sets which are being compared and compositional differences between the samples are ignored. In any case, this analysis suggests that nonporous feldspar melts along the Hugoniot only at pressures significantly higher than 46 GPa. Similar comparisons of unloading wave velocities with independently determined bulk compressibilities have been used to determine the shear properties of metals to pressures well in excess of 100 GPa (e.g., Al'tshuler et al., 1971; Simonov and Chekin, 1975).

Anorthite behaves as though it undergoes a major phase transformation under shock, as exemplified by the large density increase and anomalously high (apparent) compressibility through the "mixed-phase" region. Without specifying the details of such a transformation, the important consequence is that the properties of anorthite along the "high-pressure phase" branch of the Hugoniot must be referenced to a zero-pressure density which is significantly higher than the initial density of anorthite and that the densification through the "mixed-phase" region is reflected not as a thermal energy but as a potential energy which is imparted to the (static) lattice: that is, an energy of transformation

(ΔE_{tr}). By comparing the theoretical (untransformed) Hugoniot with the nonporous Hugoniot of anorthite at about 30 (±10) GPa pressure, a volume decrease of about 20% is found associated with the "mixed-phase" region. Hence, the high-pressure anorthite data correspond to a state with a zero-pressure density ρ_{02} = 3.40 (±0.1) Mg/m^3, a Grüneisen parameter given by Equation 2 and with $\Delta E_{tr} \sim 198 \pm 60$ kJ/mol. Here, $\Delta S_{tr} \sim 0$ was assumed and the transition pressure of 10.3 GPa derived above was used.

With these parameters constrained, a principal adiabat can immediately be derived for the porous and nonporous anorthite data corresponding to the "high-pressure phase" branch of the Hugoniot. The approach used here was to find a least-squares fit to the data with the adiabat given by either third- or fourth-order, Eulerian finite-strain theory. The appropriate equations for the forward problem (e.g., McQueen et al., 1963; Davies, 1973) are readily converted to normal equations of the form

$$\frac{2}{3}\left\{\left[1 - \frac{\gamma}{2}\left(\frac{\rho_H}{\rho_{01}}\right) - 1\right] \quad P_H + \gamma\rho_H \, \Delta E_{tr}\right\} \left\{\chi^3 \, (\chi^2-1)\right\}\zeta^{-1} = \beta_0+\beta_1 \tag{4}$$

$$(\chi^2-1) \, [\frac{\gamma}{2} \, (\chi^2-1) - \chi^2] \, \zeta^{-1}$$

with

$$\zeta = \chi^2 - \frac{3}{4}\gamma \, (\chi^2-1) + \xi_2 \, (\chi^2-1)^2 \, [\chi^2 - \frac{3}{8}\gamma \, (\chi^2-1)] \tag{5a}$$

$$\xi_2 = \frac{3}{8} K_{02}K_{02}'' + \frac{3}{8} K_0' \, (K_0' - 7) + \frac{143}{24} \tag{5b}$$

$$\chi = (\rho/\rho_{02})^{1/3} \tag{5c}$$

The least-squares solution to Equation 4 yields best estimates of the parameters $\beta_0 = K_{02}$ and $\beta_1 = K_{02}\xi_1$, where $\xi_1 = \frac{3}{4}(4-K_{0s}')$ and all properties refer to the adiabat centered at ρ_{02} (primes indicate pressure derivatives). Although equation 4 can easily be extended to the multivariate case in which ξ_2 and ΔE_{tr} could be independently estimated, these variables are so poorly constrained by a fit to the data (at least in the present case) that no further information is gained. A third-order fit (corresponding to a Birch-Murnaghan adiabat) is derived by setting $\xi_2 = 0$ in Equation (5a), resulting in

$$K_{0s} = 86.5\ (\pm 10)\ \text{GPa} \tag{6a}$$

$$K_{0s}' = 3.93\ (\pm 0.20) \tag{6b}$$

$$K_{0s}K_{0s}'' = -3.45\ (\pm 0.35) \tag{6c}$$

for the adiabat corresponding to the "high-pressure phase" Hugoniot of anorthite; the value in Equation 6c comes from Equation 5b. Alternatively, fourth-order solutions can be found for Equation 4, however these do not improve the fit to the data significantly and do not change the resulting adiabat markedly. For example, letting $K_{0s}'' = 0$ ($\xi_2 = 1.49$) yields $K_{0s} = 95.4$ GPa, $K_{0s}' = 2.93$ and an adiabat which is within about 0.7% in density from that determined by Equation 6. It is interesting to note that K_0' is essentially equal to 4 (Equation 6b), the value for the Birch, second order equation of state, whereas neither the Slater, Dugdale-MacDonald nor Free Volume estimates of γ based on this value agree with the present data (e.g., Zharkov and Kalinin, 1971).

The bulk modulus given in Equation 6a is surprisingly low given the large increase in density from ρ_{01} = 2.74 Mg/m^3 to ρ_{02} = 3.4 Mg/m^3 (compare with K_{0s} = 92 GPa for anorthite at zero pressure; Liebermann and Ringwood, 1976), however this conclusion is in complete agreement with the results originally derived by McQueen et al. (1967). Because the Grüneisen parameter was not independently known in that earlier study, they derived solutions for the principal adiabat of the "high-pressure phase" Hugoniot of anorthosite using both low (γ_0 = 1.13) and high (γ_0 = 1.73) values of γ (they assumed γ/V constant). The values of γ measured in the present study clearly favor the latter solution, which resulted in ρ_{02} = 3.46 Mg/m^3, K_{0s} = 88 GPa and K_{0s}' = 3.93, in excellent agreement with the values found here despite the different formalism used to reduce the Hugoniot data. Ironically, subsequent work in which the seismic equation of state of Anderson (1967, 1969) was assumed to hold (Anderson and Kanamori, 1968; Ahrens et al., 1969a; Davies and Anderson, 1971) had tended to favor the low-γ solution of McQueen and coworkers (ρ_{02} = 3.53 Mg/m^3, K_{0s} = 112 GPa), resulting in values of ρ_{02} between 3.57 and 3.71 Mg/m^3. In the present study, no solution could be found using Equations 2 and 4 which fit the data and which was consistent with either form of the seismic equation of state (Anderson, 1967, 1969); it is worth noting that the seismic parameter and density of anorthite are not consistent with the seismic equation of state at zero pressure.

The present results (using Equation 6) are shown in Figure 5, along with the nonporous and porous Hugoniots directly determined by the data. A metastable Hugoniot for anorthite (centered on ρ_{02} = 3.4 Mg/m^3)

can be derived by rearranging Equation 4, with $\rho_{01} = \rho_{02}$ and $\Delta E_{tr} = 0$. It is shown in Figure 5 along with a Hugoniot calculated for 10% initially porous anorthite, which is derived from Equations 1 and 2, as can be done for Hugoniots corresponding to arbitrary porosities. The bulk moduli along the adiabat, metastable Hugoniot and calculated, porous Hugoniot(s) then follow directly from the theory of finite strains (Birch, 1938, 1947; Davies, 1973), or, for the Hugoniots, from Equation 3; the results are displayed in Figure 4 (the calculated, porous Hugoniot results are left off for clarity).

In order to derive the temperatures along the compression curves shown in Figure 5, a model for the specific heat at constant volume (C_v) must be constructed, except for the case of the adiabat along which the temperature is completely determined by the Grüneisen parameter:

$$T_s(\rho) = T_{0s} \exp \frac{\gamma_0 - \gamma}{n} \tag{7}$$

where $\gamma(\rho)$ is given by Equation 2: $\gamma_0 = 2.20$, $n = 1.66$, and $T_{0s} = 300K$. The temperature along any compression curve (e.g., a Hugoniot) can be calculated from:

$$T(P,\rho) = T_s(\rho) + \int_{P_s}^{P} \frac{V\, dP'}{\gamma\, C_v} \quad ; \tag{8}$$

subscript s indicates evaluated along the principal adiabat and P' is a dummy variable. In order to solve Equation 8, a simple, Debye-Grüneisen model is used to evaluate the specific heat, as has commonly been done in previous studies (e.g., Ahrens et al., 1969b; McQueen et al., 1970). A (high-temperature) value of the Debye temperature $\theta_1 \sim 1000K$ was found from the zero-pressure specific heat data of anorthite (Robie et al.,

1978), however this must be renormalized to the high-pressure state centered at $\rho_{02} = 3.4$ Mg/m^3. According to Debye theory, the characteristic temperature is proportional to both a mean sound velocity and density, however because the mean velocity of the high-pressure state is unknown (and velocity systematics apparently do not satisfy the data) the following relation was used (see Anderson et al., 1968, for example):

$$\theta_2 \sim \theta_1 \, (\rho_{02}/\rho_{01})^{1/3} = 1075\text{K} \qquad (9)$$

In Equation 9, the mean velocity is assumed constant in going to the high-pressure state and only the density jump is accounted for. This is a rough approximation, but the approximations used here mainly affect the computed results at temperatures less than θ: about 1100 to 2200K for pressures up to 120 GPa. Note that the Debye temperature depends on volume according to a relation analogous to Equation 7. Because the temperature along the adiabat is given independently, only the temperature along the metastable Hugoniot below about 80 GPa is likely to be seriously affected either by the use of the Debye-Grüneisen model or by the choice of θ_2. We note that higher than zeroth order anharmonic contributions to the specific heat, such as the linear -T term (e.g., Wallace, 1972), are ignored although they may alter the specific heat somewhat at high temperatures. The overall effect is not likely to be very significant, however, particularly because the higher order anharmonicity is expected to decrease rapidly upon compression (Zharkov and Kalinin, 1971).

The temperatures calculated in this fashion are shown in Figure 6. The largest uncertainties arise from uncertainties in ΔE_{tr}, followed

by uncertainties in the principal adiabat of Figure 5. This might be expected since a change in ΔE_{tr} from 200 to 300 kJ/mol involves a temperature change $\delta T \sim \delta E/C_v \sim \frac{100}{0.32} \sim 300K$ at a given density, and ΔE_{tr} is not very well constrained.

The calculated temperatures also allow isotherms to be found for the high-temperature, high-pressure bulk modulus data in Figure 4. Given the uncertainties and extrapolations involved these isotherms must be considered somewhat schematic, but it is interesting to note the change in pressure derivative of the bulk modulus with temperature and also the relative insensitivity of the bulk modulus to temperature at high pressures and moderately low temperatures. For example at 100 GPa, $\left| \left(\frac{\partial K_S}{\partial T}\right)_P \right|$ apparently increases from about 6×10^{-3} GPa K^{-1} at 4000K to about 30×10^{-3} GPa K^{-1} at 7000 K, a value typical of the region of broadly spaced isotherms between the porous and nonporous Hugoniot curves in Figure 4. This range of values is also compatible with the low pressure data summarized by Anderson et al. (1968).

The coefficient of thermal expansion is given by

$$\alpha = \gamma C_v \, (VK_s - \gamma^2 T C_v)^{-1} = \frac{\gamma C_p}{V K_S} \qquad (10)$$

in which the specific heat at constant pressure (C_p) is distinguished from C_v. Equation 10 can be solved as a function of pressure and temperature from the present results on anorthite, as shown in Figure 7 in which both isobars and isochores are displayed. For comparison, the zero-pressure data for anorthite and the high-pressure Debye temperature are also shown. At temperatures below θ, the values of α in Figure 7 are subject to errors due to the possible inadequacies

of the specific heat model used. However, the thermal expansion must vanish as the temperature goes to zero and the general features of Figure 7 are not strongly model-dependent.

Although the zero-pressure thermal expansion of anorthite is subject to some uncertainty, it is significantly lower than the low-pressure thermal expansions derived from the "high pressure phase" Hugoniot data (Figure 7). As with the Gruneisen parameter, the thermal expansion of anorthite increases considerably upon compression to the high-pressure state (ρ_0 = 3.40 Mg/m^3), whence it decreases with increasing pressure. Again, this can be viewed in terms of anharmonic effects increasing sharply at a pressure-induced phase transformation, whereas pressure decreases both γ and α for a given phase. This decrease of thermal expansion with compression can be approximately related to the bulk modulus isotherms in Figure 4 since $\left(\frac{\partial \alpha}{\partial P}\right)_T = K_T^{-2}\left(\frac{\partial K_T}{\partial T}\right)_P \sim K_S^{-2}\left(\frac{\partial K_S}{\partial T}\right)_P$ (K_T is the isothermal bulk modulus).

At high temperatures ($T > \theta$) α increases with temperature, particularly at low pressures. This is due to both zeroth and first-order anharmonic effects which are approximately of equal importance in increasing α: the former through $C_p = (1+\alpha\gamma T)C_v$, while the latter derive from the decrease in the bulk modulus with temperature. It is important to note that these anharmonic contributions decrease more rapidly with pressure than does the zeroth order effect embodied in the thermal expansion itself. Hence at pressures above 80-100 GPa, α attains a "saturated", high-temperature value above the Debye temperature In this "saturated" regime, the calculated values of the thermal expansion are virtually model-independent since the Dulong-Petit value

of C_v provides a good approximation for C_p and all other variables in Equation 10 are experimentally constrained (cf. Jeanloz, 1979a). Furthermore, the relative decrease in importance of higher order anharmonic contributions relative to the lower-order (e.g., strictly quasi-harmonic) effects provides additional justification for the simple, Debye-Grüneisen model which was used for C_v. From the present data, the second Grüneisen parameter (e.g., Anderson et al., 1968) $\delta_S = \alpha K_S \left(\frac{\partial K_S}{\partial T}\right)_p$ appears to be relatively independent of temperature at high pressures and temperatures, as expected. Unfortunately, δ_S is not very well constrained ($\delta_S \sim 2.2 \pm 1.2$), however it can be evaluated over many tens of GPa and thousands of degrees, and its approximate constancy lends further support to the assumed temperature independence of γ (Anderson et al., 1968).

DISCUSSION

Much of the preceding analysis depends on the inference that anorthite undergoes, in some sense, a phase transformation under shock-loading to pressures above about 10.3 GPa. Although previous analyses have assumed this to be the case (e.g., McQueen et al., 1967; Anderson and Kanamori, 1968; Ahrens et al., 1969a, Davies and Anderson, 1971), there is a considerable doubt that polymorphic transformation occurs under shock in a fashion directly analogous to the phase transformations achieved under static conditions. Because of kinetic limitations, it is quite likely that highly nonequilibrium states are measured in these shock experiments.

One indication of such difficulties arises from a comparison of

the present reduction of the Hugoniot data on anorthite in the "high-pressure phase" regime with the densities of predicted high-pressure phases or assemblages given in Table 5. As shown in Figure 5, the zero-pressure densities of these candidate high-pressure phases are considerably higher than is found from the reduced Hugoniot data. Although neither the hollandite phase nor the mixed-oxide assemblage have been documented for anorthite, both the calcium ferrite- and sodium titanate-bearing assemblages have been synthesized in calcium-aluminum-silicate systems (Reid and Ringwood, 1969; Liu, 1978b) and Liu (1978a) has found Na-plagioclase in the hollandite structure. Previous reductions of the Hugoniot data had allowed higher zero-pressure densities than are found here. However, the new data on the Grüneisen parameter preclude such solutions and, as discussed above, the use of the seismic equation of state in those studies appears to be unwarranted. Regardless of other assumptions, no solutions could be found to Equations 2, 4 and 5 which fit the data with ρ_{02} larger than about 3.80 ($\pm$0.10) Mg/m^3. In fact, the best fits to the present data resulted from allowing $\rho_{02} < 3.0$ Mg/m^3 and $\Delta E_{tr} = 0$, however yielding seemingly unphysical values of K_{0s} (typically less than 50 GPa). These results suggest that anorthite along the Hugoniot is not transformed to an equilibrium high-pressure polymorph, particularly since less than 30 GPa pressure has been required to find the assemblages listed in Table 5. A recent study by Jeanloz (1979b) finds little evidence for the transformation of (nonporous) silicates in Hugoniot experiments either from observations on shocked olivine samples or from theoretical considerations, and anorthite may provide the first clear case of a silicate achieving

significantly more effective packing under static as compared to dynamic loading.

On the other hand, it is not certain that the results of static high-pressure experiments can be so directly compared with the shock-wave data since the temperatures achieved in the former (~1000-1500K) are for the most part considerably less than the temperatures achieved along the Hugoniot. More important, though, is the fact that strict equilibrium on a microstructural state need not be required for the kind of analysis presented here. As illustrated above for the case of melting, large energy differences are involved in this analysis such that rather substantial deviations from equilibrium values are not likely to be noted in the Hugoniot data. Furthermore, the evidence for a density increase of about 20% above 10 GPa, as well as the release adiabats of non-porous anorthite, are all indicative of the behavior of a high-pressure phase. As discussed by Jeanloz (1979b), despite the Hugoniot possibly not representing equilibrium states, the properties measured under shock appear to be very close to their equilibrium values.

There are two problems which must be specifically addressed in this context. Although values of total energy are reasonably well constrained in this analysis, the partitioning of energy may not be. In particular, the amount of thermal energy present, and hence the calculated temperatures, depend on the estimated value of ΔE_{tr}: if anorthite undergoes no manner of phase transformation under shock $\Delta E_{tr} = 0$. Jeanloz (1979b) used this fact and measured Hugoniot temperatures to argue that some form of (non-equilibrium) transformation apparently occurs in silicates under shock. Similarly, if melting occurs in the anorthite samples this would

not affect the bulk thermal or compressional properties severely, but it could change the calculated temperatures dramatically, lowering them (at a given pressure) by possibly 10^3K. Since the zero-pressure melting temperature of anorthite is 1830K, a simple scaling argument suggests that melting may occur at about 70-90 GPa on the nonporous Hugoniot or about 40-60 GPa along the porous Hugoniot. This ambiguity can, however be directly resolved by way of shock-temperature measurements or by determinations of the shear modulus along the Hugoniot. Higher order effects associated with melting, such as discussed by Grover (1971), are not likely to change the values of properties calculated here by more than 15-20% even at the highest temperatures shown in Figure 6; given the important decrease in higher-order anharmonicities with pressure this is likely to be an overly conservative estimate.

The second question is whether the phase(s) along the "high-pressure phase" Hugoniot evolve continuously with increasing pressure, as might particularly be expected if these are in highly nonequilibrium states. This is equivalent to considering all of the data presented here as being in a "mixed-phase" regime despite the break in the U_s-u_p relation documented in Figure 2 (cf. McQueen et al., 1967, for example). Some question has, in fact, been raised for other silicates (Jeanloz and Ahrens, 1977; Jackson and Ahrens, 1979) about stability in the "high-pressure phase" regime: some evidence suggests continued reaction or evolution along the Hugoniot to pressures of 100 GPa or higher. Although the measured Hugoniot densities might still be used in such a case, the reduction of the Hugoniot data and especially the values of bulk moduli derived

above would be meaningless. At present there is no compelling evidence for such a conclusion and counterexamples can be found, however, the inability to independently verify this is problematical. Hence just as the porous and nonporous Hugoniots are assumed to be directly comparable, the "high-pressure phase" branch of the Hugoniot is assumed to represent a single (possibly nonequilibrium) phase or assemblage.

LOWER MANTLE

Since theories involving inhomogeneous accretion of the planets suggest that relatively refractory compounds, such as anorthite, may exist deep within the earth, it is of interest to compare the present data with seismologically-based models of the lower mantle. In Figures 4 and 5 the density and bulk modulus of the mantle are compared with our data for anorthite. The density of anorthite is compatible with mantle densities, but only for pressures in excess of about 80 to 100 GPa. As is evident from Figure 4, however, the bulk moduli derived here for anorthite at high pressures virtually preclude its being a major component throughout the bulk of the lower-mantle (cf. McQueen et al., 1967). If the assumptions made in calculating the bulk moduli are in error, then higher (more compatible) values would be found for anorthite.

Whereas a recent study on CaO (Jéanloz et al., 1979) indicates that the lower mantle could be considerably enriched in calcium, the present data do not support anorthite as being a particularly important Ca-bearing mineral in the mantle except possibly in its lowermost portions (D" region). Because the D" region is seismologically anomalous it is

not possible to determine its properties, with great confidence. Indeed, the evidence for a decrease in velocity gradient through the D" region (see the review of Cleary, 1974, for example) is compatible with its containing 10-20% anorthite (or similar refractory compound) according to the present data, while for plausible mantle temperatures (e.g., Stacey, 1977; Jeanloz and Richter, 1979) anorthite has a density within about 1% of the observed mantle densities at this level. Although not required, an enrichment of anorthite in the D" region is therefore acceptable and would appear to be bouyantly stable. This is consistent with a simple thermal model for the lower mantle presented by Jeanloz and Richter (1979), in which the D" region is chemically distinct from the overlying mantle. An increase in refractory components toward the base of the mantle is also in qualitative agreement with inhomogeneous accretion models, however a simple zone-refining process could produce the same effect in an originally homogeneous mantle heated from below.

CONCLUSIONS

New shock-wave data have been presented for anorthite from which a full high-temperature, high-pressure equation of state has been derived. Whereas anorthite has relatively low values of thermal expansion and Grüneisen parameter at zero pressure, these attain relatively high values in the high density state corresponding to the "high-pressure phase" Hugoniot, but decrease upon compression as expected. Higher order anharmonic contributions appear to decrease more rapidly with pressure and the thermal expansion therefore saturates to a high temperature value at pressures above about 100 GPa. Reduction

of the Hugoniot data allows shock temperatures to be calculated and also yields a principal adiabat for the high pressure branch of the Hugoniot. This adiabat has an initial bulk modulus (about 87 GPa) which is essentially identical to that of anorthite, whereas the initial density is about 3.40 Mg/m^3. Because candidate, high-pressure assemblages with significantly higher densities are known for anorthite (4.05 to 4.30 Mg/m^3) and because Hugoniot states are not likely to be at equilibrium, an ambiguity arises in the interpretation of the present data which are assumed to reflect equilibrium properties. Nevertheless, this assumption appears to be valid and no inconsistencies are evident. Significantly, no solutions could be found in reducing the data with zero pressure densities for the principal adiabat above 3.8-3.9 Mg/m^3, or with bulk moduli satisfying the seismic equation of state. A reduction of these data to lower mantle conditions demonstrate that anorthite may be present in amounts of 10-20% in the D" region, but it is not likely to be a significant phase elsewhere in the lower mantle because of its apparently small bulk modulus.

ACKNOWLEDGEMENTS

We thank Dr. Y. Syono for providing anorthite crystals, and also E. Gelle, J. Long and R. Smith for their substantial help in carrying out the experimental work.

REFERENCES

Ahrens, T. J., D. L. Anderson and A. E. Ringwood, Equations of state and crystal structures of high-pressure phases of shocked silicates and oxides, Rev. Geophys., 7, 667-707, 1969a.

Ahrens, T. J., C. F. Petersen and J. T. Rosenberg, Shock compression of feldspars, J. Geophys. Res., 79, 2727-2746, 1969b.

Ahrens, T. J., I. Jackson and R. Jeanloz, Shock compression and adiabatic release of a titaniferous mare-basalt, Proc. Lunar Sci. Conf. 8th, 3437-3455, 1977.

Al'tshuler, L. V., M. I. Brazhnik and G. S. Telegin, Strength and elasticity of iron and copper at high shock-wave compression pressures, J. Appl. Mech. Tech. Phys., 12, 921-926, 1971.

Al'tshuler, L. V., S. B. Kormer, M. I. Brazhnik, L. A. Vladimirov, M. P. Speranskaya and A. I. Funtikov, The isentropic compressibility of aluminum, copper, lead and iron at high pressures, Sov. Phys. JETP, 11, 766-775, 1960.

Anderson, D. L., A seismic equation of state, Geophys. J. R. astr. Soc., 13, 9-30, 1967.

Anderson, D. L., Bulk modulus-density systematics, J. Geophys. Res., 74, 3857-3864, 1969.

Anderson, D. L., Chemical plumes in the mantle, Bull. Geol. Soc. Am., 86, 1593-1600, 1975.

Anderson, D. L. and R. S. Hart, An earth model based on free oscillation and body waves, J. Geophys. Res., 81, 1461-1475, 1976.

Anderson, D. L. and H. Kanamori, Shock-wave equations of state for rocks and minerals, J. Geophys. Res., 73, 6477-6502, 1968.

Anderson, O. L., E. Schreiber, R. C. Liebermann and N. Soga, Some elastic constant data on minerals relevant to geophysics, Rev. Geophys., 6, 491-524, 1968.

Andersson, S. and A. D. Wadsley, The crystal structure of $Na_2Ti_3O_7$, Acta Cryst., 14, 1245-1249, 1961.

Belyakov, G. V., L. D. Livshits and V. N. Rodionov, Shock-wave deformation of an inhomogeneous medium which is modeled by a set of steel balls, Izv. Earth Phys., No. 10, 665-667, 1974.

Belyakov, G. V., V. N. Rodionov and V. P. Samosadnyi, Heating of porous material under impact compression, Combustion, Explosion and Shock Waves, 13, 524-528, 1977.

Birch, F., The effect of pressure upon the elastic parameters of isotropic solids, according to Murnaghan's theory of finite strain J. Appl. Phys., 9, 279-288, 1938.

Birch, F., Finite elastic strain of cubic crystals, Phys. Rev., 71, 809-824, 1947.

Brennan, B. J. and F. D. Stacey, A thermodynamically based equation of state for the lower mantle, J. Geophys. Res., in press, 1979.

Clark, S. P., K. K. Turekian and L. Grossman, Chemical models of the Earth, in The Nature of the Solid Earth, E. C. Robertson (ed.) McGraw-Hill, New York, 3-18, 1972.

Cleary, J. R., The D" region, Phys. Earth Planet. Int., 9, 13-27, 1974.

Davies, G. F., Quasi-harmonic finite strain equations of state of solids, J. Phys. Chem. Solids, 34, 1417-1429.

Davies, G. F. and D. L. Anderson, Revised shock wave equations of state for high pressure phases of rocks and minerals, J. Geophys. Res., 76, 2617-2627, 1971.

Davies, G. F. and E. S. Gaffney, Identification of high-pressure phases of rocks and minerals from Hugoniot data, Geophys. J. R. astr. Soc., 33, 165-183, 1973.

Dziewonski, A. M., A. L. Hales and E. R. Lapwood, Parametrically simple earth models consistent with geophysical data, Phys. Earth Planet. Int., 10, 12-48, 1975.

Gay, P., The structure of the plagioclase feldspars, V., Min. Mag., 30 428-438, 1954.

Grady, D. E., Processes occurring in shock wave compression of rocks and minerals, in High Pressure Research, M. H. Manghnani and S. Akimoto (eds.), Academic Press, New York, 389-438, 1977.

Grady, D. E. and W. J. Murri, Dynamic unloading in shock compressed feldspar, Geophys Res. Lett., 3, 472-474, 1976.

Grady, D. E., W. J. Murri and P. S. DeCarli, Hugoniot sound velocities and phase transformations in two silicates, J. Geophys. Res., 80, 4857-4861, 1975.

Grossman, L., J. W. Larimer, Early chemical history of the solar system, Rev. Geophys. Space Phys., 12, 71-101, 1974.

Grover, R., Liquid metal equation of state based on scaling, J. Chem. Phys., 55, 3435, 3441, 1971.

Jackson, I. and T. J. Ahrens, Shock-wave compression of single-crystal forsterite, J. Geophys. Res., 84, 3039-3048, 1979.

Jeanloz, R., Properties of iron at high pressures and the state of the core, J. Geophys. Res., 84, 1979a.

Jeanloz, R., Shock effects in olivine and implications for Hugoniot data, J. Geophys. Res., submitted, 1979b.

Jeanloz, R. and T. J. Ahrens, Pyroxenes and olivines: structural implications of shock-wave data for high pressure phases, in High-Pressure Research, M. H. Manghnani and S. Akimoto (eds.) Academic Press, New York, 439-461, 1977.

Jeanloz, R. and T. J. Ahrens, The equation of state of a lunar anorthosite: 60025, Proc. Lunar Planet. Sci. Conf. 9th, 2789-2803, 1978.

Jeanloz, R. and T. J. Ahrens, Equations of state of FeO and CaO, Geophys. J. R. astr. Soc., submitted (1979a).

Jeanloz, R. and T. J. Ahrens, Release adiabat measurements on minerals; the effect of viscosity, J. Geophys. Res., in press, 1979b.

Jeanloz, R., T. J. Ahrens, H. K. Mao and P. M. Bell, B1/B2 transition in CaO from shock-wave and diamond cell experiments, Science (in press), 1979.

Jeanloz, R. and F. M. Richter, Convection, composition and the thermal state of the lower mantle, J. Geophys. Res., in press, 1979.

Kormer, S. B., A. I. Funtikov, V. D. Urline and A. N. Kolesnikova, Dynamic compression of porous metals and the equation of state with variable specific heat at high temperatures, Sov. Phys. JETP 15, 477-488, 1962.

Liebermann, R. C. and A. E. Ringwood, Elastic properties of anorthite and the nature of the lunar crust, Earth Planet. Sci. Lett., 31, 69-70, 1976.

Liu, L.-G., High-pressure phase transofrmation of albite, jadeite and nepheline, Earth Planet. Sci. Lett., 37, 438-444, 1978a.

Liu, L.-G., A new high-pressure phase of $Ca_2Al_2SiO_7$ and implications for the earth's interior, Earth Planet. Sci. Lett., 40, 401-406, 1978b.

Lyzenga, G. and T. J. Ahrens, The relations between the shock-induced free-surface velocity and post-shock density of solids, J. Appl. Phys., 49, 201-204, 1978.

Marvin, U. B., J. A. Wood, and J. S. Dickey, Jr., Ca-Al rich phases in the Allende meteorite, Earth Planet. Sci. Lett., 7, 346-350, 1970

McLaren, A. C., The domain structure of a transitional anorthite: a study by direct lattice-resolution electron microscopy, Contrib. Mineral. Petrol., 41, 47-52, 1973.

McQueen, R. G., J. N. Fritz and S. P. Marsh, on the equation of state of stishovite, J. Geophys. Res., 68, 2319-2322, 1963.

McQueen, R. G., S. P. Marsh and J. N. Fritz, Hugoniot equation of state of twelve rocks, J. Geophys. Res., 72, 4999-5036, 1967.

McQueen, R. G., S. P. Marsh, J. W. Taylor, J. N. Fritz and W. J. Carter The equation of state of solids from shock wave studies, in High Velocity Impact Phenomena, R. Kinslow (ed.) Academic Press, New York, 294-419 and Appendices, 1970.

Megaw, H. D., The thermal expansion of crystals in relation to their structure, Z. Kristallog., 100, 58-76, 1938.

Müller, W. F., H. R. Wenk and G. Thomas, Structural variations in anorthite, Contrib. Mineral. Petrol., 34, 304-314, 1972.

Ramakrishnan, J., R. J. Hardy and G. C. Kennedy, The Grüneisen parameter γ of KBr, RbCl and Bi through high pressure phase transitions, J. Phys. Chem. Solids, 40, 297-303, 1979.

Reid, A. F. and A. E. Ringwood, Newly observed high pressure transformations in Mn_3O_4, $CaAl_2O_4$ and $ZrSiO_4$, Earth Planet. Sci. Lett., 6, 205-208, 1969.

Rice, M. H., R. G. McQueen and J. M. Walsh, Compressibility of solids by strong shock waves, Solid State Physics, 6, 1-63, 1958.

Ringwood, A. E., Composition and Petrology of the Earth's Mantle, McGraw-Hill, New York, 618 pp., 1975.

Robie, R. A., B. S. Hemingway, and J. R. Fisher, Thermodynamic Properties of Minerals and Realted Substances, U. S. Geol. Surv. Bull. 1452, Washington, D.C., 456 pp., 1978.

Simonov, I. V. and B. S. Chekin, High-velocity collisions of iron plates, Combustion, Explosion and Shock Waves, 11, 237-242, 1975.

Skinner, B. J., Thermal expansion, in Handbook of Physical Constants, S. P. Clark, Jr. (ed.), Geol. Soc. Am. Mem. 97, 75-96, 1966.

Stacey, F. D., A thermal model of the earth, Phys. Earth Planet. Int., 15, 341-348, 1977.

Touloukian, Y. S., R. K. Kirby, R. E. Taylor and T. Y. R. Lee, Thermal Expansion, Nonmetallic Solids, IFI/Plenum, New York, 1658 pp., 1977.

Turekian, K. K. and S. P. Clark, Jr., Inhomogeneous accretion model of the earth from the primitive solar nebula, Earth Planet. Sci. Lett., 6, 346-348, 1969.

Wackerle, J., Shock-wave compression of quartz, J. Appl. Phys., 33, 922-937, 1962.

Wallace, D. C., Thermodynamics of Crystals, J. Wiley & Sons, New York, 484 pp., 1972.

Walsh, J. M., and R. H. Christian, Equation of state of metals from shock wave measurements, Phys. Rev., 97, 1544-1556, 1955.

Zharkov, V. N. and V. A. Kalinin, Equations of State for Solids at High Pressures and Temperatures, Consultants Bureau, N.Y., 257 pp., 1971.

TABLE 1

Electron Microprobe Analysis

Single-Crystal Anorthite (Miyake-zima, JAPAN)

Oxide	Weight %
Na_2O	0.51
MgO	0.04
Al_2O_3	35.28
SiO_2	44.19
K_2O	0.02
CaO	19.57
FeO	0.66
TOTAL	100.27

TiO_2, BaO, Cr_2O_3, MnO, F, Cl absent

TABLE 2

SINGLE-CRYSTAL ANORTHITE[1] HUGONIOT DATA

Experiment			Sample	Hugoniot State			Release State			
	Shot No.	Flyer/ Driver	Impact Velocity (km/s)	Initial Density Crystal (Mg/m^3)	Shock wave Velocity (km/s)	Particle Velocity (km/s)	Pressure (GPa)	Density (Mg/m^3)	Shock-wave velocity (km/s)	Particle[2] Velocity (km/s)	Pressure (GPa)	Density (Mg/m^3)
LGG	058	2024 Al	5.398	2.783	7.400	2.911	60.0	4.588	6.226	3.226	44.3	4.459
			±0.005	±0.002	±0.077	±0.012	±0.4	±0.043	±0.119	±0.075	±1.9	±0.088
LGG	038	Ta	4.925	2.756	8.628	3.791	90.2	4.916	7.982	4.333	76.2	4.455
			±0.003	±0.001	±0.057	±0.005	± 0.5	±0.030	±0.079	±0.050	±1.6	±0.127
LGG	037	Ta	5.694	2.768	9.477	4.338	113.8	5.104	8.722	4.798	92.2	4.861
			±0.004	±0.002	±0.092	±0.009	± 0.9	±0.050	±0.181	±0.113	±4.1	±0.164

NOTES: (1) [010] shock-wave propagation direction

(2) Derived from measured shock-wave velocity (U_s) through fused quartz buffer-mirror using $U_s = 1.108 + 1.587\ u_p$, $\rho_0 = 2.204\ Mg/m^3$

TABLE 3

LUNAR ANORTHOSITE (60025) HUGONIOT DATA

	Experiment			Sample		Hugoniot State				Release State			
				Initial Density									
	Shot No.	Flyer/ Driver	Impact Velocity (km/s)	Bulk (Mg/m^3)	Crystal[1] Mg/m^3	Shock-wave Velocity (km/s)	Particle Velocity (km/s)	Pressure (GPa)	Density (Mg/m^3)	Shock-wave Velocity (km/s)	Particle Velocity[2] (km/s)	Pressure (GPa)	Density (Mg/m^3)
40mm Gun	429	W	2.312 ±0.010	2.243 ±0.014	2.747 ±0.002	5.070 ±0.021	2.036 ±0.010	23.2 ± 0.2	3.749 ±0.025				
										Free Surface Velocity: 3.727 ±0.101	0		2.563 ±0.091
LGG	042	2024A1	4.971 ±0.002	2.239 ±0.010	2.751 ±0.003	6.751 ±0.038	2.964 ±0.009	44.8 ± 0.2	3.990 ±0.025	5.523 ±0.036	2.783 ±0.023	33.9 ± 0.5	3.943 ±0.025
LGG	029	Ta	4.467 ±0.006	2.244 ±0.002	2.709 ±0.003	7.732 ±0.048	3.617 ±0.004	62.7 ± 0.3	4.216 ±0.027	6.434 ±0.109	3.355 ±0.069	47.5 ± 1.8	4.137 ±0.039
LGG	059	Ta	5.240 ±0.020	2.216 ±0.002	2.767 ±0.005	8.539 ±0.046	4.211 ±0.017	79.7 ± 0.05	4.372 ±0.032	8.031 ±0.110	4.363 ±0.069	77.2 ± 2.3	4.199 ±0.314
LGG	036	Ta	5.668 ±0.003	2.199 ±0.001	2.743 ±0.006	9.150 ±0.072	4.525 ±0.006	91.1 ± 0.6	4.351 ±0.039	8.116 ±0.086	4.417 ±0.054	79.0 ± 1.8	4.333 ±0.039
LGG	026	Ta	5.762 ±0.012	2.234 ±0.003	2.713 ±0.002	9.168 ±0.129	4.591 ±0.015	94.0 ± 1.1	4.473 ±0.075	6.952 ±0.256	3.682 ±0.164	56.4 ± 4.6	4.074 ±0.096
LGG	061	Ta (thin)	6.585 ±0.005	2.230 ±0.024	2.748 ±0.006	10.142 ±0.121	5.196 ±0.019	117.5 ± 1.5	4.573 ±0.075	9.349 ±0.207	5.194 ±0.130	107.0 ± 5.1	4.573 ±0.075

Notes: (1) Archimedean density: assumes interconnected porosity. Average crystal density is 2.74 Mg/m^3 and the average porosity is about 19%.

(2) Derived from measured shock-wave velocity through fused quartz buffer-mirror using $U_s = 1.108 + 1.587\ u_p$, $\rho_0 = 2.204\ Mg/m^3$.

TABLE 4

ANORTHITE: HUGONIOT EQUATIONS OF STATE

Non-porous

$\rho_o = 2.74\ (\pm 0.02)\ Mg/m^3$, $P > 30$ GPa

$U_s = 2.37\ (\pm 0.55) + 1.82\ (\pm 0.36)\ u_p - 0.045\ (\pm 0.058)\ u_p^2$

Porous

$\rho_o = 2.23\ (\pm 0.03)\ Mg/m^3$, $P > 22$ GPa

$U_s = 1.43\ (\pm 0.35) + 1.90\ (\pm 0.20)\ u_p - 0.044\ (\pm 0.028)\ u_p^2$

TABLE 5

CANDIDATE HIGH-PRESSURE PHASES

FOR ANORTHITE ($CaAl_2Si_2O_8$)

Hollandite phase: $^{VIII}Ca\ ^{VI}(Al_2Si_2)O_8$, $\rho_o = 3.92$ Mg/m^3 (based on Liu, 1978a)

Mixed Oxides assemblage: $^{VI}CaO + {}^{VI}Al_2O_3 + 2\,{}^{VI}SiO_2$, $\rho_o = 3.95$

OR

$^{VIII}CaO + {}^{VI}Al_2O_3 + 2\,{}^{VI}SiO_2$, $\rho_o = 4.05$ Mg/m^3

(CaO data from Jeanloz, et al., 1979)

Calcium Ferrite assemblage: $^{VIII}Ca\ {}^{VI}Al_2O_4 + 2\,{}^{VI}SiO_2$, $\rho_o = 4.10$ Mg/m^3

(Reid and Ringwood, 1969)

Sodium Titanate assemblage: $\frac{1}{2}\left({}^{VIII}Ca_2\ {}^{VI}Al_2\ {}^{VI}SiO_7 + {}^{VI}Al_2O_3 + 3\ {}^{VI}SiO_2\right)$,

$\rho_o = 4.29$ Mg/m^3 (Liu, 1978b; Anderson and Wadsley, 1961)

General References: Ringwood (1975), Robie, et al., (1978)

Figure Captions

Figure 1: Anorthite and anorthosite shock-wave data from the present study and that of McQueen, et al., [1967] compared with a theoretical Hugoniot for anorthite (its uncertainty corresponds to variations in the assumed pressure derivative of the bulk modulus between 4 and 6). The porous and nonporous Hugoniot curves are from the fit listed in Table 4.

Figure 2: The data and Hugoniot curves from Figure 1 shown in the shock-wave velocity vs. particle velocity plane. The dashed line corresponds to the theoretical Hugoniot of (untransformed) anorthite, while c_0 shows the bulk sound speed of anorthite from Liebermann and Ringwood [1976].

Figure 3: Grüneisen parameter of anorthite as a function of density. The present data at densities above 3.5 Mg/m^3 are shown as individual points which can be fit by a power law in density with an exponent of 1.66 (Equation 2). Alternatively, the best-fit Hugoniots of Table 4 imply values of the Grüneisen parameter which are given by the short-dashed curve. The zero-pressure value for anorthite is shown at a density of 2.74 Mg/m^3 along with an assumed volume dependence (long dashes). Data sources: Liebermann and Ringwood [1976]; Rigby and Green, and Floyd in Touloukian, et al., [1977]; Robie, et al., [1978].

Figure 4: Adiabatic bulk modulus of anorthite as a function of pressure and temperature based on the present shock-wave data, compared with seismological values for the lower mantle [Dziewonski, et al., 1975; Anderson and Hart, 1976]. Bulk moduli based directly on data are shown for the (nonporous) Hugoniot and porous Hugoniot, along with values along the adiabat and metastable Hugoniot derived from the reduced Hugoniot data. Isotherms based on the calculated temperatures are also given (thin, solid lines), with temperatures given in K.

Figure 5: Hugoniots given by the data on anorthite (heavy lines) are compared with the derived compression curves based on the present reduction of the shock-wave data (thin lines). The density in the lower mantle according to Dziewonski et al. [1975] and Anderson and Hart [1976] is presented (dashed lines), as the zero-pressure densities of candidate high-pressure assemblages corrsponding to anorhtite (see Table 5).

Figure 6: Calculated temperatures along the porous (19%) and nonporous Hugoniot of anorthite, as well as the derived adiabat and metastable Hugoniot. Estimated errors are shown for the Hugoniot temperatures.

Figure 7: Coefficient of thermal expansion of anorthite as a function of pressure and temperature. Isobars (heavy curves) and density isopleths (thin, dashed curves; densities in Mg/m^3 in parentheses) are shown for the high-pressure state of anorthite. The Debye temperature (Θ) used in this analysis is also given, as a function of density (or pressure). Along each isobar, the circles correspond to intersections with, respectively, the adiabat (open), metastable Hugoniot (open), Hugoniot (filled) and porous Hugoniot (filled) with increasing temperature. For comparison, the thermal expansion of anorthite measured at zero-pressure is shown with a dotted curve extending to the melting temperature (marked) according to a fit to the data of Rigby and Green, and Floyd in Touloukian, et al., [1977], and also as crosses from the work of Kozu et al., [in Skinner, 1966].

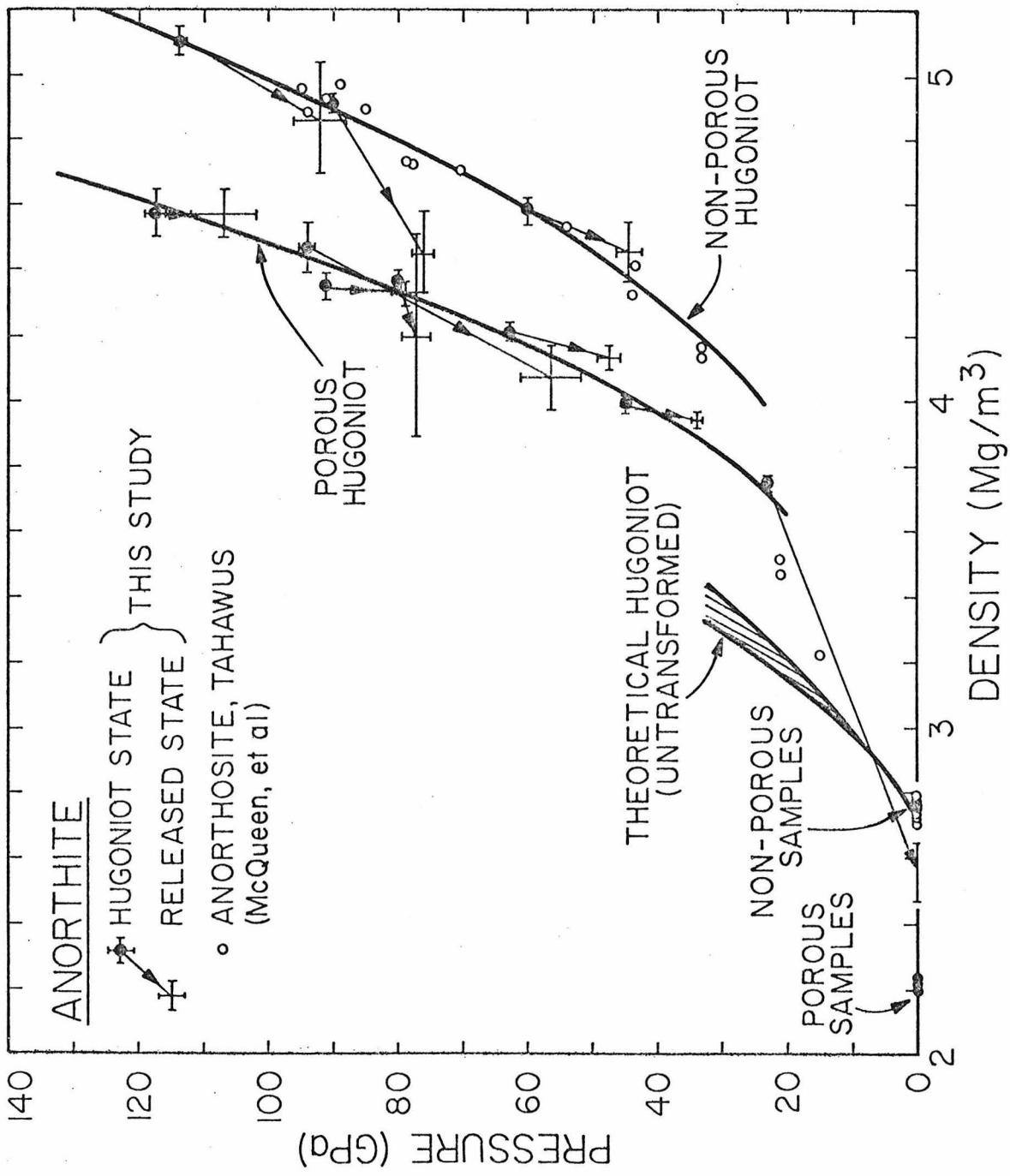
ANORTHITE
HUGONIOT STATE
RELEASED STATE
THIS STUDY
ANORTHOSITE, TAHAWUS
(McQueen, et al)
POROUS HUGONIOT
NON-POROUS HUGONIOT
THEORETICAL HUGONIOT
(UNTRANSFORMED)
NON-POROUS SAMPLES
POROUS SAMPLES
PRESSURE (GPa)
DENSITY (Mg/m3)
140
120
100
80
60
40
20
0
2
3
4
5

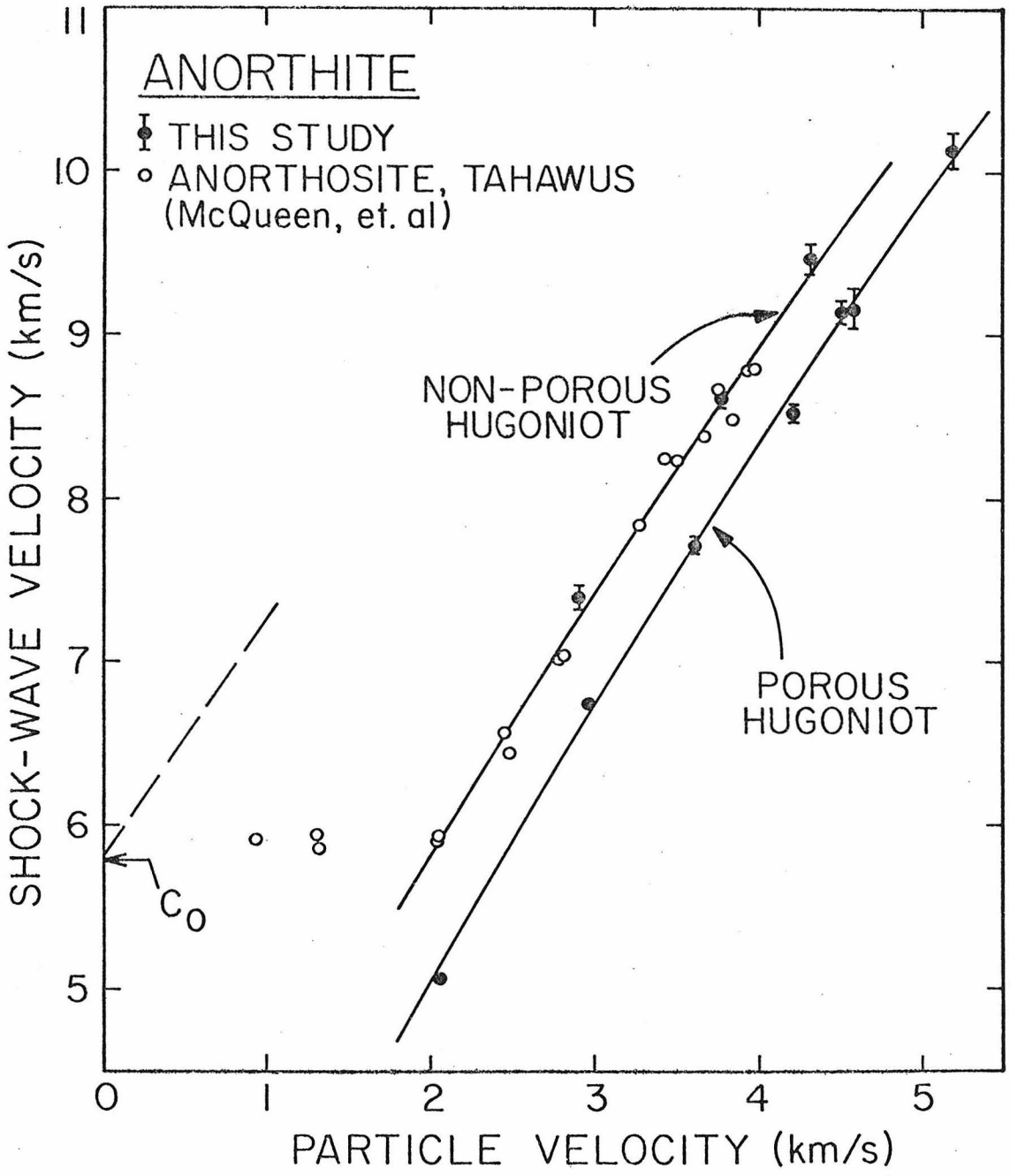
ANORTHITE
THIS STUDY
ANORTHOSITE, TAHAWUS
(McQueen, et. al)
NON-POROUS
HUGONIOT
POROUS
HUGONIOT
C_0
SHOCK-WAVE VELOCITY (km/s)
PARTICLE VELOCITY (km/s)
11
10
9
8
7
6
5
0
1
2
3
4
5

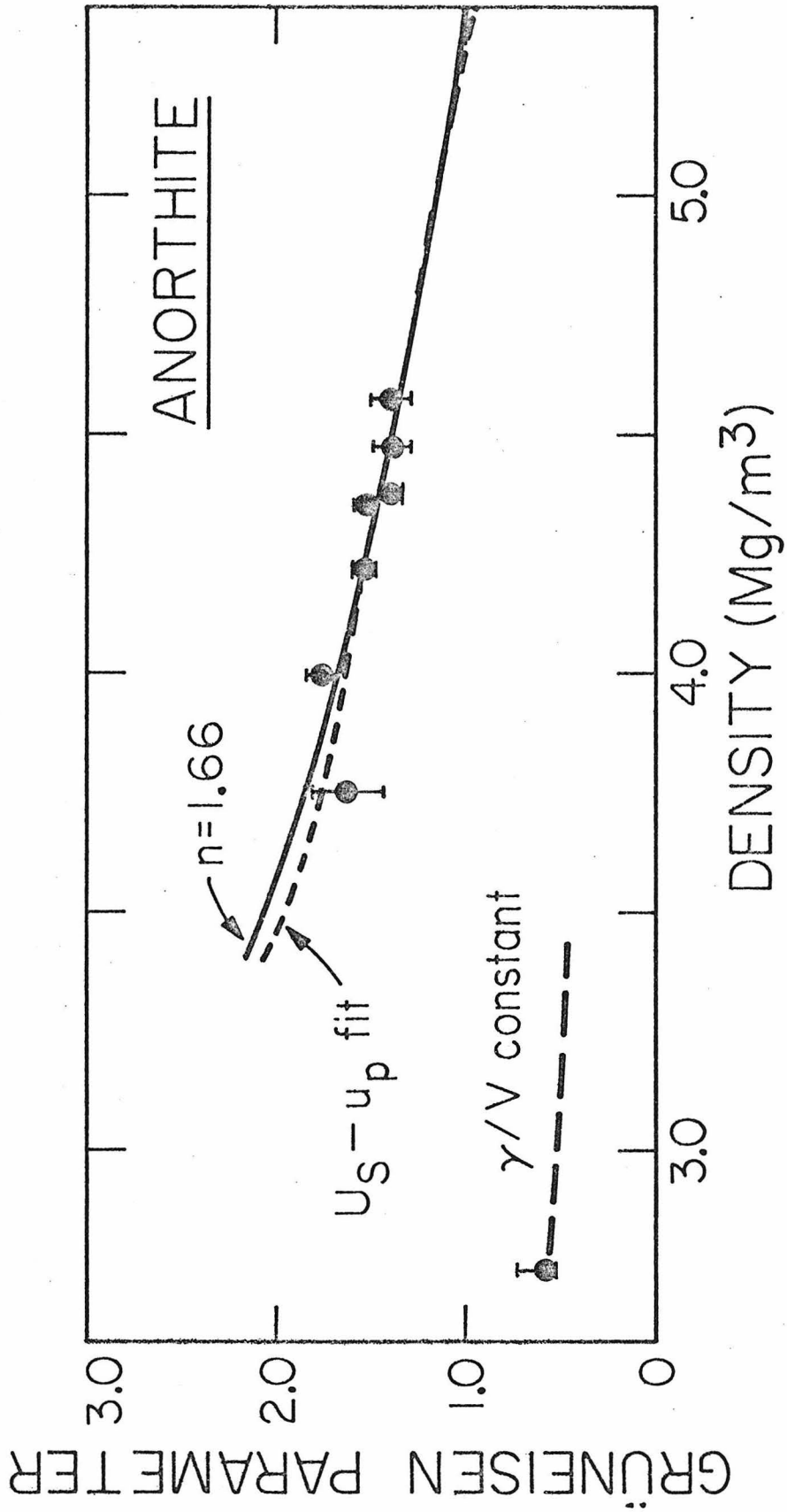
ANORTHITE
n=1.66
$U_S - u_p$ fit
γ/V constant
GRÜNEISEN PARAMETER
3.0
2.0
1.0
0
3.0
4.0
5.0
DENSITY (Mg/m^3)

Fig. 3

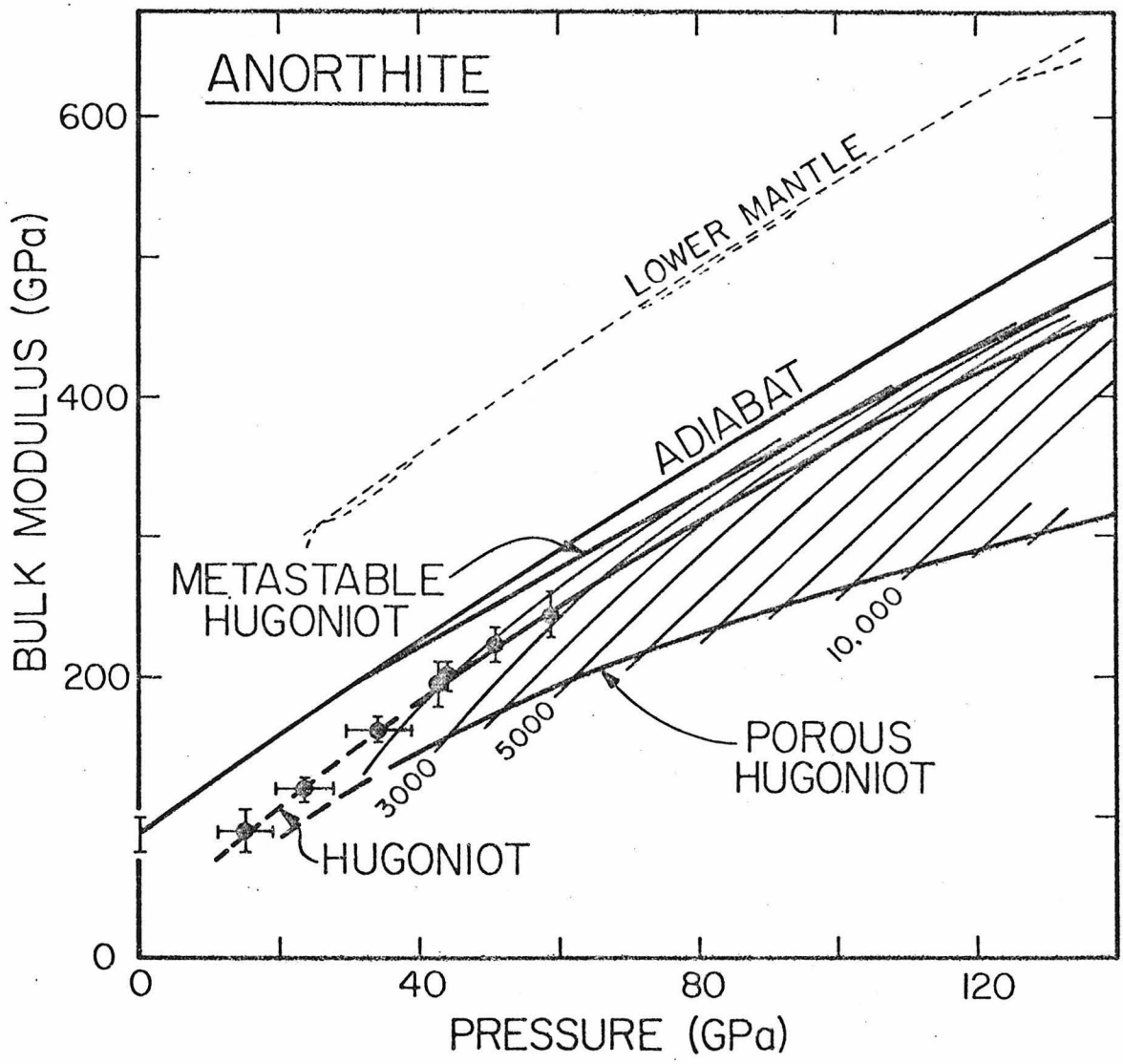
ANORTHITE
BULK MODULUS (GPa)
PRESSURE (GPa)
0
200
400
600
0
40
80
120
LOWER MANTLE
ADIABAT
METASTABLE
HUGONIOT
HUGONIOT
POROUS
HUGONIOT
3000
5000
10,000

Fig 4

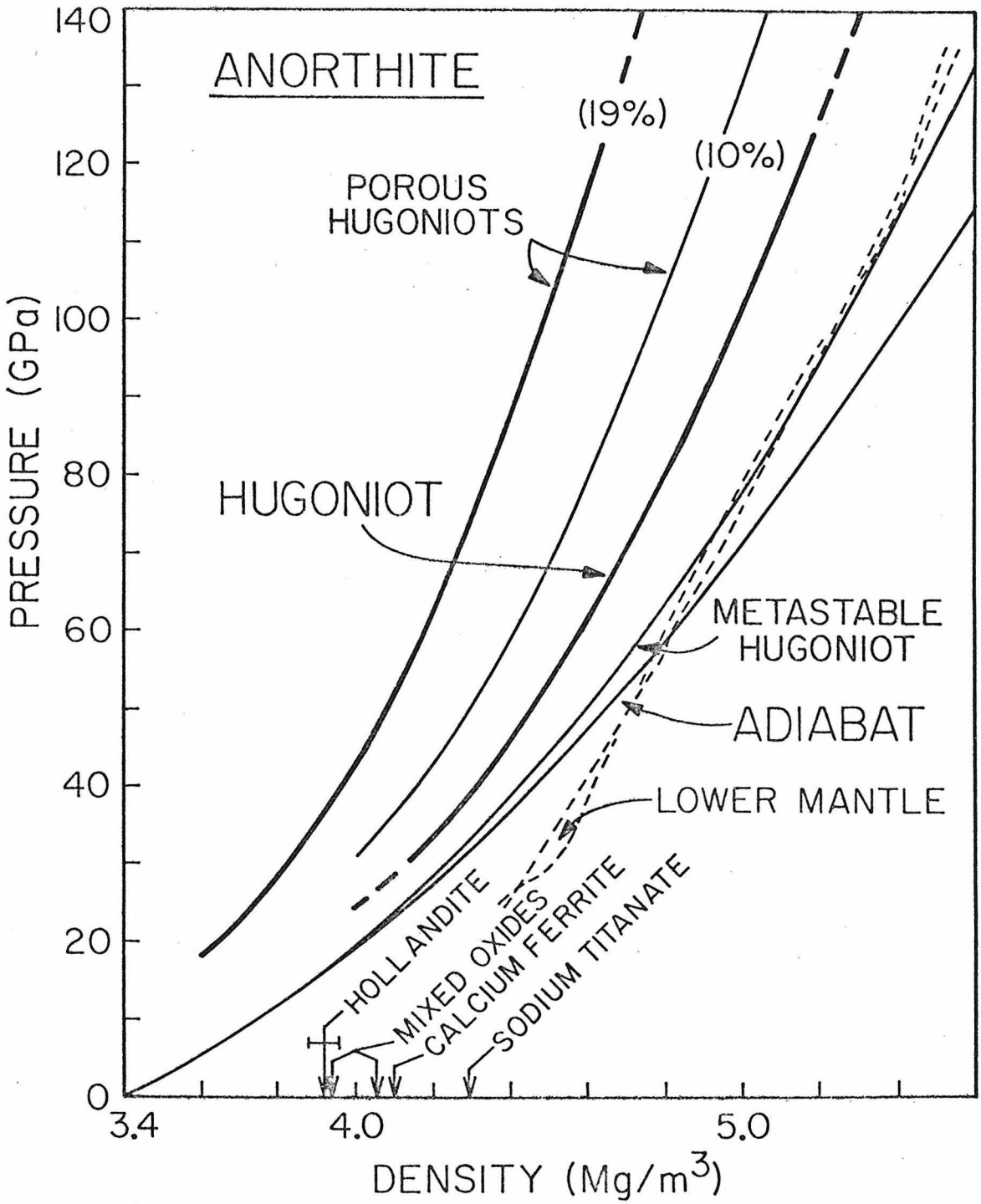
ANORTHITE
(19%)
(10%)
POROUS
HUGONIOTS
HUGONIOT
METASTABLE
HUGONIOT
ADIABAT
LOWER MANTLE
HOLLANDITE
MIXED OXIDES
CALCIUM FERRITE
SODIUM TITANATE
PRESSURE (GPa)
DENSITY (Mg/m3)
0
20
40
60
80
100
120
140
3.4
4.0
5.0

Fig. 5

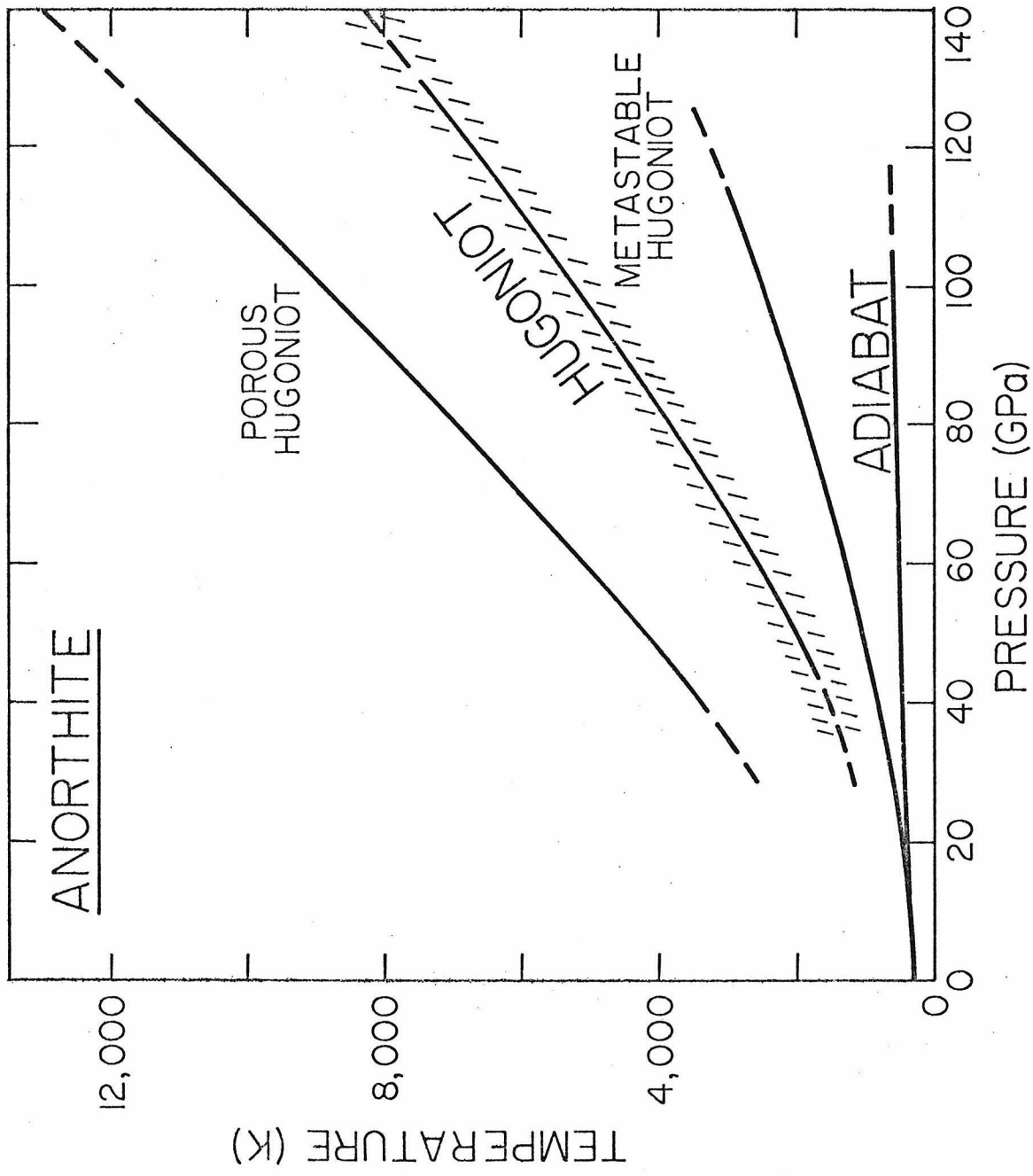
ANORTHITE
POROUS HUGONIOT
HUGONIOT
METASTABLE HUGONIOT
ADIABAT
TEMPERATURE (K)
12,000
8,000
4,000
0
0
20
40
60
80
100
120
140
PRESSURE (GPa)

Fig. 6

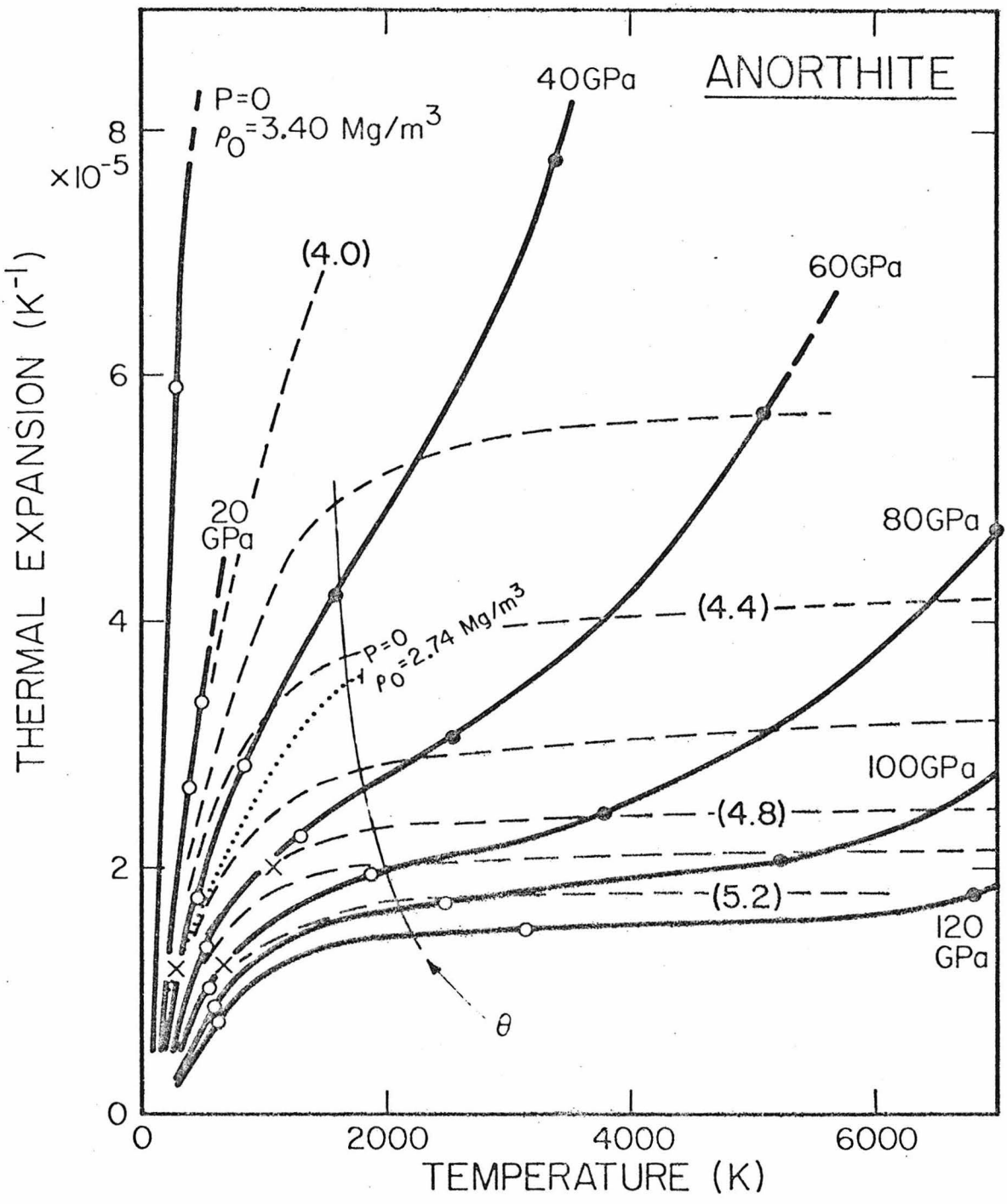
ANORTHITE
P=0
ρ_0=3.40 Mg/m^3
40GPa
60GPa
80GPa
100GPa
120 GPa
20 GPa
(4.0)
(4.4)
(4.8)
(5.2)
P=0
ρ_0=2.74 Mg/m^3
θ
THERMAL EXPANSION (K^{-1})
×10^{-5}
8
6
4
2
0
0
2000
4000
6000
TEMPERATURE (K)

Fig. 7

Chapter 8

INFRARED SPECTRA OF OLIVINE POLYMORPHS: α, β-PHASE AND SPINEL

Abstract

Infrared (IR) absorption spectra are presented for olivine (α) and apinel (γ) phases of A_2SiO_4 (A = Fe, Ni, Co) and Mg_2GeO_4. IR spectra of β-phase ("modified spinel") Co_2SiO_4 and of α-Mg_2SiO_4 are also included. These results provide reference spectra for the identification of olivine high-pressure polymorphs. Isostructural and isochemical correlations are used to support a general interpretation of the spectra and to predict the spectrum of γ-Mg_2SiO_4. A γ-Mg_2GeO_4 sample equilibrated at 1000°C shows evidence of inversion, but one equilibrated at 730°C does not. This suggests that inversion could occur in silicate spinels at elevated temperatures and pressures, however no evidence of inversion is seen in the IR spectra of the silicates.

I. INTRODUCTION

Olivine and its high-pressure polymorphs are considered to be important phases of the earth's mantle, and hence there is substantial interest in their properties (e.g., Ringwood, 1975). In this study, the infrared (IR) spectra of several olivines (α-A_2SiO_4:A = Mg, Fe, Ni, Co; α-Mg_2GeO_4) and their corresponding β-phase ("modified spinel") and spinel polymorphs have been determined. This is the first spectroscopic investigation of several of these high-pressure polymorphs; it provides new observations for determining the effects of varying either structure or composition on the IR spectra of silicates. By comparison, the structures and stability relations of the olivine and spinel polymorphs have been studied extensively (e.g., Hanke, 1965; Wenk and Raymond, 1973; Yagi, et al., 1974; Morimoto, et al., 1974; Marumo, et al., 1974, 1977; Tokonami, et al., 1972; Akimoto, et al., 1976; Ringwood, 1975; Kamb, 1968; Baur, 1972); newly determined thermochemical data are also pertinent (Navrotsky and Hughes, 1976; Navrotsky, et al., 1979).

The present study is an extension of the work of Tarte (1962, 1963a,b, 1965) who has emphasized the use of chemical substitution in understanding the infrared spectra of silicates and germanates. Polymorphism is useful in a fashion analogous to substitution (e.g., White and Roy, 1964), particularly for the case of olivine and spinel. The latter, being a highly symmetric structure, yields a simple spectrum which has the basic features of the more complex olivine spectrum. The β-phase, although closely related to the spinel structure (Morimoto, et al., 1969; Moore and Smith, 1969) also has reduced symmetry and contains Si_2O_7 groups. Thus, its spectrum is relatively complex and

includes double-tetrahedral vibrational modes.

The question of disorder between tetrahedral and octahedral cation sites (inversion) in spinels has repeatedly come up (e.g., Durif-Varambon, 1956; Dachille and Roy, 1960; Tarte, 1963b; Datta and Roy, 1967; Navrotsky and Kleppa, 1967; Ma, 1975), and because of the recent geochemical interest in this effect (Jackson, et al., 1974; Navrotsky, 1977; Liebermann, et al., 1977; Navrotsky, et al., 1979) the present data have been examined for spectroscopic evidence of inversion. Finally, these results allow IR spectroscopy to be used for the identification of olivine polymorphs independently, or in conjunction with standard x-ray diffraction techniques (Jeanloz, 1979a).

II. EXPERIMENTAL

The specimens used in this study are described in Table 1. Hand-picked sample material was ground and mixed with 200 mg (reagent grade) KBr, and pressed to form pellets about 13 mm in diameter and 0.52 (±0.03) mm thick. Spectra were measured at room temperature using a Perkin-Elmer model 180 double beam spectrophotometer over the range 2000 to 230 cm^{-1}. The use of TlBr pellets (in an attempt to match indices of refraction of sample and medium) did not significantly improve the quality of the results, and all IR spectra shown below were derived from KBr pellets. An absolute wavelength calibration was made by measuring the rotationally-split fine structure of the ν_2 fundamentals of CO_2 and H_2O (cf. Pyler, et al., 1960), as well as by correlating peaks within the overlapping spectral ranges of the gratings used. All spectra are given with a linear absorbance scale, and are normalized to 5 μmole of

sample/200 mg KBr. An absolute absorbance calibration was made using a pre-calibrated screen, however the peak heights are only accurate to within about 10 to 15%.

III. RESULTS AND DISCUSSION

The spectra can be broadly interpreted in terms of internal (molecular), tetrahedral and octahedral, versus external (lattice) modes (Tables 2 and 3). Stretching and bending vibrations of the tetrahedra can be distinguished as nearly independent modes, whereas the octahedral vibrations cannot be considered independent of the full-lattice vibrations. Recent spectroscopic studies (Preudhomme and Tarte, 1971a,b,c, 1972; Hohler and Funck, 1973; Paques-Ledent and Tarte, 1973) have emphasized the coupling between octahedral and lattice vibrations, and even between octahedral and tetrahedral modes. Evidence for such coupling is also found in the present data. Further complexities arise in the olivine spectra due to splitting of the tetrahedral and octahedral bands; symmetric and antisymmetric tetrahedral stretching modes (ν_1 and ν_2 respectively) can be distinguished, while the symmetric and antisymmetric tetrahedral bending modes (ν_2 and ν_4) are apparently closely coupled (e.g., Paques-Ledent and Tarte, 1973).

The new infrared spectra of olivine (α) and spinel (γ) phases are shown in Figures 1-5. Although γ-Mg_2SiO_4 has been produced (e.g., Ito, et al., 1974), its synthesis is difficult and none was available for this study. Similarly, the β-phase of only Co_2SiO_4 was available for study; its spectrum is included in Figure 4. The peaks in the spectra

are listed in Tables 2 and 3, and the main features are summarized in Figure 7. The present observations are consistent with those of previous studies, the quantitative agreement of spectra being especially good with respect to the more recent work (e.g., Hohler and Funck, 1973). In particular, the new spectrum of γ-Ni_2SiO_4 confirms the spurious nature of the previously observed peaks at 1034, 709 and 470 cm^{-1} (Tarte and Ringwood, 1962; Tarte, 1963b, 1965).

Spinel

The spinel spectra are characterized by three strong absorption peaks corresponding, in order of decreasing wavenumber, to tetrahedral stretching (ν_3) and bending modes (ν_4), and octahedral-lattice modes. Presumably, a fourth peak exists for the silicate spinels at a frequency below the spectral range studied here (e.g., White and DeAngelis, 1967). Although the ν_3 peak is considered to be an essentially pure Si-O or Ge-O stretching mode (Prendhomme and Tarte, 1972), there are measurable variations in the peak locations for different compositions. Single-crystal X-ray data (Yagi, et al., 1974; Marumo, et al., 1974,1977; Finger, et al., 1979) indicate no variation in the Si-O distance among the spinels studied here (165.5 ± 0.3 ppm), and both X-ray and IR data preclude significant distortions of the tetrahedral sites. Hence the variation in the Si-O stretching frequency is likely due to the influence of the octahedral cation. This is further indicated by the correlation of this vibrational frequency with the octahedral metal-oxygen distance. This correlation is not evident among the germanates, and isotope substitution in γ-Ni_2GeO demonstrates that the mode is independent of the octahedral

cation in this compound. However, from the correlation of u-parameter and lattice parameter among the silicate spinels (Akimoto, et al., 1976; Finger, et al., 1979) a short octahedral metal-oxygen distance might be expected in γ-Mg_2SiO_4: 207 pm (using a = 807.6 pm from Ito, et al., 1974). Again, this suggests the possibility of octahedral-tetrahedral interactions in the ν_3 SiO_4 absorption band.

The second (ν_4) peak also varies among the spinels of different compositions (Figure 7), and the position of this band follows that of the lower frequency octahedral mode. This is consistent with the evidence from isotope substitution for octahedral, hence full-lattice, influence on the ν_4 mode (Preudhomme and Tarte, 1972). By contrast, the octahedral vibrational mode can be readily understood in terms of a simple force model which predicts a vibrational frequency:

$$\nu \propto \sqrt{\frac{k}{\mu}} \qquad (1)$$

and

$$k \propto d^{-3} \qquad (2)$$

where μ is reduced mass, k is the force constant and d is the interatomic separation; the first expression corresponds to the frequency of a harmonic oscillator while the second derives from an ionic bonding (Coulombic) potential (e.g., Batsanov and Derbeneva, 1969). The results, Figure 8, show that the octahedral vibrational frequency is well accounted for in this way for both silicate and germanate spinels; the tetrahedral cation also influences this band, decreasing its frequency in the germanates with respect to the silicates. From this correlation and the

octahedral metal-oxygen bond distance derived above the MgO_6 peak location for γ-Mg_2SiO_4 can be predicted as shown in Figure 8.

The present interpretation of the γ-Mg_2GeO_4 spectrum differs from that of Tarte (1963b, 1965) in that the 484 cm^{-1} and 447 cm^{-1} peaks are now assigned to GeO_4 and MgO_6 vibrations, respectively. This interpretation is based on Tarte's data for solid solutions, the consistent relation between olivine and spinel spectra (Figure 7) as well as the correlation shown in Figure 8. The spectrum of γ-Mg_2GeO_4, sample B is discussed below.

Olivine

The olivine spectra are broadly similar to the corresponding spinel spectra, with the main peaks split into groups a few hundred cm^{-1} wide. Many of the peak positions can be correlated with the mass of the octahedral cation, as is shown by the work of Tarte (1963a, 1965), Burns and Huggins (1972), and the present data. This is particularly true for the main XO_4-ν_3 peak (e.g., 884 cm^{-1} in α-Mg_2SiO_4) and the XO_4-ν_1 peak, corresponding to the trend found among the silicate spinels.

For the olivine/spinel pairs studied here, the tetrahedral stretching mode of the spinel appears at approximately the same location as the ν_1 mode for the olivine, rather than near the center of the ν_3+ν_1 bands (cf., Figure 7). This is apparently associated with the approximately 1.5% increase in mean tetrahedral bond length from olivine to spinel structures (Morimoto, et al., 1974; Smyth, 1975; Hazen, 1976; Lager and Meagher, 1978; Yagi, et al., 1974; Marumo, et al., 1974, 1977; Finger, et al., 1979). By contrast, the tetrahedral bending modes for the spinels

occur near the center of the corresponding olivine bands. These olivine peaks must be assigned to combined $\nu_2+\nu_4$ vibrational modes, whereas the lower frequency peaks are essentially octahedral modes (cf., Table 2, Figure 7) (Paques-Ledent and Tarte, 1973; Hohler and Funck, 1973; Burns and Huggins, 1972). This interpretation is different from that of Tarte (1963a): the peaks which he assigned to tetrahedral ν_2 are attributed here to octahedral vibrations (cf., Duke and Stephens, 1964, as well). The octahedral mode is found at somewhat higher frequency in spinel than the mean of the corresponding bands for olivine. This is similar to the relation found for the ν_3 peaks, and is also consistent with a $\sim$1.5% change (decrease) in mean octahedral cation-oxygen bond length from olivine to spinel.

The IR spectrum of γ-Mg_2SiO_4 can be predicted from these comparisons between the spectra of corresponding olivine/spinel pairs (including the correlation shown in Figure 8): the result is included in Figure 7. There is probably also a band near 400 cm^{-1} (not shown), corresponding to the 271 cm^{-1} peak of γ-Mg_2GeO_4.

β-Phase

The most striking feature of the β-phase spectrum (Figure 4) is the appearance of a peak at 686 cm^{-1}, well away from the regions of absorption of the olivine and spinel phases. This band is due to the symmetric stretching vibration of the Si_2O_7 (double tetrahedral) units which characterize the β-phase (e.g., Lazarev, 1972). The remaining peaks can only be tentatively characterized due to the lack of spectra for closely related compounds, however the peaks at 910 and 801 cm^{-1} are undoubtedly

due to Si-O vibrations. The former is considered to be an SiO_3 mode by analogy with the pyrosilicates which show this vibration as their most intense absorption, typically at 900-950 cm^{-1} (Lazarev, 1972; Tarte, et al., 1973). An Si-O-Si antisymmetric stretching vibration is also expected in this region, and the 801 cm^{-1} peak is assigned to this mode based on the correlation between splitting of the Si-O-Si bands and Si-O-Si bond angles given by Lazarev (1972; a splitting $\Delta \sim 7\%$ is consistent with a bond angle of about 109° from Morimoto, et al., 1974). This is an anomalously low frequency for this peak, as is expected from the highly bent bond between the double tetrahedra.

The three principal peaks at 473-557 cm^{-1} are interpreted as SiO_3 bending modes, however the origin of the lower frequency peaks is uncertain. That at 343 cm^{-1} may be due to the Si-O-Si bending mode (Lazarev, 1972) or it, along with the other low frequency bands, may arise from octahedral cation vibrations. In any case, octahedral and full-lattice motions are likely to be significantly intermixed with these bands.

Spinel Inversion

In order to re-examine the possibility that inversion can occur in germanate (or silicate) spinels, IR spectra were obtained from two samples of γ-Mg_2GeO_4, A and B (Table 1), which were heated to 730°C and 1000°C, respectively. Although evidence for inversion has been inferred from X-ray diffraction studies of γ-Mg_2GeO_4 specimens which have been synthesized under similar conditions (Liebermann, et al., 1977), there has been enough controversy over the possibility of inversion in

germanate and silicate spinels (e.g., Dachille and Roy, 1960; Tarte, 1963b, 1965) that an independent analysis seems warranted.

The major spectroscopic change to be expected from inversion in these samples is that due to Ge entering octahedral coordination. A new GeO_6 peak might be expected within 100-150 cm^{-1} below the tetrahedral Ge-O stretching mode in the spectrum of inverse spinel (Tarte, 1962; Tarte and Preudhomme, 1963; Lazarev, 1972). For example, Tarte (1963) documented a GeO_6 peak at 623 cm^{-1} for $LiCrGeO_4$ spinel, whereas Tarte and Ringwood (1964) found two strong peaks near 560 and 610 cm^{-1} due to octahedral Ge in ilmenite-structured $MgGeO_3$. Similarly, new absorption bands might be expected between 500 and 700 cm^{-1} (Tarte, 1962; Lazarev, 1972) due to the presence of tetrahedral Mg in inverse spinel.

As is evident from Figures 5 and 6, γ-Mg_2GeO_4 sample A is a normal spinel, whereas sample B contains new absorption bands. The additional peak at 650 cm^{-1} is especially suggestive of a GeO_6 mode. However, this assignment is inconclusive, and ordering of cations, or other complications, may need to be invoked in support of it (White and DeAngelis, 1967). There is no clearcut evidence for a MgO_4 band, but such a mode could be strongly coupled to full-lattice vibrations.

Subtracting the spectrum of sample A from that of sample B yields a difference spectrum which is similar to that of α-Mg_2SiO_4. However, an X-ray diffraction pattern of sample B reveals no significant contamination other than a trace of MgO (one weak line). Energy-dispersive X-ray analysis shows that samples A and B contain only trace ($\sim 10^{-3}$) amounts of impurities (Si; Ni in A). Therefore the differences between

the spectra of γ-Mg_2GeO_4 samples A and B are interpreted to result from intrinsic structural differences rather than contamination.

The fact that new peaks occur in the spectrum of the high-temperature sample suggests that this spinel is partly inverse. Hence, the IR data are tentatively interpreted as showing that inversion is possible in γ-Mg_2GeO_4, in agreement with the conclusions drawn from earlier X-ray studies. However, the present results show sample A to be normal, despite the X-ray data which have been cited as evidence for inversion in γ-Mg_2GeO_4 synthesized under the same conditions (Liebermann, et al., 1977). Neutron diffraction results also imply that sample A should be normal (Von Dreele, et al., 1977).

There is no convincing evidence for inversion among the silicate spinels studied here. This is particularly true for the Fe and Ni spinels, although the asymmetric nature of the 825 cm^{-1} band of γ-Co_2SiO_4 (subsidiary peaks at 778 and 631 cm^{-1}) may reflect the presence of SiO_6, hence of inversion. However, since the frequency of the ν_3 (SiO_4) peak in silicate spinels is influenced by the presence of the octahedral cation, as shown above, the shape of this peak is probably also modified by interactions with octahedral modes. Both the 908 cm^{-1} shoulder in γ-Ni_2SiO_4 and the asymmetry of the ν_3 band of γ-Co_2SiO_4 are therefore considered to be second-nearest neighbor effects. Recent single-crystal X-ray diffraction data (Finger, et al., 1979) similarly yield no indication of inversion in γ-Fe_2SiO_4 and γ-Ni_2SiO_4.

IV. CONCLUSIONS

New infrared absorption spectra have been presented for silicate (Co, Ni, Fe) olivine/spinel pairs and also for a β-phase. Systematic trends are found for silicates and germanates, among both isostructural and isochemical analogs (Figure 7). These lead to a slight revision of previous interpretations of the olivine and spinel spectra, and also allow the spectrum of γ-Mg_2SiO_4 to be predicted. The present results provide reference spectra for the identification of high-pressure olivine polymorphs. Such an application is illustrated in the studies of Jeanloz (1979a,b).

Two γ-Mg_2GeO_4 samples were examined for evidence of inversion. The 730°C sample is normal, however additional peaks in the spectrum of the 1000°C sample are inferred to be caused by partial inversion. This is the first spectroscopic evidence for inversion in germanate spinels and it suggests that inversion may also be possible in silicate spinels. However, there is no evidence of inverse character in the silicate spinels of the present study. If such inversion occurs in silicates at high temperatures it is likely to influence the phase equilibria between olivine, β-phase, spinel, and perovskite polymorphs which are considered to be significant through the transition zone of the earth's mantle.

Acknowledgments: I am grateful to Drs. S. Akimoto (University of Tokyo), I. Jackson (Australian National University), J. Ito (University of Chicago) and H. Takei (Tohoku University) for providing the sample material used in this study. I have benefited from discussions with G. R. Rossman, and thank T. Benjamin, G. Meeker and S. Hill for technical assistance.

REFERENCES

Akimoto, S., Y. Matsui and Y. Syono. High-pressure crystal chemistry of orthosilicates and the formation of the mantle transition zone in: The Physics and Chemistry of Minerals and Rocks, (R. G. J. Strens, editor), J. Wiley & Sons, New York, pp. 327-363, 1976.

Batsanov, S. S. and S. S. Derbeneva. Effect of valency and coordination of atoms on position and form of infrared absorption bands in inorganic compounds, J. Struct. Chem. (USSR), 10, 510-515, 1969.

Baur, W. H. Computer-simulated crystal structures of observed and hypothetical Mg_2SiO_4 polymorphs of low and high density. Am. Min., 57, 709-731, 1972.

Burns, R. G. and F. E. Huggins. Cation determinative curves for Mg-Fe-Mn olivines from vibrational spectra. Am. Min., 57, 967-985, 1972.

Dachille, F. and R. Roy. High pressure studies of the system Mg_2GeO_4 with special reference to the olivine-spinel transition. Am. J. Sci., 258, 225-246, 1960.

Datta, R. K. and R. Roy. Equilibrium order-disorder in spinels. J. Am. Ceram. Soc., 50, 578-583, 1967.

Duke, D. A. and J. D. Stephens. Infrared investigation of the olivine group minerals. Am. Min., 49, 1388-1406, 1964.

Durif-Varambon, A., E. F. Bertaut and R. Pauthenet. Etude des germanates spinelles. Ann. de Chim., 1, 525-543, 1956.

Finger, L. W., R. M. Hazen and T. Yagi. Crystal structures and electron densities of nickel and iron silicate spinels at elevated temperature or pressure. Am. Min., (in press, 1979).

Hanke, K. Beitrage zu Kristallstrukturen vom Olivin-Typ., Beitr. Mineral, u. Petrog., 11, 535-558, 1965.

Hazen, R. M. Effects of temperature and pressure on the crystal structure of forsterite, Am. Min., 61, 1280-1293, 1976.

Hohler, V. and E. Funck. Schwingungsspektren von Kristallen mit Olivin-Struktur. Z. Naturforsch., 28b, 125-139, 1973.

Ito, E., Y. Matsui, K. Suito and N. Kawai. Synthesis of γ-Mg_2SiO_4. Phys. Earth Planet Int., 8, 342-344, 1974.

Jackson, I. N. S., R. C. Liebermann and A. E. Ringwood. Disproportionation of spinels to mixed oxides: significance of cation configuration and implications for the mantle. Earth Planet. Sci. Lett., 24, 203-208.

Jeanloz, R. Ringwoodite: complex aggregate misidentified as a high-pressure spinel structure, Lunar Planet. Sci. X, 619-621, 1979a.

Jeanloz, R. Shock effects of olivine and implications for Hugoniot data, 1979b.

Kamb, B. Structural basis of the olivine-spinel stability relation. Am. Min., 53, 1439-1455, 1968.

Lager, G. A. and E. P. Meagher. High-temperature structural study of six olivines. Am. Min., 63, 365-377, 1978.

Lazarev, A. N. Vibrational Spectra and Structure of Silicates, Consultants Bureau, New York, 302 pp., 1972.

Liebermann, R. C., I. Jackson and A. E. Ringwood. Elasticity and phase equilibria of spinel disproportionation reactions. Geophys. J. R. astr. Soc., 50, 553-586, 1977.

Ma, C.-B. Structure refinement of high-pressure Ni_2SiO_4 spinel, Z. Kristallog., 141, 126-137, 1975.

Marumo, F., M. Isobe and S. Akimoto: Electron-density distributions in crystals of γ-Fe_2SiO_4 and γ-Co_2SiO_4, Acta Cryst., B33, 713-716, 1977.

Marumo, F., M. Isobe, Y. Saito, T. Yagi and S. Akimoto. Electron-density distribution in crystals of γ-Ni_2SiO_4, Acta Cryst., B30, 1904-1906, 1974.

Moore, P. B. and J. V. Smith. High pressure modification of Mg_2SiO_4: crystal structure and crystallochemical and geophysical implications. Nature, 221, 653-655, 1969.

Morimoto, N., S. Akimoto, K. Koto and M. Tokonami: Modified spinel, beta-manganous orthogermanate: stability and crystal structure. Science, 165, 586-588, 1969.

Morimoto, N., M. Tokonami, M. Watanabe and K. Koto. Crystal structures of three polymorphs of Co_2SiO_4. Am. Min., 59, 475-485, 1974.

Navrotsky, A. Calculation of effect of cation disorder on silicate spinel phase boundaries. Earth Planet. Sci. Lett., 33, 437-442, 1977.

Navrotsky, A. and L. Hughes, Jr. Thermodynamic relations among olivine, spinel and phenacite structures in silicates and germanates. V. J. Solid State Chem., 16, 185-188, 1976.

Navrotsky, A. and O. J. Kleppa. The thermodynamics of cation distributions in simple spinels. J. Inorg. Nucl. Chem., 29, 2701-2714, 1967.

Navrotsky, A., F. Pintchovsky and S. Akimoto. Calorimetric study of the stability of high pressure phases in the systems $CoO-SiO_2$ and "FeO"-SiO_2 and calculation of phase diagrams in $MO-SiO_2$ systems. Phys. Earth Planet. Int. (in press), 1979.

Paques-Ledent, M. Th. and P. Tarte. Vibrational studies of olivine-type compounds-I. Spectrochim. Acta, 29A, 1007-1016, 1973.

Plyler, E. K., A. Danti, L. R. Blaine and E. D. Tidwell. Vibration-rotation structure in absorption bands for the calibration of spectrometers from 2 to 16 microns. J. Res. Nat. Bur. Stds. (U.S.), 64, 29-48, 1960.

Preudhomme, J. and P. Tarte. Infrared studies of spinels-I. Spectrochim. Acta, 27A, 961-968, 1971a.

Preudhomme, J. and P. Tarte. Infrared studies of spinels-II. Spectrochim. Acta, 27A, 845-851, 1971b.

Preudhomme, J. and P. Tarte. Infrared studies of spinels-III. Spectrochim. Acta, 27A, 1817-1835, 1971c.

Preudhomme, J. and P. Tarte. Infrared studies of spinels-IV. Spectrochim. Acta, 28A, 69-79, 1972.

Ringwood, A. E. Composition and Petrology of the Earth's Mantle, McGraw-Hill, New York, 618 pp.

Shankland, T. J. Synthetic forsterite. Bull. Am. Ceram. Soc., 46, 1160-1162, 1967.

Smyth, J. R. High Temperature crystal chemistry of fayalite. Am. Min., 60, 1092-1097, 1975.

Takei, H. Czochralski growth of Mn_2SiO_4 (tephroite) single crystal and its properties, J. Cryst. Growth, 34, 125-131, 1976.

Tarte, P. Étude infra-rouge des orthosilicates et des orthogermanates. Spectrochim. Acta, 18, 467-483, 1962.

Tarte, P. Étude infra-rouge des orthosilicates et des orthogermanates-II. Spectrochim. Acta, 19, 25-47, 1963a.

Tarte, P. Étude infra-rouge des orthosilicates et des orthogermanates-III. Spectrochim. Acta,19, 49-71, 1963b.

Tarte, P. Infra-red spectrum and tetrahedral coordination of lithium in the spinel $LiCrGeO_4$. Acta Cryst., 16, 228, 1963c.

Tarte, P. Étude éxperimentale et interpfetation du spectre infra-rouge des silicates et des germanates. Mem. Acad. Roy. Belgique, 35, (4a,b), 260 + 134 pp., 1965.

Tarte, P., M. J. Pottier and A. M. Procès. Vibrational studies of silicates and germanates-V. Spectrochim. Acta, 29A, 1017-1027, 1973.

Tarte, P. and J. Preudhomme. Infra-red spectrum and cation distribution in spinels. Acta. Cryst., 16, 227, 1963.

Tarte, P. and A. E. Ringwood. Infra-red spectrum of the spinels Ni_2SiO_4, Ni_2GeO_4 and their solid solutions. Nature, 193, 971-972, 1962.

Tarte, P. and A. E. Ringwood. Infra-red spectrum and germanium co-ordination in some high-pressure meta-germanates. Nature, 201, 819, 1964.

Tokonami, M., N. Morimoto, S. Akimoto, Y. Syono and H. Takeda. Stability relations between olivine, spinel and modified spinel. Earth Planet. Sci. Lett., 14, 65-69, 1972.

Von Dreele, R. B., A. Navrotsky and A. L. Bowman. Refinement of the crystal structure of Mg_2GeO_4 spinel. Acta Cryst., B33, 2287-2288, 1977.

Wenk, H.-R. and K. N. Raymond. Four new structure refinements of olivine. Z. Kristallogr., 137, 86-105, 1973.

White, W. B. and B. A. DeAngelis. Interpretation of the vibrational spectra of spinels. Spectrochim. Acta, 23A, 985-995, 1967.

White, W. B. and R. Roy. Infrared spectra-crystal structure correlations: II. Am. Min., 49, 1670-1687, 1969.

Yagi, T., F. Marumo and S. Akimoto. Crystal structures of spinel polymorphs of Fe_2SiO_4 and Ni_2SiO_4. Am. Min., 59, 486-490, 1974.

Table 1

SAMPLE CHARACTERISTICS

Sample	Identification Number	Amount Used (per 200 mg KBr)	Synthesis[1]	Source, Reference
Olivine				
α-Mg_2SiO_4	72472	3.15 mg		Shankland (1967)
α-Fe_2SiO_4	32877	2.08 mg		Takei (1976)
α-Ni_2SiO_4	50374 (JI#5)	2.03 mg	1200-750°C, 1°C/hr.cooling; Na_2WO_4 flux[2]	J. Ito
α-Co_2SiO_4	41078 (JI#2)	1.98 mg	1250-600°C, 1°C/hr.cooling; Na_2WO_4 flux[2]	J. Ito
α-Mg_2GeO_4	DL50967	2.34 mg	1350°C	D. Lindsley
β-Phase				
β-Co_2SiO_4[3]	90578	1.50 mg	1150°C, 7.5 GPa	S. Akimoto
Spinel				
γ-Fe_2SiO_4[3]	71775	1.89 mg	900°C, 7.2 GPa	S. Akimoto
γ-Ni_2SiO_4[3]	61277	1.39 mg	1400°C, 5.5 GPa	S. Akimoto
γ-Co_2SiO_4[3]	61377	3.06 mg	850°C, 6.8 GPa	S. Akimoto
γ-Mg_2GeO_4	Sample A 2379, 2	2.50 mg	730°C, 0.2 GPa 24 hr.	I. Jackson
γ-Mg_2GeO_4	Sample B 2379, 1	3.99 mg	1000°C, 1.5 GPa 2 hr.	I. Jackson

Notes

(1) Zero pressure, unless otherwise states.
(2) Possible contaminant.
(3) Macroscopic organic contaminents present in original material.

Table 2

INFRARED PEAKS: A_2XO_4 OLIVINE (α)

(units: cm^{-1})

	α - Mg_2SiO_4	α - Fe_2SiO_4	α - Ni_2SiO_4	α - Co_2SiO_4	α - Mg_2GeO_4
	1003 (sh)			979 ± (sh)	
ν_3 (XO_4)	985 ± 1	944 ± 1	966 ± 3	948 ± 3	816 ± 2
	957 ± 1	916 ± 3 (sh)	921 (sh)	920 (sh)	775 ± 2
	925 (sh)		900 (sh)		
ν_3 (XO_4)	884 ± 1	870 ± 1	870 ± 1	865 ± 2	721 ± 1
ν_1 (XO_4)	839 ± 1	828 ± 1	826 ± 1	825 ± 1	698 (sh)
ν_4 (XO_4)	609 ± 1	559 ± 1	576 ± 1	565 ± 1	505 ± 2
	547 (sh)		528 ± 5 (sh)		
$\nu_2+\nu_4$ (XO_4)	527 ± 2	508 ± 1	514 ± 1 (sh)	515 ± 3 (sh)	476 ± 2
	507 ± 1	475 ± 2	491 ± 1	481 ± 1	456 ± 1
(AO_6)	475 ± 1 420 ± 2	363 ± 2	389 ± 2	372 ± 1	400 ± 2
	403 ± 1			343 (sh)	
(AO_6)	361 ± 1	308 ± 1	339 ± 1	307 ± 2	355 (sh)
			315 ± 1		282 ± 2
(AO_6)	295 ± 1	253 (sh)	283 ± 1	273 (sh)	266 ± 1

sh: shoulder

Table 3

INFRARED PEAKS: A_2XO_4 SPINEL (γ) AND β-PHASE

(units: cm^{-1})

	γ-Fe_2SiO_4	γ-Ni_2SiO_4	γ-Co_2SiO_4	γ-Mg_2GeO_4 (A)	γ-Mg_2GeO_4 (B)		β-Co_2SiO_4
	1063 (sh)		1058 (sh)				960 (sh)
	965 (sh)		970 (sh)			(XO_3, st.)	910 ± 2
	908 (sh)	908 (sh)	893 (sh)				
ν_3 (XO_4)	848±1	824±2	825±1	690±2	687±2	(X_2O_7,AS)	801 ± 1
			778 (sh)		650±2*	(X_2O_7,S)	686 ± 2
	568 (sh)	626 (sh)	631 (sh)			(XO_3,b)	557 ± 1
					500 (sh)		545
ν_4 (XO_4)	503±1	515±1	503±1	484±1	484±1		503 (sh)
		404 (sh)	392 (sh)			(XO_3,b)	473 ± 2
(AO_6)	344±2	376±1	357±1	447±3	435±2		438
			310 (sh)		362±3*		343 ± 2
(AO_6)				271±1	271±1	AO_6	283

sh: shoulder

*Extra peaks (see text)

st: stretch
b: bend
s: symmetric
As: Antisymmetric

Figure Captions

Figure 1. Infrared spectrum of Mg_2SiO_4, olivine (note scale).

Figure 2. Infrared spectra of olivine (α) and spinel (γ) phases of Fe_2SiO_4.

Figure 3. Infrared spectra of olivine (α) and spinel (γ) phases of Ni_2SiO_4.

Figure 4. Infrared spectra of olivine (α), spinel (γ) and β phases of Co_2SiO_4 (note scale in bottom Figure).

Figure 5. Infrared spectra of olivine (α) and spinel (γ; sample A) phases of Mg_2GeO_4.

Figure 6. Infrared spectrum of γ-Mg_2GeO_4 sample B, exhibiting anomalous new peaks in spinel pattern.

Figure 7. Summary of the main features in the infrared spectra of silicate and germanate olivine, spinel and β phases. Date of Preudhomme and Tarte (1972) for Co-, Ni- and Fe-germanate spinels are included. Open squares show the positions of the extra peaks in the spectrum of γ-Mg_2GeO_4 sample B. The peak positions for γ-Mg_2SiO_4 have been inferred from the correlations which are described in the text.

Figure 8. Position of octahedral modes of silicate and germanate spinels as a function of the force constant function of Equations 1 and 2. The bracketed point indicates the peak of γ-Mg_2GeO_4 assigned to AO_6 by Tarte; the arrow on the bracket points to the present interpretation. The value of the force constant function expected for γ-Mg_2SiO_4 is shown: its AO_6 peak location is predicted to be near the tip of this arrow.

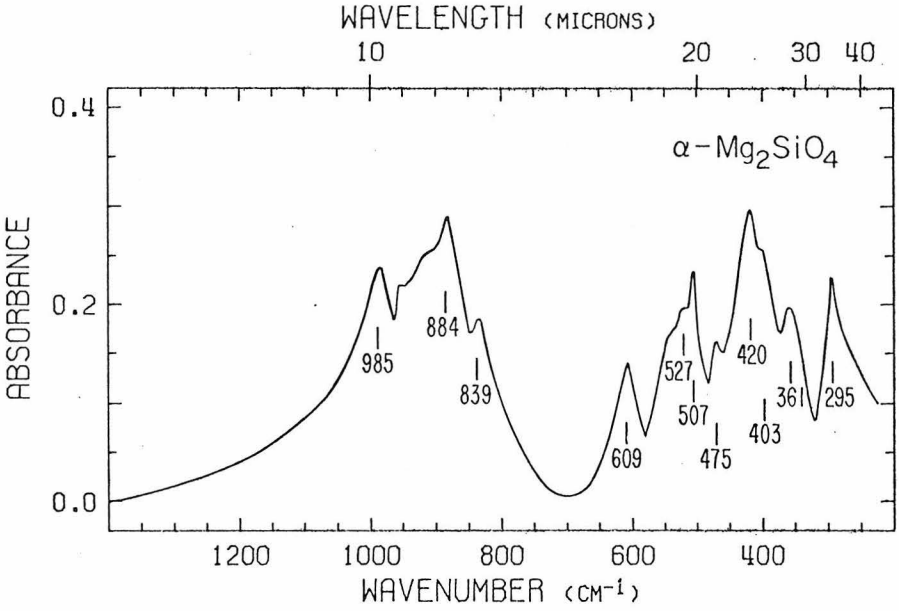
WAVELENGTH (MICRONS)
10
20
30
40
0.4
0.2
0.0
ABSORBANCE
α-Mg2SiO4
985
884
839
609
527
507
475
420
403
361
295
1200
1000
800
600
400
WAVENUMBER (CM-1)

Figure 1

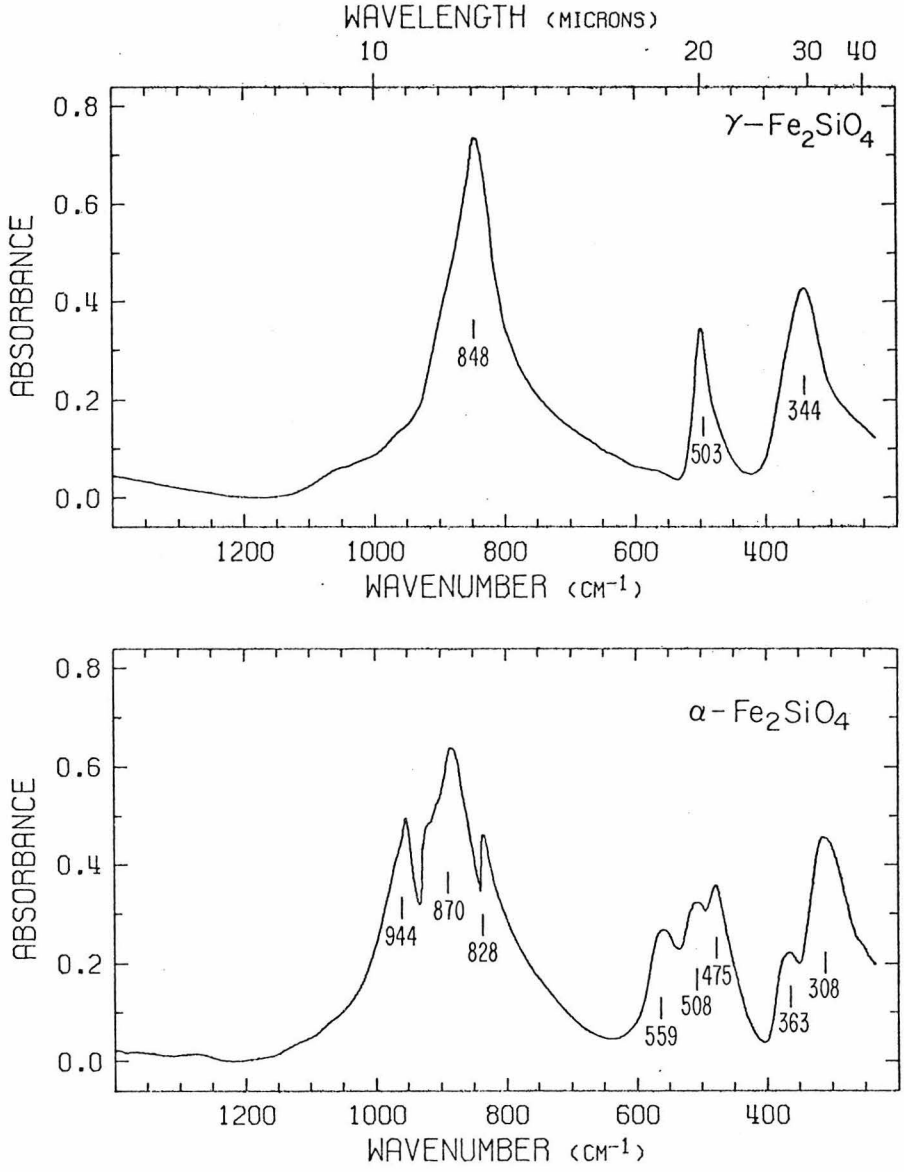
WAVELENGTH (MICRONS)
10
20
30
40
0.8
0.6
0.4
0.2
0.0
ABSORBANCE
γ-Fe2SiO4
848
503
344
1200
1000
800
600
400
WAVENUMBER (cm-1)
α-Fe2SiO4
944
870
828
559
508
475
363
308

Figure 2

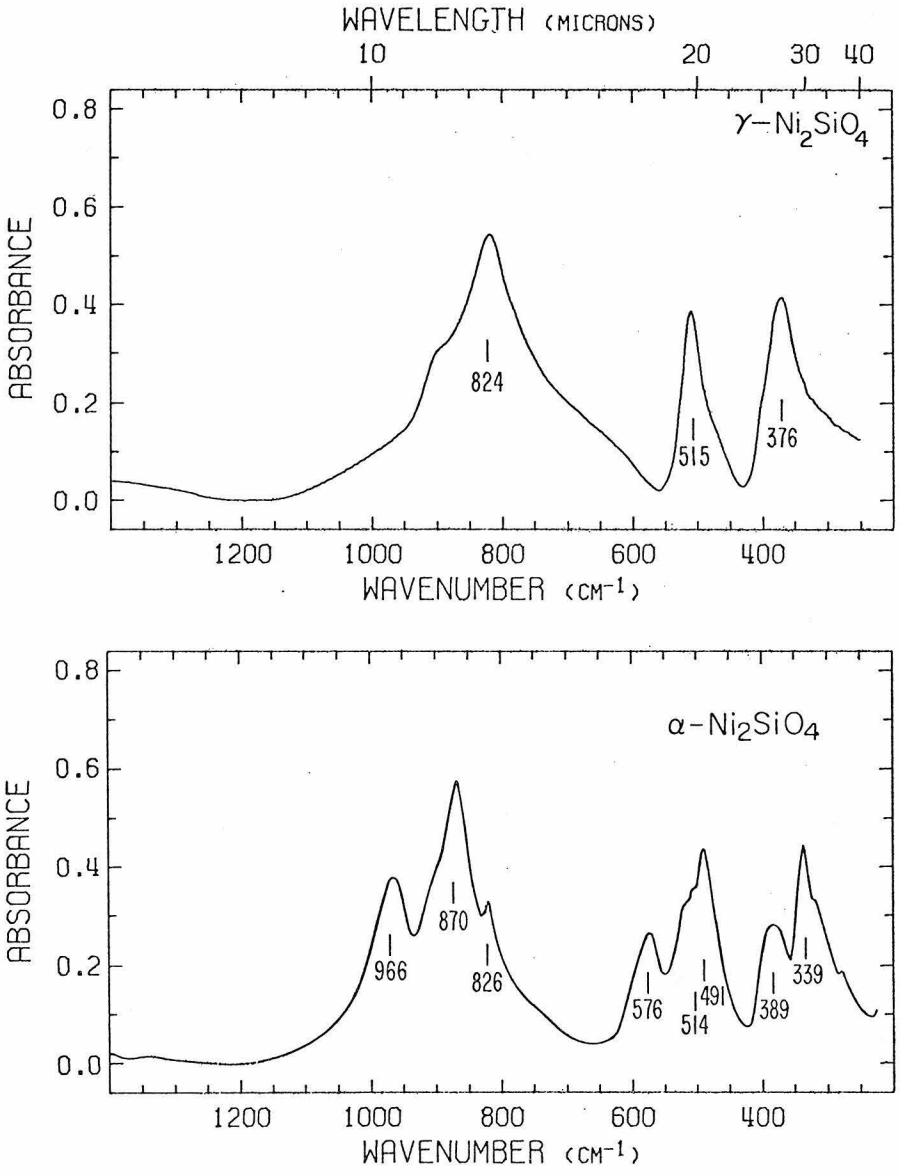
WAVELENGTH (MICRONS)
10
20
30
40
γ-Ni2SiO4
ABSORBANCE
0.8
0.6
0.4
0.2
0.0
824
515
376
1200
1000
800
600
400
WAVENUMBER (cm-1)
α-Ni2SiO4
966
870
826
576
514
491
389
339

Figure 3

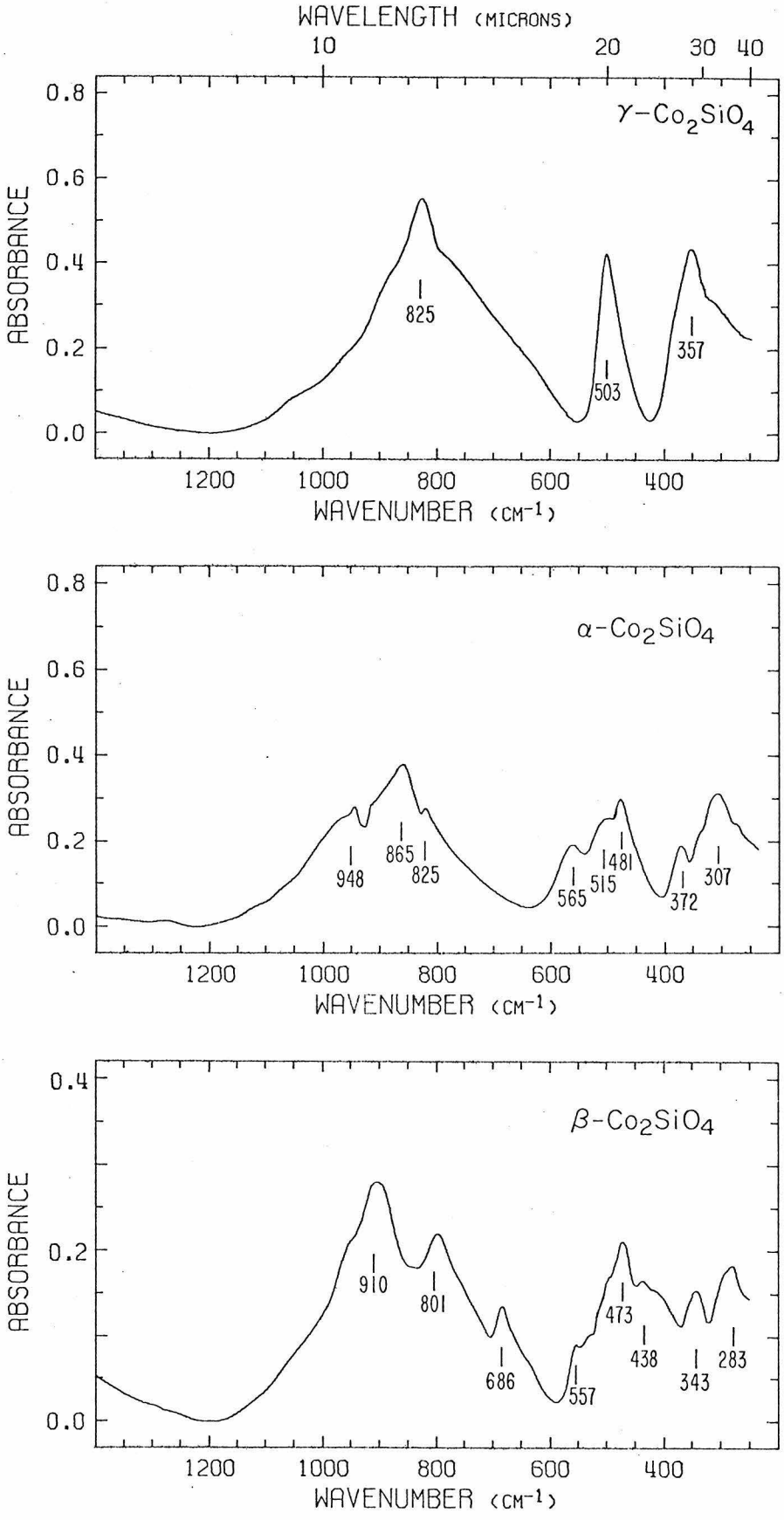
WAVELENGTH (MICRONS)
10
20
30
40
γ-Co2SiO4
ABSORBANCE
0.8
0.6
0.4
0.2
0.0
825
503
357
1200
1000
800
600
400
WAVENUMBER (CM-1)
α-Co2SiO4
948
865
825
565
515
481
372
307
β-Co2SiO4
910
801
686
557
473
438
343
283

Figure 4

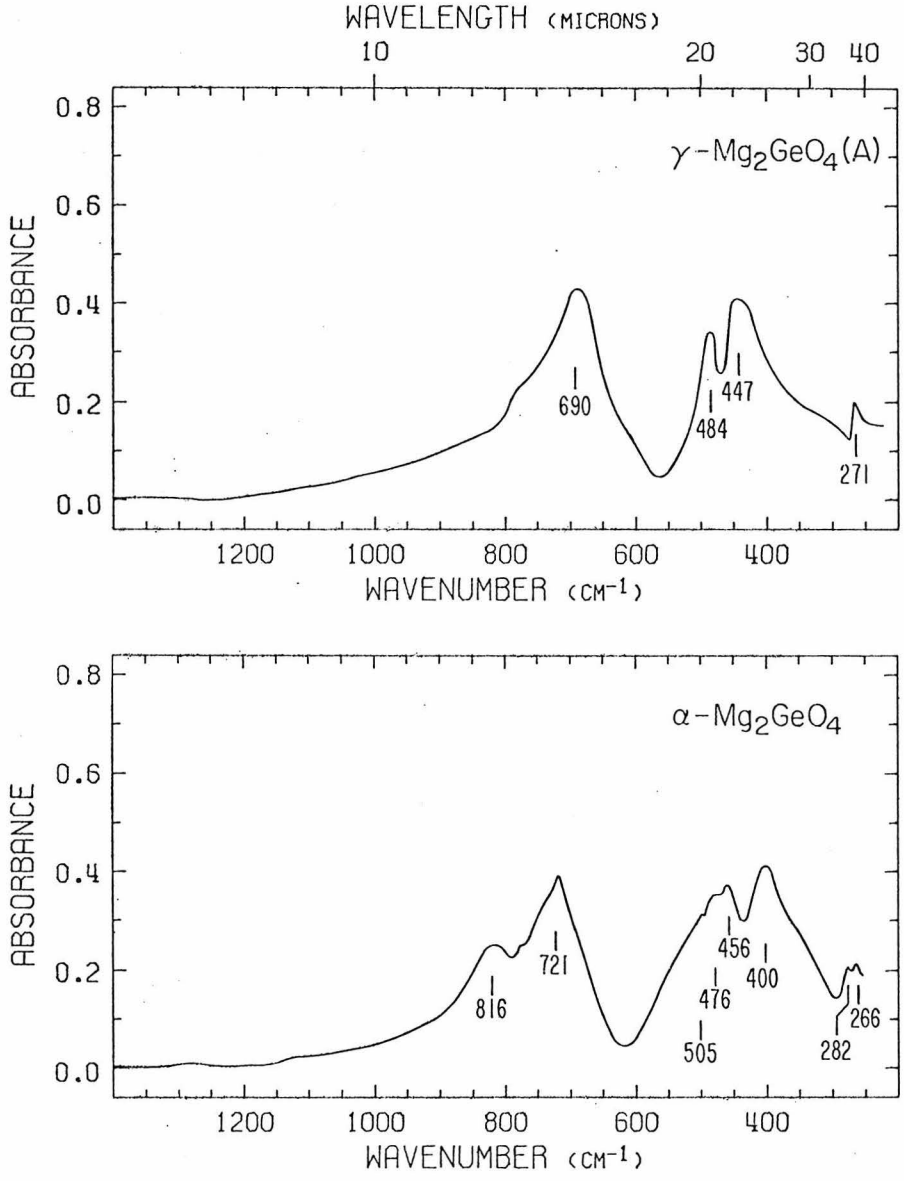
WAVELENGTH (MICRONS)
10
20
30
40
0.8
0.6
0.4
0.2
0.0
ABSORBANCE
γ-Mg2GeO4(A)
690
484
447
271
1200
1000
800
600
400
WAVENUMBER (cm-1)
α-Mg2GeO4
816
721
476
505
456
400
282
266

Figure 5

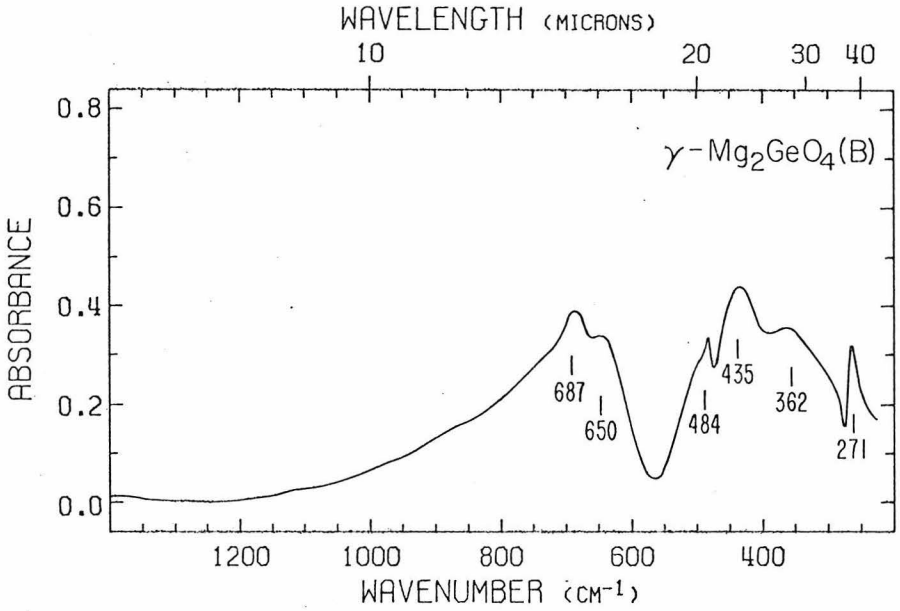
WAVELENGTH (MICRONS)
10
20
30
40
0.8
0.6
0.4
0.2
0.0
ABSORBANCE
γ-Mg2GeO4(B)
687
650
484
435
362
271
1200
1000
800
600
400
WAVENUMBER (cm-1)

Figure 6

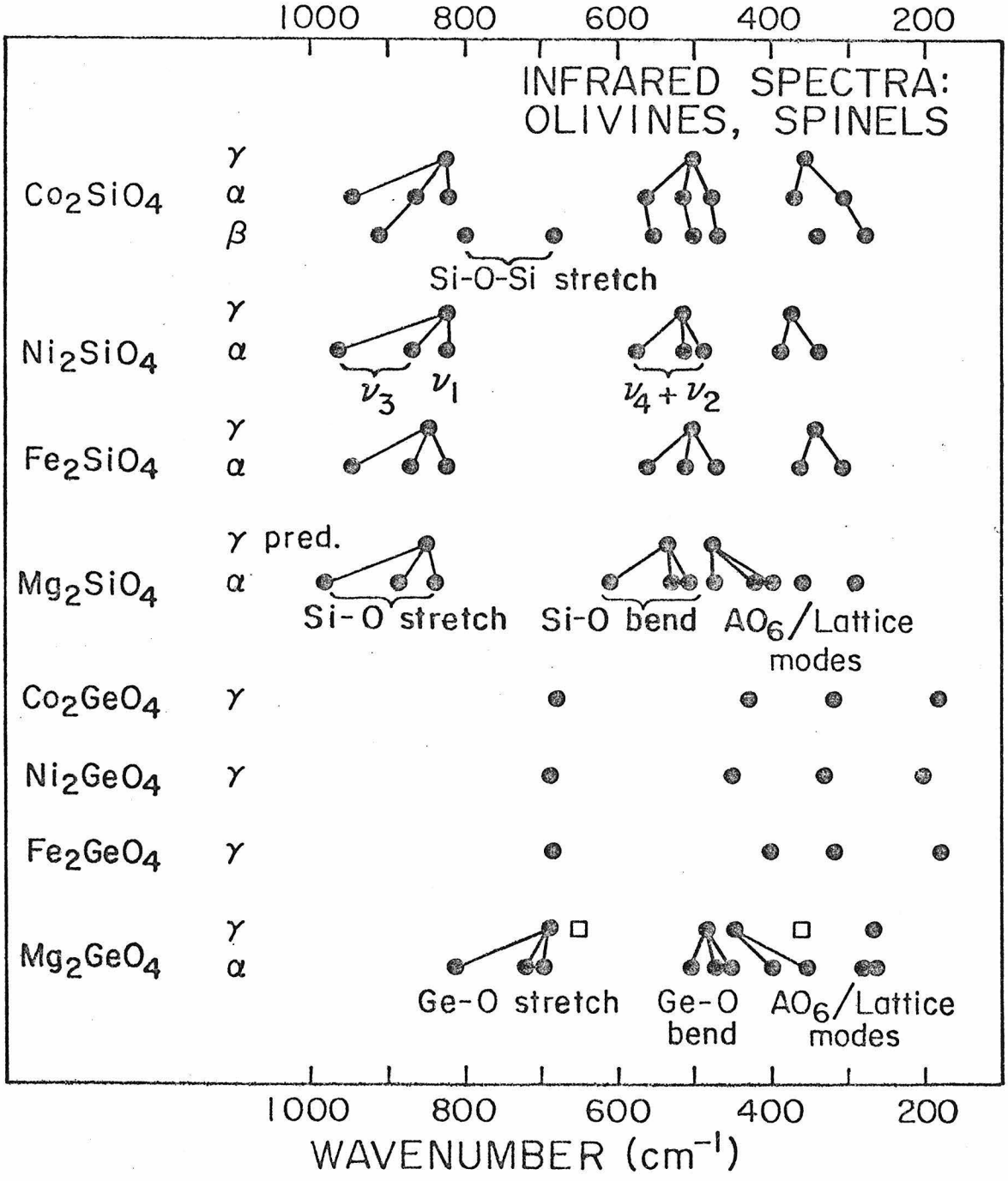
1000
800
600
400
200
INFRARED SPECTRA:
OLIVINES, SPINELS
Co_2SiO_4
γ
α
β
Si-O-Si stretch
Ni_2SiO_4
γ
α
ν_3
ν_1
$\nu_4 + \nu_2$
Fe_2SiO_4
γ
α
Mg_2SiO_4
γ pred.
α
Si-O stretch
Si-O bend
AO_6/Lattice modes
Co_2GeO_4
γ
Ni_2GeO_4
γ
Fe_2GeO_4
γ
Mg_2GeO_4
γ
α
Ge-O stretch
Ge-O bend
AO_6/Lattice modes
1000
800
600
400
200
WAVENUMBER (cm^{-1})

Fig. 7

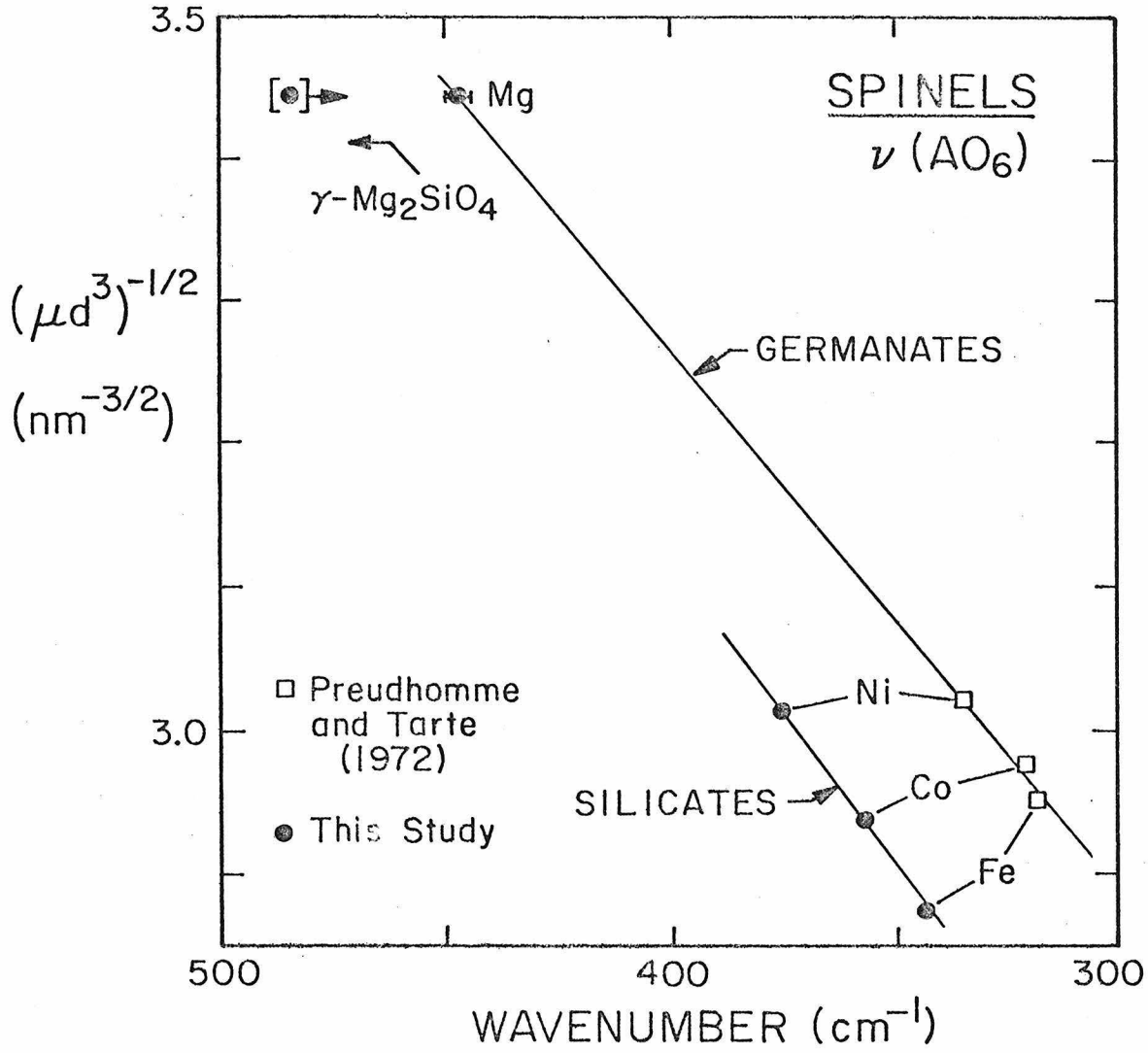
3.5
3.0
$(\mu d^3)^{-1/2}$
$(nm^{-3/2})$
[●]
Mg
γ-Mg_2SiO_4
SPINELS
ν (AO_6)
GERMANATES
SILICATES
Ni
Co
Fe
□ Preudhomme and Tarte (1972)
● This Study
500
400
300
WAVENUMBER (cm^{-1})

Figure 8

Chapter 9

SHOCK-PRODUCED OLIVINE GLASS: FIRST OBSERVATION

Abstract

Transmission electron microscope (TEM) observations of an experimentally shock-deformed single crystal of natural peridot $(Mg_{0.88}Fe_{0.12})_2SiO_4$ recovered from peak pressures of about 56 GPa revealed the presence of amorphous zones located within crystalline regions with a high density of tangled dislocations. This is the first reported observation of olivine glass. The shocked sample exhibits a wide variation in the degree of shock-deformation on a small scale, and the glass appears to be intimately associated with the highest density of dislocations. This study suggests that olivine glass may be formed as a result of shock at pressures above about 50 to 55 GPa and that further TEM observations of naturally shocked olivines may demonstrate the presence of glass.

We know of no case in which olivine liquid (Mg_2SiO_4 to Fe_2SiO_4 in composition) has been quenched to a glass. Numerous studies of the liquidus of olivine (Davis and England, 1964; Lindsley, 1965; Akimoto et al., 1967) and corresponding compositions in analogs of the system (Mg,Fe)O-SiO_2 (for example, LiF-BeF_2, Roy et al., 1954) have never resulted in the unequivocal quench of such a glass. Furthermore, attempts to produce olivine glass by means of rapid fusion and quench techniques have also been unsuccessful (Blander et al., 1976). Similarly, the presence of olivine glass has never been unambiguously demonstrated in the extensive studies of naturally and (a few) experimentally shocked olivines (Christie and Ardell, 1976; Lally et al., 1968; Carter et al. 1968; Stöffler, 1972), although it is known that most silicates that have been studied become amorphous when subjected to shock of high enough intensity (Stöffler, 1972).

We report the first observation of olivine glass and its synthesis by means of shock. A disk cut from a crystal of San Carlos, Arizona peridot $(Mg_{0.88}Fe_{0.12})_2SiO_4$ was shocked along [010] (propagation direction of the shock wave).[1] A peak pressure of 56 GPa (560 kbar) was achieved by the "multiple-reverbertation" technique for a period

---

[1]A polished disk 4.67 mm in diameter, 295 μm thick and oriented parallel to [010] was prepared from the olivine crystal (composition determined by microprobe analysis). Examination of the sample by optical microscopy before the experiment revealed no inclusions or heterogeneities other than sub-boundaries, in agreement with the observations of Kirby and Wegner (1973) and Wegner and Christie (1971) on olivine from the same locality. The disk was encased in a stainless steel container which included "momentum trap" plates (Doran and Linde, 1966) and the container was impacted with a 16-mm tungsten flyer-plate launched from a high-performance propellant gun.

of approximately 0.5 μsec[2].

Transmission electron microscope (TEM) observations[3] on ion-thinned slices of the shocked olivine revealed patchy, nondiffracting zones of no contrast within crystalline and diffracting sample material (Figure 1, a and c). The lack of diffraction contrast implies that the zones consist of material lacking crystalline order down to a scale of several nanometers. These zones grade into the surrounding crystalline olivine, and diffracting fragments within the amorphous material indicate remnants of crystalline material. There is not evidence for phase separation or other heterogeneities within the glass. Marked, spotty asterism in the diffraction pattern indicates misorientation of fragments and bending of the olivine (Figure 1d). Although the amorphous zones attain maximum dimensions of 10 μm and more (representing approximately 1 to 2 percent of the sample by volume), they were not evident during optical microscopic examination carried out on the shocked olivine prior to the TEM analysis.

Regions of low dislocation density (Figure 1b) as well as the high-density tangles (Figure 1, a and c), can be found in the shocked sample, an indication of wide variations in shock induced deformation on an

---

[2]We calculated the peak pressure, using standard impedance match techniques for multiple shock reverberations (Walsh and Christian, 1955; Al'tshuler, 1965; Gibbons and Ahrens, 1971) based on the Hugoniot equation of state data (McQueen et al., 1970) for tungsten and stainless steel, and it is accurate to within about 5 percent. The time at peak pressure is based on a calculation of the type given by Fowles (1960) and by Al'tshuler (1965).

[3]Carried out with the 1-Mev electron microscope at the U. S. Steel Research Laboratory, Monroeville, Pa., and at 200 kv at the U. S. Geological Survey, Reston, Va.

extremely small scale. Significantly, the glassy zones are located within the regions of highest dislocation density. This result may indicate that a threshold stress for the production of diaplectic glass exists, which was only achieved locally in the present experiments.

Estimates of the average temperature of the sample at peak pressure are between 740 and 1000 K, based on the equation-of-state properties of the sample container (McQueen et al., 1970)[4] and a model presented in Ahrens et al. (1976). [5] The temperature attained immediately upon the release of pressure is poorly constrained as a result of its strong dependence on the details of the irreversible thermodynamic path followed by the sample on compression and decompression (Ahrens and O'Keefe, 1973; Waldbaum, 1971). Nevertheless, a temperature well below the melting point of olivine (above 2000 K at 1 atm and presumably much higher at 56 GPa; Davis and England, 1964; Akimoto and Komada, 1967; Bowen and Schairer, 1935) is indicated at peak pressure and probably on pressure release (Ahrens et al., 1976; Ahrens and O'Keefe, 1973).

These results suggest that the shocked olivine contains diaplectic glass (glass apparently formed in the solid state by shock; Stöffler, 1972)[6]. The fact that the glassy zones are associated with the regions of the sample showing the highest amount of crystalline deformation

---

[4]We made the simplifying assumption that the temperature in the sample which has attained peak pressure by multiple reverberations is approximately the same as the temperature of the container achieved by a single shock to peak pressures.

[5]This is a maximum estimate since it is for the attainment of peak pressure by a single shock (see Al'tshuler, 1965).

[6]Note that thetomorphic and diaplectic are equivalent terms.

suggests that they possibly represent portions of the sample quenched from material which at one point was in a high pressure phase or phases. Although no microtextural evidence for the formation of any high-pressure phases was seen in the TEM studies, Hugoniot equation-of-state data for olivine indicate partial transformation to one or more high-density phases at 56 GPa (transformation is apparently initiated at pressures in excess of about 26 GPa (Ahrens et al., 1976)[7]. Intense strain would be expected in areas surrounding zones of high-pressure phases as a result of the volume changes associated with transformation. The observed glass might then represent the olivine which has re-transformed from the high-pressure phase or phases upon (or during) release, forming a metastable glass rather than crystalline olivine. Such a process has been documented for SiO_2 (Skinner and Fahey, 1963) and has even been found in static, high-pressure experiments[8] (Liu and Ringwood, 1975; Ringwood and Major, 1971). It is also possible that the phases formed in the olivine under shock compression lack long-range order and that the diaplectic glass may effectively have formed at high pressure, modified only by release to ambient conditions. In this regard, it is possible that olivine glass

---

[7]The Hugoniot data are consistent with results from static, high-pressure experiments (Liu, 1975a, b) which indicate major, reconstructive transformations at these pressures in magnesian olivine, for example, to (Mg, Fe)SiO_3 perovskite + (Mg,Fe)O rock salt phases (see Jeanloz and Ahrens, 1977). Direct evidence for similar major, reconstructive transformations and reactions in nesosilicates under shock can be found in Liu (1975c), Ahrens and Graham (1972), and Schneider and Hornemann (1975).

[8]In these experiments, $CaSiO_3$ perovskite formed (and identified) at high pressure could only be quenched to a glass.

may be more stable than a highly dislocated crystal. For dislocation densities like those in the tangles (Figure 1, a and c), the crystalline material might have a higher free energy than the glass, thus favoring spontaneous conversion to glass[9].

Alternatively, in the above calculations it is assumed that the thermal energy is uniformly distributed throughout the sample on compression and decompression (accounting for phase transformation). However, it has been argued (Grady, 1977; Grady et al., 1975) that yielding under shock is inherently inhomogeneous, leading to zones of high strain surrounding relatively unstrained material. As a result thermal energy would be localized along "adiabatic shear bands" and the final shock deformation should be highly heterogeneous, as observed in the shocked olivine sample. Such heterogeneous deformation could originate from the interaction of the shock and release waves with heterogeneities (such as sub-boundaries) in the original sample. If shear bands exist as postulated, they could generate high temperatures locally, allowing rapid, solid-state phase transformation or melting (Grady, 1977; Grady et al., 1975; Grady and Murri, 1976). In either case, (transformation to either a solid or liquid) it is easy to understand

---

[9]The free energy of a crystal is increased by an amount on the order of $1/2\ \mu b^3$ per atomic length of dislocation (where μ is the shear modulus and b is the average length of the Burgers vectors of the dislocations). Taking the dislocation density to be about 10^{12} cm^{-2} or more in the tangles, $b \sim 5$ Å, $\mu = 80$ GPa and assuming that a typical difference in free energy between silicate crystals and their glasses is about 5 kilojoules per mole, it is possible for the glass to have a lower free energy than the dislocated crystal. (See also Cotterill et al., 1975).

how glass could be formed in conjunction with heterogeneous yielding under shock.

Finally, the results presented here suggest that further TEM observations should yield some olivine glass in naturally shocked samples if peak pressures were sufficiently elevated and postshock recovery sufficiently minor. On the basis of the present study, it appears that glass forms incipiently in olivine shocked to about 50 to 55 GPa.

Addendum: Recent TEM observations have revealed traces of glass in a sample cut from the same olivine crystal and shocked to 54 GPa in a separate experiment. We also wish to note Cotterill's suggestion that there may be a "natural" upper limit to dislocation densities (Cotterill, 1977). Applying his calculations to olivine yields an estimate (probably a lower bound) on the order of 10^{13} cm^{-2} for the limiting, dynamic dislocation density.

Acknowledgments

We are grateful for discussions with I. Jackson and L. Liu and for reviews from A. Albee and D. Grady, all of which were very helpful.

REFERENCES

Ahrens, T. J., and E. K. Graham, Earth Planet. Sci. Lett., 26, 425, 1975.

Ahrens, T. J., J. H. Lower, P. L. Lagus, J. Geophys. Res., 76, 518, 1971.

Ahrens, T. J., and J. D. O'Keefe, Moon, 4, 214, 1973.

Ahrens, T. J. and C. F. Petersen, in The Application of Modern Physics to the Earth and Planetary Interiors, S. K. Runcorn (ed.), Wiley-Interscience, New York, 449, 1969.

Ahrens, T. J., F. D. Tsay, D. H. Live, Geochim. Cosmochim. Acta., (Suppl. 7), 1143, 1976.

Akimoto, S., I. Kushiro, and E. Komada, J. Geophys. Res., 72, 679, 1967.

Al'tshuler, L. V., Sov. Phys. Usp., 8, 59, 1965.

Blander, M., H. N. Planner, K. Keil, L. S. Nelson, and N. L. Richardson, Geochim. Cosmochim. Acta., 40, 889, 1976.

Bowen, N. L. and J. F. Schairer, Am. J. Sci., 29, 161, 1935.

Carter, N. L., C. B. Raleigh, P. S. DeCarli, J. Geophys. Res., 73, 5439, 1968.

Chao, E. C. T., in Researches in Geochemistry, P. Abelson (ed.), Wiley, New York, Vol. 2, 204, 1967.

Christie, J. M. and A. J. Ardell, in Electron Microscopy in Mineralogy, H. R. Wenk et al., (eds.) Springer-Verlag, Berlin, 374, 1976.

Cotterill, R. M. J., Phys. Lett., 60A, 61, 1977.

Cotterill, R. M. J., E. J. Jensen, W. Damgaard Kristensen and R. Paetsch, J. Phys. [Paris], 36, C2, 1975.

Davis, B. T. C. and J. L. England, J. Geophys. Res., 69, 1113, 1964.

Doran, D. G. and R. K. Linde, Solid State Phys., 19, 262, 1966.

Fowles, G. R., J. Appl. Phys., 31, 655, 1960.

Gibbons, R. V. and T. J.Ahrens, J. Geophys. Res., 76, 5489, 1971.

Grady, D. E., in High Pressure Research: Applications to Geophysics, M. Manghnani and S. Akimoto (eds.), Academic Press, New York, 389, 1977.

Grady, D. E., W. J. Murri, P. S. DeCarli, J.Geophys. Res., 80, 4857, 1975.

Grady, D. E., W. J. Murri, Geophys. Res. Lett., 3, 472, 1976.

Jeanloz, R. and T. J. Ahrens, in High Pressure Research: Applications to Geophysics, M. Manghnani and S. Akimoto (eds.) Academic Press, New York, 439, 1977.

Kirby, S. H. and M. W. Wegner, Trans. Am. Geophys. Un., 54, 452, 1973.

Lally, J. S., J. M. Christie, G. L. Nord., Jr., A. H. Heuer, Geochim. Cosmochim. Acta (Suppl. 7), 1845, 1976.

Lindsley, D. H., Carnegie Inst. Washington Ybook, 65, 227, 1965.

Liu, L. Geophys. Res. Lett., 2, 417, 1975a.

Liu, L., Nature (London) 258, 510, 1975b.

Liu, L., Earth Planet. Sci. Lett., 26, 425, 1975c.

Liu, L., Nature (London), 262, 770, 1976.

Liu, L. and A. E. Ringwood, Earth Planet. Sci. Lett., 28, 209, 1975.

McQueen, R. G., S. P. Marsh, J. W. Taylor, J. N. Fritz, W. J. Carter, in High Velocity Impact Phenomena, R. Kinslow (ed.) Academic Press, New York, 294, 1970.

Ringwood, A. E. and A. Major, Earth Planet. Sci. Lett., 12, 411, 1971.

Roy, D. M., R. Roy and E. F. Osborn, J. Am. Ceram. Soc., 37, 300, 1954.

Schneider, H. and U. Horenmann, Naturwissenschaften, 62, 296, 1975.

Skinner, B. J. and J. J. Fahey, J. Geophys. Res., 68, 5595, 1963.

Stöffler, D., Fortschr. Mineral., 51, 256, 1972.

Waldbaum, D. R., Nature (London) 232, 545, 1971.

Walsh, J. M. and R. H. Christian, Phys. Rev., 97, 1544, 1955.

Wegner, M. W. and J. M. Christie, Contrib. Mineral. Petrol., 43, 195, 1971.

FIGURE CAPTION

Figure 1. (a) Transmission electron microscope (TEM) image (200 kev, bright-field) of shocked olivine showing nondiffracting glassy zone (g) within diffracting and crystalline olivine (light areas) containing a high density of dislocations (presumably [001] screw dislocations; Christie and Ardell, 1976; Lally et al., 1976; Carter et al., 1968; Stoffler, 1972). (b) Bright-field TEM image (1 Mev) of shocked olivine exhibiting dislocation densities almost as low as that found in the starting material (typically 10^6 to 10^7 cm^{-2}). (c) A TEM image (1 Mev, bright-field) of shocked olivine with glassy patches (dark, no contrast) graving into crystalline material containing a high density of dislocations. Scales in (a to 3) are in micrometers. (d) Electron diffraction pattern (1 Mev) of the area in (c).

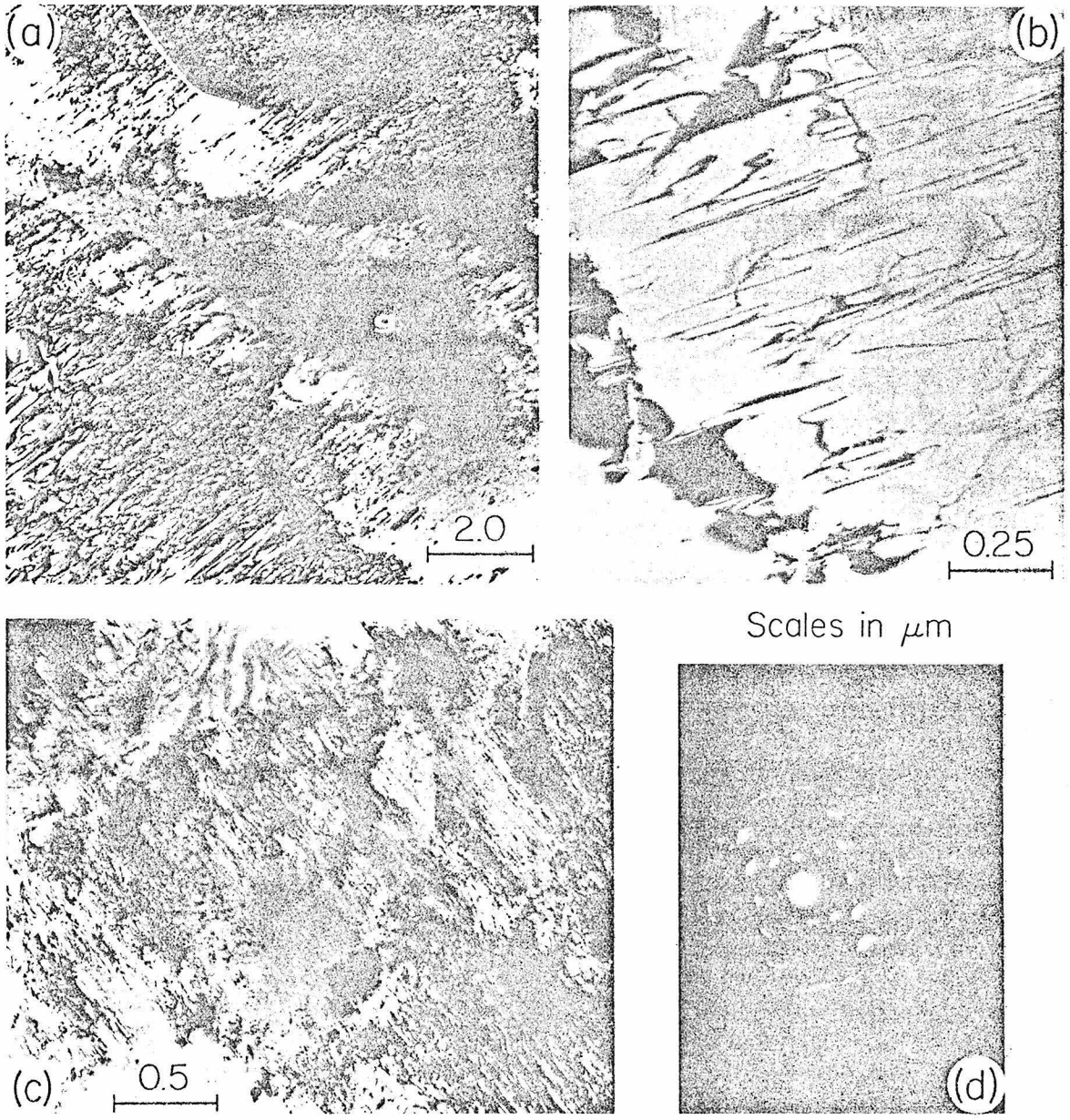
(a)
2.0
(b)
0.25
Scales in μm
(c)
0.5
(d)

Chapter 10

SHOCK EFFECTS IN OLIVINE AND IMPLICATIONS FOR HUGONIOT DATA

Abstract

Deformation produced in single-crystal olivine samples by shock-wave stresses ranging between 18 and 75 GPa are documented by microscopic and spectroscipic techniques. Significantly, no evidence was found for phase transformation throughout the "mixed-phase" region (about 25-40 GPa to 70 GPa), contrary to expectations based on the current interpretations of Hugoniot data. Samples retrieved from peak pressures above 20 GPa exhibit extensive plastic strain as elevated dislocation densities causing a distinctive microundulatory extinction (mosaicism). However shock effects in olivine are relatively minor compared to those typical of other silicates: only traces of diaplectic glass are found at pressures above about 50 GPa and no evidence for melting, recrystallization or extensive recovery is present. Although civilian (reconstructive) phase transformation has been previously inferred from the Hugoniot data on olivine, this textural evidence is inconsistent with such a process. Calculations of transformation rates for olivine similarly indicate that reconstructive phase transformation is highly unlikely under experimental shock conditions and that the Hugoniot data represent highly nonequilibrium states. A new, crystallographically-based model is presented for the behavior of olivine under shock that successfully reproduces the Hugoniot data and that is in accord with all available observations. According to this model, olivine is compressed into a transient, slightly randomized, olivine-like

structure at shock pressures above about 30 GPa and does not undergo a polymorphic transformation or an increase in cation coordination number. Some evidence indicates that many other silicates may behave similarly under shock and also not transform. The results of this study suggest that the current interpretations of shock wave data on silicates and their geophysical applications may need reappraisal.

I. INTRODUCTION

There has been considerable interest in understanding the shock-wave equation-of-state (Hugoniot) data on olivine ($(Mg,Fe)_2 SiO_4$) which extend to pressures spanning those found in the Earth's deep interior. Olivine exhibits a region of normal compression extending to about 30 GPa (0.3 Mbar: low-pressure phase region), which can be described in terms of the measured thermodynamic and compressional properties of olivine. Above about 30-40 GPa, olivine achieves substantially higher densities under shock compression than can be explained by normal compression and hence a transformation of phase is implicated. Beyond this "mixed-phase" region, above about 70 GPa, olivine exhibits the high densities which are characteristic of the Earth's lower mantle [e.g., Birch, 1952; McQueen et al., 1967; Ringwood, 1975]. Therefore, the high-pressure Hugoniot data for olivine have played an important role in deducing the properties of the phases which are believed to make up the lower mantle. This has allowed the interpretation of the seismologically observed properties of the earth's deep interior in terms of chemical composition, petrological characteristics, thermal state and compressional properties [e.g., Birch, 1964; Trunin et al., 1965; McQueen et al., 1967; Wang, 1967, 1968, 1970, 1972; Anderson and Kanamori, 1968; Ahrens, et al., 1969; Ahrens and Petersen, 1969; Anderson and Jordan, 1970; Anderson, et al., 1971; Ahrens, 1971; Ahrens, et al., 1971; Al'tshuler and Sharipdzhanov, 1971 a,b; Davies and Anderson, 1971; Kalinin et al., 1972; Davies and Gaffney, 1973; Davies, 1974; Kalinin and Pan'kov, 1974; Telegin et al., 1974; Ahrens, 1975; Graham, 1975; Ringwood, 1975; Anderson, 1977; Jeanloz and Ahrens, 1977; Jackson and Ahrens, 1979; Somerville, 1979].

Central to all of these applications is the interpretation of the Hugoniot data in terms of polymorphic transformation to high-pressure phases, consistent with the knowledge, from static high-pressure results [e.g., Ringwood, 1975; Liu, 1976a,b, 1977], that olivine undergoes several major, reconstructive (or civilian) phase transformations at pressures less than 30 GPa.

Specifically, polymorphism has been considered necessary to explain the regions of anomalous compressibility and high densities exhibited by the olivine shock-wave data [McQueen, et al., 1967; Ahrens and Petersen, 1969; Jackson and Ahrens, 1979]: an interpretation which has commonly been applied to Hugoniot data for many compounds [see review of Duvall and Graham, 1977, for example]. It is argued below that only civilian (i.e. reconstructive or diffusion-based) transformations are likely to be of importance in producing significant density increases in olivine (and probably in most silicates) under pressure, as has generally been implicitly assumed in the interpretation of Hugoniot data; major changes in cation coordination number have typically been invoked. Phase transformation (even diffusion-limited) has long been considered possible under shock conditions, despite the short time available, due to the high temperatures or shearing generated during dynamic compression [e.g., Libby, 1962; Alder, 1963; Leiserowitz et al., 1966; Dremin and Breusov, 1968; Grady, 1977; DeCarli, 1979]. Support for this conclusion comes from the agreement between densities found under static and dynamic pressures [cf., Ahrens, et al., 1969; Duvall and Graham, 1977] as well as the unambiguous demonstration that phase transformation does occur in shock-waves within certain compounds [Johnson and Mitchell, 1972; Johnson,

et al., 1972]. Consequently, McQueen et al., [1967, 1970] have discussed interpretations of Hugoniot data in terms of the details of high-pressure phase-equilibrium relations. It should be noted at the outset, however, that the beginning of the "mixed-phase" region for olivine, even if as low as about 25 GPa, is substantially higher than the pressures at which olivine is known to transform under equilibrium conditions [eg. Ringwood, 1975]. This difficulty has long been recognized for most of the Hugoniot data of silicates [McQueen, et al., 1967], and it has generally been conceded that a certain amount of "overdriving" is required in order to generate phase transformation under shock.

Phase transformation has also been invoked to explain electrical conductivity measurements of olivine under shock [Schulien, et al., 1978], as well as petrographic textures observed in shocked olivines [Carter, et al., 1968]. Furthermore, Jeanloz and Ahrens [1977] demonstrated that the Hugoniot data are very consistent with the most recent of data on high pressure polymorphs of olivine derived from static experiments by showing that the densities and bulk moduli implied by the olivine Hugoniot are at least as high as those determined from the static experiments [see also Jackson and Ahrens, 1979]. These considerations, along with the reported discoveries of high pressure phases of olivine both in naturally shocked meteorites [ringwoodite: Binns, et al., 1969; Binns, 1970; Smith and Mason, 1970; Coleman, 1977] and in experimentally shocked samples [Schneider and Hornemann, 1977; Schneider, 1978], represent the evidence for phase transformation occurring in dynamically compressed olivine. However, the time at high pressure can be significantly longer in natural impacts than in laboratory shock experiments and a direct

comparison between these cases may not be valid [eg, Chao, 1968; James, 1969; Stöffler, 1972].

There is also considerable interest in the deformation produced in olivine (and other minerals) by dynamic compression because of the importance of shock due to meteorite impact in nature [e.g., Stöffler, 1971, 1972, 1974]. Thus, deformation features have been compared between experimentally and naturally shocked olivines in the study of "shock metamorphism" effects [e.g., Carter, et al., 1968; Lafleur, et al., 1968; Binns, et al., 1969; Müller and Hornemann, 1969; Short, 1968; Dobretsov, et al., 1970; Smith and Mason, 1970; Dymek, et al., 1975; Ashworth and Barber, 1975, 1977; Snee and Ahrens, 1975; Ahrens, et al., 1976; Christie and Ardell, 1976; Lally, et al., 1976; Levi, 1976; Coleman, 1977; Jeanloz, et al., 1977; Reimold and Stöffler, 1978; Bauer, 1978]. Again, many of the observed shock effects are interpreted in terms of phase transformation upon compression to high pressure, consistent with the standard interpretations of the Hugoniot data [cf., Stöffler, 1971, 1972]. Phase transformation is also thought to play an important role in the cratering process of planetary surfaces [O'Keefe and Ahrens, 1977, 1978].

The purpose of this paper is to present new observations which strongly suggest that reconstructive phase transformation does not occur in shock-compressed olivine to pressures extending through the "mixed-phase" region or about 75 GPa. This conclusion is at odds with the current interpretations of Hugoniot data which assume that the "mixed-phase" regions commonly found for silicates in the 5-100 GPa pressure range are due to major, reconstructive transformations similar (or

identical) to those which are known to occur under equilibrium conditions. A new, nonequilibrium model is presented for the behavior of olivine under shock which explains the densification associated with the "mixed-phase" region and which is consistent with all available observations, yet which bears little similarity to the equilibrium behavior of olivine at high pressures. However, the major geophysical conclusions which have been drawn to date from the standard reduction of Hugoniot data (assuming rigorous thermodynamic equilibrium) and their application to the earth's interior, appear to be valid. Despite the Hugoniot data representing states which are far from an equilibrium configuration on a microstructural level, the equations of state which are measured under shock apparently (perhaps fortuitously) do not deviate strongly from their equilibrium values.

II. EXPERIMENTAL METHODS

All samples for the present set of experiments were cut from a single crystal of peridot from San Carlos, Arizona (U.S.A.) with a composition of Fo(88). Samples were cored, lapped and polished to produce discs about 4.5 mm in diameter, 200-300 μm thick, and with surfaces smooth to a 0.5 μm finish. All samples were optically oriented parallel to either (010) or (100) and they were found to be free of any inhomogeneities at the scale of optical microscopy, except for the subboundaries evident in Figure 1. Wegner and Christie [1974] and Kirby and Wegner [1978] have described these subboundaries and, likewise, found no evidence for other heterogeneities in olivines from the same locality. Parallelism of the surfaces could be maintained to within about 5 (±5) μm

over the central area of the discs (approximately 75% of the radius), however some rounding of the sample edges was unavoidable. Because of this and other edge effects (e.g., sample/container impedance mismatch) only the central portions of each sample are, in principle, reliable for post-shock analysis. However, edge effects were not observed in the shocked samples.

Each sample disc was placed inside a spacer which, in turn, was sandwiched between two polished plugs and screwed into a container. All parts of the container, which were made of stainless steel 304, were lapped to conform to the geometry of the individual sample discs. Each container was pressed into a target block, machined flat and fitted with "momentum trap" plates [cf. Doran and Linde, 1966]. The target block was attached to the end of a 20-mm propellant gun using nylon screws and impacted under vacuum ($\lesssim 10^{-3}$ torr) by a lexan projectile bearing (except for shot #453) a tungsten or stainless steel flyer-plate. Upon impact, the nylon screws are sheared and the sample container is ejected away from the gun muzzle.

Because the projectile is never in free flight with the present design, a normal impact was assured for every shot. In all experiments the sample container was quenched to room temperature within 30-45 sec after impact using a burst of pressurized air. Although post-shock temperatures are not likely to be more than a few hundred degrees centigrade for these samples [Raikes and Ahrens, 1979], this quenching further minimizes any possible post-shock annealing in the olivine samples.

The primary measurement in each experiment is that of the projectile (impact) velocity measured by timing the successive obstruction of two

laser beams (about 58 mm apart) just prior to impact [see Gibbons and Ahrens, 1977; Raikes and Ahrens, 1979]. Velocities are usually measured to within 0.1-0.8%, and can be estimated to within about 5% from the amount of propellant used. Peak pressures are determined by standard impedance matching techniques for multiple shock reverberations [Walsh and Christian, 1955; Al'tshuler, 1965; Gibbons and Ahrens, 1971] based on the Hugoniot equation of state data of McQueen, et al., [1970] for tungsten and stainless steel and of Carter and Marsh [1979] for lexan.

After an experiment, the remains of the sample container are machined open, an air hose being frequently used in order to keep the container cool during the machining. Chemical composition and X-ray emission spectra of the samples were determined with an electron microprobe operating at 15 kV accelerating potential. Doubly polished thin sections used for petrographic observations and microprobe analyses were thinned by Ar^+-beam bombardment to produce "foils" for transmission electron microscopy, which was carried out at 200 kV accelerating potential. Separate aliquots destined for IR spectroscopic analyses were prepared and studied as in Jeanloz [1979]. Finally, individual chips of sample material were mounted and gold-coated for scanning electron microscopy.

III. RESULTS

The experimentally shocked samples were studied at three (overlapping) ranges of magnification: by optical and scanning electron microscopy, by means of transmission electron microscopy, and spectroscopically. The stresses achieved in the shock experiments are summarized in Figure 2 and Table 1.

The most dramatic effect observed in the shock-deformed olivine samples occurs at about 20 GPa peak pressure when massive plastic deformation is imparted to the crystalline structure. Whereas blocky fracturing is the most obvious deformation below 20 GPa (Figure 3a), for all samples retrieved from higher shock pressures a distinctive undulatory extinction is seen (Figure 4), indicating extensive plastic strain.

The blocky fracturing found in sample 13 (15.9 GPa peak pressure) is homogeneously distributed, and fracture orientations are more or less controlled by the cleavage directions of olivine. They are reminiscent of the fractures described by Levi [1973, 1976] and may have a thermal origin, or alternatively may reflect massive brittle failure at the Hugoniot Elastic Limit. The fractures separate blocks which are slightly misoriented with respect to each other but which exhibit no undulatory extinction, implying essentially no plastic strain within these blocks. This interpretation is confirmed by TEM observations (Figure 3b) which show nearly perfect crystalline material, along with a relatively low density ($\sim 10^{12} m^{2}$) of dislocation segments. These are interpreted as cold-work dislocations produced by the shock wave ([001] screw dislocations: see Christie and Ardell [1976]), presumably at stresses above about 9 GPa (the dynamic yield strength of olivine). The crystal is not very deformed, however, and yields a single-crystal electron diffraction pattern free of asterism.

By contrast, the undulatory extinction or mosaicism [Carter, et al., 1968; Reimold and Stöffler, 1978] seen optically in all of the other samples (Figure 4) is indicative of significant plastic deformation [e.g., Vernon, 1975]. This texture consists of domains about 10-30 μm

across which are slightly misoriented with respect to each other, although there is little large scale (sample-wide) misorientation: the sample is uniformly close to extinction, within a range of 5-10°. The texture is well developed even in sample 12 (21.7 GPa peak stress) and does not appear to change as a function of increasing pressure.

The mosaicism represents a high (spatial) frequency warping of the crystalline lattice associated with extensive plastic deformation, as is also shown by the high dislocation densities and complex selected area electron diffraction patterns observed by TEM [Figure 5; also Jeanloz, et al., 1977]. This is in contrast to the much longer wavelength undulatory extinction characteristic of typical metamorphic rocks which are deformed at very low strain rates [e.g., Spry, 1969], and appears to correlate with the high strain rates achieved under shock. The dimensions of the mosaics are of the order of plausible shock-front widths in olivine, based on measurements of shock-wave rise times in silicates and oxides [corresponding to $\tau \sim 1$ to 10 ns: see Grady, 1977].

The observation of mosaicism at pressures above about 20 GPa agrees with previous observations both on single crystals and poly-crystals [Carter, et al., 1968; Bauer, 1978; Reimold and Stöffler, 1978], as well as with the X-ray data of Hörz and Quaide [1973]. It appears that the mosaicism found in polycrystalline samples (including natural examples) is substantially more irregular than that seen in this study, a result suggesting that more complex wave interactions may be occurring in shocked polycrystals than single crystals, as is indicated by simple theoretical analyses [Rinehart, 1968; Guz', et al., 1974; Meyers and Carvalho, 1976; Brinkman, 1976]. Naturally shocked samples are commonly

further complicated by recovery and recrystallization processes [e.g., Lally, et al., 1976].

Fracturing becomes increasingly complex with increasing pressures; typically two scales of fractures are evident at pressures above 20 GPa. Large scale fractures cut across the samples in braided zones some 20-100 μm wide (Figure 6a). These zones of localized deformation surround regions of relatively unbroken olivine, suggesting the occurrence of heterogeneous yielding under shock, perhaps similar to that discussed by Grady [1977]. At a smaller scale, however, the regions between these fractured zones contain numerous micro-cracks (Figure 6b) which are oriented along cleavage planes [see Snee and Ahrens, 1975; Reimold and Stöffler, 1978; Levi, 1973, 1976]. With increasing pressure these small fractures tend to lose their planarity and apparent crystallographic constraint, sometimes taking on a wavy (flow-like) appearance (Figure 6c).

In all samples, the larger fractures actually represent faults cutting through the entire specimen (Figure 6d) with offsets as large as 50-500 μm [cf., Ananin, et al., 1974 a,b; Kanel', et al., 1977]. The faces of these microfaults are invariably polished and striated. The fact that striated and polished surfaces can be produced in silicates with such minute amounts of differential motion under shock implies that naturally occurring, shock-produced striae can not necessarily be used to infer large scale motions of ejecta [Chao, 1976]. However, the orientations and character of these fractures are undoubtedly affected by the experimental geometry, since they occur on a scale comparable to that of the sample.

The heterogeneous nature of deformation evident in the fracturing on a scale of millimetres is also seen in the strain at the submicroscopic scale, where deformation can vary noticeably within a few μm or less (Figure 5). This heterogeneity is thus characteristic of shock deformation even for single-crystal samples in nearly ideal, one-dimensional geometry.

Similarly, the occurrence of glassy regions in olivine samples shocked to pressures above about 50 GPa [described by Jeanloz, et al., 1977] is considered to represent localized areas of intense strain. The glassy regions comprise no more than a few percent of any sample, and there is no evidence that larger proportions are produced with increasing shock pressure (within the range studied here). Although it is possible that the glassy zones result from local melting, or transformation, the gradational boundaries between glass and crystalline sample, the lack of correlation between the amounts of glass and peak pressures, as well as the current estimates of shock and post-shock temperatures all make this mechanism implausible [Jeanloz, et al., 1977; Bauer, 1978; Raikes and Ahrens, 1979]. Rather, the glass apparently represents regions within which the crystalline structure was locally so intensely dislocated during shock that it was effectively disordered [cf., Cotterill, 1977]. Thus at a microstructural level as well as on the scale of the whole sample, shock-induced strain is not uniformly distributed.

In general, however, the shock effects found in olivine are significantly less pronounced than the effects typically seen in other silicates [e.g., Stöffler, 1972, 1974]; this is undoubtedly due, at least in part, to the refractory nature of olivine. For example, IR spectra of the

shocked samples are virtually identical to the spectrum of unshocked material (Figure 7). Significantly, the spectra show no evidence of any phases other than crystalline olivine in the shocked samples (the few percent of glass present in some of the samples is insufficient to be detected). Also, X-ray emission spectra [e.g., White, 1973] have resolved no changes in the nature of the Si-O bonding in shocked as compared with unshocked olivines (spectral resolution for the Si K_β peak is $\lesssim$0.1 eV).

There is no evidence for any new phases from the microscopic observations (Figures 3-6), and they indicate that there was no significant amount ($\gtrsim$1%) of phase transformation in these samples during the shock compression. This conclusion is based on the fact that not only have no new phases been found in these samples, but also that they exhibit no recrystallization. Given the high strains achieved in the shocked olivines, any significant amount of recrystallization should be readily observed. Thus, had there been any melting or solid state (reconstructive) transformations, the specimens should have contained either a remnant of the new phase(s) or areas of new (recrystallized) olivine replacing the high pressure-phase due to its instability upon decompression. There is no evidence of recovery (annealing) extensive enough to mask such features. The microstructural evidence, then, puts rather strict constraints on the nature of the shock-compression in these samples and indicates that they remained essentially as olivine (although internally highly sheared) within the range of pressures studied. This result is somewhat different from previous observations made on experimentally shocked olivines. For example, Carter, et al., [1968], Reimold and

Stöffler [1978] and Bauer [1978] all describe varying amounts of recrystallization in samples shocked to pressures above about 37 to 59 GPa. Such recrystallization is not a high-pressure shock phenomenon per se, but rather represents the post-shock thermal annealing of the shock-produced deformation structure, and it depends on the details of the pressure release, post-shock thermal history and target geometry. Thus, recovery and recrystallization processes often obliterate the shock effects of primary interest [Lally, et al., 1976] and introduce an ambiguity concerning phase transformations under shock. Nevertheless, Reimold and Stöffler [1978] come to the same conclusions as given here: they find essentially no evidence for phase transformation in olivines shocked to pressures of 60-70 GPa.

Schneider and Hornemann [1977] and Schneider [1978], however, have reported dramatic changes in the IR spectra of olivines experimentally shocked to nearly 58 GPa. They interpret these changes as indicating strong evidence for transformation(s) to oxide phases at high pressures under shock. The data presented here are in disagreement with their results, as are IR spectra of independently shocked olivines [described by Snee and Ahrens, 1975] and also the spectra and observations of Reimold and Stöffler [1978] and Bauer [1978]. The reasons for Schneider and Hornemann's contrasting results are not clear but may be due to unique post-shock thermal histories experienced by their samples, possibly involving thermal decomposition [Nitsan, 1975]. This speculative explanation is consistent with the fact that different studies appear to indicate different amounts of recrystallization upon release from similar shock pressures, thus implying different post-shock thermal histories.

Finally, in the olivines studies here (as well as in previous work: Reimold and Stöffler [1978]; Bauer [1978]) a distinct brown color appears in the samples shocked to pressures above about 40 GPa. The origin of this color is not understood, but it is not a surface property, nor does it apparently represent oxidation of iron [Reimold and Stöffler, 1978]. It has not been observed in naturally shocked olivines.

IV. DISCUSSION

The shock effects produced in olivine should, in principle, be explicable in terms of measured Hugoniot equation-of-state data as has been done for many other silicates [see Stöffler's 1972 review]. The relevant data for olivines of compositions similar to that studied here are shown in Figure 8 [McQueen, et al., 1967; Ahrens and Petersen, 1972], with a dynamic yield strength located at about 9 GPa (recently confirmed for single crystal forsterite by Raikes and Ahrens [1979]).

In the "mixed-phase" region, at pressures above about 25-40 GPa and below about 70 GPa, the Hugoniot data define a region of anomalous compressibility, as is typically found in silicates under shock [e.g., McQueen, et al., 1967; Ahrens, et al., 1969; Duvall and Graham, 1977]. The "mixed-phase" region has been ascribed to phase transformation and according to the transformation model of Ahrens, et al., [1976], for example, olivine shocked to about 60 GPa should transform approximately 60% to the ultimate high pressures phase(s). This must be considered a lower bound for the proportion transformed since olivine could transform to intermediate high-pressure phases through the "mixed-phase" region. For example, the spinel phase of olivine (ringwoodite) identified in

naturally shocked meteorites [e.g., Binns, 1970; Smith and Mason, 1970] must be considered such an intermediate phase since it has a density higher than that of olivine but significantly lower than that exhibited by the "high-pressure phase" regime of the Hugoniot. Consequently, sample 06 (60 GPa peak pressure) would be expected to exhibit evidence of at least 60 percent transformation, whereas evidence for even a few percent was not found. The present study of shock effects in olivine is in marked disagreement with the results expected from analyses of Hugoniot data, since no evidence was found of any phase transformations in the samples retrieved from pressures extending throughout the "mixed-phase" region.

However, there are two important differences between the present experiments and standard Hugoniot experiments: these involve temperature and time scale. In the first place, Hugoniot data reflect a high-pressure state achieved via a single shock front, whereas the present samples were brought to peak pressures via multiple reverberations between sample and container. The latter process, being more nearly isentropic, involves a smaller increase in thermal energy than direct shock compression and therefore leads to a lower temperature at peak pressure. However, the differences in internal energy increase calculated for the multiple reverberation paths shown in Figure 3 as compared with direct shock compression are small, amounting only to about 4% for the 60 GPa peak stress. Assuming the energy difference to be purely thermal (as a limiting case), this corresponds to a temperature difference on the order of 100 K (for a specific heat of about 10^3 J kg^{-1} K^{-1}), or less than 10% of the estimated Hugoniot temperature of 1200 K [Ahrens, et al.,

1976]. For comparison, Ahrens, et al.,'s [1976] phase transformation model would still predict over 50% transformation at 60 GPa, for the lower temperature state resulting from multiple reverberations. In the present experiments the samples are at peak pressures for about 300 to 1000 ns (Figure 2), whereas Hugoniot measurements represent properties achieved within the rise-time of the shock front (assuming a steady shock), i.e. of the order of 1 to 10 ns [Grady, 1977]. Thus if transformation is kinetically limited it would be expected to go further towards completion in the present shock recovery experiments than in the direct Hugoniot experiments. This only increases the present dilemma.

The problem of phase transformations under shock can to some extent be theoretically analyzed. The following is largely based on Christian [1975]. The objective here is to verify that the experimental observations indicating no transformation under shock are theoretically plausible.

Although it is conceivable that a high pressure phase of olivine might be formed under shock by a military (diffusionless, shear-based) transformation, followed by a complete reversion to olivine upon decompression (and with no evidence left to indicate that a transformation had occurred), no such transformation has yet been found associated with any significant density increase in olivine or any related silicate. Whereas military transformations are known to proceed readily under shock [Kormer, et al., 1966; Al'tshuler, et al., 1967; Johnson and Mitchell, 1972; Johnson, et al., 1972; Livshits, et al., 1972; Barker and Hollenbach, 1974], these are almost certainly not accessible to olivine in the present situation. For example, Sung and Burns [1978] have shown that the olivine-

spinel transition must be of civilian (diffusional) nature despite the lack of coordination change. Coordination changes might be expected for the much larger density increases characteristic of the "mixed-phase" regions of silicates, further diminishing the likelihood of any military character. In general, military mechanisms are not expected to play an important role in the major transformations which occur at high pressures in silicates because of the extensive rearrangements that are required in these complex structures.

Although specific models have been presented which predict extensive local transformation associated with very heterogeneous (and locally very high) temperature distributions in shocked samples ["shear-bands": Ananin, et al., 1974 a,b; Grady, et al., 1975; Grady, 1977; Kanel', et al., 1977; or "hot spots":DeCarli, 1979], such models are inadequate in the present context. These models are undoubtedly realistic for explaining partial transformations of initially porous samples or similarly heterogeneous media [e.g. Kieffer, et al., 1976; DeCarli, 1979], but the local temperatures that are required are much higher than the average shock temperatures in nonporous samples. Therefore, such models can not explain the large mixed phase regions in most of the Hugoniot data. Furthermore, there is little observational evidence for shear bands [Grady, 1977] or similar zones of high local temperatures in the samples discussed here. Nevertheless, this discussion does not preclude the formation of high pressure phases under shock in porous specimens, as has been observed [e.g., DeCarli and Milton, 1965; Kleeman and Ahrens, 1973; Kieffer, et al., 1976; DeCarli, 1979] and as is consistent with the Hugoniot data for such samples [Jeanloz and Ahrens, 1977]. Rather, this analysis deals with the

average or bulk properties of olivine under shock in terms of nucleation and growth of a high pressure phase. The conclusion from the following application of transformation theory is that no (observable) amount of transformation would be expected in any of the samples studied here because of the sluggish kinetics involved.

Near the top of the "mixed-phase" region (about 65-70 GPa) less than 1 percent (i.e. no evidence of) transformation was found in the present study, after a time of about 300-500 ns and at temperatures of the order 1400-1500 K [Ahrens, et al., 1976]. Under these conditions, the driving force for transformation ($\Delta G \sim \Delta V \Delta P$) is of the order of $\Delta G/k \lesssim 2.5 \times 10^3$ K (assuming the Hugoniot data to represent metastable and untransformed olivine, as is inferred from this study; k is Boltzmann's constant). This value is low, by a factor of 3, for the extreme assumption that the Hugoniot data reflects material which is transformed from the metastable extension of the low pressure Hugoniot (Figure 8). In either case, critical nuclei have molecular dimensions for bulk nucleation [$2\text{-}6 \times 10^{-10}$ m with surface energy $\sigma \sim 1$ J m^{-2}: e.g., Brace and Walsh, 1962 for typical values]. Similarly, nucleation on dislocations is essentially unimpeded under these conditions, using Cahn's [1957] model as a limiting case [e.g., Gómez-Ramírez and Pound, 1973, would predict more difficult nucleation on dislocations].

The extent of transformation for time t is given by

$$\zeta \sim 1 - \exp(-\pi \gamma^3 I t^4/3)$$

where I is the volume nucleation rate and γ is the equivalent isotropic

growth rate. Thus at the top of the mixed phase region the present observations indicate that $\gamma^3 I \lesssim 1.5 \times 10^{23}$ s^{-4} (for $\zeta \lesssim 10^{-2}$ and $t \sim 5 \times 10^{-7}$ s). This is a conservative bound since this analysis assumes quasi-steady state nucleation [e.g., Zel'dovich, 1943; Turnbull, 1948; Aleksandrov and Kedyarov, 1974]. The most plausible sites for nucleation are along dislocations, especially in light of the large dislocation densities observed in the olivine samples. Then, for v_N^D the number of nucleii along dislocations and an activation energy $\Delta g^{\pm}$,

$$I \sim v_N^D \frac{kT}{h} \exp(-\Delta g^{\pm}/kT),$$

at temperature T (h is Planck's constant) and assuming unimpeded nucleation. An approximate estimate of $\Delta g^{\pm}/k \sim 3.9 \times 10^4$ K is given by the measured activation energy of the olivine-spinel transition [Sung and Burns, 1978; Sung, 1979]. Any transformations involving major increases in coordination number and density might have significantly higher activation energies, and this estimate is also extremely conservative since it assumes no activation volume. For example, a minimal estimate of 5×10^{-6} m^3 mol^{-1} for the activation volume [e.g., Misener, 1974] doubles the activation energy used here at 70 GPa; the activation volume for oxygen-limited diffusion [13.4×10^{-6} m^3 mol^{-1}: Ross, et al., 1979] is a more plausible value and increases $\Delta g^{\pm}$ to about 3.8 times its zero pressure value.

Taking a dislocation density of $\rho_D \sim 10^{16}$ m^{-2} [a generous estimate of the maximum observed, and probably close to the maximum possible: Jeanloz, et al., 1977] and assuming that every molecule on a dislocation line

could be a nucleus gives ${}^{v}N_D \lesssim 10^{26}$. At the top of the "mixed-phase" region, then, $I \sim 1.6 \times 10^{28}$ s^{-1} m^{-3} is predicted. Bulk nucleation is probably much less effective than this, but even if every molecule is considered a nucleation center I is only increased by a factor of about 100. In order to get $\zeta \sim 10^{-2}$, $\gamma \sim 2 \times 10^{-2}$ m s^{-1} would be needed ($\gamma \sim 4 \times 10^{-3}$ m s^{-1} for every molecule being a nucleation site). However, γ is determined by the thickness of the growth interface λ:

$$\gamma \sim \lambda \frac{kT}{h} \exp(-\Delta g^{\pm}/kT)[1 - \exp(-\Delta G/kT)].$$

Taking $\lambda \lesssim 5 \times 10^{-10}$ m [e.g., Sung, 1979], $\gamma \sim 8 \times 10^{-8}$ m s^{-1} at the top of the "mixed-phase" region (even allowing the associated driving force $\Delta G \rightarrow \infty$) and $\zeta < 10^{-12}$. That is, essentially no amount of transformation occurs and it is not surprising that evidence for transformation has not been found in olivines.

It is possible that the temperature estimates used are inaccurate, yet nucleation becomes significant only above 2000 K and substantial transformation requires temperatures close to 2500 K (about 8×10^{3}K, using Ross, et al.,'s [1979] activation volume). It is highly unlikely that the estimates are inaccurate to this degree, especially in the light of recent measurements of shock temperatures in oxides (including forsterite) which are in close agreement with the theoretical calculations [Lyzenga, et al., 1979]. Furthermore, the present calculations of transformation rates probably underestimate drastically the temperatures required for significant phase transformation within the available time, given the numerous assumptions made, all of which maximize the amount of transformation allowed.

Hence from the perspective of transformation theory phase, transformation is not expected in experimentally shocked olivine, and the previous interpretations of the high-pressure Hugoniot data for olivine which call upon phase transformation appear to require revision. It is not necessary, however, to invoke phase transformations (in the conventional sense, and in particular involving coordination changes or disproportionation reactions) in order to explain the Hugoniot data for olivine. The high densities achieved by olivine at elevated shock pressures can be derived from a simple, crystallographically-based model in which the shock wave compresses the olivine structure essentially instantaneously (with respect to any but vibrational lattice relaxation processes) to a closely related and more efficient packing which is partly random on a local scale. Upon decompression, then, the compressed "lattice" can readily pop back into its original configuration with minimal rearrangement: no diffusive motion or coordinated rearrangement is required.

In particular, the properties of olivine reflect mainly the behavior of its oxygen sublattice which can be considered to be in a slightly distorted hexagonal closest packing (hcp). However, the packing is far from being efficient and the density of olivine is well below an ideal hcp density because its structure is distended in the [100] direction in comparison with hcp. By contrast, corundum (Al_2O_3) and bromellite (BeO) possess an oxygen sublattice very nearly in ideal hcp, while kyanite is only slightly less efficiently packed [e.g., Fairbairn, 1943]. Densities of olivine (Fo 90) corresponding to such efficient packings would be about 4.31, 4.42 and 4.17 Mg m^{-3}, respectively: much higher than the normal olivine density of 3.32 Mg m^{-3}.

Thus, olivine can be crudely modeled as a set of hcp sheets of oxygen in (100) orientation with cations interlayered between the sheets. Above the Hugoniot Elastic Limit, the structure is compressed to a state more efficiently packed than the original structure, thus accounting for the anomalous compressibility throughout the "mixed-phase" region. At high pressures, oxygen will tend to be in ideal hcp layers along (100), but it appears unlikely that the packing could become ideal hcp in the direction normal to the sheets of oxygen. This is because of the intervening cations and the complex but coordinated rearrangements required between the sheets within the time scale of the shock-compression. Rather, a random closest packing (rcp) might be expected in this orientation. Such a model assumes approximate long range order in shock-compressed olivine, but with locally significant deviations. For the purpose of quantitative estimates, the highest packing densities achieved by olivine under shock are modeled by a 2 + 1 dimensional hcp + rcp oxygen sublattice. This is not a unique model, but is proposed merely as a plausible description for the crystallographically expected behavior of olivine under rapid compression and it serves as an illustrative example.

Such a model does, in fact, reproduce the high-pressure, high-density Hugoniot data for olivine remarkably well: a comparison of the data with a theoretical Hugoniot for the present model is shown in Figure 9 [see Davies and Gaffney, 1973 and Jeanloz and Ahrens, 1977 for details; alternatively, thermal corrections can be ignored and a direct oxide-mixing model such as presented by McQueen, et al., 1967, 1970 and

Al'tshuler and Sharipzhanov, 1971a yields the same result]. The Hugoniot data for Al_2O_3 (corrected to a density corresponding to the molecular weight of olivine) have been used to define the compression curve for an ideal hcp oxygen sublattice, while the efficiency of rcp was determined from the work of Bernal [1959, 1964] on liquid structures. Although BeO also represents ideal hcp, corundum is preferred as an analog for olivine since the ionic radii of Al and Mg are similar while that of Be is significantly smaller. In this way, the presence of cations is accounted for, with the largest cation being taken as the most important in limiting the packing efficiency. These considerations would suggest that the Hugoniot of single-crystal olivine might exhibit slightly higher densities for shocks propagated along [100] than in other orientations, to the extent that the present model remains valid on a microscopic scale.

Alternative models exist: for example, the ideal packing for olivine might be modeled by a 2:1 combination of the hcp compression curves derived from Al_2O_3 and BeO (Figure 9). This is in direct analogy with the oxide-mixing models just referred to, and the ionic radii of Mg and Si are matched by Al and Be respectively. This would yield a compression curve for cp olivine of slightly higher density than that found in the model above, implying that olivine along the Hugoniot is even less efficiently packed than in that model (a 1:1 hcp:rcp packing would satisfy the Hugoniot data in this case). The present models suggest that significantly higher densities might be achieved by olivine than is indicated by the Hugoniot data, were the structure permitted to achieve an ideally

efficient packing. Olivine achieves a packing efficiency at the top of the "mixed-phase" region which is more nearly like that of kyanite than that of ideal closest packing. Presumably, ideal packing densities ($\rho_0 \sim 4.30 - 4.35$ Mg m^{-3}) might be achieved in static experiments (at low temperatures, in particular) although such densities are significantly larger than can be ascribed to any high pressure polymorphs of olivine found to date. If such packings are found (i.e., densities significantly larger than implied by the Hugoniot data), this will lend strong support to the models suggested here (plagioclase appears to provide an example for which recent, static high pressure data [Liu, 1978a,b] imply a high pressure polymorph with a density greater than those indicated by the Hugoniot data [Jeanloz and Ahrens, 1978, 1979]). By contrast, Al_2O_3 and BeO which are initially in ideal hcp exhibit no "mixed-phase" regions to pressures of 150 and 90 GPa, respectively.

An important problem remains, however, with respect to the partitioning of energy in olivine at high dynamic pressures. For example, in the calculations of Hugoniot temperatures quoted above, an energy of transformation (E_{tr}) is assumed to be partitioned into the (static) lattice, thus diminishing the thermal energy. For a typical value of $E_{tr} \sim 10^3$ kJ kg^{-1} [e.g., Ahrens, et al., 1976; Jeanloz and Ahrens, 1977], this corresponds to a temperature of about 10^3K (for a specific heat of about 1 kJ kg^{-1} K^{-1}) by which the Hugoniot temperature is assumed to be decreased due to phase transformation. If transformation does not occur then the calculated Hugoniot temperatures must be revised upwards by about 10^3K at high pressures, although this is not consistent with the

available measurements of shock temperature. In the present model, olivine is visualized as attaining a transient and partly random configuration upon shock loading, and it is assumed that about 10^3 kJ kg^{-1} (or 4×10^{-17} J $atom^{-1}$) is lost to the lattice at high shock-pressures, as required to bring calculated and observed temperatures into agreement. For example, the present model predicts a significant increase in entropy associated with the random nature of the packing achieved under shock. This is analogous to melting and is expected to significantly decrease the temperature of the crystal, as has been documented for several compounds which are believed to melt under shock [Kormer, et al., 1965; Kormer, 1968]. Taking a value of $\Delta S/3k \sim 0.5$ for the entropy gain per atom in randomizing the lattice under shock (this is of the order of magnitude which is typical for melting) yields the appropriate energy loss to the structure (the temperatures of Ahrens, et al., [1976] are assumed). Also, this amount of energy could be accounted for by the breaking of only one bond per 10-100 atoms resulting, nevertheless, in a highly unstable structure. Essentially, this reflects the small proportion of the static lattice energy which E_{tr} represents [e.g., Gaffney and Ahrens, 1970]. Finally, simple calculations [Bragg, 1948; Friedel, 1964; Christian, 1975] show that a large fraction ($\gtrsim$20%) of this energy could be stored in the cores of the dislocations which are formed during the shock compression (based on the parameters quoted in Jeanloz, et al., [1977]. These considerations are simplistic and speculative, however it is not clear how much reliance should be placed in the calculations of energy partitioning and temperature in the first place, since these must rigorously assume thermodynamic equilibrium at the Hugoniot state,

contrary to the conclusions deduced above.

If these conclusions are valid then several concepts which have been widely used in the interpretation of shock-wave data are invalid. In particular, olivine does not undergo large increases in cation coordination number and achieve the density of (ideally) close-packed oxides, as has long been presumed [e.g., McQueen, et al., 1967; Wang, 1967; Ahrens, et al., 1969]. Cation coordination number (CN) is not relevant in the present context: an oxygen sublattice corresponding to BeO (CN = 4) has a significantly higher density than one corresponding to Al_2O_3 (CN = 6). The concept of phase transformations, as it has been applied to the Hugoniot data for olivine, appears to be invalid and the olivine structure is approximately retained along the "high-pressure phase" branch of the Hugoniot, despite this structure being extremely unstable. As envisioned here, the process which occurs under shock is more analogous to a lattice relaxation (absorption) process than a transformation from one structure to another. Most important, then, the assumption of equilibrium which is central to the reduction and application of shock-wave data can not be justified in principle, although it is remarkable how well the properties of the olivine Hugoniot in the "high-pressure phase" region reflect the properties expected of the appropriate (equilibrium) high pressure polymorphs [eg, Jeanloz and Ahrens, 1977].

Although the data and discussion presented above are directly relevant only to olivine under shock, there is some evidence that these conclusions may also apply to other silicates. For example, careful analyses of shocked pyroxene and quartz suggest that these do not undergo phase transformation in the bulk, as their Hugoniot data have been inferred to

demonstrate. The shock-recovery experiments of Gibbons [1974, 1975] and Schaal and Hörz [1977] produced no evidence of phase transformation in pyroxenes to pressures of 53 to 100 GPa, consistent with the results of Pollack and DeCarli [1969] and Dundon and Haffner [1971]; for comparison, Ahrens and Gaffney [1971] inferred from their Hugoniot data that the "mixed-phase" region of bronzite begins at 15 GPa. Similarly, Kieffer et al., [1976] found no evidence for the formation of stishovite in the bulk (within grains rather than at their boundaries) in the Coconino sandstone, in one of the most extensive studies of shock-deformation to date [see also Chao 1967, 1968]. Also, the experiments of Hörz [1968] on single crystal quartz samples did not yield amounts of diaplectic glass (inferred to be formed by reversion of the high pressure phase) which correlate well with the Hugoniot data for SiO_2 [Wackerle, 1962; McQueen, et al., 1963; Grady, et al., 1974]. Podurets and Trunin [1974] and Podurets, et al., [1976] have discussed similar difficulties in presenting two speculative models for the possible transformation mechanism of quartz under shock. On the other hand, the apparent evidence for phase transformation in shocked garnets [Ahrens and Graham, 1972; Liu, 1975; Stähle, 1975] remains enigmatic in the context of the present study [see also Graham and Ahrens, 1973].

V. CONCLUSIONS

New observations of shock deformation in single-crystal olivine are presented for the range in peak pressures from about 18 to 75 GPa. There is clear evidence of extensive plastic deformation throughout most of this range, but no indication of substantial recovery or of any recrystallization. No evidence could be found of any high pressure phases

having formed in these samples under shock, and textural evidence seems to preclude any having formed and reverted to olivine. Previous identification of high pressure phases in experimentally shocked olivines appear to be spurious. Therefore, these results indicate that nonporous olivine does not undergo (reconstructive) phase transformation under experimental shock conditions to pressures extending through the "mixed-phase" region, and that previous interpretations of the shock-wave data may not be well founded. Because of the much higher temperatures which are achieved in porous samples under shock, these may achieve states very nearly at equilibrium and a substantial amount of phase transformation is not precluded.

A new interpretation of the response of olivine to shock is presented which does not invoke phase transformation (at least in the usual, equilibrium sense), yet which reproduces the Hugoniot data very well. This is a crystallographically-based model which considers the olivine structure under shock to be in a compressed, somewhat randomized configuration which nevertheless corresponds closely to the olivine structure. Hence, the "high-pressure phase" regime of the olivine Hugoniot does not correspond to the compression of an ideally close-packed oxide or of an equilibrium high-pressuje phase of olivine; increases in cation coordination number can not be inferred from the data. There is some evidence suggesting that other silicates may also be untransformed along their high-pressure Hugoniots. In this model, the Hugoniot is considered to consist of highly metastable, transient states, hence violating the assumptions which are fundamental to the reduction of Hugoniot data and their geophysical applications. However, the Hugoniot data appear to

reflect, at least approximately, the packing densities which are attained at the high pressures and temperatures relevant to the Earth's interior. Nevertheless, the results of this study suggest that a reappraisal of the geophysical applications of high-pressure shock-wave data may be necessary.

Acknowledgments. I am particularly indebted to J. M. Christie and T. J. Ahrens for their generous help and advice throughout this study. TEM examination (and sample preparation) was carried out in the Departments of Geology and Materials Science, University of California, Los Angeles, through the hospitality of A. J. Ardell and J. M. Christie. Spectroscopic facilities were provided by G. R. Rossman (California Institute of Technology). I appreciate very much numerous discussions with T. J. Ahrens, J. M. Christie, D. E. Grady, I. Jackson, S. W. Kieffer, and G. R. Rossman. Their comments and ideas have considerably improved this paper.

REFERENCES

Ahrens, T. J., D. L. Anderson and A. E. Ringwood, Equations of state and crystal structures of high-pressure phases of shocked silicates and oxides, Rev. Geophys., 7, 667-707, 1969.

Ahrens, T. J. and C. F. Petersen, Shock wave data and the study of the earth, in The Application of Modern Physics to the Earth and Planetary Interiors, S. K. Runcorn (ed.), J. Wiley and Sons, New York, 449-461, 1969.

Ahrens, T. J., Shock-wave equations of state of minerals, in Mantle and Core in Planetary Physics, L. Corso (ed.) Academic Press, New York, 157-187, 1971.

Ahrens, T. J. and E. S. Gaffney, Dynamic compression of enstatite, J. Geophys. Res., 76, 5504-5513, 1971.

Ahrens, T. J., J. H. Lower and P. L. Lagus, Equation of state of forsterite, J. Geophys. Res., 76, 518-528, 1971.

Ahrens, T. J. and E. K. Graham, A shock-induced phase change in iron-silicate garnet, Earth Planet. Sci. Lett., 14, 87-90, 1972.

Ahrens, T. J., Equations of state of the earth, Rev. Geophys. Space Phys., 13, 335-339, 1975.

Ahrens, T. J., F.-D. Tsay and D. H. Live, Shock-induced fine-grained recrystallization of olivine: evidence against subsolidus reduction of Fe^{2+}, Proc. Lunar Sci. Conf., 7th, 1143-1156, 1976.

Alder, B. J., Physics experiments with strong pressure pulses, in Solids Under Pressure, W. Paul and D. M. Warschauer (eds.) McGraw-Hill Book Co., New York, 385-420, 1963.

Aleksandrov, L. N. and B. I. Kedyarov, Stochastic theory of non-steady state nucleation, J. Cryst. Growth, 24/25, 507-510, 1974.

Al'tshuler, L. V., Use of shock waves in high-pressure physics, Sov. Phys. Uspekhi, 8, 52-91, 1965.

Al'tshuler, L. V., M. N. Pavlovskii and V. P. Drakin. Peculiarities of phase transitions in compression and rarefaction shock waves. Sov. Phys. J.E.T.P., 25, 260-265, 1967.

Al'tshuler, L. V. and I. I. Sharipdzhanov. Additive equations of state of silicates at high pressures. Izv. Acad. Sci. USSR Earth Phys., no. 3, 167-177, 1971a.

Al'tshuler, L. V. and I. I. Sharipdzhanov. Distribution of iron in the earth and its chemical differentiations. Izv. Acad. Sci. USSR, Earth Phys., no. 4, 231-239, 1971b.

Anan'in, A. V., O. N. Breusov, A. N. Dremin, S. V. Pershin and V. F. Tatsii. The effect of shock waves on silicon dioxide. I. Quartz. Fiz. Goren. Vzryva, 10, 426-436, 1974a.

Anan'in, A. V., O. N. Breusov, A. N. Dremin, S. V. Pershin, A. I. Rogacheva and V. F. Tatsii. Action of shock waves on silicon dioxide II. Quartz glass. Fiz. Goren. Vzryva, 10, 578-583, 1974b.

Anderson, D. L. and H. Kanamori. Shock-wave equations of state for rocks and minerals. J. Geophys. Res., 73, 6477-6502, 1968.

Anderson, D. L. and T. Jordan. The composition of the lower mantle. Phys. Earth and Planet. Int., 3, 23-35, 1970.

Anderson, D. L., C. Sammis and T. Jordan. Composition and evolution of the mantle and core. Science, 171, 1103-1112, 1971.

Anderson, D. L. Composition of the mantle and core. Ann. Rev. Earth Planet. Sci., 5, 179-202, 1977.

Ashworth, J. R. and D. J. Barber. Electron petrography of shock-deformed olivine in stony meteorites. Earth Planet. Sci. Lett., 27, 43-50, 1975.

Ashworth, J. R. and D. J. Barber. Electron microscopy of some stony meteorites. Phil. Trans. R. Soc. Lond., A286, 493-506, 1977.

Barker, L. M. and R. E. Hollenbach. Shock wave study of the $\alpha \rightleftarrows \varepsilon$ phase transition in iron. J. App. Phys., 45, 4872-4887, 1974.

Bauer, J. F. Shock-induced deformation in olivines from polycrystalline dunites and particulate samples. Lunar Planet. Sci. IX, 55-57, 1978.

Bernal, J. D. A geometrical approach to the structure of liquids. Nature, 183, 141-147, 1959.

Bernal, J. D. The structure of liquids. Proc. Roy. Soc. Lond., A 280, 299-322, 1964.

Binns, R. A., R. J. Davis and S. J. B. Reed. Ringwoodite, natural $(Mg, Fe)_2SiO_4$ spinel in Tenham meteorite. Nature, 221, 943-944, 1969.

Binns, R. A. $(Mg, Fe)_2SiO_4$ spinel in a meteorite. Phys. Earth Planet. Int., 3, 156-160, 1970.

Birch, F. Elasticity and constitution of the earth's interior. J. Geophys. Res., 57, 227-286, 1952.

Birch, F. Density and composition of mantle and core. J. Geophys. Res., 69, 4377-4388, 1964.

Birch, F. Compressibility; elastic constants, in: Handbook of Physical Constants (S.P. Clark, Jr., ed.) Geol. Soc. Am. Mem. 97, pp. 97-173, 1966.

Brace, W. F. and J. B. Walsh. Some direct measurements of the surface energy of quartz and orthoclase. Am. Min., 47, 1111-1122, 1962.

Bragg, L. Effects associated with stresses on a microscopic scale, in: Symposium on Internal Stresses, in Metals and Alloys, Inst. of Metals, London, pp. 221-226, 1948.

Brinkman, J. A. Effects of focused collisions on shock-wave propagation in crystalline solids. J. App. Phys., 47, 1374-1384, 1976.

Cahn, J. W. Nucleation on dislocations, Acta Met., 5, 169-172, 1957.

Carter, N. L., C. B. Raleigh and P. S. DeCarli. Deformation of olivine in stony meteorites. J. Geophys. Res., 5439-5461, 1968.

Carter, W. J. and S. P. Marsh. Hugoniot equations of state of polymers. J. Chem. Phys. (in press), 1979.

Chao, E. C. T. Shock effects in certain rock-forming minerals. Science, 156, 192-202, 1967.

Chao, E. C. T. Pressure and temperature histories of impact metamorphosed rocks - based on petrographic observations, in: Shock Metamorphism of Natural Materials (B. M. French and N. M. Short, eds.) Mono Book Corp., Baltimore, Md. pp. 135-158, 1968.

Chao, E. C. T. Mineral-produced high-pressure striae and clay polish: key evidence for nonballistic transport of ejecta from Ries Crater. Science, 194, 616-618, 1976.

Christian, J. W. The Theory of Transformations in Metals and Alloys, Part I, Pergamon Press, New York, 586 pp., 1975.

Christie, J. M. and A. J. Ardell. Deformation structures in minerals, in: Electron Microscopy in Mineralogy, (H.-R. Wenk, ed.), Springer-Verlag, Berlin, pp. 374-403, 1976.

Coleman, L. C. Ringwoodite and majorite in the Catherwood meteorite. Can. Min., 15, 97-101, 1977.

Cotterill, R. M. J. Does dislocation density have a natural limit? Phys. Lett., 60A, 61-62, 1977.

Davies, G. F. and D. L. Anderson. Revised shock-wave equations of state for high-pressure phases of rocks and minerals. J. Geophys. Res., 76, 2617-2627, 1971.

Davies, G. F. and E. S. Gaffney. Identification of high-pressure phases of rocks and minerals from Hugoniot data. Geophys. J. R. astr. Soc., 33, 165-183, 1973.

Davies, G. F. Limits on the constitution of the lower mantle. Geophys. J. R. astr. Soc., 38, 479-503, 1974.

DeCarli, P. S. and D. J. Milton. Stishovite: synthesis by shock wave. Science, 147, 144-145, 1965.

DeCarli, P. S. Nucleation and growth of cubic diamond in shock wave experiments, in: High-Pressure Science and Technology, Vol. 1 (K. D. Timmerhaus and M. S. Barber, editors), Plenum Press, New York, pp. 940-943, 1979.

Dobretsov, N. L., A. A. Deribas and V. I. Maly. Shock compression of powdered SiO_2, Mg_2SiO_4, $ZrSiO_4$ and other materials. Phys. Earth Planet. Int., 3, 348-355, 1970.

Doran, D. G. and R. K. Linde. Shock effects in solids. Solid State Physics, 19, 229-290, 1966.

Dremin, A. N. and O. N. Breusov. Processes occurring in solids under the action of powerful shock waves. Russ. Chem. Rev., 37, 392-402, 1968.

Dundon, R. W. and S. S. Haffner. Cation disorder in shocked orthopyroxene. Science, 174, 581-583, 1971.

Duvall, G. E. and R. A. Graham. Phase transitions under shock-wave loading. Rev. Mod. Phys., 49, 523-579, 1977.

Dymek, R. F., A. L. Albee and A. A. Chodos. Comparative petrology of lunar cumulate rocks of possible primary origin: dunite 72415, troctolite 76535, norite 78235, and anorthosite 62237. Proc. Lunar Sci. Conf. 6th, 301-341, 1975.

Fairbairn, H. W. Packing in ionic minerals. Bull. Geol. Soc. Am., 54, 1305-1374, 1943.

Fowles, G. R. Attenuation of the shock wave produced in a solid by a flying plate. J. App. Phys., 31, 655-661, 1960.

Friedel, J. Dislocations, Pergamon Press, New York, 491 pp., 1964.

Gaffney, E. S. and T. J. Ahrens. Stability of mantle minerals from lattice calculations and shock wave data. Phys. Earth Planet. Int., 3, 204-212, 1970.

Gibbons, R. V. and T. J. Ahrens. Shock metamorphism of silicate glasses. J. Geophys. Res., 76, 5489-5498, 1971.

Gibbons, R. V. Experimental Effects of High Shock Pressure on Materials of Geological and Geophysical Interest: PhD Thesis, California Institute of Technology, 215 pp., 1974.

Gibbons, R. V., Controlled shock experiments on pyroxene and plagioclase, Geol. Assoc. Canada Abs. Prog., 7, 36, 1975.

Gibbons, R. V. and T. J. Ahrens. Effects of shock pressures on calcic plagioclase, Phys. Chem. Min., 1, 95-107, 1977.

Gómez-Ramírez, R. and G. M. Pound, Nucleation of a second solid phase along dislocations, Metal. Trans., 4, 1563-1570, 1973.

Grady, D. E., W. J. Murri and G. R. Fowles. Quartz to stishovite: wave propagation in the mixed phase region, J. Geophys. Res., 79, 332-338, 1974.

Grady, D. E., W. J. Murri and P. S. DeCarli. Hugoniot sound velocities and phase transformations in two silicates, J. Geophys. Res., 80, 4857-4861, 1975.

Grady, D. E. Processes occurring in shock wave compression of rocks and minerals, in: High-Pressure Research, (M. H. Manghnani and S. Akimoto, eds.) Academic Press, New York, pp. 389-438, 1977.

Graham, E. K. and T. J. Ahrens. Shock wave compression of iron-silicate garnet, J. Geophys. Res., 78, 375-392, 1973.

Graham, E. K. On the occurrence of (Mg, Fe)SiO_3 in the lower mantle, Geophys. J. R. astr. Soc., 42, 993-1009, 1975.

Guz', I. S., V. N. Peretyat'ko and G. S. Demina. Study of structural changes in polycrystals under explosive loads. Fiz. Goren. Vzryva, 10, 452-455, 1974.

Hörz, F. Statistical measurements of deformation structures and refractive indices in experimentally shock loaded quartz, in: Shock Metamorphism of Natural Materials (B. M. French and N. M. Short, eds.) Mono Book Corp., Baltimore, Md., pp. 243-253, 1968.

Hörz, F. and W. L. Quaide. Debye-Scherrer investigations of experimentally shock loaded quartz, in: Shock Metamorphism of Natural Materials, (B. M. French and N. M. Short, eds.) Mono Book Corp., Baltimore, Md., pp. 243-253, 1968.

Hörz, F. and W. L. Quaide. Debye-Scherrer investigations of experimentally shocked silicates, The Moon, 6, 45-82, 1973.

Jackson, I. and T. J. Ahrens. Shock-wave compression of single-crystal forsterite, J. Geophys. Res., 84, 3039-3048, 1979.

James, O. B., Jadeite: shock-induced formation from oligoclase, Ries Crater, Germany, Science, 165, 1005-1008, 1969.

Jeanloz, R. and T. J. Ahrens. Pyroxenes and olivines: structural implications of shock-wave data for high pressure phases, in: High-Pressure Research, (M. H. Manghnani and S. Akimoto, eds.) Academic Press, New York, pp. 439-461, 1977.

Jeanloz, R., T. J. Ahrens, J. S. Lally, G. L. Nord Jr., J. M. Christie and A. H. Heuer. Shock-produced olivine glass: first observation, Science, 197, 457-459, 1977.

Jeanloz, R. and T. J. Ahrens. The equation of state of a lunar anorthosite: 60025, Proc. Lunar Planet. Sci. Conf. 9th, 2789-2803, 1978.

Jeanloz, R., Infrared spectra of olivine polymorphs: α, β-phase and spinel, 1979.

Jeanloz, R. and T. J. Ahrens. Equation of state of lunar anorthosite and anorthite, criteria for impact melting and vaporization, Lunar Planet. Sci. X, 622-624, 1979.

Johnson, Q., A. C. Mitchell and L. Evans. X-ray diffraction study of single crystals undergoing shock-wave compression, App. Phys. Lett., 21, 29-30, 1972.

Johnson, Q. and A. C. Mitchell. First X-ray diffraction evidence for a phase transition during shock-wave compression, Phys. Rev. Lett., 29, 1369-1371, 1972.

Kalinin, V. A., V. L. Pan'kov and V. N. Zharkov. Equations of state of dunites and bronzitites undergoing polymorphic transformations under pressure, Izv. Acad. Sci. USSR, Earth Phys., no 7, 419-426, 1974.

Kanel', G. I., A. M. Molodets and A. N. Dremin. Investigation of singularities of glass strain under intense compression waves. Fiz. Goren. Vzryva, 13, 906-912, 1977.

Kieffer, S. W., P. P. Phakey and J. M. Christie. Shock processes in porous quartzite: transmission electron microscope observations and theory, Contrib. Min. Pet., 59, 41-93, 1976.

Kirby, S. H. and M. W. Wegner. Dislocation substructure in mantle-derived olivine as revealed by selective chemical etching and transmission electron microscopy, Phys. Chem. Min., 3, 309-330, 1978.

Kleeman, J. D. and T. J. Ahrens. Shock-induced transition of quartz to stishovite, J. Geophys. Res., 78, 5954-5960, 1973.

Kormer, S. B., M. V. Sinitsyn, G. A. Kirillov and V. D. Urlin, Experimental determination of temperature in shock-compressed NaCl and KCl and of their melting curves at pressures up to 700 Kbar, Sov. Phys. J.E.T.P., 21, 689-700, 1965.

Kormer, S. B., K. B. Yushko and G. V. Kirshkevich. Dependence of the refractive index on the density of the solid and liquid phases of shock-compressed ionic crystals. Relaxation time of phase transformation under shock compression. Zh. E.T.F. Pis'ma, 3, 39-42, 1966.

Kormer, S. B. Optical study of the characteristics of shock-compressed condensed dielectrics, Sov. Phys. Uspehki, 11, 229-254, 1968.

LaFleur, L. D., C. D. Goodman and E. A. King. Mössbauer investigation of shocked and unshocked iron meteorites and fayalite, Science, 162, 1268-1270, 1968.

Lally, J. S., J. M. Christie, G. L. Nord, Jr. and A. H. Heuer. Deformation, recovery and recrystallization of lunar dunite 72417, Proc. Lunar Sci. Conf. 7th, 1845-1863, 1976.

Leiserowitz, L., G. M. J. Schmidt and A. Shamgar. Shock-induced irreversible phase transitions in inorganic solids, J. Phys. Chem. Solids, 27, 1453-1457, 1966.

Levi, F. A. Thermal fatigue: a possible source of structural modifications in meteorites, Meteorites, 8, 209-221, 1973.

Levi, F. A. Thermally induced fractures in olivines of stony meteorites, Min. Mag., 40, 519-521, 1976.

Libby, W. F. High pressure chemistry, I: ultra rapid rates at very high pressures, Proc. Nat. Acad. Sci., U.S., 48, 1475-1480, 1962.

Liu, L.-G., High pressure reconnaissance investigation in the system $Mg_3Al_2Si_3O_{12}$ - $Fe_3Al_2Si_3O_{12}$, Earth Planet. Sci. Lett., 26, 425-433, 1975.

Liu, L.-G. The post-spinel phase of forsterite, Nature, 262, 770-772, 1976a.

Liu, L.-G. Orthorhombic perovskite phases observed in olivine, pyroxene and garnet at high pressures and temperatures, Phys. Earth Planet. Int., 11, 289-298, 1976b.

Liu, L.-G. The post-spinel phases of twelve silicates and germanates, in: High-Pressure Research, (M. H. Manghnani and S. Akimoto, eds.) Academic Press, New York, pp. 245-253, 1977.

Liu, L.-G. High-pressure phase transformations of albite, jadeite and nepheline, Earth Planet. Sci. Lett., 37, 438-444, 1978a.

Liu, L.-G. A new high-pressure phase of $Ca_2Al_2SiO_7$ and implications for the earth's interior, Earth Planet. Sci. Lett., 40, 401-406, 1978b.

Livshits, L. D., L. V. Larionov and Y. N. Ryabinin. Kinetic features of polymorphic transitions from NaCl type structure to CsCl type structure at high pressure (in the case of polymorphic transformations in RbI and KCl). Izv. Acad. Sci. USSR, Earth Phys., no 11, 730-735, 1972.

Lyzenga, G., T. J. Ahrens and A. C. Mitchell. Optical measurement of shock temperatures in dielectrics and metals. Bull. Am. Phys. Soc. (in press) 1979.

McQueen, R. G., J. N. Fritz and S. P. Marsh. On the equation of state of stishovite, J. Geophys. Res., 68, 2319-2322, 1963.

McQueen, R. G., S. P. Marsh and J. N. Fritz. Hugoniot equation of state of twelve rocks, J. Geophys. Res., 72, 4999-5036, 1967.

McQueen, R. G., S. P. Marsh, J. W. Taylor, J. N. Fritz and W. J. Carter. The equation of state of solids from shock wave studies in: High Velocity Impact Phenomena, (R. Kinslow, ed.) Academic Press, New York, pp. 294-419, and Appendices, 1970.

Meyers, M. A. and M. S. Carvalho. Shock-front irregularities in polycrystalline metals, Mater. Sci. Eng., 24, 131-135, 1976.

Misener, D. J.. Cationic diffusion in olivine to 1400°C and 35 Kbar, in: Geochemical Transport and Kinetics (A. W. Hoffmann, B. J. Giletti, H. S. Yoder, Jr. and R. A. Yund, eds.), Carnegie Institute of Washington Publication 634, Washington, D.C., pp. 117-129, 1974.

Müller, W. F. and U. Hornemann. Shock-induced planar deformation structures in experimentally shock-loaded olivines and in olivines from chondritic meteorites, Earth Planet. Sci. Lett., 7, 251-264, 1969.

Neal, T. Second Hugoniot relationship for solids, J. Phys. Chem. Solids, 38, 225-231, 1977.

Nitsan, U. Stability field of olivine with respect to oxidation and reduction, J. Geophys. Res., 79, 706-711, 1975.

O'Keefe, J. D. and T. J. Ahrens. Impact ejecta on the moon, Proc. Lunar Sci. Conf. 7th, 3007-3025, 1977.

O'Keefe, J. D. and T. J. Ahrens. Impact flows and crater scaling on the moon, Phys. Earth Planet. Int., 16, 341-351, 1978.

Podurets, M. A. and R. F. Trunin. On the microstructure of the dense phase of shock-compressed quartz, Izv. Acad. Sci. USSR, Earth Phys., no 7, 427-429, 1974.

Podurets, M. A., G. V. Simakov and R. F. Trunin. On the phase equilibrium in shock-compressed quartz and on the kinetics of phase transitions, Izv. Acad. Sci. USSR, Earth Phys., no 7, 419-424, 1976.

Pollack, S. S. and P. S. DeCarli. Enstatite: disorder produced by a megabar shock event, Science, 165, 591-592, 1969.

Raikes, S. and T. J. Ahrens. Post-shock temperatures in minerals, Geophys. J. R. astr. Soc., (in press), 1979.

Reimold, W. U. and D. Stöffler. Experimental shock metamorphism of dunite, Proc. Lunar Planet. Sci. Conf. 9th, 2805-2824, 1978.

Rinehart, J. S. Intense destructive stresses resulting from stress wave interactions, in: Shock Metamorphism of Natural Materials (B. M. French and N. M. Short, eds.) Mono Book Corp., Baltimore, Md. pp. 31-42, 1968.

Ringwood, A. E. Composition and Petrology of the Earth's Mantle, McGraw-Hill, New York, 618 pp., 1975.

Ross, J. V., H. G. Ave'Lallement and N. L. Carter. Activation volume for creep in the upper mantle, Science, 203, 261-263, 1979.

Schaal, R. B. and F. Hörz. Shock metamorphism of lunar and terrestrial basalts, Proc. Lunar Sci. Conf. 8th, 1697-1729, 1977.

Schneider, H. and U. Hornemann. Preliminary data on the shock-induced high-pressure transformation of olivine, Earth Planet. Sci. Lett., 36, 322-324, 1977.

Schneider, H. The shock-induced high pressure transformation of olivine, Phys. Chem. Min., 3, 89-90, 1978.

Schulien, S., U. Hornemann and D. Stöffler. Electrical conductivity of dunite during shock compression from 12.5 to 45 GPa, Geophys. Res. Lett., 5, 345-348, 1978.

Short, N. M. Shock metamorphism of basalt: Report X-644-69-117, Goddard Space Flight Center, Greenbelt, Md., 39 pp., 1969.

Smith, J. V. and B. Mason. Pyroxene-garnet transformation in Coorara meteorite, Science, 168, 832-833, 1970.

Snee, L. W. and T. J. Ahrens. Shock-induced deformation features in terrestrial peridot and lunar dunite, Proc. Lunar Sci. Conf. 6th , 833-842, 1975.

Somerville, M. Temperature of earth's lower mantle according to homogeneous and layered models, Geophys. J. R. astr. Soc., (in press), 1979.

Spry, A. Metamorphic Textures, Pergamon Press, New York, 350 pp., 1969.

Stähle, V. Natural shock behavior of almandite in metamorphic rocks from the Ries Crater, Germany, Earth Planet. Sci. Lett., 25, 71-81, 1975.

Stöffler, D. Progressive metamorphism and classification of shocked and brecciated crystalline rocks at impact craters, J. Geophys. Res., 76, 5541-5551, 1971.

Stöffler, D. Deformation and transformation of rock-forming minerals by natural and experimental shock processes: I Fortschr, Miner., 49, 40-113, 1972.

Stöffler, D. Deformation and transformation of rock-forming minerals by natural and experimental shock processes: II, Fortsch, Miner., 51, 256-289, 1974.

Sung, C.-M. and R. G. Burns. Crystal structural features of the olivine→spinel transition, Phys. Chem. Min., 2, 177-197, 1978.

Sung, C.-M. Kinetics of the olivine→spinel transition under high pressure and temperature: experimental results and geophysical implications, in: High-Pressure Science and Technology, Vol. 2, (K. D. Timmerhaus and M. S. Barber, editors), Plenum Press, New York, pp. 31-42, 1979.

Telegin, G. S., V. A. Bugayeva and R. F. Trunin. Determination of the metastable adiabat of the dense phase of silica from the results of measurements of the dynamic compressibility of minerals, Izv. Acad. Sci. USSR, Earth Phys., no. 12, 793-794, 1974.

Trunin, R. F., V. I. Gon'shakova, G. V. Simakov and N. E. Galdin. A study of rocks under the high pressures and temperatures created by shock compression, Izv. Acad. Sci. USSR, Earth Phys., no. 9, 579-586, 1965.

Turnbull, D. Transient nucleation, Trans. A.I.M.E., 175, 774-783, 1948.

Van Thiel, M., editor, Compendium of Shock Wave Data, Report UCRL-50108 Lawrence Livermore Laboratory, University of California, Livermore, CA, 1977.

Vernon, R. H. Metamorphic Processes, J. Wiley and Sons, New York, 247 pp., 1975.

Wackerle, J. Shock-wave compression of quartz, J. App. Phys., 33, 922-937, 1962.

Walsh, J. M. and R. H. Christian. Equation of state of metals from shock wave measurements, Phys. Rev., 97, 1544-1556, 1955.

Wang, C. Phase transitions in rocks under shock compression, Earth Planet. Sci. Lett., 3, 107-113, 1967.

Wang, C. Constitution of the lower mantle as evidenced from shock wave data for some rocks, J. Geophys. Res., 73, 6459-6476, 1968.

Wang, C. Density and constitution of the mantle, J. Geophys. Res., 75, 3264-3284, 1970.

Wang, C. Temperature in the lower mantle, Geophys. J. R. astr. Soc., 27, 29-36, 1972.

Wegner, M. W. and J. M. Christie. Preferential chemical etching of terrestrial and lunar olivines, Contrib. Min. Pet., 43, 195-212, 1974.

White, E. W. Applications of soft x-ray spectroscopy to chemical bonding studies with the electron microprobe, in: Microprobe Analysis, (C. A. Andersen, ed.) J. Wiley and Sons, New York, pp. 349-369, 1973.

Zel'dovich, Y. B. The theory of new phase formation; cavitation, Acta. Physicochim, 18, 1-22, 1943.

TABLE I

Shot No.	Sample No.	Orientation	Thickness (mm)	Peak Pressure (GPa)	Initial Pressure* (GPa)	Impact Velocity (km/s)	Flyer Plate
453	OL-13	[100]	0.292	15.9	11.5	2.650 ±0.001	Lexan
451	OL-12	[100]	0.254	21.7	15.5	1.03** ±0.10	SS 304
431	OL-04	[010]	0.295	31.5	22.1	1.421 ±0.002	SS 304
429	OL-11	[100]	0.193	40.8	28.1	1.34 ±0.01	W
388	OL-03	[010]	0.314	53.6	36.2	1.68 ±0.01	W
339	OL-02	[010]	0.293	56.3	37.9	1.75 ±0.01	W
457	OL-06	[010]	0.221	59.7	40.1	1.835 ±0.001	W
460	OL-07	[010]	0.287	75.8	49.4	2.22** ±0.10	W

* Multiple wave structures neglected.

** Velocity measurement uncertain for these experiments: quoted velocities are based on the empirical correlation of powder loads with velocity.

FIGURE CAPTIONS

Figure 1: Starting material: Sample 03. Views of the central portion of the sample disc used in the experiment, before shocking (crossed polarizers); note the low angle boundaries.

Figure 2: Stress-time histories with peak pressures (and indicated error bars) calculated from the impact velocities given in Table 1 using standard impedance matching calculations. Stress rise is derived from iterative impedance mismatch calculations for a one-dimensional geometry [e.g., Al'tshuler, 1965] based on the Hugoniot of dunite [McQueen et al;, 1967], while shock duration is determined by rarefaction catch-up from the back of the impactor plate [Fowles, 1960]. The calculations are approximate in that they neglect the formation of multiple wave structures, the interactions due to edge effects, and (small) thermal differences between first and multiple Hugoniot states [e.g. Neal, 1977].

Figure 3: a) Blocky fracturing in Sample 13 (15.9 GPa: plane polarized light). b) Bright field TEM image of short dislocation segments in a moderately deformed portion of Sample 13.

Figure 4: Mosaicism in Samples 11 (a) and 04 (b) (40.8 and 31.5 GPa). Optical micrographs between crossed polarizers.

Figure 5: a) Bright field TEM image of Sample 11 (40.8 GPa). b) Bright field TEM image of Sample 06 (59.7 GPa); note the transition from relatively undeformed (lower right hand corner) to more highly deformed (upper left hand corner) in (b). c) Dark field TEM image of a relatively highly dislocated region in Sample 06.

d) Electron diffraction pattern showing asterism; this denotes that the crystal is "blocky" on a very fine scale within the ∿1 μm diameter of the selecting aperture (Sample 06).

Figure 6: a) Sample 11 (40.8 GPa) under crossed polarizers showing fractured zones (arrows). b) Sample 03 (53.6 GPa; plane polarized light) with arrows indicating the approximately perpendicular orientations of the two sets of microfractures. c) Sample 07 (about 75 GPa): note the "wavy" appearance of many of the fractures (arrow). Sets of microfractures are also evident. d) Scanning electron micrograph of the face of a fracture (0.28 mm vertical dimension) formed in a sample disc (top surface marked S) of single crystal olivine resting against one wall of the container within which it was shocked (C).

Figure 7: Infrared absorption spectrum of shocked (solid line; Sample 06, 59.7 GPa) and unshocked (dashed line) samples. All shocked samples have identical spectra at this scale and show no evidence of any phases other than olivine.

Figure 8: Hugoniot equation-of-state data for Twin Sisters Dunite [Fo 90: McQueen et al., 1967] in a) the pressure (P)-volume (V) and b) the shock-wave velocity (U_S) - particle velocity (u_P) planes. For comparison, a third-order finite strain adiabat (P_{3S}) and theoretical Hugoniot (P_{3H}) for olivine are shown in (a) along with data of Ahrens and Petersen [1969] which indicate the Hugoniot Elastic Limit (HEL). The "mixed-phase" region is located between A and B in both figures.

Figure 9: Hugoniot data for olivine compared with the theoretical Hugoniot predicted for a 2 + 1 dimensional closest packed (CP) and randomly closest packed (RCP) model of olivine (see text). For comparison, Hugoniots of olivine corresponding to the (CP) packing efficiencies illustrated by Al_2O_3 and BeO are shown, as are zero-pressure densities of slightly less than ideal packing efficiencies corresponding to kyanite and the present 2 + 1 CP/RCP model. Shock-wave data on Al_2O_3 [McQueen and Marsh: quoted in Birch, 1966] and BeO [in Van Thiel, 1977] have been transposed to olivine densities with equivalent oxygen packing. Initial densities of high-pressure phases of olivine which have previously been derived from the olivine Hugoniot data [e.g., Ahrens et al., 1969; Davies and Gaffney, 1973] are also indicated.

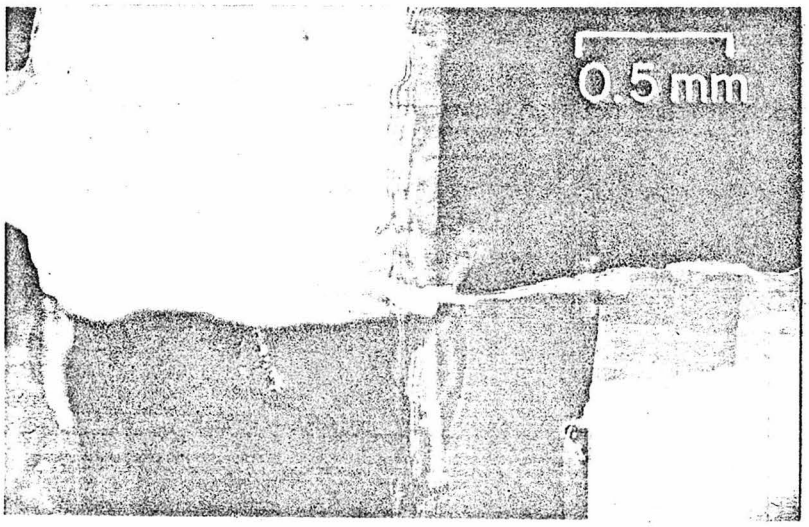

Figure 1.

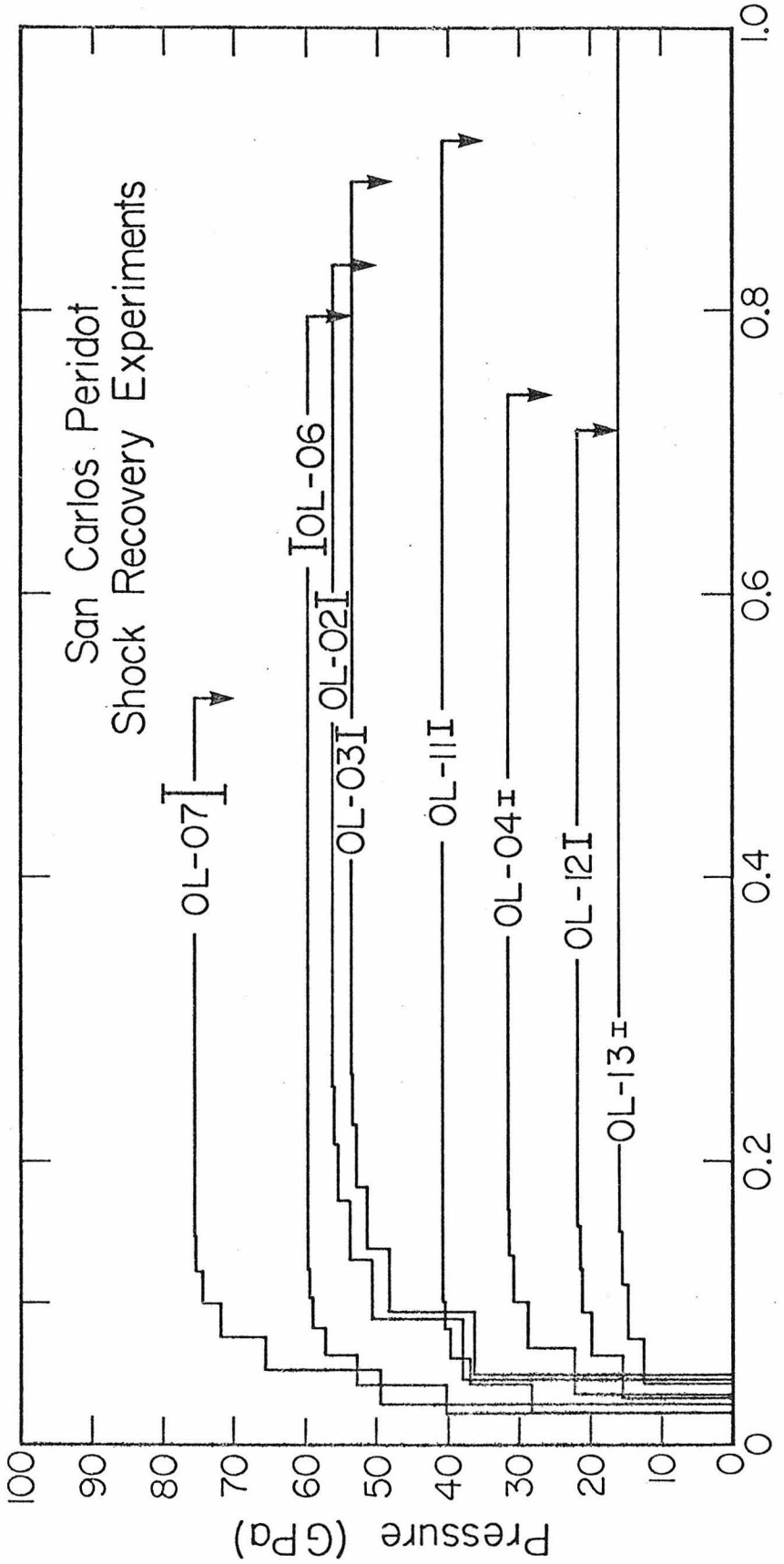
San Carlos Peridot
Shock Recovery Experiments
OL-07
OL-06
OL-02
OL-03
OL-11
OL-04
OL-12
OL-13
Pressure (GPa)
Time (μs)
0
10
20
30
40
50
60
70
80
90
100
0.2
0.4
0.6
0.8
1.0

Fig. 2

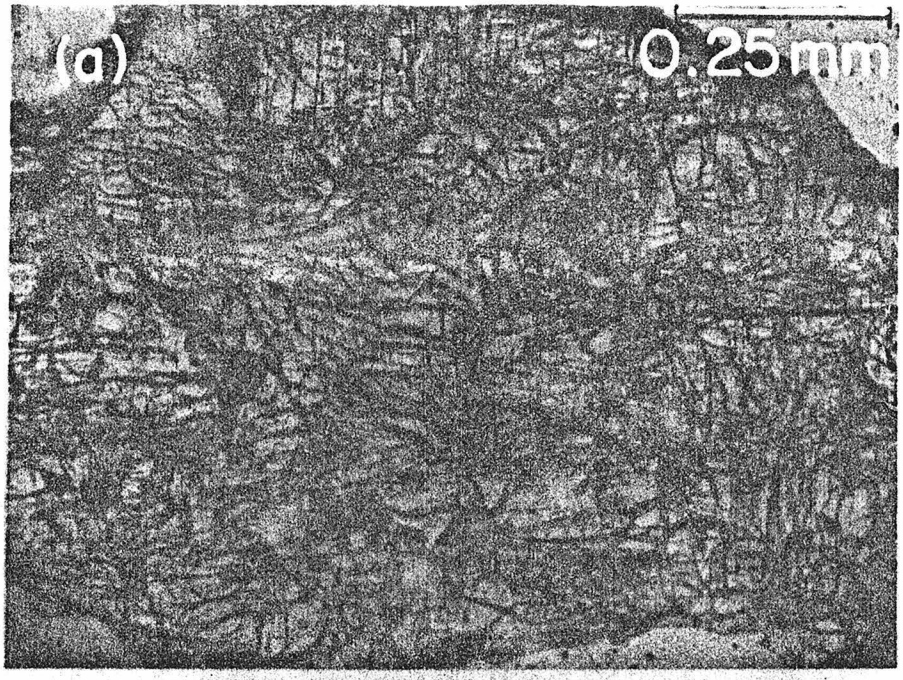

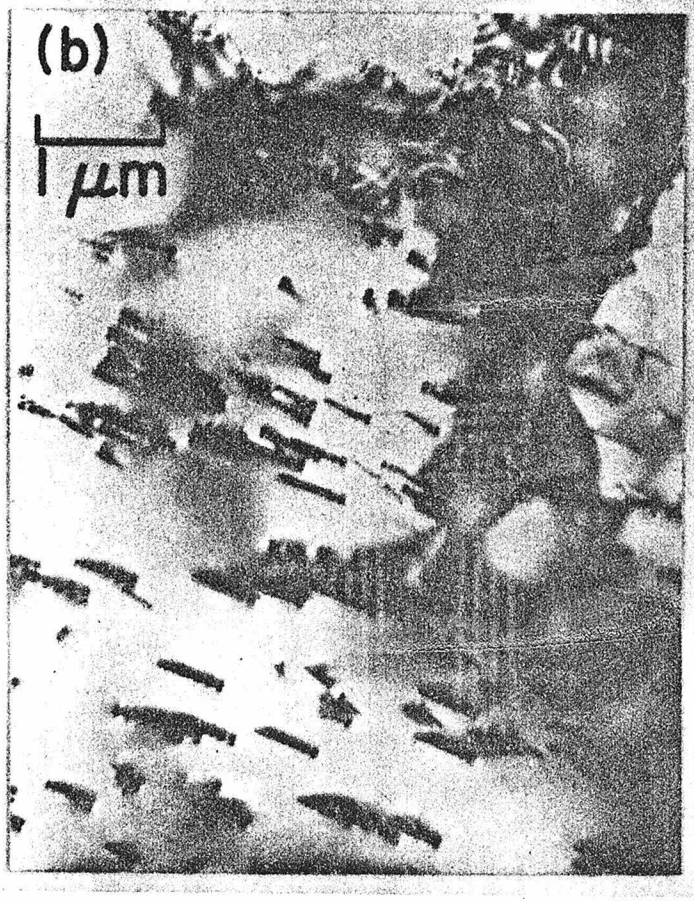

Figure 3.

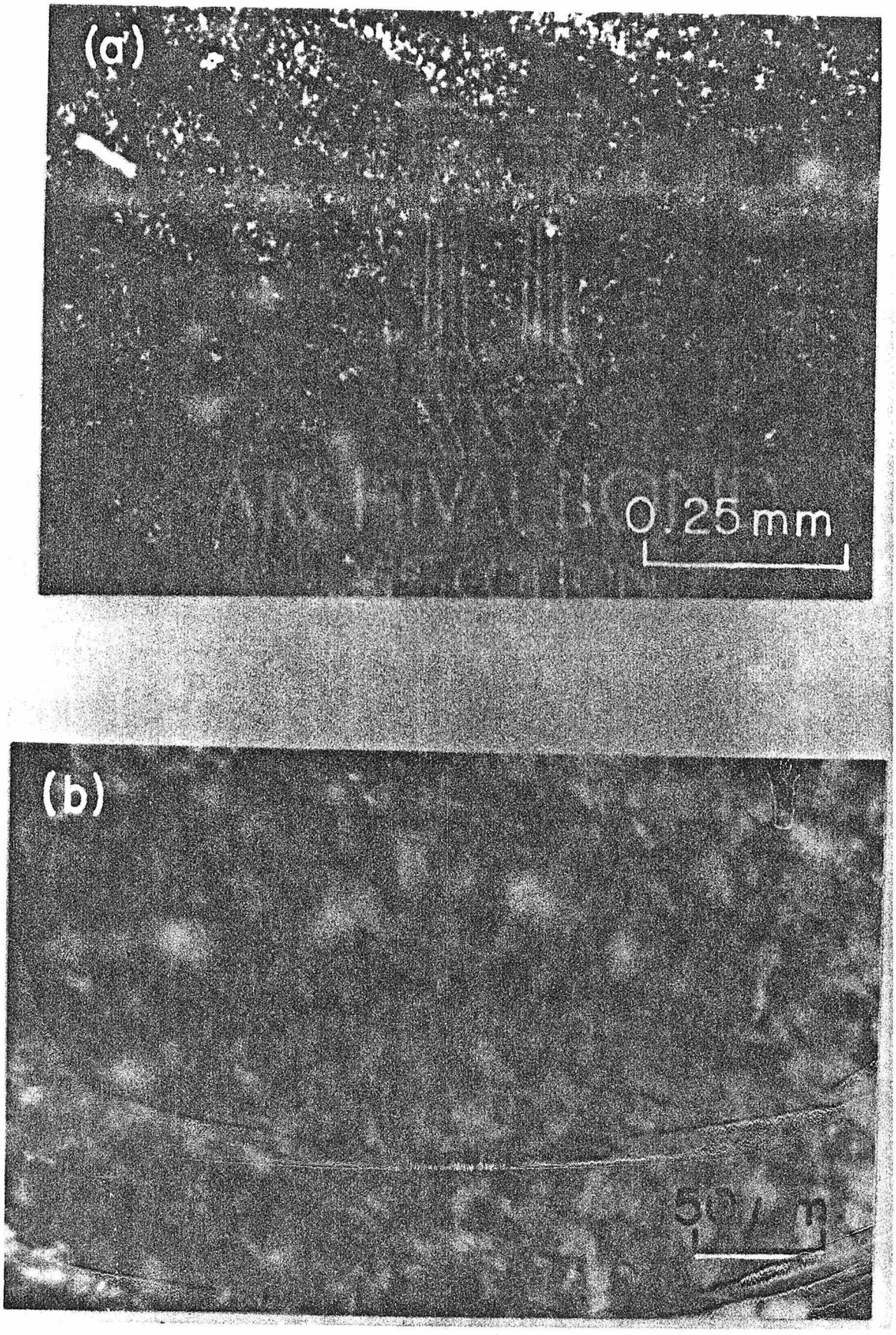

Figure 4.

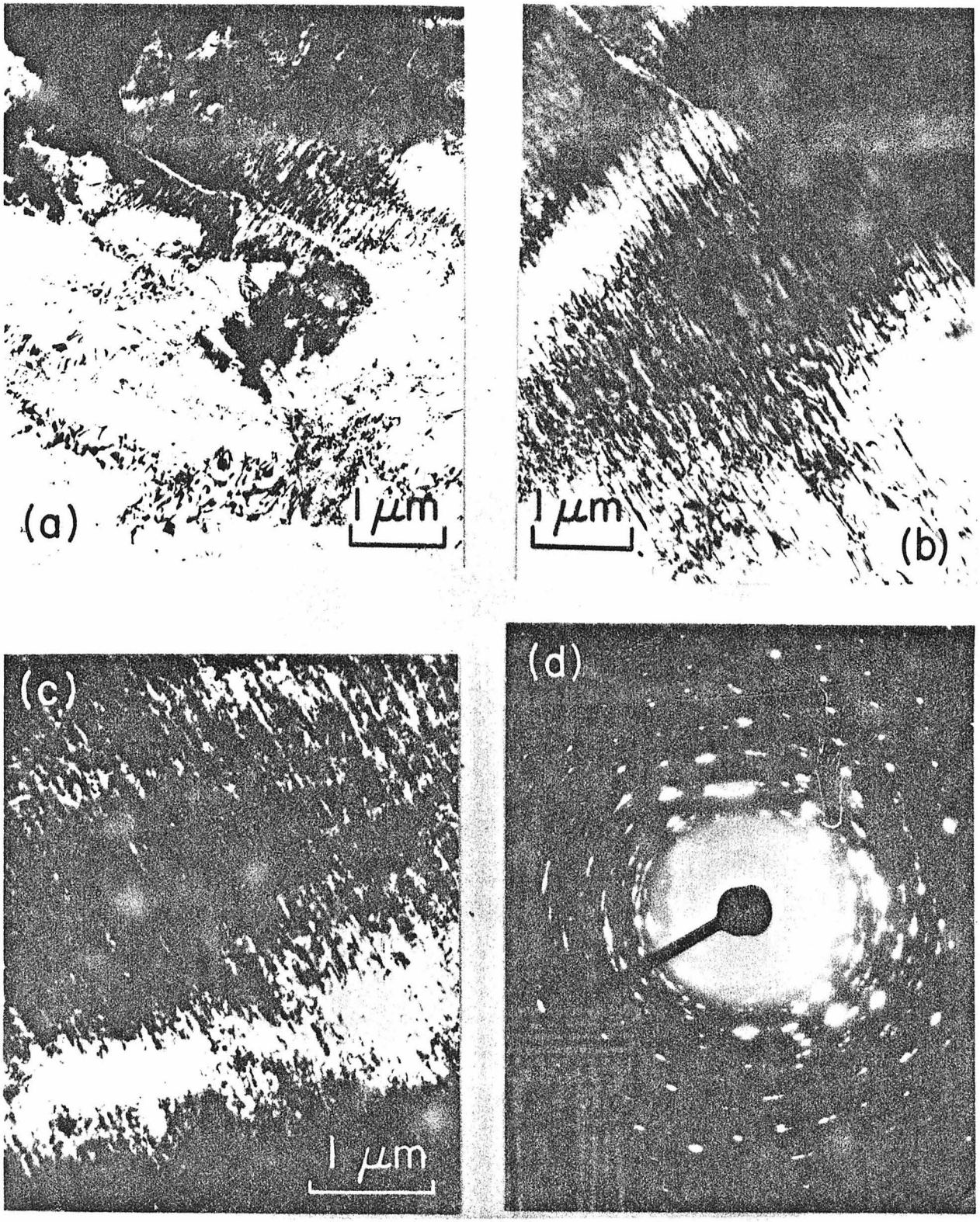

Figure 5.

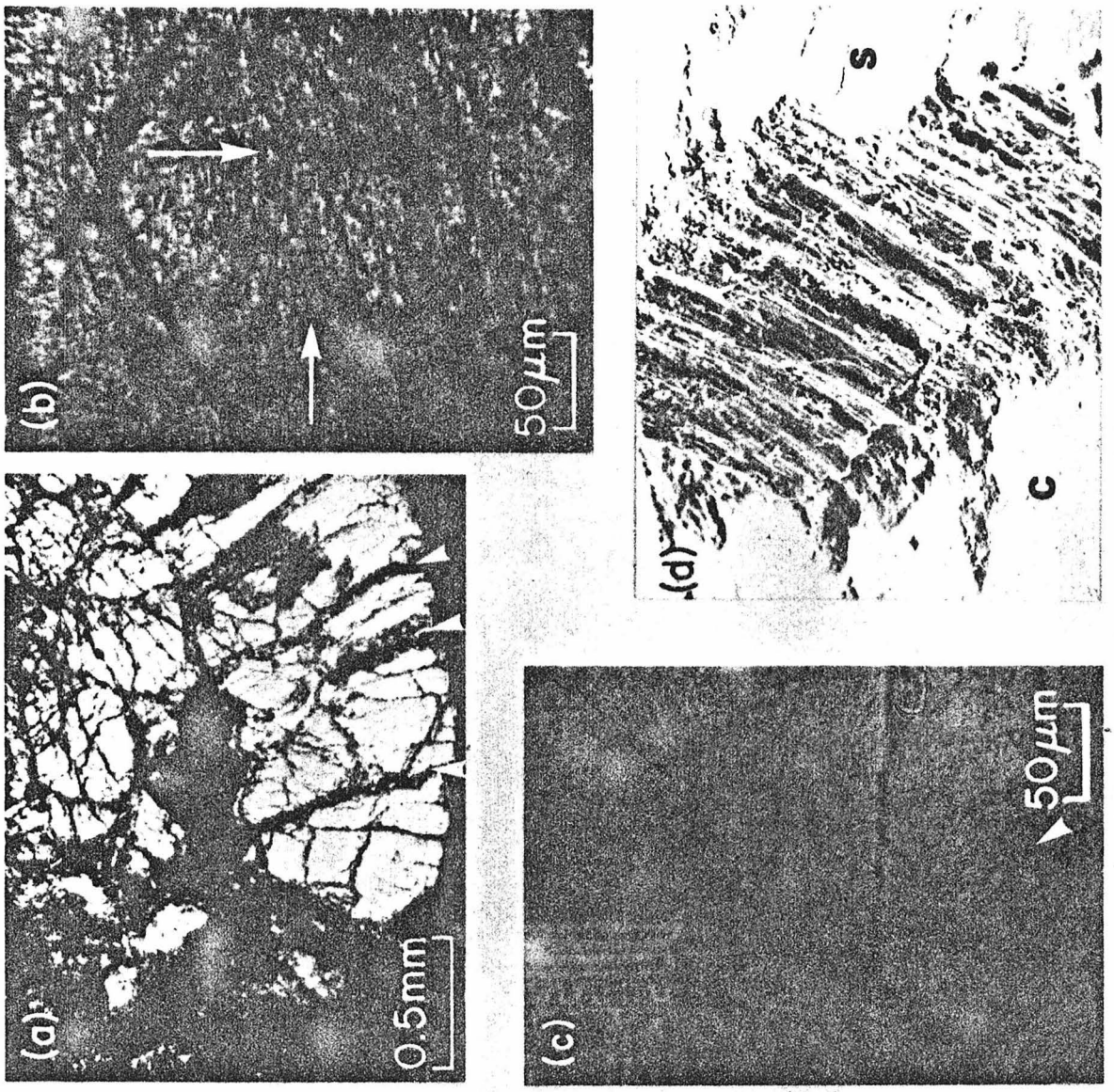

Fig. 6

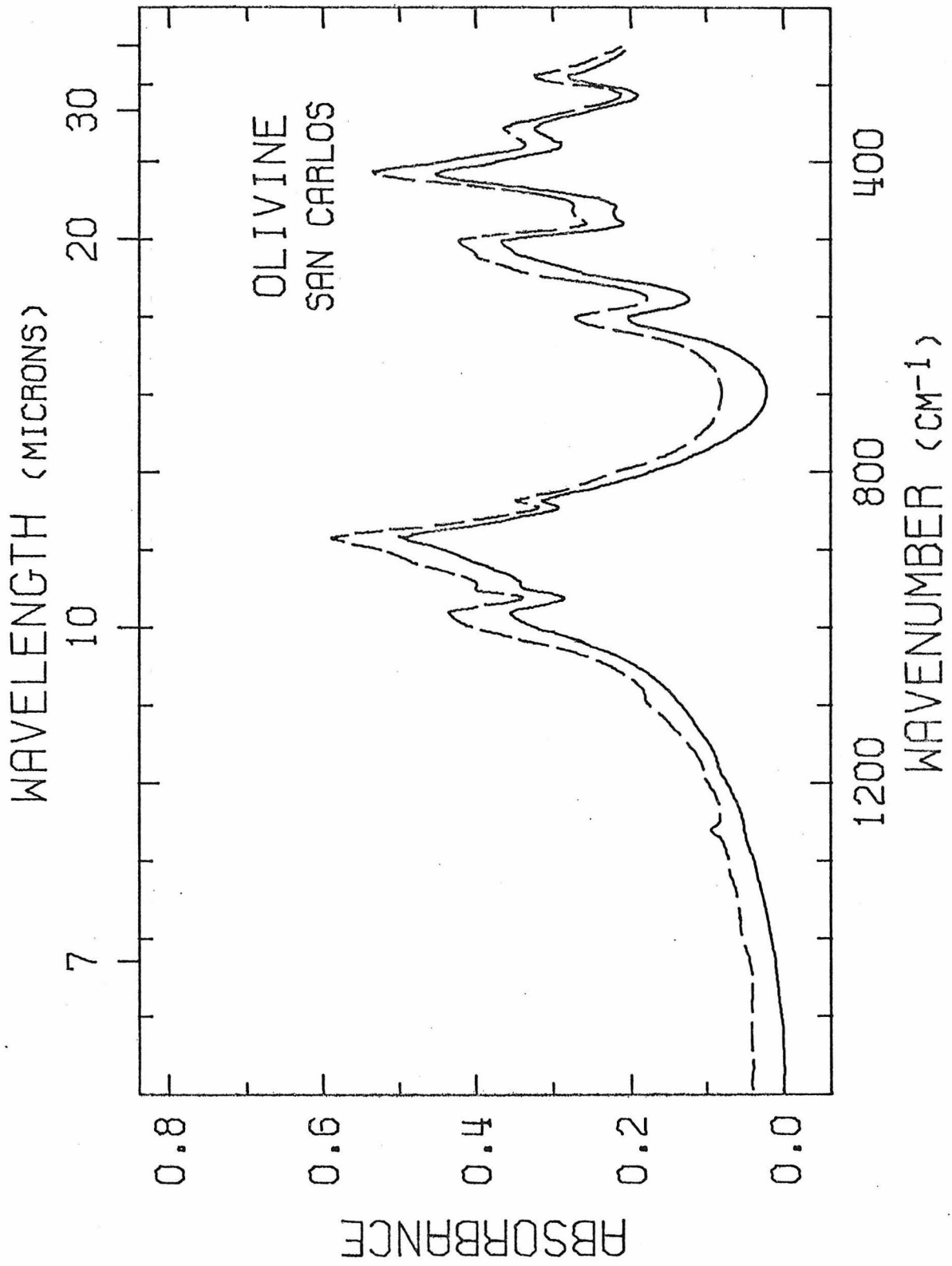
OLIVINE
SAN CARLOS
WAVELENGTH (MICRONS)
7
10
20
30
WAVENUMBER (CM-1)
1200
800
400
ABSORBANCE
0.0
0.2
0.4
0.6
0.8

Fig. 7

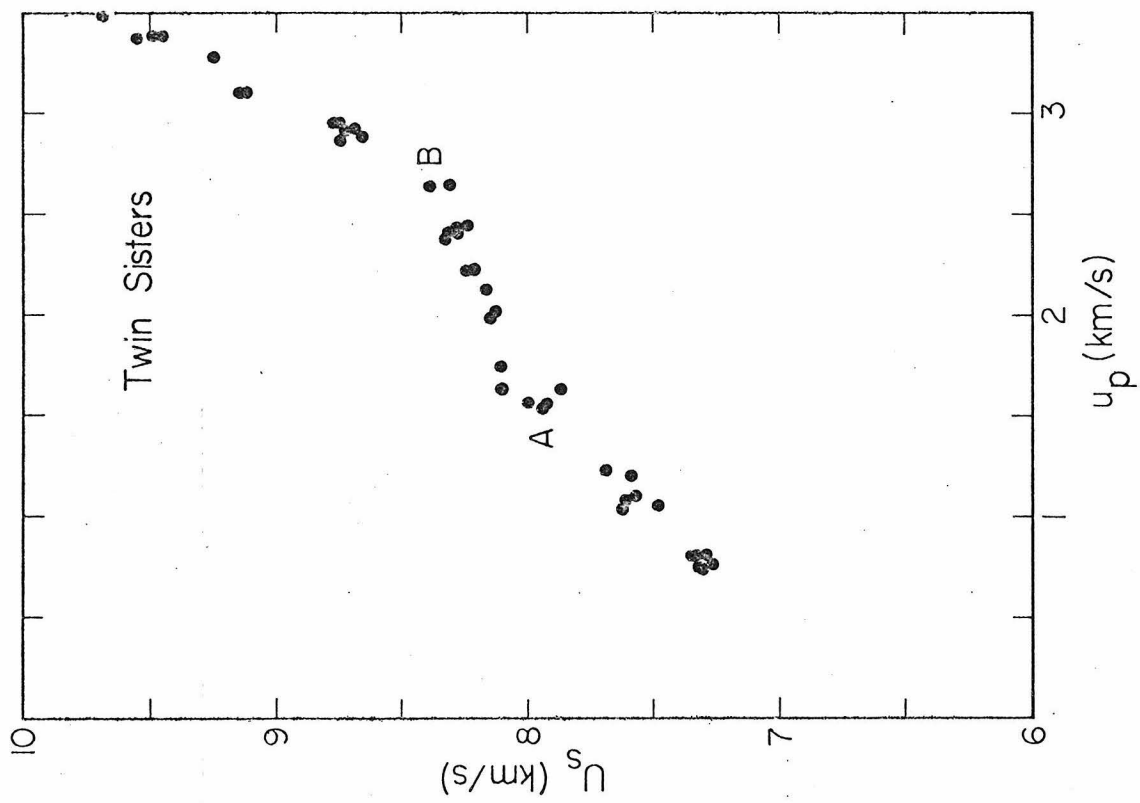
Twin Sisters
B
A
U_s (km/s)
u_p (km/s)

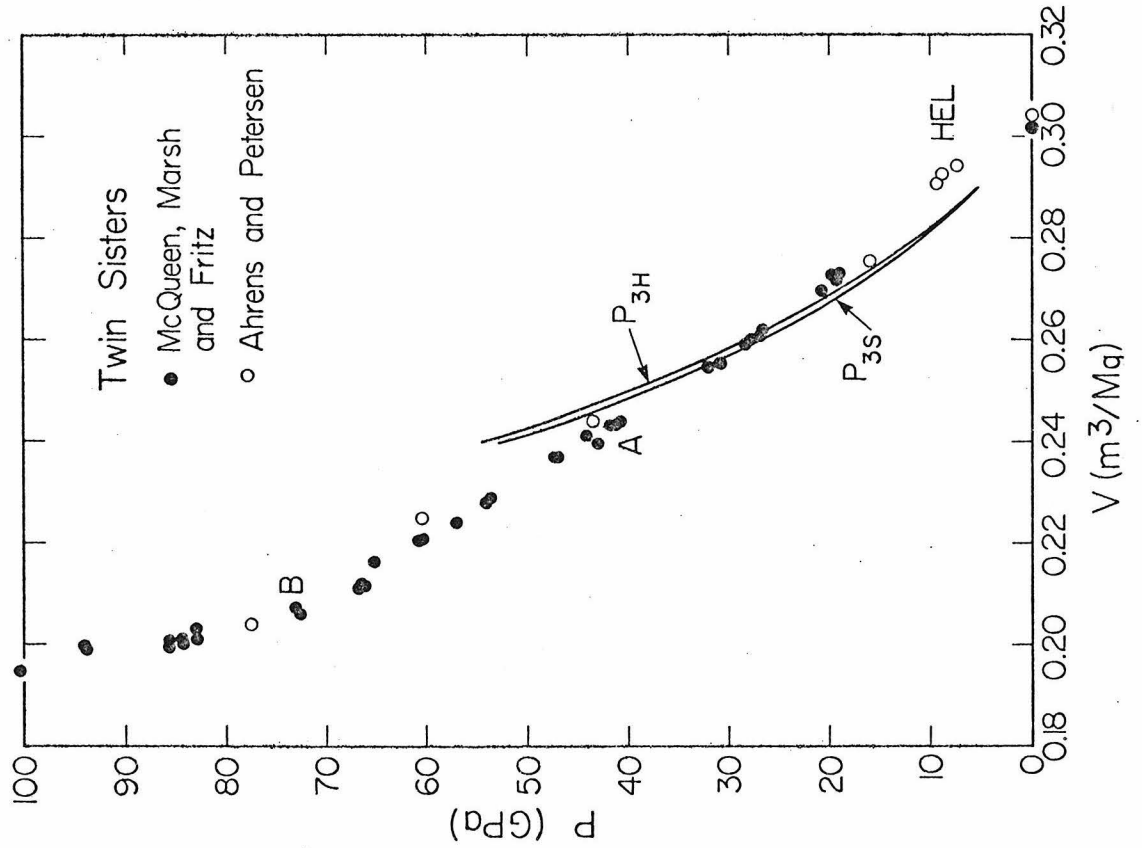
Twin Sisters
McQueen, Marsh and Fritz
Ahrens and Petersen
B
A
P_{3H}
P_{3S}
HEL
P (GPa)
V (m^3/Mg)

Fig. 8

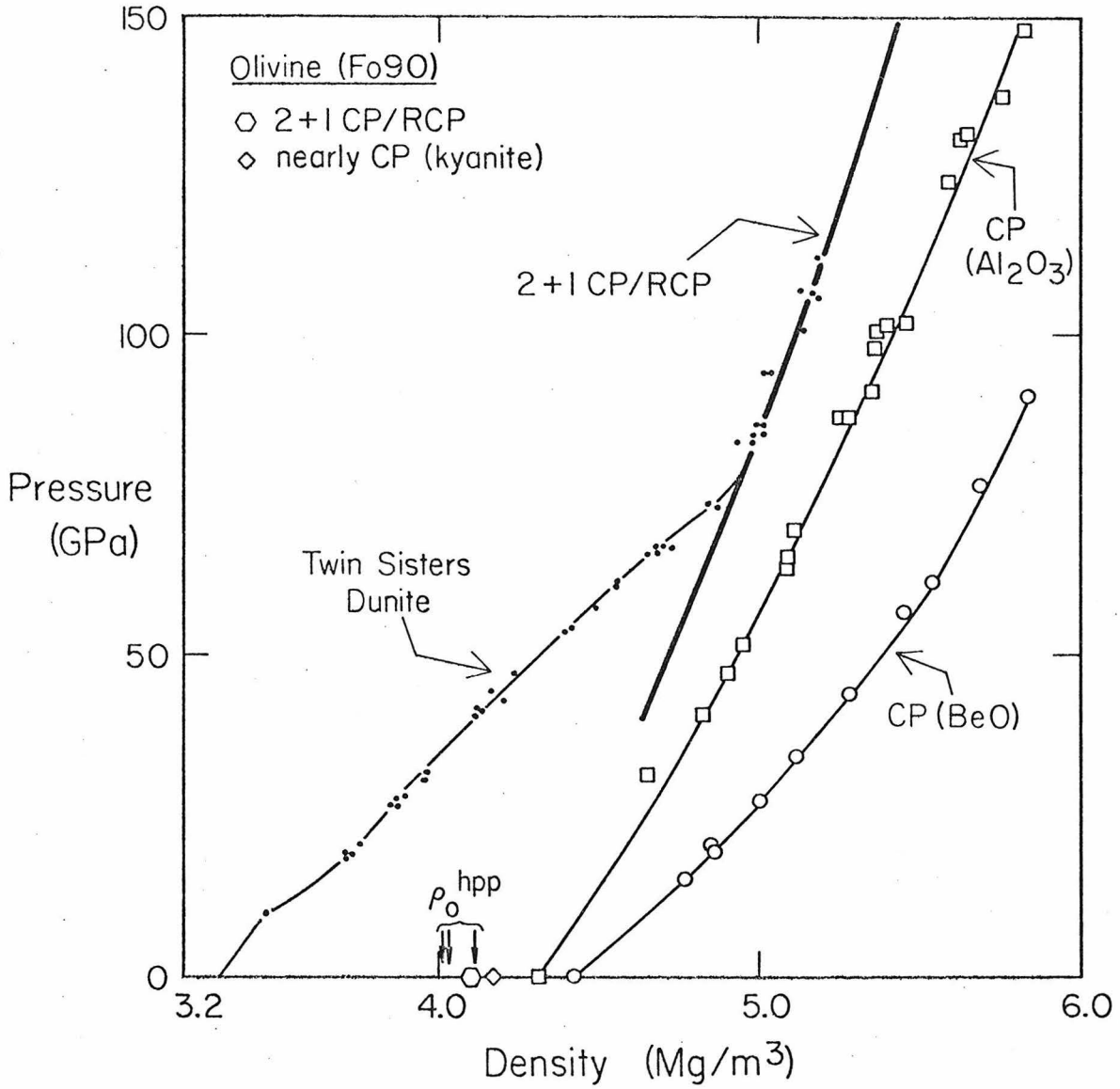
150
100
50
0
Pressure
(GPa)
Olivine (Fo90)
2+1 CP/RCP
nearly CP (kyanite)
2+1 CP/RCP
CP
(Al2O3)
Twin Sisters
Dunite
CP (BeO)
ρ0 hpp
3.2
4.0
5.0
6.0
Density (Mg/m3)

Fig. 9

Chapter 11

CONVECTION, COMPOSITION AND THE THERMAL STATE OF THE LOWER MANTLE

Abstract

We present a thermal model for the lower mantle which is constructed from petrologically derived estimates of the temperature in the transition zone and from an adiabat based on the thermal properties of MgO and SiO_2 measured at high pressures. Superadiabatic contributions to the geotherm through the lower mantle, including those from possible phase transformations but excluding those from thermal boundary layers, are negligibly small. A thermal boundary layer is required at the base of the mantle in order to satisfy our estimate of the lowest possible temperature in the core (about 2800K); its thickness of about 100 km is well constrained. Even so, our model suggests that we either require a significantly larger heat flux from the core than has been considered reasonable (> 50 mWm^{-2}) or we require the presence of a further thermal boundary layer within the lower mantle in order to arrive at more likely core temperatures (about 3200-3500K). This latter alternative appears the more plausible, and such a boundary layer requires a barrier to convection. Guided by the present seismological evidence, we suggest that a thermal boundary layer is associated with a chemical discontinuity either at the top of the lower mantle or near its base (D" region). If seismological data require the D" layer to be significantly thicker than about 100 km, this is support for a chemically distinct D" region with multiple thermal boundary layers. Otherwise, the results of this study

suggest that the upper and lower mantle may be chemically distinct, hence precluding whole-mantle convection.

I. INTRODUCTION

The composition and dynamic state of the earth's lower mantle have evoked considerable attention recently, in particular with reference to arguments being presented for or against mantle-wide convection [Davies, 1977; Jordan, 1977; O'Connell, 1977; Richter and McKenzie, 1978]. Similarly, it has been argued that seismological data, combined with measured and extrapolated physical properties of candidate minerals, do or do not require a difference in bulk chemical composition between the upper and lower mantle [e.g., Birch, 1961; Press, 1968, Anderson, 1968, 1977; Anderson, et al., 1972; Mao, 1974; Davies, 1974; Ringwood, 1975; Burdick and Anderson, 1975; Watt, et al., 1975; Liu, 1979]. These two questions are, of course, coupled in that whole-mantle convection is not compatible with a compositional change between the upper and lower mantle.

We propose a different approach for addressing this problem by examining the thermal state of the lower mantle, and the ensuing implications for convection and chemical composition throughout the mantle. We find that the temperature gradient through the lower mantle is well enough constrained to indicate the existance of a thermal boundary layer at the base of the mantle. Furthermore, our preferred solution requires a second boundary layer elsewhere within the lower mantle, most likely either close to its base or associated with the transition zone. This strongly suggests the existence of a chemical transition which is a barrier to convection either at the top of the lower mantle or in a complex region at its base. A thermal structure with only one thermal boundary layer within the lower mantle (presumably at the core-mantle

boundary) is only acceptable if the outer core is at a lower temperature than has previously been estimated or if the heat flux from the core is significantly larger than has been considered reasonable.

II. ADIABATIC GRADIENTS

We examine the following equation for the increase in temperature from the top of the lower mantle (T(700)) to the top of the outer core (T(2900)):

$$T(2900) - T(700) = [\Delta T_S + \bar{\beta}\Delta z] + \Sigma\ \Delta T(P.T.) + \Sigma\ \Delta T(B.L.). \qquad [1]$$

The bracketed term contains the nearly adiabatic temperature rise through the lower mantle, appropriate to a convecting and homogeneous system ($\bar{\beta}$ is the average superadiabatic gradient and Δz is the thickness of the lower mantle). The remaining terms allow for temperature increases associated with regions of phase transformations ($\Delta T.(P.T.)$) and thermal boundary layers ($\Delta T(B.L.)$), respectively [cf; Verhoogen, 1965; McKenzie, et al., 1974]. We constrain first the left hand side of [1] and then evaluate each term on the right hand side in succession.

We presume throughout this discussion that the lower mantle is convecting, as is strongly indicated by the fact that it is very nearly adiabatic throughout [e.g. Jordan and Anderson, 1974; Dziewonski, et al., 1975; see also Stacey, 1977a]. Since an adiabatic gradient is not a steady solution to the conduction equation, it can exist only under very special circumstances and the most likely interpretation is that the planetary interior is adiabatic due to sufficiently vigorous convection.

The temperature at the top of the outer core is poorly constrained, however we estimate that a minimum plausible value is about 2800K. We

have estimated both liquidi and solidi for the Fe-S system under core conditions based on extrapolations of Usselman's [1975a,b] high-pressure data for the eutectic and Liu's [1975] analysis of the melting curve of iron, corrected upward slightly to conform with the nonzero shear modulus observed in iron at 180 GPa under shock [Al'tshuler, et al., 1971]. Taking Ahrens' [1979] bounds on the maximum sulfur content allowed in the core and assuming that the core is at a temperature at least as high as the mean between eutectic and liquidus, we arrive at a lowest estimate of about 2800K (under these conditions the outer core would already be a slurry consisting of at least 5-10% crystals according to our extrapolations). Our bound of 2800K is substantially less than most estimates of the temperature in the core [cf. Jacobs, 1975], and is less than or comparable to previously suggested lower bounds [e.g., Birch, 1972; Usselman, 1975b]. Furthermore, we have only considered sulfur as the light element in the outer core: sulfur is likely to decrease the melting temperature of iron significantly more than other plausible candidates [e.g., Brett, 1976], in particular oxygen which is currently considered a strong candidate [Ringwood, 1978]. In this case a minimum estimate for T(2900) would be above 3000-3200K, taking the zero pressure phase equilibria [Darken and Gurry, 1953] and assuming that the effect of pressure in the Fe-O system can be scaled to that in the Fe-S system [see also Ringwood, 1978]. Thus a more plausible value for T(2900) might lie between about 3200 and 3500K, in accord with recent analyses [e.g., Stacey, 1972, 1977b; Verhoogen, 1973; Usselman, 1975].

The temperature at the base of the transition zone can best be constrained petrologically, yielding estimates of about 1900-2000K for

T(700) [Ahrens, 1973; Akimoto, et al., 1976]. For example, taking the transition from olivine to β-spinel as beginning at about 390 km depth [Burdick and Helmberger, 1978] provides a temperature "fixed-point" of about 1700K [e.g., Akimoto, et al., 1976]. This implies a temperature of about 2000K at the base of the transition zone, for plausible values of thermal expansion, specific heat and Clapeyron slope [cf. Verhoogen, 1965; Mao, et al., 1969; Schubert, et al., 1975; Navrotsky, et al., 1979]. Because of the sensitivity of the estimated temperatures on the detailed phase equilibria as well as the uncertainties in our estimates of the thermochemical properties in the transition zone, our values for T(700) are somewhat uncertain, perhaps by as much as 100-200K. However a recent, in situ determination of the olivine-spinel phase boundary [Akimoto, et al., 1977] suggests that our values of temperature may, if anything, be high. Furthermore, independent evaluations of the temperature at the top of the lower mantle are very compatible with our result (e.g., Banks, 1969; Graham and Dobrzykowski, 1976; Watt and O'Connell, 1978]. Thus, we estimate the difference in temperature between the top of the lower mantle and the outer core to be no smaller than 800K, and more likely of the order of 1300K.

If we assume, initially, that the lower mantle is homogeneous (in phase and composition) the bracketed term in [1] should yield the rise in temperature from top to bottom of the lower mantle. Following Jeffreys [1930], dynamic stability requires a Rayleigh number less than about 10^3, and this provides an estimate of the superadiabatic temperature increase through the lower mantle of $\overline{\beta\Delta z} \sim$ 1K. Here, the constraints currently available for the viscosity [Peltier and Andrews, 1976; see

Table 1 for representative parameter estimates] have been used and this estimate is only accurate to about one order of magnitude. In any case, the superadiabatic gradient is negligibly small.

The adiabatic temperature gradient is given by the Grüneisen parameter, $\gamma = \left(\frac{\partial \ln T}{\partial \ln \rho}\right)_S$, as a function of density (ρ). We have determined γ for the lower mantle from experimental data on MgO and SiO_2 throughout the pressure range of interest. Shock-wave data on porous (or amorphous) and nonporous samples yield values of γ directly as a function of pressure or density [see Carter, et al., 1971, for example]; for MgO and SiO_2 these values are quite similar as a function of pressure [data base: Wackerle, 1962; Al'tshuler, et al., 1965; Hart and Skidmore, 1965; Anderson, 1967; Jones, et al., 1968; Ahrens and Rosenberg, 1968; Carter, et al., 1971; Trunin, et al., 1970, 1971; Podurets, et al., 1976]. Figure 1 shows the values of γ derived from these data for mixtures of the oxides corresponding to olivine and pyroxene stoichiometry. The differences between these two cases are not resolvable in this study. Taking MgO and SiO_2 at high pressures to be representative of the earth's deep interior, this supplies the ratio of temperatures at the top and bottom of the lower mantle along an aidabat by applying seismologically determined density profiles [e.g., Dziewonski, et al., 1975]. Consequently ΔT_s, the adiabatic temperature increase across the lower mantle, corresponds to about 460K (with an average $\bar{\gamma} = \frac{\Delta \ln T}{\Delta \ln \rho} \sim 0.88$), and the bracketed term in [1] amounts to no more than about 500K. This is approximately 300K less than even our limiting estimate of the left hand side of [1].

That our estimate of the Grüneisen parameter is similar to those resulting from independent analyses is shown in Figure 1. The different estimates do not strongly affect ΔT_S in that increasing $\bar{\gamma}$ from 0.88 to 1.0 raises the ratio of temperatures at the top and bottom of the lower mantle by only 3%. However, our analysis has the advantage of being constrained by experimental data measured at the appropriate pressures.

III. SUPERADIABATIC GRADIENTS

In the discussion above we have estimated the temperature at a depth of 700 Km, a lower bound on the temperature at the core-mantle boundary and the Grüneisen parameter, which specifies the adiabatic gradient between these two points. Our results are illustrated in Figure 2 and it is apparent that a single adiabat does not join the two temperature estimates. Therefore one or more regions of superadiabatic gradients are likely to exist between 700 km depth and the core-mantle boundary. The required superadiabatic temperature increase is so large as to further validate our initial assumption that convection is inevitable. We now explore how such superadiabatic gradients can arise in a convecting mantle.

If regions of phase transformation exist within the convecting lower mantle, they could contribute superadiabatic temperature increases, depending on the enthalpies of reaction involved. The occurrence of phase transformations has indeed been inferred from several seismological studies [e.g. Kanamori, 1967; Johnson, 1969; Vinnik and Nikolayev, 1970; Wright and Cleary, 1972; Butler and Anderson, 1978] and, although the evidence is still open to question [e.g., Wiggins, et al., 1973], as many

as five seismic discontinuities have been identified [Johnson, 1969]. Whether these transitions are univariant or polyvariant, the additional change in temperature associated with each transformation is very nearly [Verhoogen, 1965]

$$\Delta T(P.T.) \sim \frac{T}{C} \left(\frac{dP}{dT}\right) \Delta V,$$

where T is the temperature, C an appropriate (averaged) specific heat, $\frac{dP}{dT}$ the Clapeyron slope and ΔV the volume change associated with the transformation. The inferred lower mantle discontinuities are known to be small (velocity jumps less than about 1%) and we take $\Delta V \sim 2\%$ as a generous upper limit. For typical values of the Clapeyron slope (2-3 MPa K^{-1}) we find $\Delta T(P.T)$ no larger than 20-30K at each transition, and hence the total contribution from phase transformations to the temperature change throughout the lower mantle amounts to no more than about 100-150K, as shown in Figure 2. Of course, if smaller (or negative) Clapeyron slopes are considered for any of the inferred transitions (as might be appropriate for transformations involving disproportionation) the total $\Delta T(P.T.)$ is smaller than our calculated values (or even negative). Clearly, the effect of phase transformations is insufficient to reconcile our two temperature estimates and we are therefore forced to consider further sources for superadiabatic temperature increases within the lower mantle.

An obvious place for non-adiabatic gradients would be immediately above the core-mantle boundary if a significant fraction of the earth's total heat flow is supplied to the mantle from the core. Heat flowing

out of the core will result in a thermal boundary layer at the base of the mantle and we need an appropriate convection model to estimate the characteristic thickness and temperature change across this boundary layer. One complication is that the required model will have to take into account the effects of compressibility and spherical geometry when applied to such a deep layer but to date these two properties have only been studied separately, and in the case of spherical geometry over a very limited parameter range. Nevertheless the existing results are sufficient to evaluate the way in which the boundary layers from incompressible, plane layer convection models will be modified.

We will first consider the boundary layers that are found in plane layer calculations which assume negligible compressibility, uniform viscosity and a surface heat flux of 5.85×10^{-2} Wm^{-2}, which is close to the average measured terrestrial heat flow. The material properties of the convecting material are given in Table 1. The resulting horizontally averaged temperature for three models of heating are given in Figure 3. When all of the heat is supplied from below, the averaged temperature structure consists of two equal boundary layers joined by an isothermal interior region. The characteristic boundary layer thickness δ is about 100 km and the associated temperature change $\Delta T(B.L.)$ is approximately 300K.

A simple boundary layer analysis [see McKenzie, et al., 1974] can be used to determine the dependence of the boundary layer properties on the heat flux and material properties of the layer:

$$\delta \propto \left(\frac{\rho C_p \kappa^2 \nu}{g\alpha} \right)^{1/4} F^{-1/4} \qquad [2]$$

and

$$\Delta T(B.L.) \propto \left(\frac{\nu}{g\alpha\kappa^2 \rho^3 C_p^3} \right)^{1/4} F^{3/4}, \qquad [3]$$

where the symbols and their typical values for mantle materials are given in Table 1. Equations [2] and [3] are consistent with the idea that the thermal boundary transmits the flux F conductively:

$$\rho\ C_p\ \kappa \frac{dT}{dz} \sim \rho\ C_p\ \kappa \frac{\Delta T}{\delta} = F$$

An important point regarding the boundary layer properties is that uncertainties in the flux across a given boundary layer affect the estimated temperature change much more than the boundary layer thickness. This effect can be seen in Figure 3, which includes a case in which half the heating is from below and half from within (by internal heat sources). The thickness of the lower boundary layer is not much different than in the case fully heated from below, but the temperature change is substantially reduced. The fully internally heated case (i.e., no flux from the core) is also shown in Figure 3 to illustrate the absence of any lower boundary layer under such conditions.

The next question is how does spherical geometry affect the results given above? A useful calculation relevant to this question is by Young [1974] who considered finite amplitude convection between isothermal shells. Figure 4 compares the horizontally averaged thermal structure of convection in a spherical shell to that of convection between plane isothermal boundaries. The spherical case has a relatively low Rayleigh

number of about five times critical and a Prandtl number of five, which means that inertial terms in the momentum equation are not negligibly small. The plane layer case has a somewhat larger Rayleigh number of about 15 times critical and the Prandtl number is assumed to be infinitely large. The two calculations thus differ in more than geometry alone but the major effect on the thermal boundary layer structure does appear to be simply related to the geometric differences. The plane layer case has symmetric boundary layers. In the spherical case both the inner and the outer boundaries transmit the same total amount of heat, but since they differ in surface area by a factor of about three, the heat flux per unit area is three times greater across the lower boundary. As one would expect from relations [2] and [3] this difference in heat flux has little effect on the boundary layer thickness but results in an almost three times greater temperature drop across the lower boundary layer. As a first approximation, the effect of spherical geometry can be taken into account by simply using the local heat flux for estimating boundary layer properties.

The effect of compressibility is illustrated in Figure 5. The incompressible temperature profile shown for reference is the same as in Figure 3 but now using a specific depth extent of 700 km. The thermal structure is taken from a recent study of convection in a compressible material by Jarvis and McKenzie [1979]. The importance of compressibility in such a calculation is measured by the ratio of the layer depth d to the thermal scale height H_T ($H_T = C_p/g\alpha$). This scale height is the vertical distance a parcel of material must be displaced for its temperature to change by a factor e due to adiabatic compression. The

case used to illustrate the effect of compressibility on the average thermal structure assumes $d/H_T = 0.5$, which results in a reasonably large effect. Comparing the two calculations one can see that the interior temperature is no longer constant in the compressible case, and in fact the interior temperature gradient is found to be almost exactly adiabatic as we have taken it to be in our earlier discussion. The boundary layers are not very much affected by the compressibility because they are small compared to H_T. When considering the mantle, we argue that compressibility will not greatly affect the thermal boundary layers because $\delta/H_T << 1 (\delta \sim 100$ Km, $H_T \sim 5000$ Km) but the interior temperature gradient joining the boundary layers must be considered to be adiabatic.

Guided by the discussion on the effects of sphericity, we will assume that 1/4 of the total terrestrial heat flow arises originally in the core. The heat flow per unit area out of the core is then almost exactly equal to the surface heat flow and we expect, based on the arguments given above, that the boundary layer at the base of the mantle will be about 100 km thick and with a temperature change of approximately 300K. A smaller flux from the core would result in a smaller boundary layer, both in thickness and in superadiabatic temperature gain (equations [2] and [3]). Similarly, because we have ignored the temperature dependence of viscosity within the thermal boundary layer, our values of δ and ΔT may be somewhat large. However, taking our best estimate of the temperature at the top of the mantle, combined with our adiabatic gradient ($\pm$ contributions from phase transformations),

we can satisfy estimates of the minimum core temperature once we include a thermal boundary layer at the bottom of the mantle.

Independently, there is considerable evidence from seismology [see Cleary, 1974, for example] that the lowermost mantle [the D" region, extending to about 100-200 km above the core-mantle boundary: Bullen, 1949] is distinct from the overlying mantle and does not behave as an adiabatic and homogeneous region. The seismological anomalies corresponding to this region may therefore reflect the properties of a thermal boundary layer. We note that our estimated average temperature gradient through this layer ($\sim$ 3K km^{-1}) is probably smaller by a factor of 2 to 4 than the critical gradient required to make the gradients in density or seismic parameter vanish; however dispersion may significantly affect the seismologically observed velocities. Allowing the values quoted in Table 1 to vary within reasonable limits does not significantly change our estimate of the thermal boundary layer thickness, therefore if the seismological data require an anomalous layer thicker than about 100 km at the base of the mantle, this should be taken as evicence that something more than a single thermal boundary layer is present.

IV. CHEMICAL COMPOSITION

We have presented our best estimates of the temperature field through the lower mantle and have found that a solution can be derived which is in agreement with our minimum bounds on the core temperature. We are required, however, to insert a significant thermal boundary layer at the core-mantle interface (Figure 6a). This conclusion is not affected by the presence (or lack thereof) of phase transformations in

the lower mantle because we found that such transitions have a minor if not negligible effect on the overall geothermal gradient. We note that the thermal boundary layer near the earth's surface involves a much larger ΔT than that at the base of the mantle due largely to the temperature dependence of the effective viscosity.

Although this model is acceptable, it barely satisfies our bounds and we find it a rather extreme solution. If the lower mantle contains only one boundary layer, we estimate a temperature at the top of the core which is very low: about 2800-3000K. Such temperatures can not be considered unreasonable, however they are significantly lower than recent estimates [e.g., Verhoogen, 1973; Stacey, 1977b; Bukowinski, 1977] and especially previous results ranging between 4000 and 5000K (cf. Jacobs, 1975].

One possible factor might come from our having underestimated the heat flux from the core. Since $\Delta T(B.L.)$ is proportional to $F^{3/4}$ (equation [3]), a larger flux might allow a large enough temperature jump across the boundary layer to yield more plausible core temperatures. If the total flux from the core is comparable to the total heat flux through the earth's surface then our mantle temperatures are essentially compatible with our best estimates for the core. Such a large flow of heat from the core has, however, been generally considered unreasonable [e.g., Stacey, 1972; Verhoogen, 1973]: our value of 1/4 of the total output at the surface represents the maximum for steady state. This is within a factor of two of the estimated minimum [Stacey, 1972, 1977a] and is probably a fairly good estimate.

Thus, we find that if the lower mantle contains only one boundary layer at its base, the core must be at a significantly lower temperature than has previously been considered (essentially consistent with Tolland's [1974] conclusions). Alternatively, if a temperature of about 2900-3000K is considered to be too low for the outer core, the lower mantle must contain other boundary layers in addition to that at the core-mantle boundary. We conclude, therefore, that a second boundary layer within the lower mantle is suggested by our results up to this point.

From our analysis we can not constrain at which depth such a boundary layer might be found, although we can rule out the possibility that there could be many such boundary layers within the lower mantle since the resultant temperatures in the core would most likely be well above the melting point of iron at the inner core - outer core boundary.

We consider two depth, as shown in Figures 6b and c, as the most plausible locations for such a boundary layer based on seismological evidence: either at the transition zone or near the base of the mantle. The lowermost mantle, for example, is known to be anomalous and it has been inferred to contain significant inhomogeneities [e.g., Phinney and Alexander, 1969; Davies and Sheppard, 1972; Kanasewich, et al., 1973; Haddon and Cleary, 1974; Doornbos, 1976; van de berg, et al., 1978]. Thus, if layer D" is chemically distinct from the overlying mantle it could contain a boundary layer both at its top and bottom, and the temperature could increase by about 900K within the lowermost 200-300 km of the mantle, easily satisfying currently accepted temperatures for the core (Figure 6b). Such a model has, in principal, already been proposed

[e.g., Sacks and Beach, 1974; Snoke and Sacks, 1976] and it has been shown to be compatible with some of the seismological data. However, numerous difficulties remain [e.g., Husebye, et al., 1976; Miller, et al., 1977] and this model must be considered speculative at present. An attempt to explain the observations from the lowermost mantle, such as the velocity anomalies and apparent scattering, in terms of a simple (single) boundary layer could provide an important seismological test on the constitution of the lower mantle.

The remaining possibility is to place a thermal boundary layer at the top of the lower mantle (associated with the transition zone) as well as at its base (Figure 6c). Again, this possibility can not be critically assessed for lack of data, however it has important implications in that it precludes whole mantle convection. Such a boundary layer would most likely be associated with a change in chemical composition from upper to lower mantle [cf. Richter and Johnson, 1974] and is therefore consistent with suggestions to this effect. Indeed, if the independent arguments in support of a change in composition across the transition zone are correct [e.g., Anderson, 1968, 1977; Press, 1968; Anderson and Jordan, 1970; Anderson, et al., 1972; Burdick and Anderson, 1975; Liu, 1979], then a boundary layer would be expected at the top of the transition zone and temperatures through the lower mantle would be some 500-700 K higher than we have shown in Figure 2. With regards to experimental, high pressure phase equilibria, the situation at present is that no adequate explanation has apparently been found for the large velocity and density jump at the base of the transition zone [e.g., Hart, et al., 1977; Burdick and Helmberger, 1978] in terms of polymorphic phase

transformations alone [Anderson, 1976; Liu, 1979], and therefore a change in bulk chemical composition is strongly implicated for the transition zone. Similarly, recent isotopic and trace element data can be interpreted to suggest the existence of a separate, relatively undepleted geochemical reservoir underlying a more depleted upper mantle reservoir [DePaolo and Wasserburg, 1976; O'Nions, et al., 1978, 1979].

V. CONCLUSIONS

The central point of this study is that there is good evidence for regions of non-adiabatic gradients within the lower mantle and these are most likely confined to thermal boundary layers. We have evaluated the adiabatic thermal gradient through the lower mantle by using high pressure experimental data on the Grüneisen parameter and have found that this gradient is compatible with a lower bound on the temperature in the core only after allowing for a thermal boundary layer at the core-mantle boundary. Even with a thermal boundary layer at the core-mantle boundry we require a very low core temperature, and therefore we discussed the possibility of further non-adiabatic regions within the lower mantle. Our analysis relies upon having properly estimated the temperature at the top of the lower mantle and other constraints on the nature of the transition zone from high-pressure experimental petrology would be very useful in this regard. However our geotherm can be arrived at by several lines of reasoning and it is therefore considered to be adequately constrained.

We can not resolve the effects of possible phase transformations within the lower mantle since they appear to have only minor consequences

for its thermal state, within the scope of our study. The thermal boundary layer properties depend on the thermal flux assumed from the core, and our conclusions regarding the need for more than one thermal boundary layer within the lower mantle, may not be valid if a significantly larger flux is allowed from the core than has previously been considered acceptable. Alternatively, we find that either the temperature in the core must be lower than has been considered plausible, or there must be a barrier to convection within the lower mantle which results in additional thermal boundary layers. We find this latter possibility more plausible, however we can not constrain the depth at which such a barrier may be found. Guided by seismological evidence, we suggest the existence of a transition in chemical composition either at the top of the lower mantle or toward its base (D" region) as being the most likely cause of extra thermal boundary layers. This, then, provides us with a large enough increase in temperature across the lower mantle to allow plausible core temperatures (about 3500K). If a complex zone with multiple thermal boundary layers and separate convection within it is required to explain the observed (anamalous) properties of the D" region then we estimate an increase in temperature of about 1000K within the lowermost 200-300 km of the mantle. Alternatively, the transition zone is a likely candidate for a region across which the bulk chemical composition changes; this could readily explain a thermal boundary layer located there.

Acknowledgments. We thank D. L. Anderson for numerous helpful and stimulating discussions; D. L. Anderson, T. J. Ahrens, B. H. Hager and R. J. O'Connell also provided helpful comments on this paper.

REFERENCES

Ahrens, T. J. and J. T. Rosenberg, Shock-metamorphism: experiments on quartz and plagioclase, in Shock Metamorphism of Natural Materials, B. M.French and N. M. Short (eds.) Mono Book Corp., Baltimore, Md. 59-81, 1968.

Ahrens, T. J., Petrologic properties of the upper 670 km of the earth's mantle; geophysical implications, Phys. Earth Planet. Sci. Lett., 7, 167-186, 1973.

Ahrens, T. J., Equations of state of iron sulfide and constraints on the sulfur content of the earth, J. Geophys. Res., (in press) 1979.

Akimoto, S.-I., M. Akaogi, K. Kawada and O. Nishizawa, Mineralogic distribution of iron in the upper half of the transition zone in the earth's mantle, Am. Geophys. Un. Monograph, 19, 399-405, 1976.

Akimoto, S., T. Yagi and K. Inoue, High temperature-pressure phase boundaries in silicates using in situ x-ray diffraction, in High-Pressure Research, Applications in Geophysics, M. H. Manghnani and S. Akimoto (eds.) Academic Press, New York, 585-602, 1977.

Al'tshuler, L. V., R. F. Trunin and G. V. Simakov, Shock-wave compression of periclase and quartz and the composition of the earth's lower mantle. Izv. Acad. Sci. USSR, Earth Phys. Ser. No. 10, 657-660, 1965.

Al'tshuler, L. V., M. I. Brazhnik and G. S. Telegin, Strength and elasticity of iron and copper at high shock-wave compression pressures, J. Appl. Mech. Tech. Phys., 12, 921-926, 1971.

Anderson, D. L. and T. H. Jordan, The composition of the lower mantle, Phys. Earth Planet. Int., 3, 23-35, 1970.

Anderson, D. L., Chemical inhomogeneity of the mantle, Earth Planet. Sci. Lett., 5, 89-94, 1968.

Anderson, D. L., C. Sammis and T. Jordan, Composition of the mantle and core, in The Nature of the Solid Earth, E. C. Robertson (ed.) McGraw-Hill, New York, 41-66, 1972.

Anderson, D. L., The 650 km mantle discontinuity, Geophys. Res. Lett., 3, 347-349, 1976.

Anderson, D. L., Composition of the mantle and core, Ann. Rev. Earth Planet. Sci., 5, 179-202, 1977.

Anderson, G. D., in Compendium of Shock Wave Data, M. van Thiel (ed.) Lawrence Livermore Laboratory Report UCRL-50108, 1967.

Banks, R. J., Geomagnetic variations and the electrical conductivity of the upper mantle, Geophys. R. astr. Soc., 17, 457-487, 1969.

Birch, F., Composition of the earth's mantle, Geophys. J. R. astr. Soc., 4, 295-311, 1961.

Birch, F., The melting relations of iron, and temperatures in the earth's core, Geophys. J. R. astr. Soc., 29, 373-387, 1977.

Brennan, B. J. and F. D. Stacey, A thermodynamically based equation of state for the lower mantle (in press), 1979.

Brett, R., The current status of speculations on the composition of the core of the earth, Rev. Geophys. Space Phys., 14, 375-383, 1976.

Bukowinski, M. S. T., A theoretical equation of state for the inner core, Phys. Earth Planet. Int., 14, 333-344, 1977.

Bullen, K. E., Compressibility-pressure hypothesis and the earth's interior, Mon. Nat. R. astr. Soc. Geophys. Suppl., 5,355-368, 1949.

Burdick, L. and D. L. Anderson, Interpretation of velocity profiles of the mantle, J. Geophys. Res., 80, 1070-1074, 1975.

Burdick, L. J. and D. V. Helmberger, The upper mantle P velocity structure of the western United States, J. Geophys. Res., 83, 1699-1712, 1978.

Butler, R. and D. L. Anderson, Equation of state fits to the lower mantle and outer core, Phys. Earth Planet. Int., 17, 147-162, 1978.

Carter, W. J., S. P. Marsh, J. N. Fritz and R. G. McQueen, The equation of state of selected materials for high-pressure references, in Accurate Characterization of the High-Pressure Environment, E. C. Lloyd (ed.) Nat. Bur. Stand. (U.S.) Spec. Pub. 326, 146-158, 1971.

Cleary, J. R., The D" region, Phys. Earth Planet. Int., 9, 13-27, 1974.

Darken, L. S. and R. W. Gurry, Physical Chemistry of Metals, Mc Graw-Hill Book Co., New York, 535 pp., 1953.

Davies, D. and R. M. Sheppard, Lateral heterogeneity in the earth's mantle, Nature, 239, 318-323, 1977.

Davies, G. F., Limits on the constitution of the lower mantle, Geophys. J. R. astr. Soc., 38, 479-503, 1974.

Davies, G. F., Whole-mantle convection and plate tectonics, Geophys. J. R. astr. Soc., 49, 459-486, 1977.

DePaolo, D. J. and G. J. Wasserburg, Inferences about magma sources and mantle structure from variations of $^{143}Nd/^{144}Nd$, Geophys. Res. Lett., 3, 743-746, 1976.

Doornbos, D. J., Characteristics of lower mantle inhomogeneities from scattered waves, Geophys. J. R. astr. Soc., 44, 447-470, 1976.

Dziewonski, A. M., A. L. Hales and E. R. Lapwood, Parametrically simple earth models consistent with geophysical data, Phys. Earth Planet. Int., 10, 12-48, 1975.

Graham, E. K. and D. Dobrzykowski, Temperatures in the mantle as inferred from simple compositional models, Am. Mineral., 61, 549-559, 1976.

Haddon, R. A. W. and J. R. Cleary, Evidence for scattering of seismic PKP waves near the mantle-core boundary, Phys. Earth Planet. Int., 8, 211-234, 1974.

Hart, R. S., D. L. Anderson and H. Kanamori, The effect of attenuation on gross earth models, J. Geophys. Res., 82, 1647-1654, 1977.

Hart, S. and I. C. Skidmore, in Compendium of Shock Wave Data, M. van Thiel (ed.) Lawrence Livermore Laboratory Report UCRL-50108, 1967.

Husebye, E. S., D. W. King and R. A. W. Haddon, Precursors to PKIKP and seismic wave scattering near the mantle-core boundary, J. Geophys. Res., 81, 1870-1882, 1976.

Jacobs, J. A., The Earth's Core, Academic Press, New York, 253 pp., 1975.

Jarvis, G. T. and D. P. McKenzie, Infinite Prandtl number compressible convection, J. Fluid Mech. (in press), 1979.

Jeffreys, H., The instability of a compressible fluid heated from below, Proc. Camb. Phil. Soc., 26, 170-172, 1930.

Johnson, L. R., Array measurements of P-velocities in the lower mantle, Bull. Seism. Soc. Am., 59, 973-1008, 1969.

Jones, A. A., W. M. Isbell, F. H. Shipman, R. O. Perkins, S. J. Green and C. J. Maiden, Material properties measurements for selected materials, Rep. NAS2-3427, Gen. Motors Mater. and Struct. Lab., Warren, Mich., 56 pp., 1968.

Jordan, T. H. and D. L. Anderson, Earth structure from free oscillations and travel times, Geophys. J. R. astr. Soc., 36, 411-459, 1974.

Jordan, T. H., Lithospheric slab penetration into the lower mantle beneath the sea of Okhotsk, J. Geophys., 43, 473-496, 1977.

Kanamori, H., Upper mantle structure from apparent velocities of P waves recorded at Wakayama Micro-earthquake Observatory, Bull. Earthquake Res. Inst., Tokyo Univ., 45, 657-678, 1967.

Kanasewich, E. R., R. M. Ellis, C. H. Chapman and P. R. Gutowski, Seismic array evidence of a core boundary source for the Hawaiian linear volcanic chain, J. Geophys. Res., 78, 1361-1371, 1973.

Kieffer, S. W., Lattice thermal conductivity within the earth and consideration of a relationship between the pressure dependence of the thermal diffusivity and the volume dependence of the Grüneisen parameter, J. Geophys. Res., 81, 3025-3030, 1967.

Liu, L.-G., On the (γ, ε, 1) triple point of iron and the earth's core, Geophys. J. R. astr. Soc., 43, 697-705, 1975.

Liu, L.-G., On the 650-km seismic discontinuity (in press), 1979.

Mao, H.-K., T. Takahashi, W. A. Bassett, J. S. Weaver and S.-I. Akimoto Effect of pressure and temperature on the molar volumes of wüstite and of three $(Fe, Mg)_2 SiO_4$ spinel solid solutions, J. Geophys. Res., 74, 1061-1069, 1969.

Mao, N.-H., Velocity-density systematics and its implications for the iron content of the mantle, J.Geophys. Res., 79, 5447-5452, 1974.

McKenzie, D. P., J. M. Roberts and N. O. Weiss, Convection in the earth's mantle: Towards a numerical simulation, J. Fluid Mech., 62, 465-538, 1974.

Müller, G. H., A. H. Mula and S. Gregersen, Amplitudes of long-period PcP and the core-mantle boundary, Phys. Earth Planet. Int., 14, 30-40, 1977.

Navrotsky, A., F. S. Pinchovski, and S.-I. Akimoto, Calorimetric study of the stability of high pressure phases in the systems $CoO-SiO_2$ and "FeO"-SiO_2 and calculation of phase diagrams in $MO-SiO_2$ systems, Phys. Earth Planet. Int. (in press) 1979.

O'Connell, R. J., On the scale of mantle convection, Tectonophys., 38, 119-136, 1977.

O'Nions, R. K., N. M. Evensen, P. J. Hamilton and S. R. Carter, Melting of the mantle past and present: isotope and trace element evidence, Phil. Trans. R. Soc. Lond., A258, 547-559, 1978.

O'Nions, R. K., S. R. Carter, N. M. Evensen and P. J. Hamilton, Upper mantle geochemistry, in The Sea, Vol. VII, E. Emiliani (ed.) (in press) 1979.

Peltier, W. R. and J. T. Andrews, Glacial-isostatic adjustment - I, Geophys. J. R. astr. Soc., 46, 605-646, 1976.

Phinney, R. A. and S. S. Alexander, The effect of a velocity gradient at the base of the mantle on diffracted P waves in the shadow J. Geophys. Res., 74, 4967-4971, 1969.

Podurets, M. A., L. V. Popov, A. G. Sevast'yanova, G. V. Simakov and R. F. Trunin, On the relation between the size of studied specimens and the position of the silica shock adiabat, Izv. Acad. Sci. USSR, Earth Phys., No. 11, 727-728, 1976.

Press, F., Density distribution in earth, Science, 160, 1218-1220, 1968.

Richter, F. M. and C. E. Johnson, Stability of a chemically layered mantle, J. Geophys. Res., 79, 1635-1639, 1974.

Richter, F. and D. McKenzie, Simple plate models of mantle convection, J. Geophys., 44, 441-471, 1978.

Ringwood, A. E., Composition and Petrology of the Earth's Mantle, McGraw-Hill, New York, 618 pp., 1975.

Ringwood, A. E., Composition of the core and implications for origin of the earth, Geochemical J., 11, 111-136, 1978.

Sacks, I. S. and L. Beach, Lateral heterogeneity at the base of the mantle -- an indication of whole mantle convection, Carnegie Inst. Wash. Yrbook, 73, 1020-1032, 1974.

Schatz, J. F. and G. Simmons, Thermal conductivity of earth materials at high temperatures, J. Geophys. Res., 77, 6966-6983, 1972.

Schubert, G., D. A. Yuen, and D. L. Turcotte, Role of phase transitions in a dynamic mantle, Geophys. J. R. astr. Soc., 42, 705-735, 1975.

Snoke, J. A. and I. S. Sacks, A model for laterally heterogeneous velocity structure at the base of the mantle, Carnegie Inst. Wash. Yrbook, 75, 233-239, 1976.

Stacey, F. D., Physical properties of the earth's core, Geophys. Surv., 1, 99-119, 1972.

Stacey, F. D., Applications of thermodynamics to fundamental earth physics, Geophys. Surv., 3, 175-204, 1977a.

Stacey, F. D., A thermal model of the earth, Phys. Earth Planet. Int., 15, 341-348, 1977b.

Tolland, H. G., Thermal regime in the earth's core and lower mantle, Phys. Earth Planet. Int., 8, 282-286, 1974.

Trunin, R. F., G. V. Simakov, M. A. Podurets, B. N. Moiseyev and L. V. Popov, Dynamic compressibility of quartz and quartzite at high pressure, Izv. Acad. Sci. USSR, Earth Phys., No. 1, 8-12, 1970.

Trunin, R. F., G. V. Simakov and M. A. Podurets, Compression of porous quartz by strong shock waves, Izv. Acad Sci. USSR, Earth Phys., No. 2, 102-196, 1971.

Usselman, T. M., Experimental approach to the state of the core, Part I, Am. J. Sci., 275, 278-290, 1975a.

Usselman, T. M., Experimental approach to the state of the core, Part II, Am. J. Sci., 275, 291-303, 1975b.

van den Berg, A. P., S. A. P. L. Cloetingh and D. J. Doornbos, A comparison of PKP precursor data from several seismic arrays, J. Geophys., 44, 499-510, 1978.

Verhoogen, J., Phase changes and convection in the earth's mantle, Phil. Trans. R. Soc., Lond., A258, 276-283, 1965.

Verhoogen, J., Thermal regime of the earth's core, Phys. Earth Planet. Int., 7, 47-58, 1973.

Vinnik, L. P. and A. V. Nikolayev, The velocity profile of the lower mantle from direct measurements of $dT/d\Delta$, Izv. Acad. Sci. USSR, Earth Phys., 24-40, 1970.

Wackerle, J., Shock-wave compression of quartz, J. Appl. Phys., 33, 922-937, 1962.

Watt, J. P., T. J. Shankland and N.-H. Mao, Uniformity of mantle composition, Geology, 3, 91-94, 1975.

Wiggins, R. A., G. A. McMechan and M. N. Toksöz, Range of earth nonuniqueness implied by body wave observations, Rev. Geophys. Space Phys., 11, 87-113, 1973.

Wright, C. and J.-R. Cleary, P wave travel-time gradient measurements for the Warrumunga Seismic Array and lower mantle structure, Phys. Earth Planet. Int., 5, 213-230, 1977.

Young, R. E., Finite-amplitude thermal convection in a spherical shell, J. Fluid Mech., 63, 695-721, 1974.

Table 1

Lower Mantle Properties

Density:	$\rho \sim 4$ to 5.5 Mg m^{-3}	(1)
Acceleration of Gravity:	$g \sim 10$ ms^{-2}	(1)
Specific Heat at Constant Pressure:	$C_p \sim 1.2 \times 10^3$ J $Kg^{-1}K^{-1}$	(2)
Kinematic Viscosity:	$\nu \sim 1$ to 10×10^{17} m^2 s^{-1}	(3)
Thermal Diffusivity:	$\kappa \sim 1$ to 2×10^{-6} m^2 s^{-1}	(4)
Coefficient of Thermal Expansion:	$\alpha \sim 1$ to 2×10^{-5} K^{-1}	(5)
Heat Flux From Core:	$F = 5.85 \times 10^{-2}$ W m^{-2}	(6)

Sources

(1) Measured

(2) Dulong-Petit value

(3) Peltier and Andrews [1976]

(4) Schatz and Simmons [1972]; Kieffer [1976]

(5) This study: $\alpha = \frac{\gamma C_p \rho}{K_s}$; also, Stacey [1977b]

(6) Assumed equivalent to the flux through the earth's surface: see text.

Figure Captions

Figure 1 Grüneisen parameter through the lower mantle based on experimental high pressure data for MgO and SiO_2 (this study) compared with the theoretical formulations of Stacey [1977b] and Brennan and Stacey [1979].
O and P refer to mixtures of the oxides corresponding to olivine and pyroxene stoichiometry, respectively.

Figure 2 The temperature profile for a homogeneous and adiabatic lower mantle (solid line) is compared with profiles including the effects of possible phase transformations (dashed line) and a thermal boundary layer at the core-mantle boundary (dotted). Fixed reference points in the transition zone are shown, along with our best estimate and lowest plausible values of temperature in the core.

Figure 3 Horizontally averaged temperature as a function of depth from numerical simulations of convection in an incompressible fluid layer. [McKenzie, Roberts and Weiss, 1974]. The flux at the upper surface is 5.85×10^{-2} Wm^{-2} and relevant material properties are given in Table 1.

a) All heating from below

b) All heating internal

c) Half heating from below, half internally heated

The boundary layer thickness δ is measured from the boundary to the first point where $dT/dz = 0$.

Figure 4 Horizontally averaged temperature from numerical calculations of convection between isothermal boundaries.

a) Plane layer: $Ra = 10^4$, $Pr = \infty$

b) Spherical shell: $Ra = 4 \times 10^3$, $Pr = 5$ and ratio of inner radius to outer radius of 0.6 [axially symmetric mode, taken from Young, 1974]

$Ra = \frac{g\alpha\Delta T\, d^3}{\kappa\nu}$, $Pr = \nu/\kappa$ and $\Delta T = T_2 - T_1$

The vertical axis is depth in fractions of d, the total layer depth.

Figure 5 Horizontally averaged temperature for both incompressible and compressible convection.

a) Same as in Figure 3a but with depth of 700 Km

b) Compressible case [Jarvis and McKenzie, 1978; case B 10]

Assumes depth = 700 Km, $d/H_T = 0.5$ and flux of 5×10^{-2} Wm^{-2} from below.

Figure 6 Temperature profiles through the earth's mantle: three acceptable models. Thermal boundary layers (B.L.) are indicated in the upper and lower mantle, while dynamic barriers associated with possible chemical transitions in the lower mantle are shown as dashed lines. The preferred core temperature and its plausible lower bound are also shown. Note the fundamental asymmetry of the profiles caused by the large decrease in temperature through the lithosphere: an effect which has no counterpart at depth within the earth and which is due to temperature-dependent rheology.

Figure 6 (continued)

(a) Adiabat through lower mantle with one thermal boundary layer at the core-mantle boundary and with the core at a relatively low temperature. Taken from Figure 2.

(b) Adiabat with two thermal boundary layers near the base of the mantle corresponding to a seismologically complex and chemically distinct D" region.

(c) Adiabat with a thermal boundary layer at the top and the bottom of the lower mantle. In this case, the lower and upper mantle are separate chemical and dynamic systems.

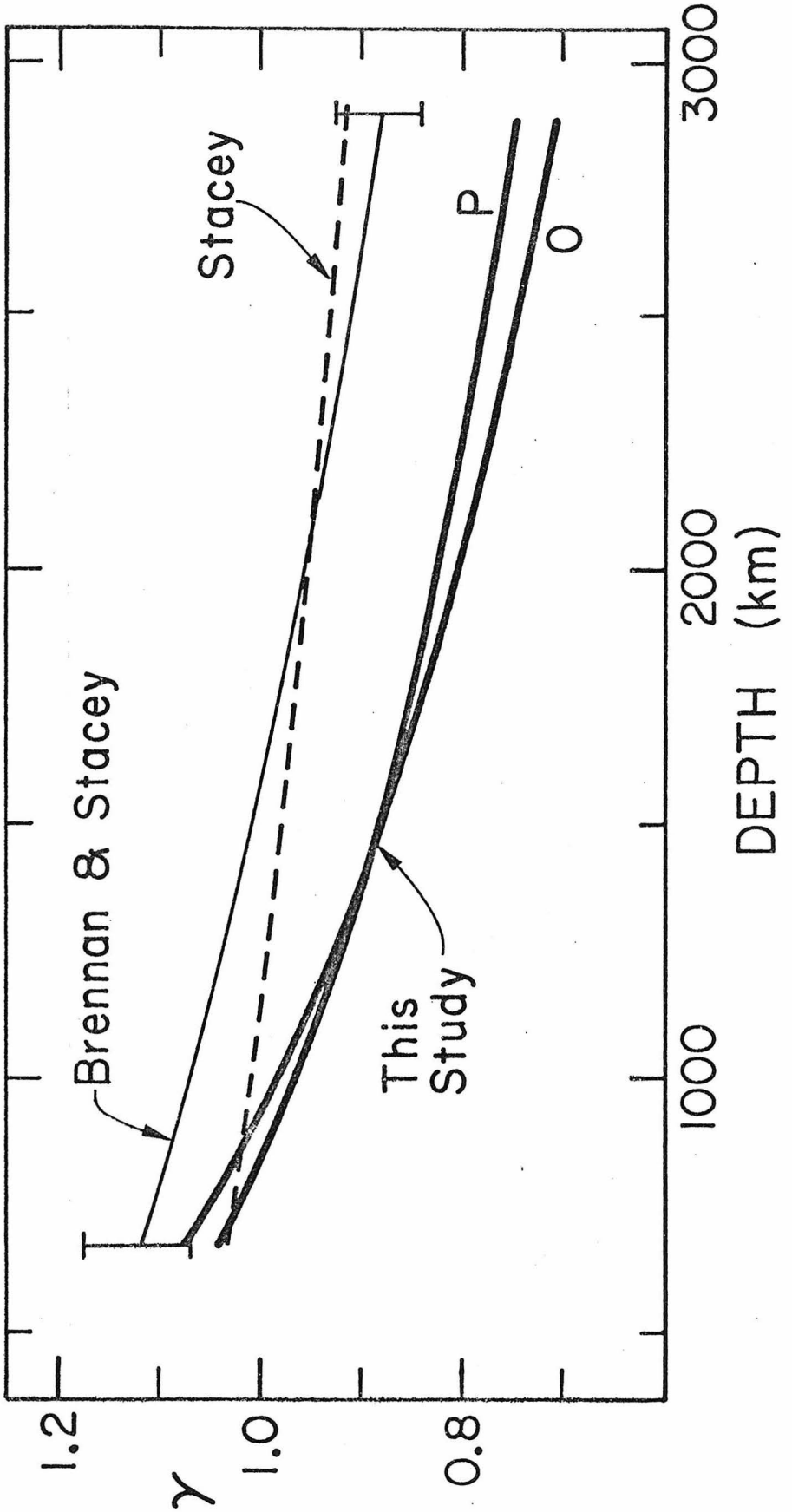
Brennan & Stacey
Stacey
P
Q
This Study
1.2
1.0
0.8
γ
1000
2000
3000
DEPTH (km)

Fig. 1

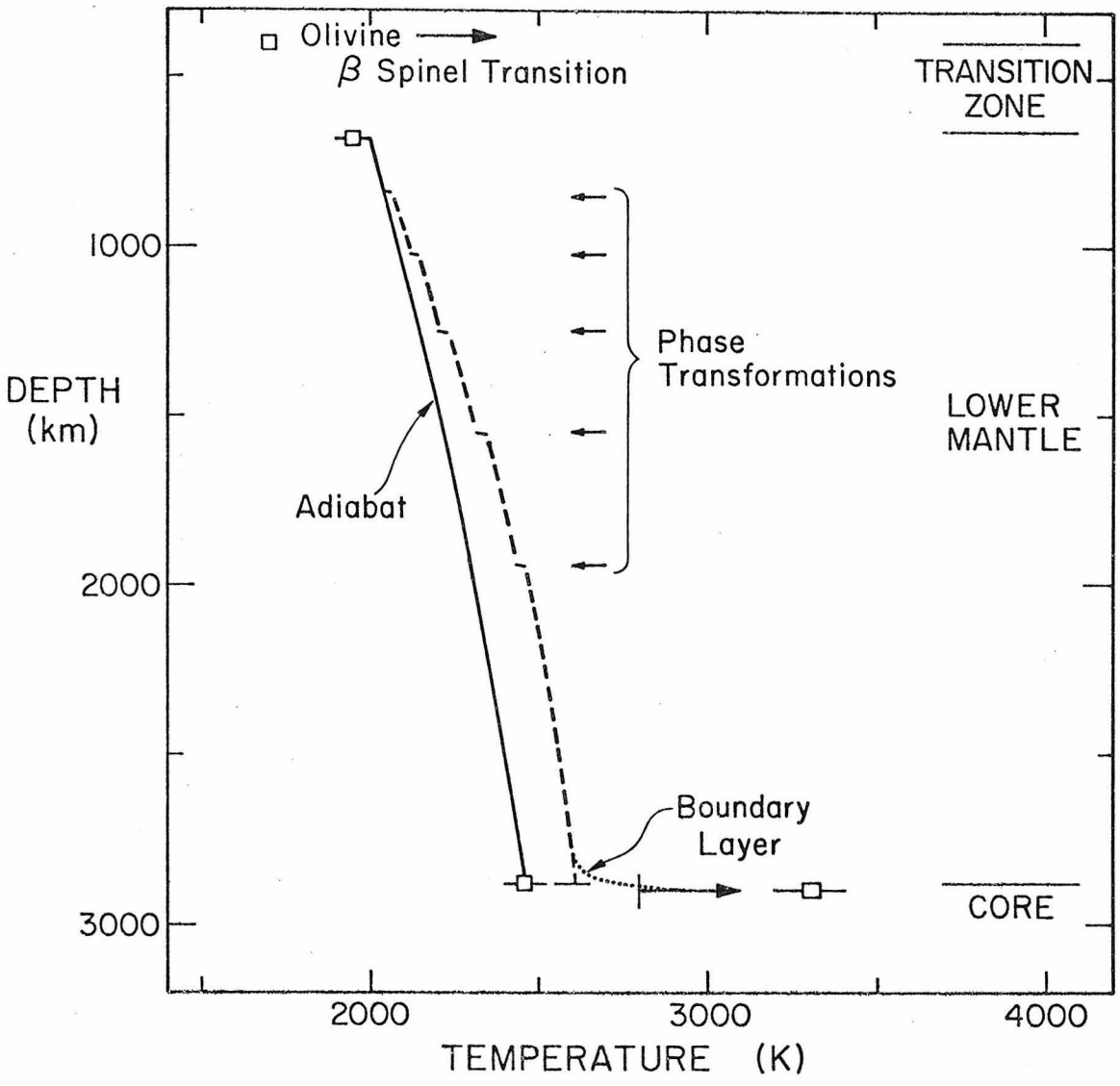
Olivine
β Spinel Transition
TRANSITION ZONE
1000
DEPTH (km)
Phase Transformations
LOWER MANTLE
Adiabat
2000
Boundary Layer
3000
CORE
2000
3000
4000
TEMPERATURE (K)

Fig. 2

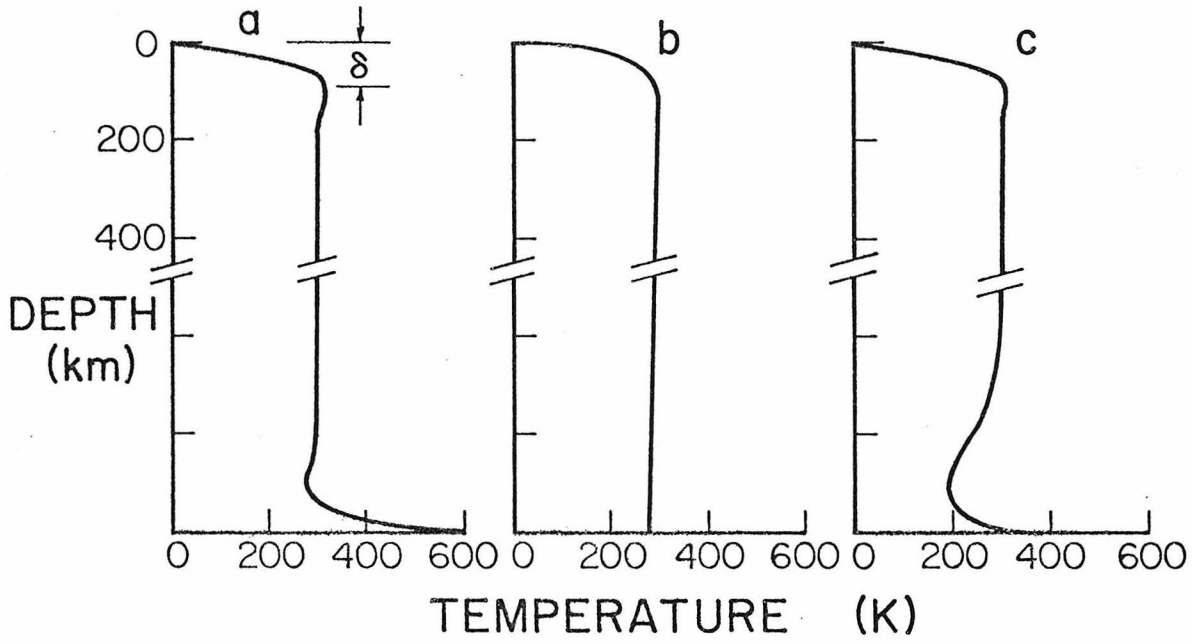
a
b
c
δ
0
200
400
DEPTH
(km)
0 200 400 600
0 200 400 600
0 200 400 600
TEMPERATURE (K)

Fig. 3

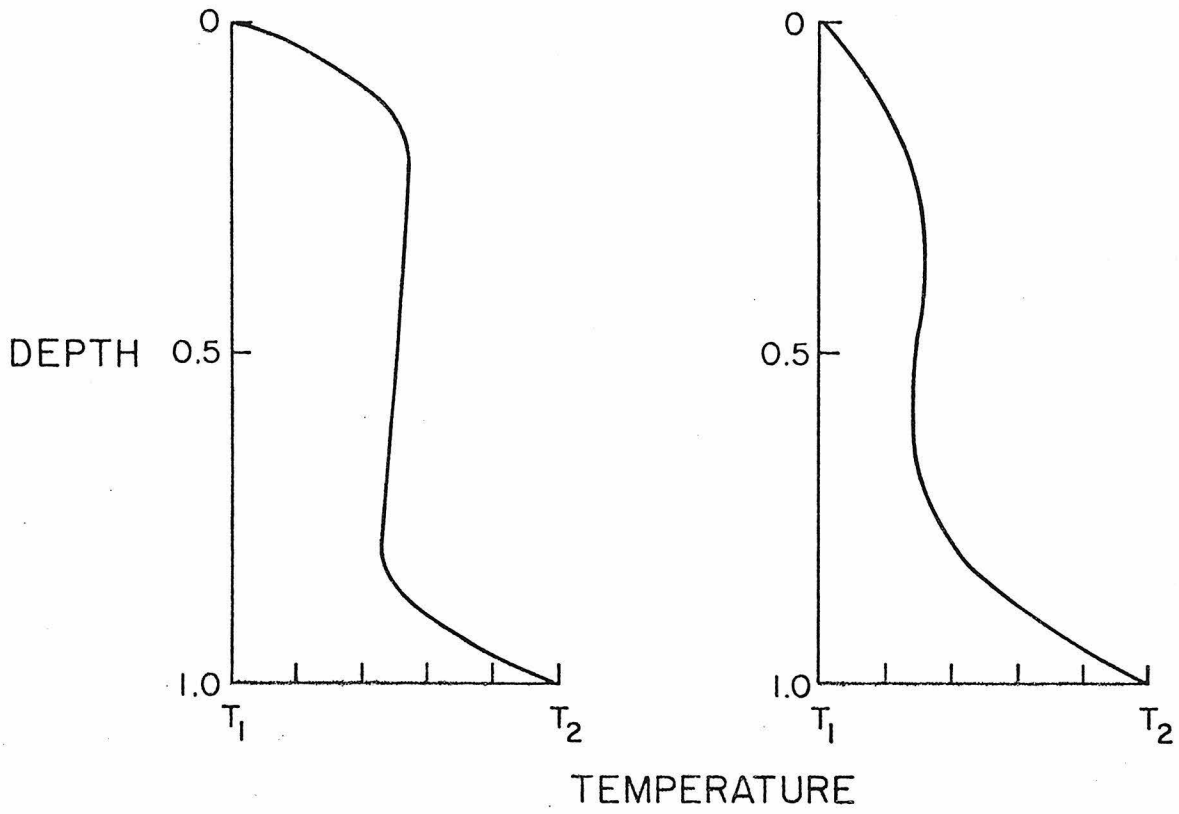

Fig 4

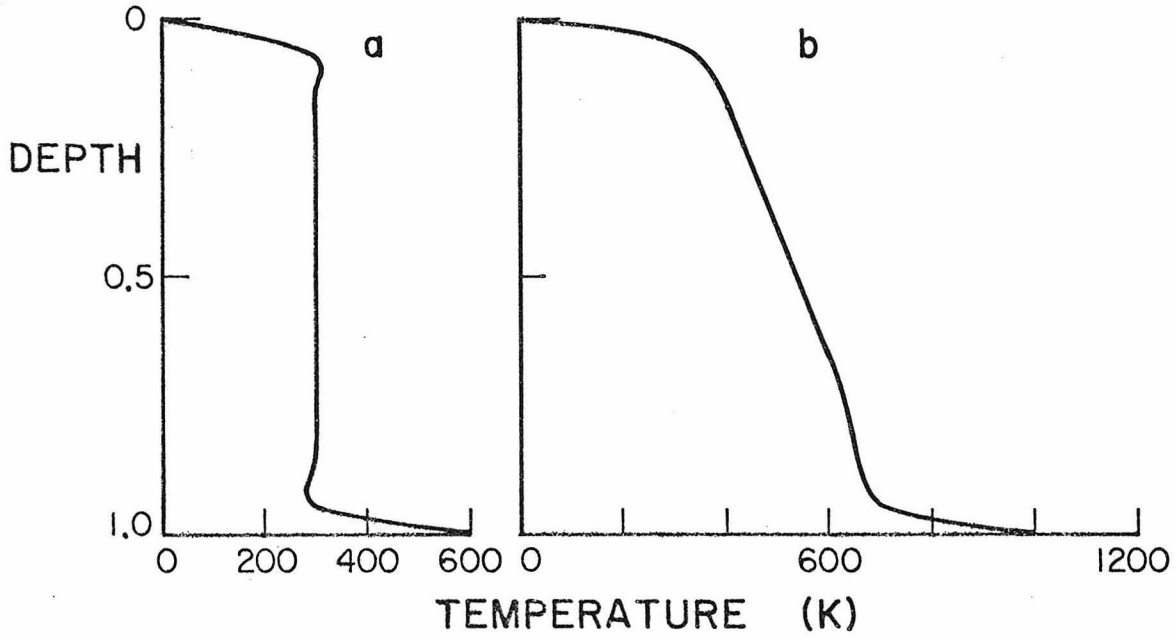

Fig. 5

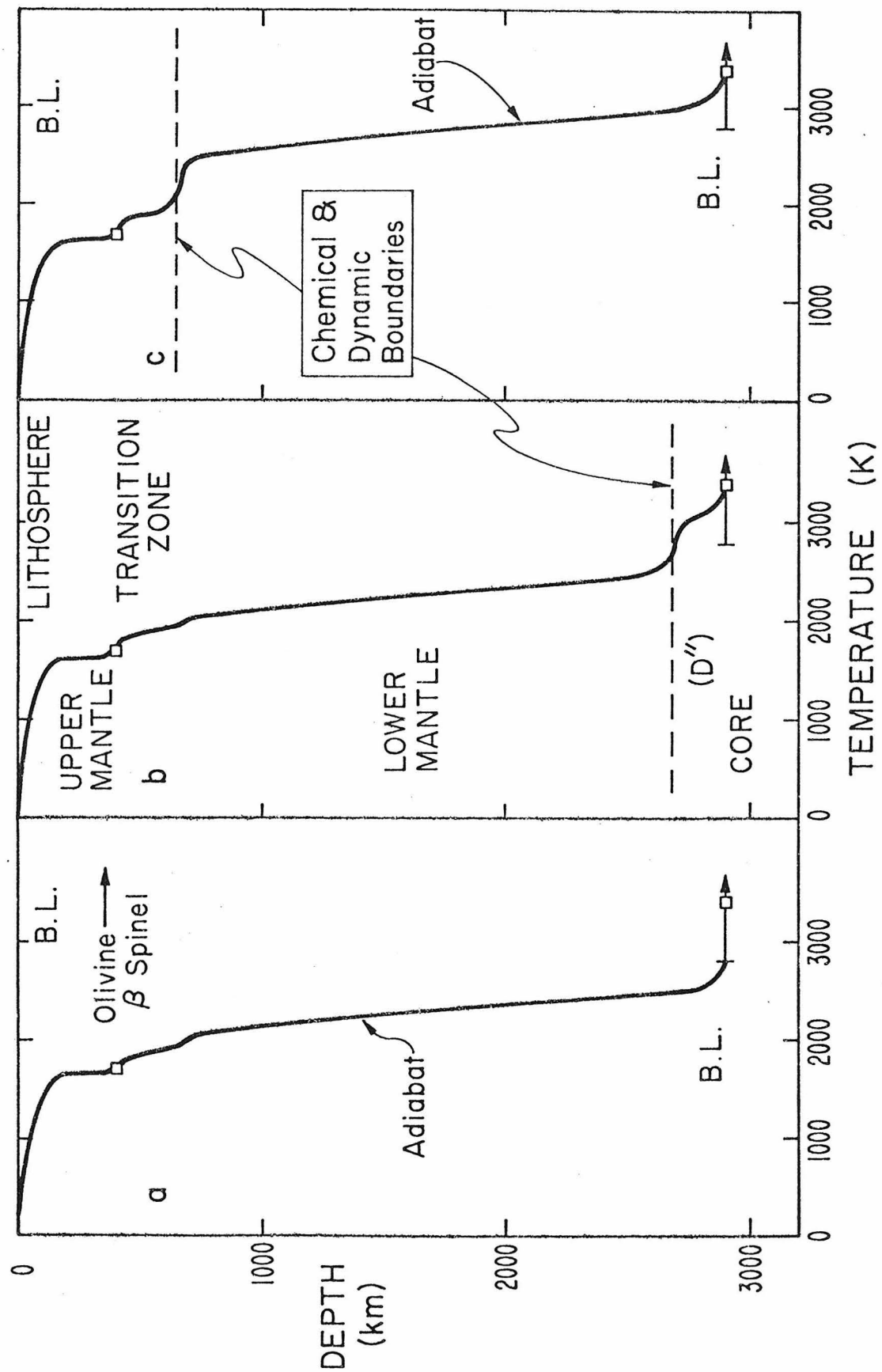
DEPTH (km)
0
1000
2000
3000
TEMPERATURE (K)
0
1000
2000
3000
a
B.L.
Olivine
β Spinel
Adiabat
B.L.
b
LITHOSPHERE
UPPER MANTLE
TRANSITION ZONE
LOWER MANTLE
(D'')
CORE
c
B.L.
Adiabat
B.L.
Chemical & Dynamic Boundaries

Fig. 6